RL-TR-94-222
Final Technical Report
December 1994

LINEWIDTH-INSENSITIVE COHERENT ANALOG OPTICAL LINKS

Stanford University

L.G. Kazovsky, J. Fan, T.K. Fong, R.F. Kalman,
D.J.M. Sabido IX, and M. Tabara

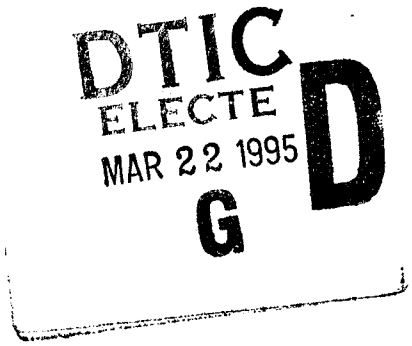

APPROVED FOR PUBLIC RELEASE; DISTRIBUTION UNLIMITED.

Rome Laboratory
Air Force Materiel Command
Griffiss Air Force Base, New York

This report has been reviewed by the Rome Laboratory Public Affairs Office (PA) and is releasable to the National Technical Information Service (NTIS). At NTIS it will be releasable to the general public, including foreign nations.

RL-TR-94-222 has been reviewed and is approved for publication.

APPROVED: James R. Hunter

JAMES R. HUNTER
Project Engineer

FOR THE COMMANDER: Donald W. Hanson

DONALD W. HANSON
Director of Surveillance & Photonics

If your address has changed or if you wish to be removed from the Rome Laboratory mailing list, or if the addressee is no longer employed by your organization, please notify RL (OCPC) Griffiss AFB NY 13441. This will assist us in maintaining a current mailing list.

Do not return copies of this report unless contractual obligations or notices on a specific document require that it be returned.

REPORT DOCUMENTATION PAGE

Form Approved
OMB No. 0704-0188

1. AGENCY USE ONLY (Leave Blank)	2. REPORT DATE	3. REPORT TYPE AND DATES COVERED
	December 1994	Final Oct 91 - Sep 94

4. TITLE AND SUBTITLE

LINEWIDTH-INSENSITIVE COHERENT ANALOG OPTICAL LINKS

5. FUNDING NUMBERS

C - F30602-91-C-0141
PE - 63726F
PR - 2863
TA - 92
WU - 52

6. AUTHOR(S)

L.G. Kazovsky, J. Fan, T.K. Fong, R.F. Kalman,
D.J.M. Sabido IX, and M. Tabara

7. PERFORMING ORGANIZATION NAME(S) AND ADDRESS(ES)

Stanford University
Department of Electrical Engineering, STARLAB/SEL
Stanford CA 94305-4055

8. PERFORMING ORGANIZATION REPORT NUMBER

N/A

9. SPONSORING/MONITORING AGENCY NAME(S) AND ADDRESS(ES)

Rome Laboratory (OCPC)
25 Electronic Pky
Griffiss AFB NY 13441-4515

10. SPONSORING/MONITORING AGENCY REPORT NUMBER

RL-TR-94-222

11. SUPPLEMENTARY NOTES

Rome Laboratory Project Engineer: James R. Hunter/OCPC/(315) 330-3143

12a. DISTRIBUTION/AVAILABILITY STATEMENT

Approved for public release; distribution unlimited.

12b. DISTRIBUTION CODE

13. ABSTRACT (Maximum 200 words)

This program has analyzed the performance of four classes of links as quantified by spurious-free dynamic range (SFDR), RF power transfer ratio and noise figure, and compared them to conventional detection links. The four classes analyzed were coherent links, optically amplified links, angle modulated links, and combinations of these. Experimental validation of the analysis was accomplished at 2 GHz and is described. The linewidth-insensitive operation in all cases using both semiconductor laser and solid-state Nd:YAG lasers has been demonstrated.

14. SUBJECT TERMS

Analog optical links, Optical modulation, Fiber optic analog links, Analog optical remoting

15. NUMBER OF PAGES

260

16. PRICE CODE

17. SECURITY CLASSIFICATION OF REPORT	18. SECURITY CLASSIFICATION OF THIS PAGE	19. SECURITY CLASSIFICATION OF ABSTRACT	20. LIMITATION OF ABSTRACT
UNCLASSIFIED	UNCLASSIFIED	UNCLASSIFIED	UL

NSN 7540-01-280-5500

Standard Form 298 (Rev. 2-89)
Prescribed by ANSI Std. Z39-18
298-102

TABLE OF CONTENTS

SCOPE OF THIS REPORT

This report covers the work performed during the three-year duration of Air Force Contract No. F30602-91-C-0141. The termination date of the project is September 30, 1994. The report is organized as follows: The project objectives are presented. The work performed during the project is briefly summarized. Part 1 gives introduction, definitions, and background. Within Part 1, Chapter 1 presents an introduction to analog optical links, to previous work in the field, and to advanced techniques. Chapter 2 defines the fundamental performance measures by which analog links are evaluated and gives background on the conventional direct detection analog link.

Part 2 describes our work on amplitude modulated coherent and optically amplified links. Chapter 3 describes our theoretical analysis of homodyne and heterodyne coherent WIRNA (WIdeband - Rectifier - NArrowband) links. Chapter 4 describes and compares our experimental implementations of a directly and externally modulated heterodyne WIRNA and direct detection links. Chapter 5 describes our work on optically amplified direct detection and coherent links. Chapter 6 describes our improvement of link performance using higher power, lower RIN lasers and linearized modulators. Chapter 7 summarizes our work on AM links and gives recommendations for directly related future work.

Part 3 describes our work on angle modulated links. Chapter 8 describes our theoretical analysis of the performance and linewidth sensitivity of coherent phase modulated and frequency modulated links. Chapter 9 describes our investigation of conventional reference transport links, which are not adequate for wide-deviation analog applications, and our development of a new class of linewidth-insensitive angle modulated analog links: interferometric links. We present both theoretical analysis and the results of our proof-of-concept experimental interferometric link. Chapter 10 presents our theoretical analysis of the performance of optically amplified interferometric links. Chapter 11 presentes our analysis of the improvement of angle modulated link performance using discriminator linearization. Chapter 12 presents theoretical linewidth and relative intensity noise limitations on coherent angle modulated and interferometric subcarrier multiplexed links for a variety of applications. Chapter 13 summarizes our work on angle modulated links and gives recommendations for directly related future work.

Part 4 provides conclusions to the project. Chapter 14 compares the performance of AM and angle modulated links for a variety of applications. Chapter 15 gives

recommendations for potential future work on analog links which is of great interest. Chapter 16 lists publications stemming from this project. Chapter 17 lists contributors.

Part 5 provides appendices. Appendix A discusses system noises and their properties. Appendix B provides derivations of amplitude modulated link equations. Appendix C provides derivations of angle modulated link equations.

PROJECT OBJECTIVES

The objective of this project is to unite the potential of coherent analog optical techniques with the practical advantages of semiconductor lasers. At the commencement of this project, we anticipated that we would produce:

- A general theory predicting the performance of coherent optical analog links utilizing wide linewidth semiconductor lasers. This theory will apply to systems utilizing a wide variety of modulation formats and demodulation techniques.
- Models of critical components appropriate for our analysis, including semiconductor lasers, optical amplitude and phase modulators, optical amplifiers, and microwave rectifiers and delay-line discriminators.
- Linewidth-insensitive system designs.
- Demonstrations of linewidth-insensitive links.
- Characterization and evaluation of experimental linewidth-insensitive links.
- Suggestions of directions for future work leading to more robust, higher performance fielded systems.

EXECUTIVE SUMMARY

During this project, we have analyzed the performance of four classes of links as quantified by spurious-free dynamic range (SFDR), RF power transfer ratio, and noise figure, and compared them to conventional direct detection links. These four classes are coherent links, optically amplified links, angle modulated links, and combinations of the above. To show the validity of our analyses, we have also constructed links which fall into the above four classes. We have measured the performance of these experimental implementations as quantified by the above performance measures. We have met the project objectives in our investigation of coherent and angle modulated links and have exceeded them in our investigation of optically amplified links.

During our investigation of linewidth-insensitive amplitude-modulated links, we have studied theoretically four types of these links:

- homodyne AM-WIRNA links:
  - (a) 2-port homodyne link;
  - (b) K-port homodyne link; and
  - (c) 2K-port homodyne link, with K>1;
- heterodyne AM-WIRNA links;
- optically amplified direct detection links;
- optically amplified heterodyne AM-WIRNA links.

We show that the 2-port homodyne link suffers from degradation caused by baseband processing, while the 2K-port link obtains the best performance, although the structure is complicated in practice. The 2K-port link is the only homodyne link which has an FLDR which is not inherently limited by receiver noise cross terms at high received optical powers. The 2K-port homodyne system has very similar performance to the heterodyne system., except that in the heterodyne system the bandwidth of the IF filter should be twice as much as that in the homodyne system. In both cases, the bandwidth of the IF filter must be sufficiently large to avoid the conversion of the phase noise characteristic of semiconductor lasers to amplitude noise during receiver processing.

We have successfully built and tested the following links operating at 2 GHz:

- a conventional direct detection link;
- a heterodyne AM-WIRNA link;
- a direct detection link with a semiconductor amplifier;

- a direct detection link with an erbium-doped fiber amplifier;
- a heterodyne AM-WIRNA link with a semiconductor amplifier;
- a heterodyne AM-WIRNA link with an erbium-doped fiber amplifier;

We have demonstrated linewidth-insensitive operation in all cases using both semiconductor lasers and solid-state Nd:YAG lasers. Using semiconductor lasers, we have demonstrated that coherent links significantly outperform direct detection links for received optical powers below 100 μW. Using optical amplifiers, we have demonstrated that for medium loss (link loss between 10 to 25 dB), direct detection links perform better than coherent links because of the stronger impact of RIN on the coherent AM link. However, the coherent AM link outperforms the DD link for high loss (loss greater than 28 dB) links due to the better sensitivity of the coherent receiver caused by the presence of an LO laser.

For low received optical power (< 100 μW), optical amplification, coherent detection, or both can be used to improve the dynamic range of the links. However, for high received optical power (>1 mW), the conventional direct detection link gives the best performance. The shot noise-limited SFDR of the conventional direct detection link is 2 dB higher than that of the amplified direct detection and coherent AM link; this is due the 3 dB noise figure of the optical amplifier in the amplified link and the extra signal processing in the coherent receiver for the coherent AM link. We have also shown that the coherent AM links are more sensitive to RIN than the direct detection links. The RIN-limited SFDR of the coherent AM links is 4 dB worse than that of the direct detection links.

Our experiments provide strong evidence that the dynamic range of coherent AM links can be improved by using better devices. The SFDR of 115 $dB \cdot Hz^{2/3}$ we obtained using Nd:YAG lasers, a linearized modulator, and a balanced receiver is the best dynamic range ever attained with a coherent analog link; it was obtained using modest optical powers of 1 mW LO and 0.5 mW received optical signals, and this was because we were limited by the saturation of our photodetector for higher optical powers. We are confident that even higher SFDR values can be obtained using much better devices. In addition, we have experimentally obtained up to 34 dB reduction in third-order IMD, the largest reported for any modulator linearization scheme for any type of analog optical link.

Due to the large potential transmission bandwidth of optical fiber, optical transmission systems are well-suited to handle the expanded bandwidth of wideband angle modulated signals. Our investigation of angle modulated links during this project

has been motivated by a desire to see the same signal-to-noise ratio (SNR) improvements in fiber systems that are exploited in commercial FM radio and video.

We present the spurious-free dynamic ranges (SFDRs), RF power transfer ratios, and noise figures of coherent phase modulated (PM) and frequency modulated (FM) links using either direct modulation of the grating section current of a laser diode or external phase modulation. We found that coherent angle modulated systems are intrinsically sensitive to phase noise because their signal information is contained in the optical phase. For a combined transmitter laser and local oscillator laser linewidth of 20 MHz, phase noise is the dominant noise in PM and FM links for received optical power levels above -30 dBm, and limits the SFDR to 30 dB and 31 dB in a 1 GHz bandwidth for PM and FM links, respectively. For a combined linewidth of 10 kHz, phase noise dominates the noise characteristics for received optical power levels above -5 dBm, and limits the SFDR to 51 dB and 53 dB in a 1 GHz bandwidth for PM and FM links, respectively. Angle modulated links can exhibit substantial RIN insensitivity through the use of a limiter in the receiver and by operating at an IF well above the RIN roll-off frequency. The linearity of angle modulated links tends to improve for high IFs due to the improved linearity of the phase or frequency discriminator in the receiver.

We find that externally angle modulated coherent links are inherently more lossy than externally amplitude modulated links, due to the large losses of the integrator and discriminator filters in these links. Extra amplification is required before these filters for these links to attain their SFDR potential. The directly frequency modulated coherent link, on the other hand, is less lossy than externally amplitude modulated links due to its high conversion efficiency of input RF power to optical frequency deviation. The difficulty with directly frequency modulated links is that it is difficult to guarantee a linear frequency versus current characteristic over many GHz in conjunction with a sufficiently low linewidth.

We then consider reference transport as a means of transmitter phase noise cancellation (PNC) in angle modulated analog links. We found that reference transport in links using direct frequency modulation is not a useful means of PNC because laser phase noise in links using direct FM is equivalent to white noise in the original applied RF signal. We found that reference transport in externally angle modulated links requires frequency shifting of the reference to facilitate demodulation of the PM or FM signal. As a result, we analyzed a novel class of linewidth-insensitive analog links: interferometric angle modulated links. Linewidth insensitivity is attained through the transport of a reference derived from the transmitter laser in the same fiber as the optical field carrying the desired signal. The IF frequency shift required for demodulation of FM and PM

signals is generated using a novel electro-optic quasi-single sideband (SSB) frequency shifter in heterodyne interferometric links and using mixers at the receiver in homodyne interferometric links.

We present the SFDRs, RF power transfer ratios, and noise figures of heterodyne and homodyne interferometric PM and FM links. Since interferometric links are more linear than externally amplitude modulated links for high intermediate frequencies, the phase modulated interferometric links (HIPM and HPM) show about a 2 dB SFDR advantage over amplitude modulated links at low received optical powers. The frequency modulated interferometric links (HIFM and HFM) show a corresponding 5 dB SFDR advantage. As laser relative intensity noise (RIN) becomes dominant for received optical powers above 1 mW, the potential SFDR advantage of the interferometric links increases. At a received optical power of 10 mW, the HIFM link shows an 11 dB SFDR advantage over a direct detection link for a laser RIN of -155 dB/Hz. For a laser RIN of -130 dB/Hz, the HIPM link shows a 24 dB SFDR advantage over the direct detection link. Heterodyne interferometric links are partially insensitive to laser RIN because the signal information is in the optical phase. However, they are not completely insensitive to laser RIN due to the RIN of the optical reference. Homodyne interferometric links are less insensitive to laser RIN because baseband RIN is converted up to the intermediate frequency of the receiver.

Interferometric links are also significantly more lossy than externally amplitude modulated links. They share the lossy integrator and discriminator filters of the coherent angle modulated links and have additional optical losses due to the optical reference transport. As a result, significant amplification is again required for interferometric links to reach their SFDR potential.

We briefly describe a proof-of-concept experimental demonstration of an HIPM link to verify the potential of interferometric links. A 23 dB suppression of third-order nonlinearities (7.7 dB SFDR improvement) over that of a conventional direct detection link is obtained using an HIPM link with an intermediate frequency of 650 MHz and signal frequencies of 47.5 and 52.5 MHz. Data is presented which shows the significant impact of receiver nonidealities, indicating that the SFDR improvement can be nearly twice as large in a carefully optimized system.

We consider the use of optical amplifiers to increase the available optical power in interferometric links. We derive the SFDR expressions for optically amplified interferometric PM and FM links and show that for realistic antenna remoting system parameters (including modulator and link losses), the HIPM and HIFM links have the

potential to improve link SFDRs by 6 dB and 9 dB, respectively, over an optically amplified direct detection link.

We consider a simple method for discriminator linearization to improve angle modulated link SFDR. Assuming realistic antenna remoting system parameters, a linearized HIPM link can potentially gain 7 dB of SFDR over an unlinearized HIPM link at a received optical power of 10 mW.

We consider the use of subcarrier multiplexing (SCM) as a means of transmitting many narrowband channels using a single transceiver. The derived results are used to find signal power, laser linewidth, and laser RIN requirements for analog video systems, SCM digital systems, and antenna remoting systems. For AM video and antenna remoting applications, low-linewidth sources such as Nd:YAG lasers are needed for PM and FM coherent systems. For these same applications, the amplitude modulated links need extremely high received optical powers and low RIN due to the high required CNRs. Even if optical amplifiers (OAs) are used in the amplitude modulated links, noise associated with the spontaneous emission of OAs and the received power limitations on the photodiode may prevent the fulfillment of the SFDR requirements in that link. For FM video and SCM digital applications, presently available semiconductor laser diodes can easily fulfill the requirements on the laser transmitter in the direct detection and the coherent systems. Interferometric links behave similarly to the direct detection and coherent AM links, with less stringent RIN requirements.

The fundamental conclusion which we draw from our work on angle modulated links is that coherent angle modulated links are promising for low received powers (< 1 mW) and low laser linewidths, while interferometric angle modulated links are promising for high received powers (> 1 mW). As a result, coherent angle modulated links are potentially useful in distribution and other high-loss links using solid-state Nd:YAG or low-linewidth (< 100 kHz) semiconductor lasers. Interferometric links do not have linewidth requirements but do require high-power semiconductor lasers and optical amplification. All externally angle modulated links are lossy in the RF domain and require more RF amplification than in externally amplitude modulated links.

PART 1:

INTRODUCTION, DEFINITIONS, AND BACKGROUND

Chapter One

Introduction to Advanced Analog Optical Links

1.1 Introduction

Applications involving multiple remote antennas require the transport of wideband analog signals. Optical fiber provides a nearly ideal signal transport medium due to its extremely low frequency-independent loss and low dispersion.

The objective of an analog link is to transport an analog signal from one site to another with high fidelity. The fidelity is commonly characterized by a number of performance measures. A very important performance measure is the dynamic range. The spurious-free dynamic range (SFDR) is the ratio of the largest usable output signal to the smallest. The largest usable signal is often limited by the spurious signals resulting from intermodulation products (IMPs) produced by the system nonlinearities while the smallest usable signal is limited by the noise power. Another fundamental measure is the RF power transfer ratio, that measures the efficiency with which the link transfers the input microwave power to the output. It is important to achieve high transfer ratio, especially at high frequencies, because low noise electronic amplifiers are not trivial to implement. In addition, the links' noise performance has to be addressed, which is often characterized by the noise figure (NF).

Analog links often require high dynamic range, high RF transfer ratio and low noise figure. These have been difficult to achieve with current approaches. In Section 1.2, we will review the current approaches in constructing analog optical links and some of the techniques studied in improving their performance. Section 1.3 will outline the background of the advanced technique we proposed to studies in this project while a scope of this project is contained in Section 1.4.

1.2 Previous Work and Current Approaches

The most straightforward modulation technique is amplitude modulation (AM). AM can be used in direct detection analog optical systems. To date, the two most popular AM direct detection links are: direct modulation of semiconductor lasers and

external modulation of lasers using lithum niobate integrated optical Mach Zehnder modulators.

1.3 Advanced Techniques

1.3.1 Coherent Detection

The use of coherent detection allows considerable flexibility in the implementation of analog optical systems. Coherent systems can utilize alternative modulation formats such as phase and frequency modulation, which can lead to improved dynamic range and noise figure. In WDM systems, coherent detection offers the additional advantage of excellent frequency selectivity. Because coherent analog systems preserve optical phase information, fiber dispersion effects can be compensated in their receivers. This may be important for long, high bandwidth links.

1.3.2 Optical Amplification

Optical amplifiers have been heavily deployed in the field of long-distance digital telecommunications. In such applications, optical amplification is used to overcome propagation losses incurred over long spans of fiber. The motivation for optical amplifiers in analog links is somewhat different than for long-distance digital links. Many (but not all) analog link applications involve relatively modest optical losses between the transmitter and receiver. Despite this fact, there is still substantial motivation to investigate optical amplifiers for our application, including:

- improving the RF power transfer ratio. Because low noise high bandwidth electronic amplifiers are not trivial to implement, this is an important contribution to the link performance;
- compensating for optical power splitting losses in analog distribution systems. There are various applications in which it is desirable to distribute one or more microwave signals to multiple signal processors. In these applications, the signal power may be split many ways, and the gain provided by optical amplifiers can compensate for this splitting loss.

1.3.3 Angle Modulation

Angle modulation can potentially improve analog optical link performance as compared to AM in exchange for wider bandwidth. However, there are several difficulties which must be overcome for wideband angle modulated links to become feasible alternatives for conventional AM links. Some of these include:

- Nonuniform laser FM response and nonlinear frequency versus current characteristics in directly modulated FM systems.
- Construction of microwave discriminators which are highly linear over a frequency range of several to upwards of 10 GHz.
- Development of linewidth-insensitive angle modulated links which enable the use of rugged, compact, and efficient conventional semiconductor lasers without linewidth-induced performance degradation.

There have been few researchers who have attempted to conquer the problems of angle modulated analog optical links. Plessey et al., during a recent Air Force funded project, investigated linewidth-insensitive separate-fiber reference transport configurations. These types of reference transport links, though feasible for digital phase-shift-keying systems, are not feasible for angle modulated analog links, as is explained in Chapter 9 of this report. Seeds et al. [2] built a directly modulated coherent FM link but had difficulties with a nonoptimal receiver. Neither of these groups provided a comprehensive theoretical analysis of angle modulated analog optical links or developed an angle modulated analog link which is potentially linewidth-insensitive.

1.3.4 Technical Challenges

There exist a variety of difficulties in implementing these techniques. Semiconductor lasers are attractive for use in the transmitter and local oscillator in coherent optical links due to their small size and weight, high electrical-to-optical power conversion efficiency, and rugged construction. However, semiconductor lasers have wide optical linewidths, which can cause substantial degradation of the performance of coherent analog links; this phenomenon represents a major obstacle to the practical application of coherent techniques to analog optical links and to the use of angle modulation in analog optical links.

As with other amplifiers, optical amplifiers add noise to the amplified signal. Broadband spontaneous emission noise is generated in the course of amplification and can result in substantial degradation in performance.

1.4 Scope of the Project

The objective of this project is to unite the potential of coherent analog optical techniques with the practical advantages of semiconductor lasers. Our goals have been to produce:

- A general theory predicting the performance of coherent optical analog links utilizing wide linewidth semiconductor lasers. This theory will apply to systems utilizing a wide variety of modulation formats and demodulation techniques.
- Models of critical components appropriate for our analysis, including semiconductor lasers, optical amplitude and phase modulators, optical amplifiers, and microwave rectifiers and delay-line discriminators.
- Linewidth-insensitive system designs.
- Demonstrations of linewidth-insensitive links.
- Characterization and evaluation of experimental linewidth-insensitive links.
- Suggestions of directions for future work leading to more robust, higher performance fielded systems.

During this project, we have analyzed the performance of analog optical links as quantified by spurious-free dynamic range (SFDR), RF power transfer ratio, and noise figure, and compare their performance to that of conventional direct detection links. The advanced links which we have considered are coherent links, optically amplified links, angle modulated links, and combinations of the above. To show the validity of our analyses, we have also constructed several of the above advanced links. We have measured the performance of these experimental implementations as quantified by the above performance measures. We have met the project objectives in our investigation of coherent and angle modulated links and have exceeded them in our investigation of optically amplified links.

1.5 References

[1] C. E. Cox, G. E. Betts, and L. M. Johnson, "An analytic and experimental comparison of direct and external modulation in analog fiber-optic links," IEEE Trans. MTT, vol. 38, no. 5, 1990.

[2] A. J. Seeds and B. Cai, "Transparent Optical Links Using Optical FM," presented at LEOS Summer Topicals '93 on Optical Microwave Interactions, Santa Barbara, CA, July 1993, pp. 69-70.

Chapter Two

Definitions and Background

In this chapter, we review some background material that will be used extensively in the succeeding chapters. Section 2.1 presents the analog link performance measures: dynamic range, link gain and noise figure. Section 2.2 gives a theoretical analysis of the direct detection link since this link will be used as the "baseline" system from which other links suggested and studied will be compared to.

2.1 Analog Link Performance Measures

In this section, the three most widely used performance measures for analog links are defined and estimates of the theoretical performance of the coherent AM link are presented. This section starts with a discussion of the spurious-free dynamic range, followed by the link gain, and then the noise figure.

2.1.1 Dynamic Range

The dynamic range (DR) is defined as the ratio of the maximum input RF power $P_{in,max}$ to the minimum input RF power $P_{in,min}$ that can be carried by the fiber optic link [1]:

$$DR = 10\log\left(\frac{P_{in,\max}}{P_{in,\min}}\right) \tag{2.1}$$

Since the square of the modulation index m is proportional to the input RF power, Eq. (2.1) can be rewritten as follows:

$$DR = 10\log\left(\frac{m_{\max}^2}{m_{\min}^2}\right) \tag{2.2}$$

where m_{min} and m_{max} are the minimum and maximum modulation indices that the system can handle, respectively. m_{min} is the modulation index of the input signal that results in equal signal and noise powers (SNR = 1). For systems with inherent nonlinearities in its components (in other words, for all practical systems), the maximum modulation index is limited by third order intermodulation distortions (IMD). To evaluate the relative magnitude of the IMDs, two equal amplitude signals at frequencies ω_1 and ω_2 are transmitted through the system and the amplitude of the third order terms at frequencies $2\omega_1 - \omega_2$ and $2\omega_2 - \omega_1$ are measured. The third order IMDs increase as the cube of the input voltage while the useful signal grows linearly. This behavior is illustrated in Fig. 2-1(a). m_{max} is the value of m that makes the IMD power equal to the noise power:

$$\left\langle i_{IMD}^2 \right\rangle \Big|_{m_{max}} = \left\langle i_{noise}^2 \right\rangle \Big|_{m_{max}} \tag{2.3}$$

where i_{IMD} and i_{noise} are the third order distortion and noise currents at the output of the receiver, respectively. When m_{max} is defined as per Eq. (2.3), the ratio defined by Eq. (2.2) is called the spurious-free dynamic range (SFDR):

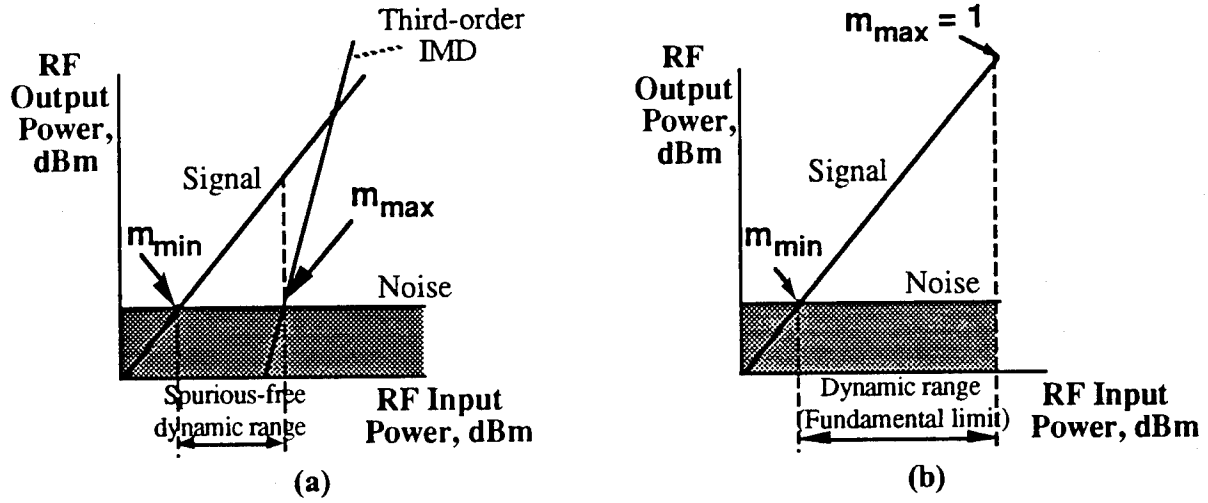

Fig. 2-1. Definitions of the dynamic range: (a) The spurious-free dynamic range (SFDR); (b) The fundamental limit of the dynamic range.

$$SFDR = 10\log\left[\frac{m^2\big|_{IMD=noise}}{m^2\big|_{signal=noise}}\right] \tag{2.4}$$

In the absence of any nonlinearities m_{max} equals one and Eq. (2.2) becomes

$$FLDR = 10\log\left(\frac{1}{m_{\min}^2}\right) \tag{2.5}$$

where FL*DR* is the fundamental limit of the dynamic range (FLDR) illustrated in Fig. 2-1(b). Clearly, SFDR can never exceed FLDR.

2.1.2 Link Gain

The **RF power transfer ratio,** or **link gain,** G of the link is defined as the ratio of the RF power at the link output, S_o to the RF power at the link input, S_i:

$$G = \frac{S_o}{S_i} \tag{2.6}$$

2.1.3 Noise Figure

Noise figure measures the degradation in the signal-to-noise ratio (SNR) between the input and output of a link and is defined as:

$$F = \frac{S_i/N_i}{S_o/N_o} = \frac{N_o}{GN_i} \tag{2.7}$$

where S_i and N_i are the input signal and noise powers; S_o and N_o are the output signal and noise powers; and G is the link gain discussed in the previous section. By definition, the input noise power is the noise power from a matched resistor, $N_i = kTB$, where k is Boltzmann's constant; T is the resistor temperature; and B is the signal bandwidth. The output noise power can be expressed by:

$$N_o = GN_i + \eta B \tag{2.8}$$

where hB is the additive noise introduced by the link. Substituting $N_i = kTB$, we can express the noise figure as:

$$F = 1 + \frac{\eta}{GkT} \tag{2.9}$$

2.2 Theoretical Analysis of the Direct Detection Link

In this section, we review direct detection links. The results of this section will serve as a basis for comparison with the coherent links presented in the succeeding chapters.

The block diagram of an externally modulated direct detection system is shown in Fig. 2-2. The light from the transmitting laser is modulated by an external Mach-Zehnder modulator.

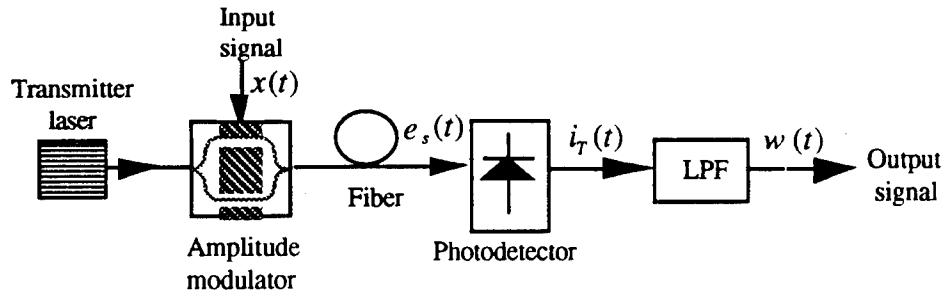

Fig. 2-2. Block diagram of a direct detection receiver.

It can be shown that the received optical field $e_S(t)$ is given by:

$$e_s(t) = \sqrt{\frac{P_s}{2}}\left\{\exp\left(j\left[\omega_s t + \phi_{ns}(t) + m \cdot x(t)\right]\right) + \exp\left(j\left[\omega_s t + \phi_{ns}(t) + \frac{\pi}{2}\right]\right)\right\} \tag{2.10}$$

where $x(t)$ is the input RF voltage (normalized to unity amplitude); P_S is the received optical power; ω_S and $\phi_{nS}(t)$ are the optical carrier frequency and phase noise of the laser transmitter, respectively; and m is the modulation index defined by the following expression:

$$m = \frac{\pi}{2}\frac{V_p}{V_\pi} \tag{2.11}$$

where Vp is the peak amplitude of the applied RF voltage and V_p is the half-wave voltage of the modulator. The output current of the photodetector is:

$$i_T(t) = R|e_s(t)|^2 + n(t) = RP_s[1 + \sin(m \cdot x(t))] + n(t) \tag{2.12}$$

where R is the photodetector responsivity and $n(t)$ is the additive white Gaussian noise at the output of the photodetector consisting of the shot and thermal noises. The single-sided PSD of $n(t)$ is given by:

$$S_n(f) = \eta = \eta_{sh} + \eta_{th} = 2eRP_s + \frac{4kT}{r}, \qquad \text{for } 0 < f < \infty \tag{2.13}$$

where h_{sh} and h_{th} are the PSD's of the shot noise and thermal noise, respectively, e is the electron charge, k is the Boltzmann's constant, T is the receiver noise temperature, and r is the input resistance of the amplifier.

To determine the fundamental limit of the performance of this system, we assume for a moment that the external modulator is replaced by an ideal modulator having no nonlinear distortions in the region of operation. Then $\sin(mx(t)) = mx(t)$ and Eq. (2.12) becomes:

Fundamental limit: $$i_T(t) = RP_s[1 + m \cdot x(t)] + n(t) \tag{2.14}$$

The SFDR is evaluated by assuming a nonlinear external modulator with the third order terms being the dominant IMDs. In this case,

$$\sin[m \cdot x(t)] \approx m \cdot x(t) - \frac{[m \cdot x(t)]^3}{3} \tag{2.15}$$

and Eq. (2.12) becomes

$$i_T(t) = RP_s\left\{1 + m \cdot x(t) - \frac{[m \cdot x(t)]^3}{3}\right\} + n(t) \tag{2.16}$$

Similar to [2] and [3], we assume the low pass filter to have an impulse response of

$$h_L(t) = \begin{cases} 2B, & \text{for } t \in \left[0, \frac{1}{2B}\right] \\ 0, & \text{for } t \notin \left[0, \frac{1}{2B}\right] \end{cases} \tag{2.17}$$

where B is the noise equivalent bandwidth. The output signal $w(t)$ is then expressed as:

$$w(t) = h_L(t) \cdot i_T(t) \tag{2.18}$$

Substituting Eqs. (2.14) and (2.17) into Eq. (2.18) and evaluating the total received power, the SNR and FLDR are found to be:

$$SNR = \frac{1/2 \cdot m^2 R^2 P_s^2 \cdot \text{sinc}^2\left(\frac{\omega_m}{4\pi B}\right)}{\eta B} \tag{2.19}$$

$$FLDR = 10 \log\left[\frac{R^2 P_s^2 \cdot \text{sinc}^2\left(\frac{\omega_m}{4\pi B}\right)}{2\eta B}\right] \tag{2.20}$$

where η is the PSD of the additive noise given by Eq. (2.13), and ω_m is the frequency (or center frequency of the two-tone signal) of the transmitted RF signal. Similarly, using (2.16) in (2.18) and evaluating the total output power, the SFDR is found to be:

$$SFDR = 10 \log\left[4\left(\frac{R^2 P_s^2 \cdot \text{sinc}^2\left(\frac{\omega_m}{4\pi B}\right)}{\eta B}\right)^{2/3}\right] \tag{2.21}$$

The numerators of Eqs. (2.19), (2.20), and (2.21) represent the signal while their denominators represent the noise.

Using (2.6) and following the procedure outlined in [4, 5], the gain for the direct detection link, G_{dd}, is given by:

$$G_{dd} = \left(\frac{\pi R_s R P_s}{V_\pi} \right)^2 \tag{2.22}$$

while using Eq. (2.9), the noise figure is:

$$F_{dd} = 1 + \frac{\eta_{dd}}{G_{dd} kT} \tag{2.23}$$

where η_{dd} and G_{dd} are given by Eqs. (2.13) and (2.22), respectively.

2.3 References

[1] W. E. Stephens and T. R. Joseph, "System characteristics of direct modulated and externally modulated RF fiber-optic links", *J. Lightwave Technol.*, vol. LT-5, no. 3, March 1987.

[2] J. R. Barry, E. Lee, "Performance of coherent optical receivers", *Proceedings of the IEEE*, vol. 78, no. 8, August 1990.

[3] L. G. Kazovsky, P. Meissner, and E. Patzak, "ASK multiport optical homodyne receivers", *J. Lightwave Technol.*, vol. LT-5, no.2, pp. 770-791, June 1987.

[4] R. Simons, "Microwave Fiber Optic Links," *Optical Control of Microwave Devices*, chap. 5, Boston: Artech House, 1990, pp. 121-155.

[5] C. H. Cox, "Gain and Noise Figure in Analogue Fiber-Optic Links," *IEE Proceedings - J*, vol. 139, no. 4, pp. 238-242, August 1992.

PART 2:

AMPLITUDE MODULATED COHERENT AND OPTICALLY AMPLIFIED LINKS

Chapter Three

Theory of Coherent AM Links

In Chapter 1, we have seen that the laser phase noise associated with the wide linewidth of semiconductor lasers can cause substantial performance degradation in coherent analog links. This phenomenon represents a major obstacle to the application of coherent techniques to analog optical links.

Conventional synchronous receivers requires phase-locking between the transmitter and the LO lasers. The phase-locking is difficult to achieve and leads to extremely stringent requirements on the laser linewidth. Asynchronous receivers using WIRNA (WIdeband-Rectifier-NArrowband filter) processing have been shown to be effective in achieving laser linewidth insensitive performance in ASK (amplitude shifted keying) homodyne and heterodyne digital systems [1], [2]. Since the phase information is discarded in the WIRNA receiver, it works effectively with amplitude modulation.

In this chapter, the analog version of the ASK-WIRNA homodyne and heterodyne digital systems are analyzed. In Section 3.1, a multiport homodyne WIRNA link is studied while Section 3.2 investigates the performance of a heterodyne WIRNA link. Section 3.3 examines the practical issues encountered in the implementation of these links.

3.1 Homodyne AM-WIRNA Links

In homodyne systems, the frequency of the incoming signal and the LO are the same. Since the electrical output of the photodetector is a baseband signal, large bandwidth photodetectors are not required. Also, baseband processing can avoid degradation due to overlapping of the signal spectrum with the noise peak of semiconductor lasers.

In this section, we discuss three types of homodyne WIRNA links: (a) a 2-port homodyne link, (b) a K-port homodyne link and (c) a 2K-port homodyne link (for K>1). We show that the 2-port homodyne link suffers from degradation caused by baseband processing, while the 2K-port link obtains the best performance, although the structure is complicated in practice.

3.1.1 2-Port Homodyne Link Description

The block diagram of an externally modulated coherent AM link using an optical 90° hybrid phase diversity WIRNA homodyne receiver is shown in Fig. 3-1. The optical signal from the transmitter laser is modulated by an electro-optic modulator. The optical frequency of the local oscillator is same as that of the optical signal. The optical signal and the local oscillator output are combined by an optical 90° hybrid. The polarization state of the received optical signal is tracked using a polarization controller and a feedback control technique is used to match the polarization state of $E_{LO}(t)$ with $E_s(t)$. In addition, an automatic frequency control (AFC) loop is used to keep the LO laser frequency equal to the laser frequency of the transmitter. Each of the two outputs of the optical 90° hybrid is sent to a photodetector and then through a DC block to a wideband lowpass filter. Then, using square-law detectors, each signal is multiplied with itself. The two output signals are combined at this point, and the phase noise terms are canceled due to the phase difference produced by the optical 90° hybrid. Finally, the combined signal passes through a DC block and a narrowband lowpass filter.

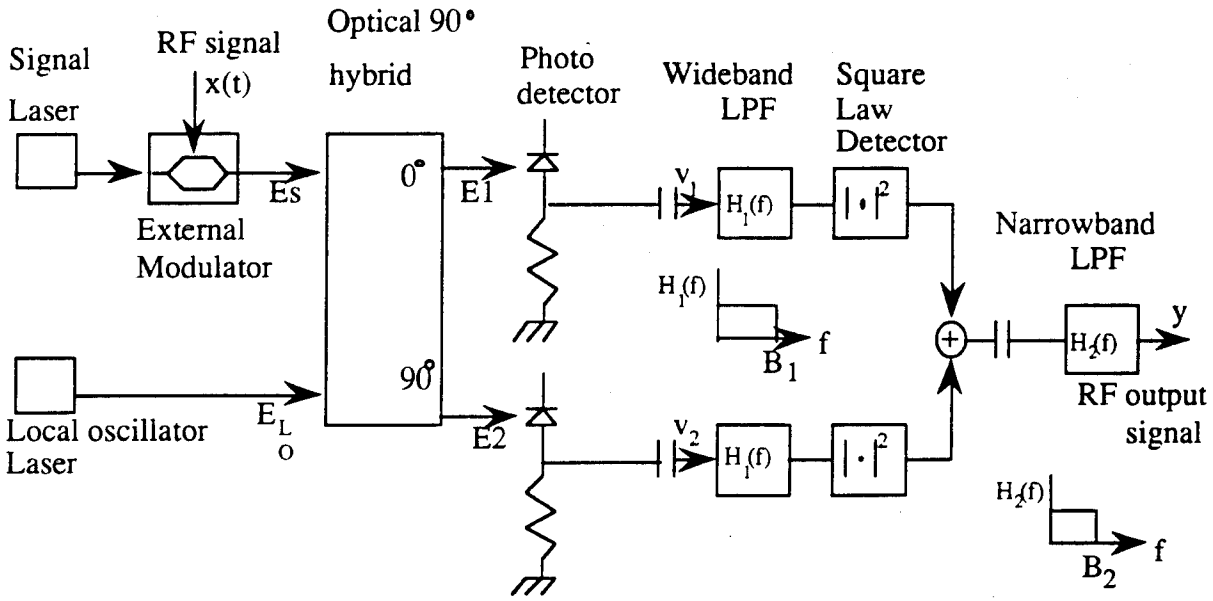

Fig. 3-1. Block diagram of the homodyne AM-WIRNA link.

Table 3-1. Definition of the variables

E_S , E_{LO}	Phasor of the optical signal and local oscillator
E_1, E_2	Output phasor of the optical hybrid port 1 and port 2
ω_S, ω_{LO}	Optical signal and local oscillator frequency
φ_S, φ_{LO}	Phase noise of the optical signal and local oscillator
$f(t)$	Combined linewidth of the signal and the local oscillator lasers
m	Modulation index to the external modulator
$x(t)$	Normalized RF input signal to the modulator
P_S	Received optical power
P_{LO}	Local oscillator optical power
L	Total loss of the optical hybrid from an input port to an output port
A	=RL; coefficient of the signal amplitude for homodyne links
C	$=R\sqrt{2P_sP_{LO}}$; coefficient of the signal amplitude for homodyne links
B_1	Bandwidth of the lowpass filter (first stage: wide bandwidth)
B_2	Bandwidth of the lowpass filter (last stage: narrow bandwidth)

3.1.2 System Evaluation

The light from the transmitter laser is modulated by an external Mach-Zehnder modulator. To accomplish quasi-linear modulation, the modulator is biased at the half power point; the output optical power of the modulator can be expressed as:

$$E_s(t)=\sqrt{\frac{P_s}{2}\left[1+r_s(t)\right]}\left\{\exp\left[j\left(\omega_s t+\phi_s(t)+m\cdot x(t)\right)\right]+\exp\left[j\left(\omega_s t+\phi_s(t)+\pi/2\right)\right]\right\} \quad (3.1)$$

The output of the LO laser has a complex amplitude $E_{LO}(t)$ given by:

$$E_{LO}(t)=\sqrt{P_{LO}\left[1+r_{LO}(t)\right]}\cdot\exp\left\{j\left[\omega_{LO}t+\phi_{LO}(t)\right]\right\} \quad (3.2)$$

After the photodetector, the signal current is as follows:

$$i(t)=s(t)+n(t) \quad (3.3)$$

where $s(t)$ is the IF signal and $n(t)$ is the additive noise process. The receiver performance is affected by noise in two ways: (a) phase noise and (b) additive noise. A description of

the noise processes and their properties can be found in Appendix A. The output current of the photodetectors are given by:

$$i_1(t) = A\left(P_s \sin x(t) + \sqrt{2P_s P_{LO}}\left\{\cos[x(t)+\phi(t)] - \sin\phi(t)\right\}\right) + n_1(t) \qquad (3.4)$$

$$i_2(t) = A\left(P_s \sin x(t) + \sqrt{2P_s P_{LO}}\left\{\sin[x(t)+\phi(t)] + \cos\phi(t)\right\}\right) + n_2(t) \qquad (3.5)$$

where $f(t)$ is combined phase noise of the signal laser and the local oscillator laser given by $f(t)=f_S(t)-f_{LO}(t)$, and $n_1(t)$ and $n_2(t)$ are two independent additive white Gaussian noise processes with power spectral densities $\eta_1 = \eta_2 = \eta = \eta_{th} + 2qRL(P_s + P_{LO})$. To evaluate the SNR of the system in Fig. 3-2, we assume a normalized sinusoidal RF input signal $x(t) = \cos(2\pi f_m t + \theta)$, where f_m is the signal frequency and q is the random initial phase uniformly distributed between 0 and 2p. The output of the link contains five terms:

(a) recovered signal with the power P_S;
(b) direct detection squared term P_{2HD} (second harmonic term);
(c) direct detection - phase noise product with the power $P_{direct\text{-}phase}$;
(d) signal-cross-white additive noise product with the power $P_{signal\text{-}noise}$;
(e) white additive noise squared term with the power $P_{white\text{-}white}$.

We assume that the bandwidth of the wideband lowpass filters is sufficiently large such that the amplitude noise to phase noise conversion is negligible. This filter helps to reduce the impact of the white additive noise [1].

Evaluating the power of each component, the output signal-to-noise ratio (SNR) can be expressed as:

$$SNR = \frac{P_{signal}}{P_{2HD} + P_{direct-phase} + P_{signal-white} + P_{white-white}}$$

$$= \frac{8A^4 P_s^2 P_{LO}^2 m^2}{\frac{1}{2}A^4 P_s^4 m^4 + 8A^4 P_s^3 P_{LO} m^2 (1-\Gamma_1) + 16A^2 P_s P_{LO} B_2 \eta (1-\Gamma_2) + 2\eta^2 B_2 (4B_1 - B_2)} \qquad (3.6)$$

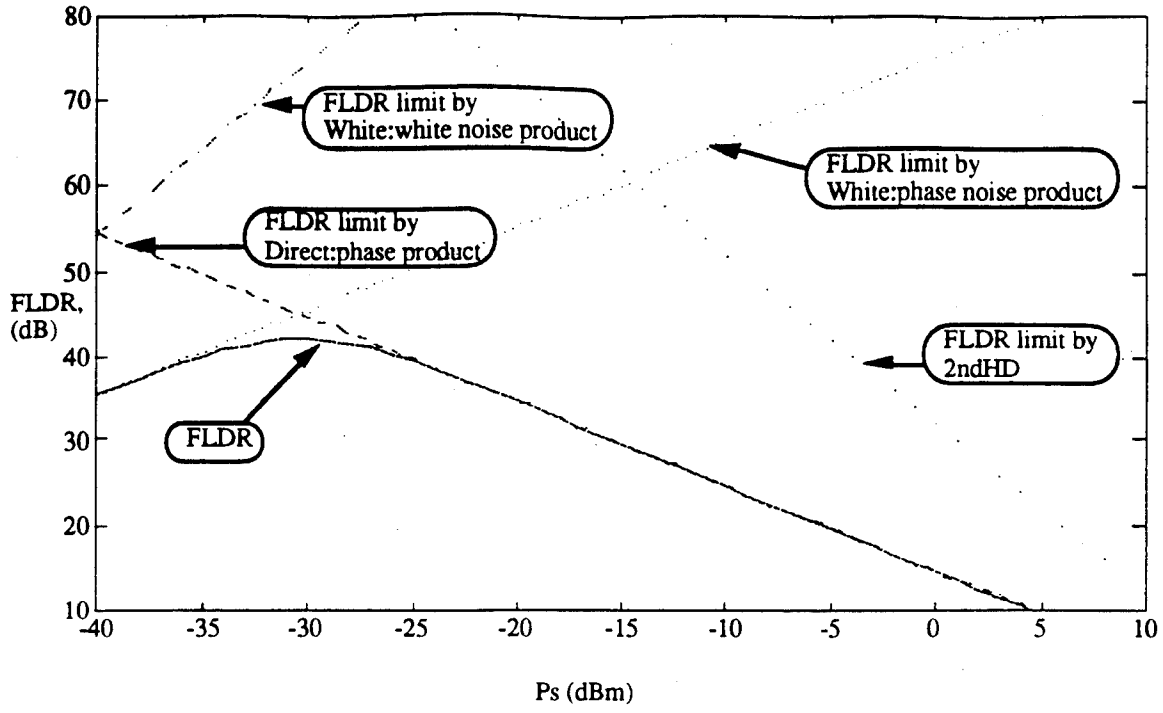

Fig. 3-2. FLDR of the 2-port homodyne AM-WIRNA receiver vs. received optical power.

where G_1 and G_2 expresses a portion of the noise power outside the signal bandwidth given by

$$\Gamma_1 = \begin{cases} \frac{1}{\pi}\tan^{-1}\frac{4\Delta\nu B_2}{4B_2^2 - \Delta\nu^2} & , \quad \text{if } \Delta\nu < 2B_2 \\ 1 - \frac{1}{\pi}\tan^{-1}\frac{4\Delta\nu B_2}{\Delta\nu^2 - 4B_2^2} & , \quad \text{if } \Delta\nu > 2B_2 \end{cases} \tag{3.7}$$

$$\Gamma_2 = \frac{\Delta\nu}{2\pi B_2}\ln\left(\frac{B_1 + B_2}{B_1 - B_2}\right) \tag{3.8}$$

$\Delta\nu$ is the total linewidth of the signal and local oscillator lasers and B_1 and B_2 are the wideband and narrowband filter bandwidth, respectively. From Eq. (3.6), the FLDR is obtained as:

$$FLDR = \frac{8A^4P_s^2P_{LO}^2}{\frac{1}{2}A^4P_s^4 + 8A^4P_s^3P_{LO}(1-\Gamma_1) + 16A^2P_sP_{LO}B_2\eta(1-\Gamma_2) + 2\eta^2B_2(4B_1 - B_2)} \tag{3.9}$$

Fig. 3-2 shows the dependency of the FLDR on the optical received power. For this graph, values of the parameters are chosen as B_1 = 1 GHz, B_2 = 6 MHz, $\Delta\nu$ = 20MHz, and P_{LO} = 10dBm. Inspection of the graph reveals that for high received optical power, the FLDR becomes worse. It is because of the noise term generated by the multiplication of the direct detection term and the phase noise term. From this graph, we conclude that the 2-port homodyne system cannot achieve high dynamic range.

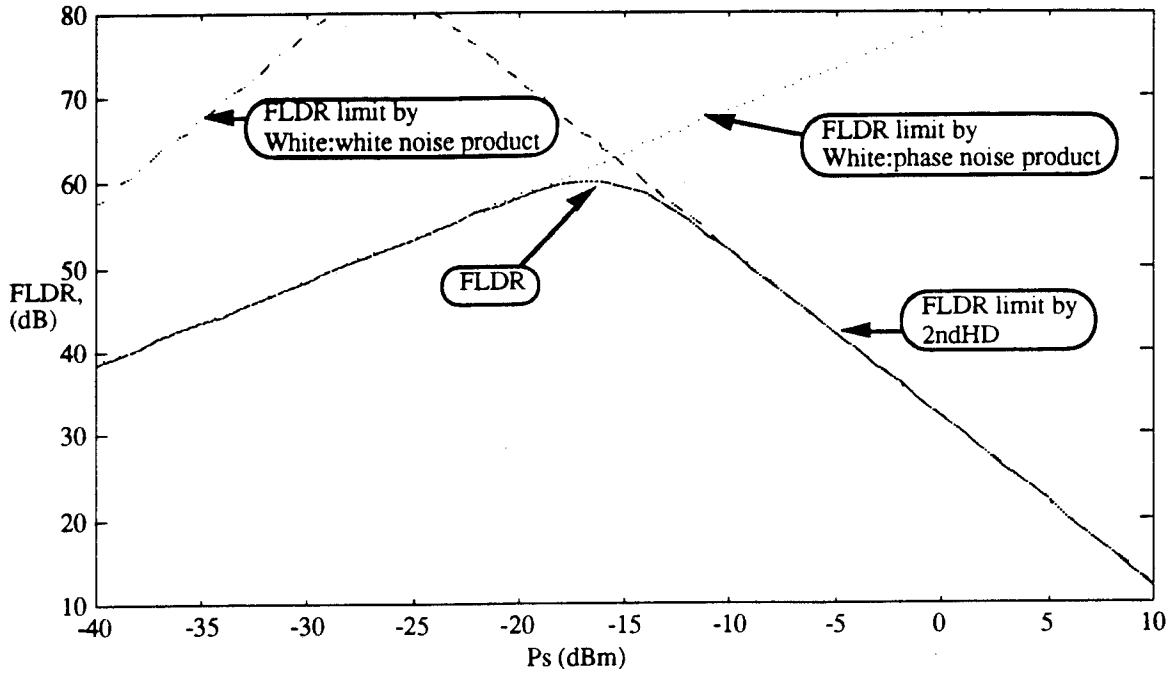

Fig. 3-3. FLDR of the multi-port homodyne AM WIRNA receiver vs. received optical power.

3.1.3 K-port Homodyne Link Description

To increase the dynamic range, a multi-port homodyne system can be used. In a K-port homodyne system, the $P_{direct\text{-}phase}$ noise term, which limits the performance in the 2-port homodyne system, is canceled because of the symmetry in the optical hybrid. The structure of this system is similar to the 2-port system, except it uses an K-port optical hybrid and K sets of receivers [1]. The resulting FLDR is

$$FLDR = \frac{P_{signal}}{P_{2HD} + P_{signal-white} + P_{white-white}} = \frac{2N^2A^4P_s^2P_{LO}^2}{\frac{N^2}{8}A^4P_s^4 + 8NA^2P_sP_{LO}B_2\eta(1-\Gamma_2) + N\eta^2B_2(4B_1 - B_2)} \quad (3.10)$$

Higher dynamic range is obtained by this structure than the 2-port system. However, as seen in Fig. 3-3, a limit still exists for high optical signal input. This limit stems from the noise term generated by the squaring operation of the direct detection term, i.e., second harmonic noise.

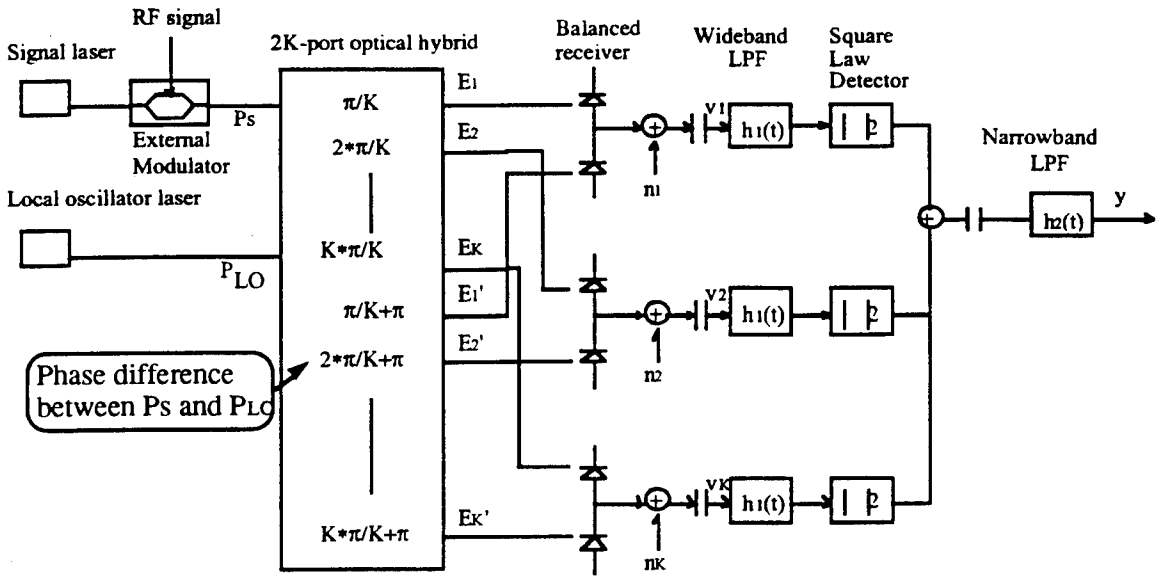

Fig. 3-4. block diagram of 2K-port homodyne receiver.

3.1.4 2K-port Homodyne Link Description

For further improvement of the link, a balanced receiver structure can be introduced. The block diagram of a 2K-port homodyne link is shown in Fig. 3-4. In this receiver, a balanced receiver structure is applied, as well as a 2K-port optical hybrid. The optical signal and the local oscillator output are combined by a 2K-port optical hybrid (2K means the number of the output ports is even number, but not two). We choose the *n*th and *(n+K)*th outputs as a pair of outputs. Each of the paired outputs of the 2K-port optical hybrid is sent to a balanced receiver. Since balanced receivers reject the common mode signals, the direct detection term and the common mode noises, such as the LO

RIN, are canceled at this point. Each balanced receiver output is sent through a DC block and a wideband lowpass filter to a square-law detector. All of the output signals are combined at this point, and the phase noise terms are canceled due to the phase difference produced by the multiport optical hybrid. Finally, the combined signal passes through a DC block and a narrowband lowpass filter. In this way, we make use of the WIRNA structure, balanced receivers and a phase diversity receiving method.

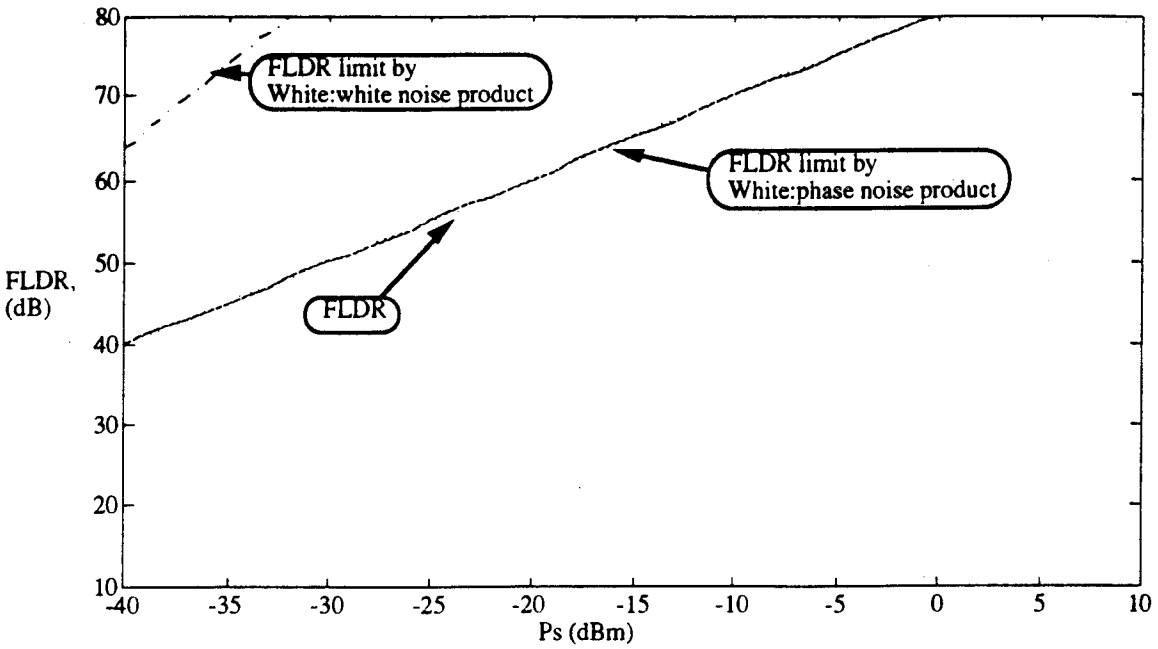

Fig. 3-5. FLDR of the 2-port homodyne AM WIRNA receiver vs. received optical power.

By similar analysis, we obtained the FLDR of this system as:

$$FLDR = \frac{P_{signal}}{P_{signal-white} + P_{white-white}} = \frac{8(2K)^2 A^4 P_s^2 P_{LO}^2}{16(2K)A^2 P_s P_{LO} B_2 \eta_3 (1-\Gamma_2) + \frac{2K}{2}\eta_3^2 B_2 (4B_1 - B_2)} \tag{3.11}$$

where

$$\eta_3 = \eta_{th} + 4qRL(P_s + P_{LO}) \tag{3.12}$$

By this double canceling technique, noise terms with large *Ps* dependency are eliminated. Fig. 3-5 shows that there is no dependency of the FLDR on the optical received power. This system can achieve good performance.

3.2 Heterodyne WIRNA Link

3.2.1 Link Description

The block diagram of an externally modulated coherent AM-WIRNA link is shown in Fig. 3-6. The link consists of an optical transmitter, fiber and a coherent optical receiver. The optical transmitter is the same as the one used in a conventional direct detection receiver. The RF input signal modulates the optical carrier using an external modulator. During coherent detection, the received optical signal is mixed with the output of the local oscillator (LO) laser before it is incident on the photodetector. The polarization state of the receiver optical signal is tracked using a polarization controller, and a feedback control technique is used to match the polarization state of $E_{LO}(t)$ with $E_s(t)$. In addition, an automatic frequency control (AFC) loop is used to maintain a fixed intermediate frequency (IF) by tuning the LO laser frequency. In the receiver, the output current of the balanced receiver is an IF signal; the RF signal is recovered by a square-law detector (SLD) and a lowpass filter (LPF). A bandpass filter (BPF) is used to filter excess additive noise before squaring.

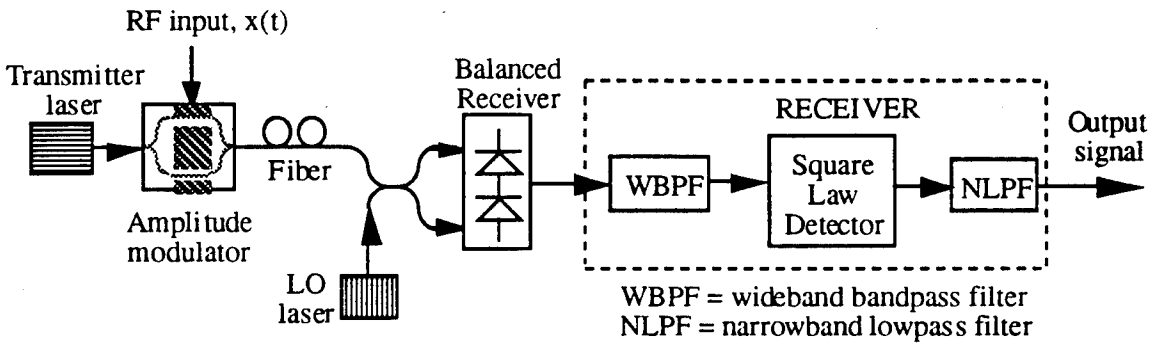

Fig. 3-6. Block diagram of the heterodyne AM-WIRNA link.

3.2.2 System Evaluation

In this section, we analyze the coherent AM link shown in Fig. 3-6. The results of this section will serve as a basis for comparison of the coherent AM link with the

direct detection link. The definitions of the variables used in this analysis are listed in Table 3-1. The output signal of the balanced receiver is an IF signal *s(t)* and can be expressed as:

$$\begin{aligned} s(t) &= C\left\{\cos\left[\omega_{IF}t + \phi(t) + m \cdot x(t)\right] - \sin\left[\omega_{IF}t + \phi(t)\right]\right\} \\ &= \text{Real}\left\{\hat{s}(t) \cdot e^{j\omega_{IF}t}\right\} \end{aligned} \tag{3.13}$$

where $\hat{s}(t) \equiv Ce^{j\phi(t)}\left[e^{jm \cdot x(t)} + e^{j\pi/2}\right]$ is the complex envelope of the IF signal. The IF signal is processed by the SLD, whose output voltage is:

$$\left|\hat{s}(t)\right|^2 \equiv 2C^2\left\{1 + \sin\left[m \cdot x(t)\right]\right\} \tag{3.14}$$

Assuming that the modulation index is small (m«1),

$$\left|\hat{s}(t)\right|^2 \approx 2C^2\left[1 + m \cdot x(t)\right] \tag{3.15}$$

Thus, ideally, in the absence of additive noise, the transmitted signal can be recovered upon the removal of the DC term in Eq. (3.15).

However, as a result of the spectral broadening due to the phase noise, the selection of the IF bandwidth is critical to the system performance. If the bandwidth of the BPF is too narrow, some of the signal power will be lost, and the laser phase noise will be converted to intensity noise at the output of the SLD; if it is too wide, more additive noise will be collected [3].

A single test tone is used to study the degradation of the link performance due to the phase noise. Consider a sinusoidal RF input signal $x(t) = \cos\left(2\pi f_m t + \theta\right)$, where f_m is the signal frequency and q is the random initial phase uniformly distributed between 0 and 2p. For m«1, the output signal-to-noise ratio (SNR) can be expressed as:

$$\begin{aligned} SNR &\approx \frac{P_{signal}}{P_{signal-white} + P_{white-white}} \\ &\approx \frac{2m^2C^4}{8C^2\eta B_2\left(1 + \frac{m^2}{4}\right)\left[1 + \frac{2}{\pi}\tan^{-1}\left(\frac{2B_1}{\Delta\nu}\right)\right] + 4\eta^2 B_2\left(4B_1 - B_2\right)} \end{aligned} \tag{3.16}$$

The first term in the denominator of Eq. (3.8) is due to the beat between the signal and the additive noise. The second term is due to the squared additive noise.

3.2.3 Link Dynamic Range

To evaluate the FLDR, we use a single-tone signal as the RF input. From Eq. (3.16), the FLDR for a coherent heterodyne AM link can be expressed as:

$$FLDR \approx \frac{2C^4}{16C^2\eta B_2 + 4\eta^2 B_2(4B_1 - B_2)} \tag{3.20}$$

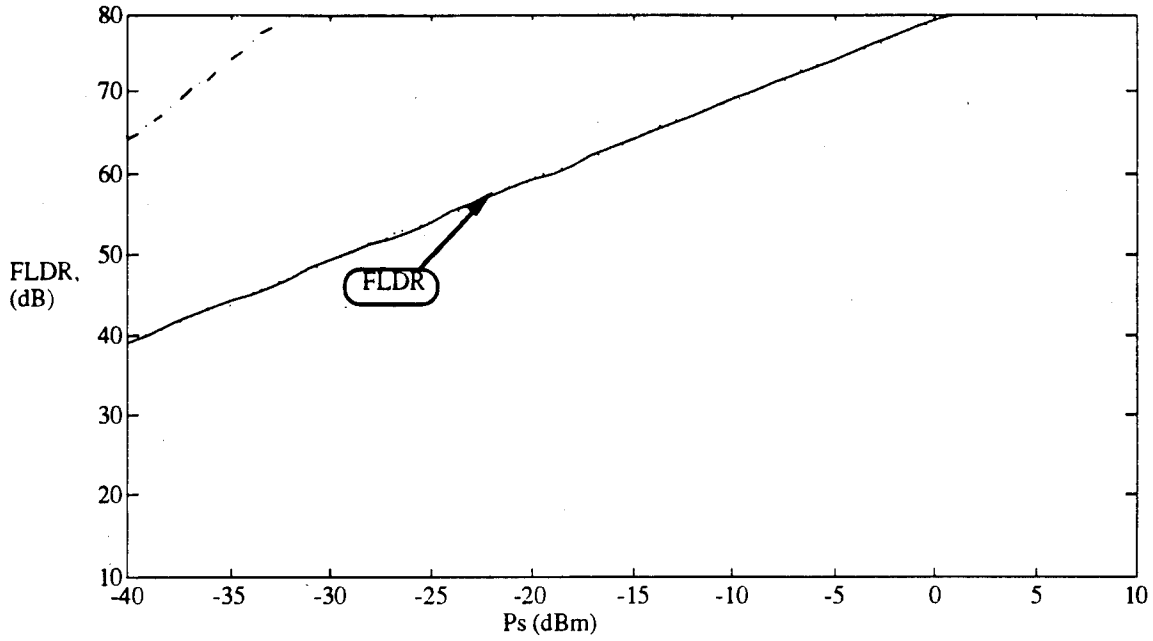

Fig. 3-7. FLDR of the heterodyne AM WIRNA receiver vs. received optical power.

3.3 Comparison between the techniques

To summarize, we explain the difference in the system performance intuitively in this section. Fig. 3-8 shows the comparison of the performance of each system for a typical values of the parameters, B_1 = 1 GHz, B_2 = 6 MHz, $\Delta\nu$ = 20 MHz, and P_{LO} = 10 dBm. In Fig. 3-9, the spectra before and after the square-law detector in the homodyne WIRNA systems are shown and compared with those in the heterodyne WIRNA system. In the heterodyne system, the direct detection term is outside the passband of the IF bandpass filter. Thus, it is rejected, and there is no $P_{direct\text{-}phase}$ term

at the receiver output; as the result, the SNR of heterodyne WIRNA systems is close to the $P_{signal\text{-}white}$-limited condition. Therefore, the larger the P_s, the larger the FLDR. In the 2-port homodyne system, the main noise term is caused by the multiplication of the direct detection signal and the phase noise. Since a homodyne system uses the same frequency region for the signal processing as that of the RF signal, it is impossible to remove this noise term. This noise term increases proportionally to P_s^3 and degrades the FLDR for large values of P_s. The achievable SNR is thus much smaller than that of the heterodyne system. To overcome this problem, in the 2K-port homodyne system, the balanced receivers are utilized to reject direct detection terms with their common mode rejection effect. The noise components contained in the 2K-port homodyne system are effectively identical to those in heterodyne system. Thus the 2K-port homodyne system has very similar performance to the heterodyne system. Note that in the heterodyne system the bandwidth of IF filter should be twice as much as that in the homodyne system. This leads to larger noise power. But it affects only the white:white noise product, which is not usually the dominant noise term. Therefore, the heterodyne system can achieve similar performance with simpler structure despite the larger IF bandwidth required.

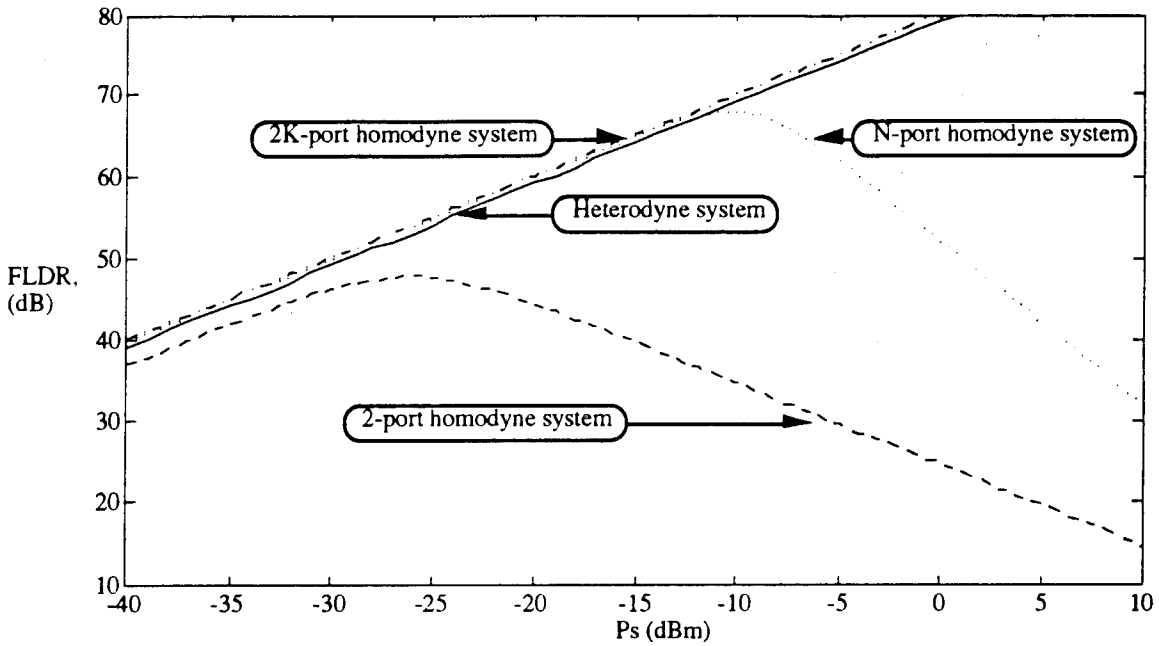

Fig. 3-8. Comparison of the homodyne and heterodyne system .

Table 3-2. Noise terms contained in each system.

Power	2-port homodyne	K-port homodyne	2K-port homodyne	Heterodyne
P_{signal}	$8\left(R^2L^2P_sP_{LO}\right)^2$	$2\left(KR^2L^2P_sP_{LO}\right)^2$	$8\left[(2K)R^2L^2P_sP_{LO}\right]^2$	$4(2R^2P_sP_{LO})^2$
P_{2HD}	$\frac{1}{2}\left(RLP_s\right)^4$	$\frac{1}{8}\left(KR^2L^2P_s^2\right)^2$	—	—
$P_{direct-phase}$	$8R^4L^4P_s^3P_{LO}\left(1-\Gamma_1\right)$	—	—	—
$P_{signal-white}$	$16R^2L^2P_sP_{LO}$ $\cdot B_2\eta\left(1-\Gamma_2\right)$	$8KR^2L^2P_sP_{LO}$ $\cdot B_2\eta\left(1-\Gamma_2\right)$	$16(2K)R^2L^2P_sP_{LO}$ $\cdot B_2\eta_3\left(1-\Gamma_2\right)$	$16(2R^2P_sP_{LO})\eta B_2$
$P_{white-white}$	$2\eta^2B_2\left(4B_1-B_2\right)$	$K\eta^2B_2\left(4B_1-B_2\right)$	$\frac{2K}{2}\eta_3^2B_2\left(4B_1-B_2\right)$	$4\eta^2B_2\left(4B_1-B_2\right)$

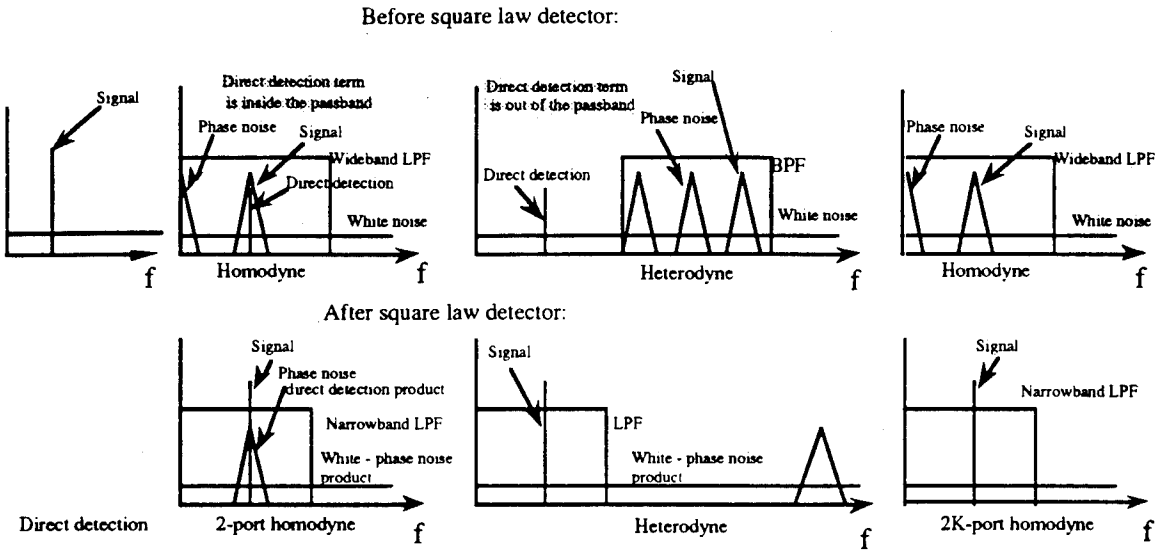

Fig. 3-9. Comparison of the homodyne and heterodyne system .

3.4 References

[1] L. G. Kazovsky, P. Meissner, and E. Patzak, "ASK multiport optical homodyne receivers," *J. Lightwave Technol.*, vol. LT-5, no. 3, pp. 770-791, June 1987.

[2] L. G. Kazovsky, and O. K. Tonguz, "ASK and FSK coherent lightwave systems: A simplified approximate analysis," *J. Lightwave Technol.*, vol. LT-8, no. 3, pp. 338-352, Mar. 1990.

[3] T. K. Fong, D. J. M. Sabido, R. F. Kalman and M. Tabara, and L. G. Kazovsky "Linewidth-Insensitive Coherent AM Optical Links: Design, Performance, and Potential Applications," *J. Lightwave Technol.*, vol. LT-12, no. 3, pp. 526-534, Mar. 1994.

[4] L. G. Kazovsky, "Impact of laser phase noise on optical heterodyne communication systems," *J. Optical Communicat.*, vol. 7, no. 2, pp. 66-78, 1986.

Chapter Four

Experimental Coherent AM Links

In Chapter 3 we concluded that it is possible to construct a linewidth-insensitive coherent AM-WIRNA* heterodyne link. In this chapter, we experimentally investigate the link performance of this AM-WIRNA heterodyne link, and compare these results to those for a similar direct detection link. For this and the succeeding chapters, when we write *coherent AM link*, we refer to the *coherent AM-WIRNA heterodyne link.*

This chapter is organized as follows: Section 4.1 contains a description of the various types of optical transmitter and receivers we constructed and investigated in this chapter. In this section, we also present the two-tone signal generator set-up. Section 4.2 deals with the comparison between directly and externally modulated coherent AM links to determine which optical transmitter would give the better performance for the coherent AM-WIRNA system. The better link would then be used for further investigations into the properties of coherent AM links. The theoretical analyses of the link performance measures -- the spurious-free dynamic range, link gain and noise figure -- are discussed in Section 4.3. Section 4.4 demonstrates phase noise cancellation by the coherent AM-WIRNA heterodyne link The impact of system parameters such as linewidth, IF bandwidth, laser relative intensity noise (RIN), received signal power and laser local oscillator (LO) power is discussed in Section 4.5. In Section 4.6 we present the link gain and noise figure, and in Section 4.7 the link loss measurements of both coherent AM and direct detection links are discussed. Section 4.8 contains the references while the appendix lists the devices used in our experimental investigations.

4.1 System Description

Shown in Fig. 4-1 is a conceptual block diagram of an analog optical link illustrating the flow of the RF signal from the optical transmitter through an optical attenuator used to vary the received optical power, several meters of optical fiber, and

* AM-WIRNA stands for Amplitude Modulation-WIdeband filter-Rectifier-NArrowband filter.

then finally to the optical receiver. In our experiments, angled optical connectors are used throughout the optical link to minimize reflections.

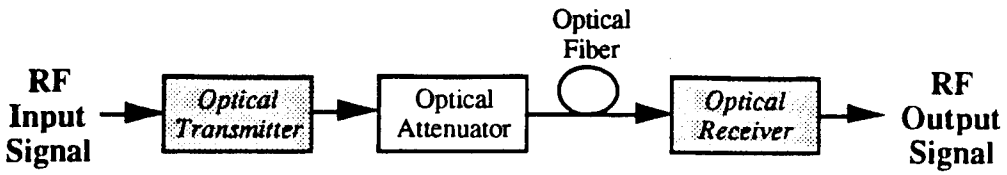

Fig. 4-1. Block diagram of an analog optical link.

There are two types of transmitters and receivers used in the experimental investigations, and these will be discussed in Sections 4.1.1 and 4.1.2. Section 4.1.3 will talk about the type and structure of RF input test signal used for our measurements.

4.1.1 Optical Transmitter

An optical transmitter can either be externally or directly modulated. In an externally modulated system, the input signal is applied to a separate device other than the laser source, while for the directly modulated system, the RF signal is applied directly to the laser source. In this section, we describe these two types of transmitters and in section 4.2, we compare their performances.

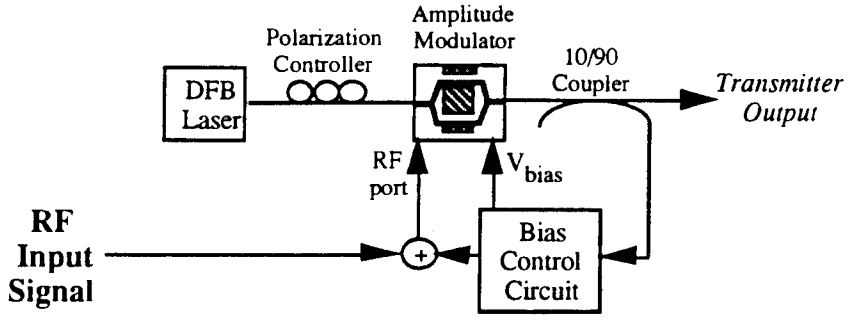

Fig. 4-2. Block diagram of the externally modulated optical transmitter.

4.1.1.1 Externally Modulated Optical Transmitter

The block diagram of the externally modulated optical transmitter which we constructed and investigated is shown in Fig. 4-2. The transmitter laser is a 1.55 μm distributed feedback (DFB) laser with a built-in optical isolator and a thermoelectric

cooler. The laser launches approximately 2 mW of optical power into the fiber and has a RIN of -153 dB/Hz to -140 dB/Hz, depending on the drive current and temperature.

The RF signal modulates the optical carrier via a $LiNbO_3$ Mach-Zehnder modulator. The modulator has an optical insertion loss of 7 dB and its π-voltage for 100% modulation is 16 V. A manual polarization controller is used to align the polarization of the laser light to that allowed by the electro-optic modulator (EOM).

The modulator is biased at its half-power point to eliminate even harmonics and even intermodulation products (operating at this bias point essentially adds an additional 3 dB loss in the optical link). It is important that the bias remain at this half power point; thus, we implemented an automatic bias control circuit in our set-up. We use the zeroing of the second-order distortion to implement a closed-loop control of the bias. This is done by applying a small, low frequency (10 kHz) pilot tone to the modulator. The level of the second harmonic of the pilot tone is then monitored at a detector and used in a feedback loop which controls the bias voltage.

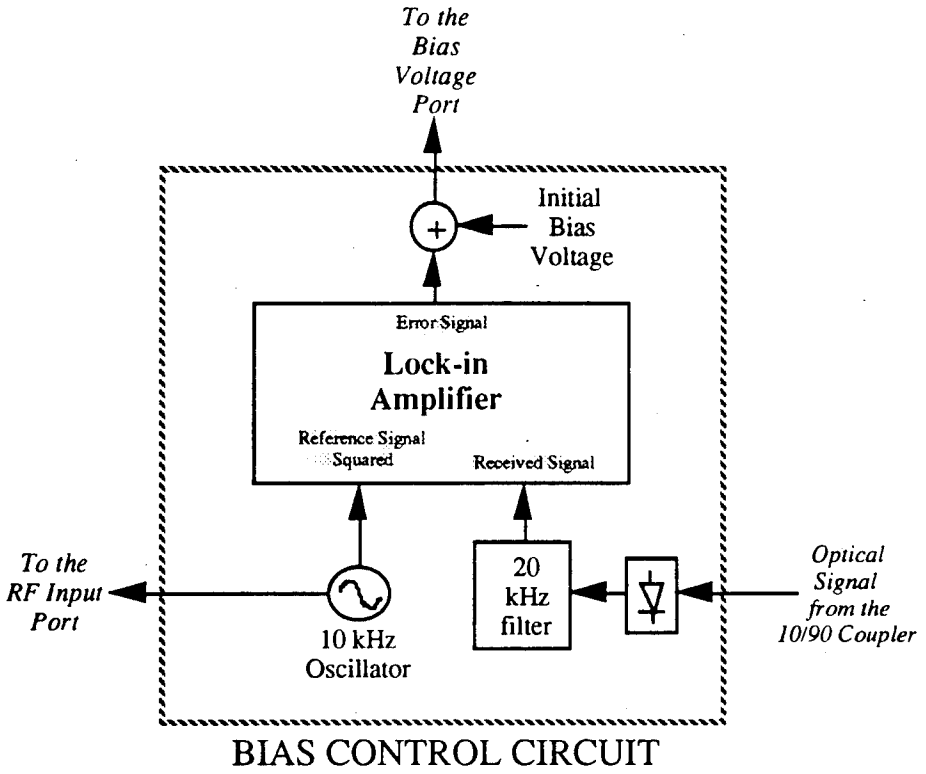

Fig. 4-3. Block diagram of the automatic bias control circuit for the externally modulated optical transmitter.

The detailed block diagram of the bias control circuit is shown in Fig. 4-3. The pilot tone is combined with the RF input signal and is applied to the RF port of the EOM.. A small portion of the optical output of the EOM is tapped with a 10/90 coupler; this portion is fed to a photodetector (with a 1 GHz frequency response) and a lock-in amplifier. The pilot signal is also used as the reference signal by the lock-in amplifier to determine the appropriate bias voltage error. This error voltage from the lock-in amplifier is then added to the original bias voltage and is fed into the bias voltage port of the EOM.

Only a small portion of the optical output of the modulator is used for the bias control circuitry. Most of the optical signal is sent through the link as the transmitter output.

4.1.1.2 Directly Modulated Optical Transmitter

The experimental set-up of the directly modulated optical transmitter we investigated is shown in Fig. 4-4. The RF signal is applied directly to the laser source; thus, the optical output of the laser is the transmitter output. We used the same DFB laser for this experiment as that for the externally modulated link.

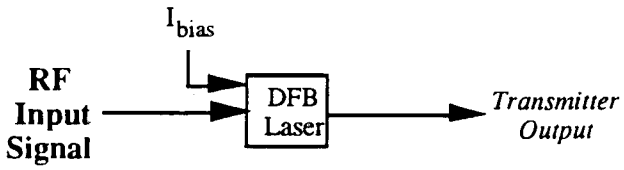

Fig. 4-4. Block diagram of the directly modulated optical transmitter.

We determined the DFB laser's threshold current to be 20 mA and specifications indicate a safe maximum drive current of 80 mA. Therefore, we set the bias current to be 50 mA.

4.1.2 Optical Receiver

As discussed in Chapter 1, an optical receiver can either be a coherent detection receiver or a direct detection receiver. This project focuses on investigating coherent detection techniques for analog optical links, but to serve as a benchmark for comparison, we also constructed, performed experiments on, and determined the link performance of

direct detection links. In this section, we describe these two types of receivers and in the following sections, we compare their performances.

4.1.2.1 Coherent Detection AM-WIRNA Receiver

The block diagram of the coherent detection AM-WIRNA receiver is shown in Fig. 4-5. The incoming optical signal is combined with the optical output of the LO laser via a 3 dB coupler. An external cavity tunable semiconductor laser (TSL) is used as the LO laser. This laser has a built-in optical isolator and a temperature controller. The TSL has an output power of 600 μW, RIN of -148 dB/Hz and linewidth of 20 kHz. A manual polarization controller is used to align the polarization of the LO laser to that of the incoming optical signal. In a field system, the polarization alignment can be handled using polarization-maintaining fiber, automatic polarization control, or a polarization diversity receiver [1]. All these methods are compatible with our system.

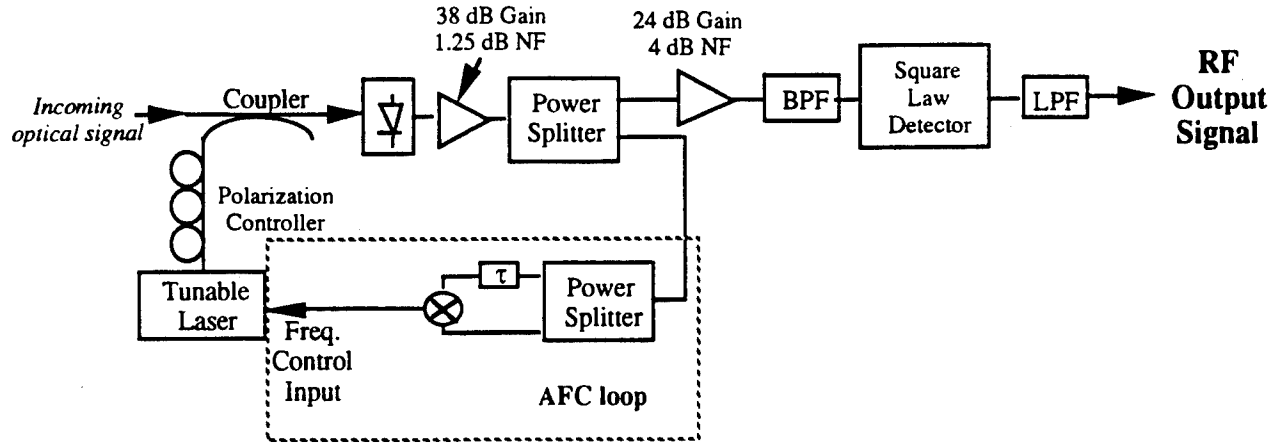

Fig. 4-5. Block diagram of the coherent detection AM-WIRNA receiver. BPF = bandpass filter; LPF = lowpass filter.

The optical receiver consists of a single-photodetector with a 3 dB bandwidth greater than 15 GHz, and a 38 dB gain, 1.25 dB noise figure 8 to 12 GHz preamplifier. After the preamplifier, the signal is split into the demodulation path and the automatic frequency control (AFC) loop. The AFC loop maintains a fixed receiver intermediate frequency (IF) at 10 GHz. Without the AFC loop, thermal effects in the semiconductor lasers were observed to cause the IF to drift by roughly 2 to 5 GHz/hr. The AFC loop consists of a frequency discriminator (constructed from a power splitter, two cables of different lengths, and a mixer) whose output is fed into the external frequency control

connector of the LO laser. The zero-crossing point of the discriminator is set at the IF of 10 GHz. For IFs larger than 10 GHz, the output of the filter generates a positive error voltage which drives the LO laser to a lower optical frequency; IFs of less than 10 GHz drive the LO laser to a higher optical frequency.

For demodulation, the signal passes through an amplifier, bandpass filter, square law detector and lowpass filter. We refer to the combination of a bandpass filter (BPF), square law detector (SLD) and lowpass filter (LPF) in the receiver as the WIRNA (which stands for WIdeband filter-Rectifier-NArrowband filter) structure [2, 3].

4.1.2.2 Direct Detection Receiver

To serve as a benchmark for comparison with the coherent AM link, we constructed a direct detection link, shown in Fig. 4-6. The receiver employs the same photodetector as used for the coherent receiver, and a 0.5 to 2 GHz preamplifier with a 38 dB gain and 1.25 dB noise figure.

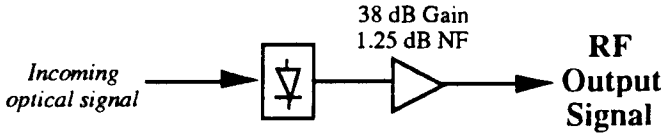

Fig. 4-6. Block diagram of the direct detection receiver.

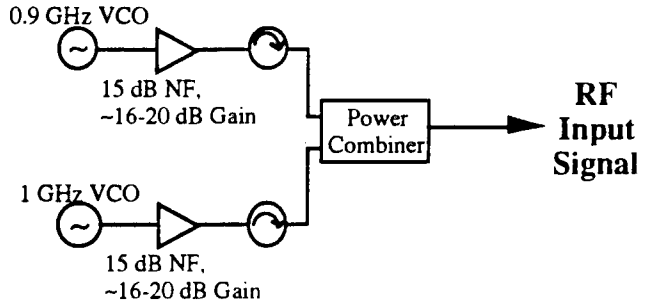

Fig. 4-7. Block diagram of the two-tone signal generator.

4.1.3 Two-Tone RF Input Signal

To measure the link performance measures experimentally, we generated a two-tone RF input test signal using two voltage controlled oscillators (VCO) running at 0.9 GHz and 1.0 GHz; the circuit diagram is shown in Fig. 4-7. To control the amplitudes, and, therefore, the modulation indices of the test signals, each VCO is connected to a

variable gain amplifier. The signals are then combined with a power combiner through microwave isolators and applied to the RF input port of the EOM. The isolators are needed to minimize the interference of the two signals. The amplitudes of the fundamental, the third order IMDs, and noise floor at the link output are then measured using a spectrum analyzer and from this information, the dynamic range, link gain, and noise figure are determined.

4.2 Direct Modulation Versus External Modulation

In this section, we focus on comparing directly and externally modulated links to determine which would give better performance for the coherent AM-WIRNA system. The better link would then be used for further investigations into the properties of coherent AM links. Fig. 4-8 contains the experimental measurements we obtained for the SFDR as a function of the received optical power for the coherent AM link [4].

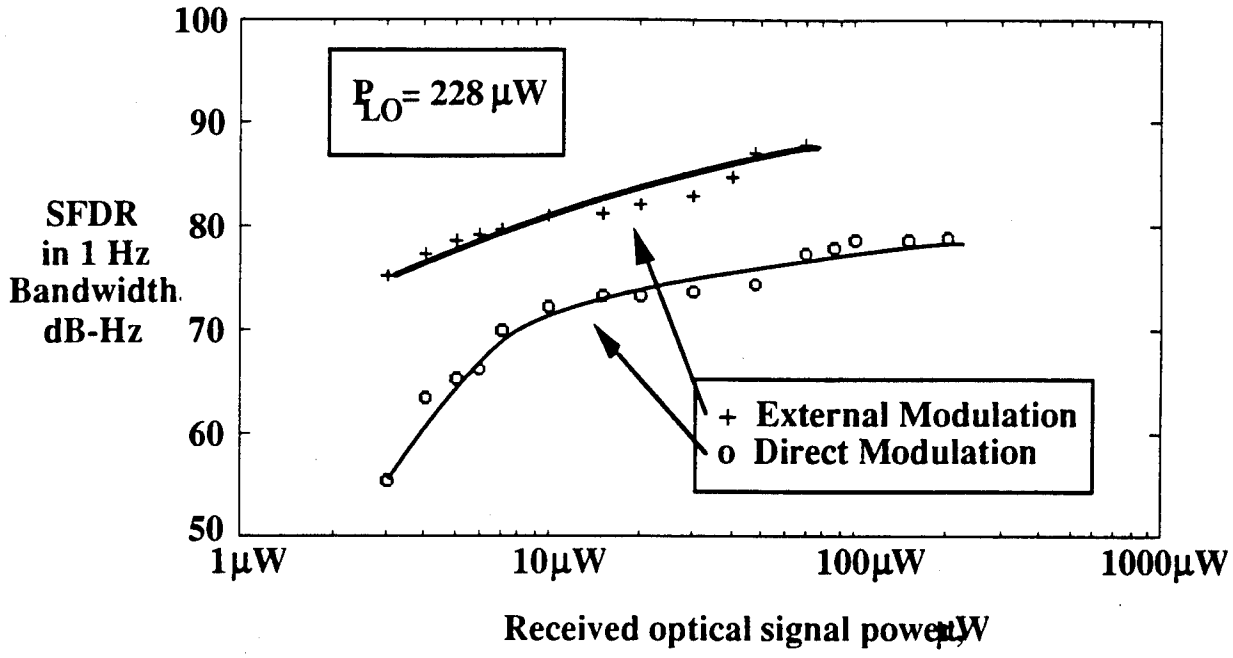

Fig. 4-8. Spurious-free dynamic range versus the received optical power for the externally and directly modulated coherent AM link.

Results show that for the device parameters and optical power levels we used, the externally modulated coherent AM-WIRNA heterodyne link exhibited a much higher SFDR (from 8 dB up to 20 dB) than the corresponding directly modulated coherent AM link. The reason for the poorer performance of the directly modulated link is primarily

due to the frequency chirping of the lasers and the finite IF bandwidth of the coherent receiver. Directly modulating a laser causes chirping, which is a change in the output frequency of the laser as a function of applied current. This results in the widening of the signal spectrum; due to the presence of a finite IF bandwidth, part of the signal is cut off and lost, resulting in both an increased noise floor and a smaller output signal power.

Thus, it is fair to conclude that for coherent AM links, a better dynamic range is achieved using an external modulator. In the succeeding sections, we will focus on investigating the performance, properties and behavior of coherent AM links using the externally modulated transmitter. The entire externally modulated coherent AM link is shown in Fig. 4-9(a), while for comparison, we show the externally modulated direct detection link in Fig. 4-9(b).

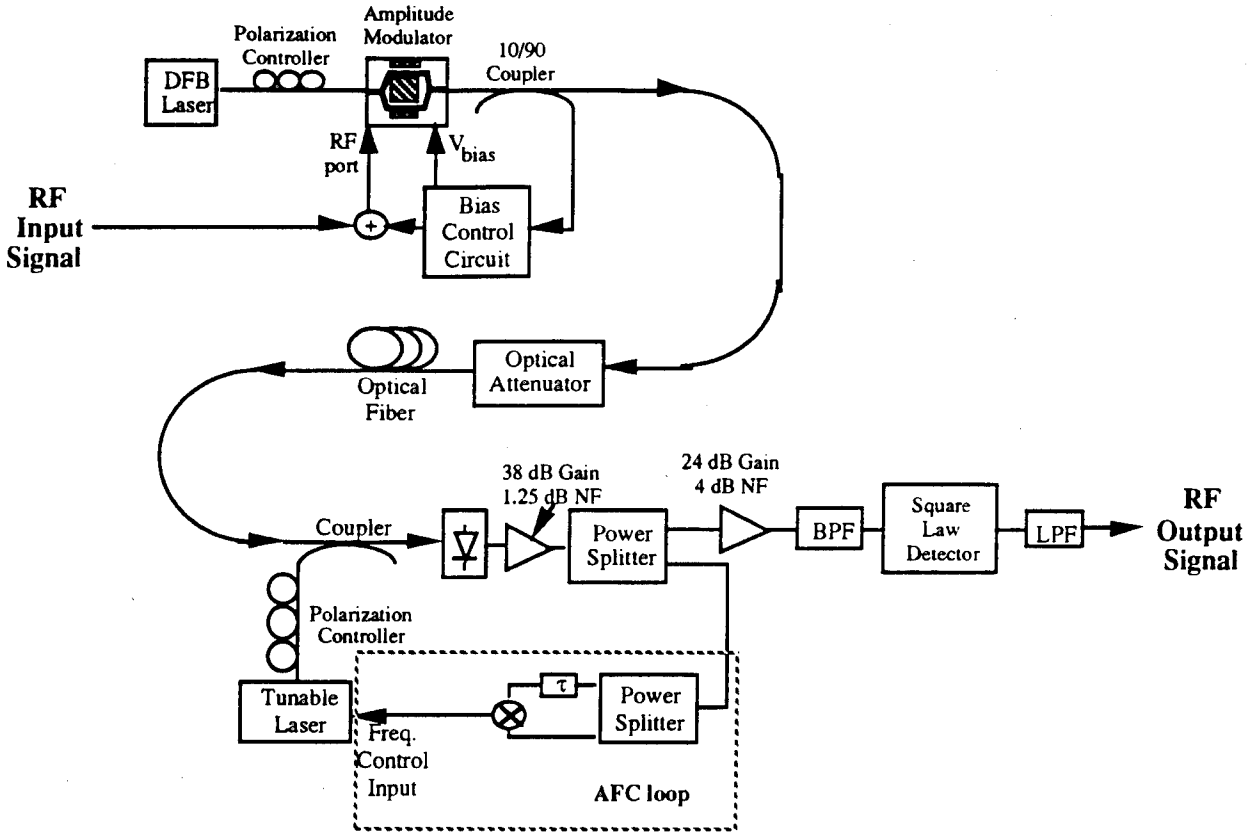

Fig. 4-9(a). Block diagram of the externally modulated coherent AM link.

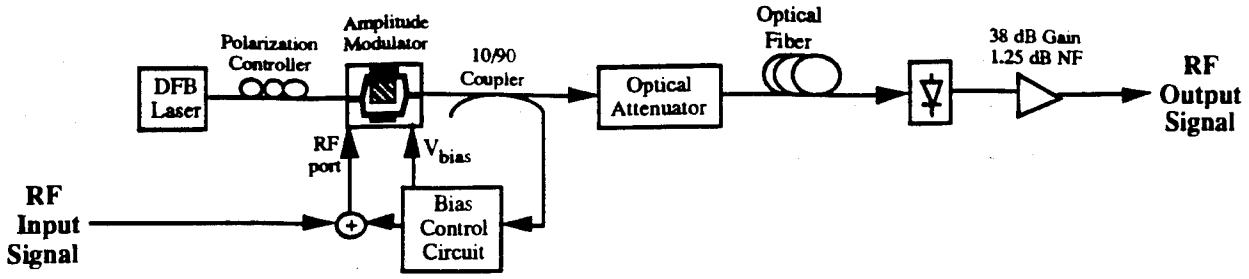

Fig. 4-9(b). Block diagram of the externally modulated direct detection link.

4.3 Analog Link Performance Measures: Theoretical Analysis

In this section, the three most widely used performance measures for analog links are defined and estimates of the theoretical performance of the coherent AM and direct detection links shown in Fig. 4-9 are presented. The analysis is a continuation of that started in Chapter 3. This section starts with a discussion of the spurious-free dynamic range, followed by the link gain, and then the noise figure.

4.3.1 Spurious-Free Dynamic Range

One of the most crucial performance measures for an analog link is the **spurious-free dynamic range** (SFDR). It is a measure of the variation in the RF signal level that can be carried by the link and is defined as the ratio of the maximum RF power, which is limited by the third order intermodulation distortions (IMD) produced by the nonlinearities in the link's components, to the minimum power, which is limited by the receiver noise [5, 6]:

$$SFDR \equiv \frac{RF\ Power|_{IMD=noise}}{RF\ Power|_{signal=noise}} = \frac{m^2|_{IMD=noise}}{m^2|_{signal=noise}} \tag{4.1}$$

m is the RF modulation index. For the links shown in Fig. 4-9, the maximum RF power is usually limited by the nonlinearities of the EOM [5].

The resulting SFDR for the coherent AM-WIRNA heterodyne link is given by [7] (see Table 4-1 for symbol definitions):

$$SFDR_{cd} \approx 4\left[\frac{A^4}{16A^2\eta_{cd}B_2 + 16\eta_{cd}^2 B_2(4B_1 - B_2)}\right]^{2/3} \Gamma_\phi^{2/3} \tag{4.2}$$

where A is the IF signal amplitude, h_{cd} is the additive noise density, and Gf represents the reduction in the dynamic range due to phase noise-to-amplitude noise conversion in the BPF. These quantities are given by:

$$A = R\sqrt{2P_sP_{LO}} \tag{4.3}$$

$$\eta_{cd} = \eta_{th} + qR(P_s + P_{LO}) + \frac{1}{4}(2R^2P_sP_{LO} + R^2P_{LO}^2)10^{\frac{RIN}{10}} \tag{4.4}$$

$$\Gamma_\phi \equiv \frac{4}{\pi}\tan^{-1}\frac{2B_1}{\Delta\nu} + \frac{2}{\pi}\tan^{-1}\frac{2B_1}{\Delta\nu} - 2 \tag{4.5}$$

Table 4-1. Definitions of Variables

P_s	Received optical signal power
P_{LO}	Received optical local oscillator power
RIN	Average RIN of the transmitter and LO lasers
h_{th}	Power spectral density of the receiver thermal noise
B_1	IF bandwidth for the coherent AM link
B_2	Signal bandwidth for the coherent AM link
Dn	Combined linewidth of the transmitter and LO lasers
R	Photodiode responsivity
R_s	Receiver source impedance = 50 W
a	Conversion loss factor of the square law detector
V_p	Voltage required to achieve p optical shift in the modulator

Phase noise-to-amplitude noise conversion results from the spectral broadening caused by the laser phase noise and by the IF filtering in the bandpass filter [2].

The SFDR for the direct detection link is [7]:

$$SFDR_{dd} = 4\left(\frac{R^2P_s^2}{\eta_{dd}B}\right)^{2/3} \tag{4.6}$$

where η_{dd} is the power spectral density of the additive noise at the output of the photodetector, given by

$$\eta_{dd} = \eta_{th} + 2qRP_s + R^2P_s^2 10^{\frac{RIN}{10}} \tag{4.7}$$

and B is the signal bandwidth.

4.3.2 Link Gain

The **RF power transfer ratio,** or **link gain**, G, of the link is defined as the ratio of the RF power at the link output, S_O to the RF power at the link input, S_i:

$$G = \frac{S_o}{S_i} \tag{4.8}$$

The gain for the coherent AM optical link, G_{cd}, and for the direct detection link, G_{dd}, are given by [8, 9]:

$$G_{cd} = \frac{\alpha P_s P_{LO}}{2}\left(\frac{\pi R_s R}{V_\pi}\right)^2 \tag{4.9}$$

$$G_{dd} = \left(\frac{\pi R_s R P_s}{V_\pi}\right)^2 \tag{4.10}$$

where the variables are defined in Table 4-1.

4.3.3 Noise Figure

Noise figure measures the degradation in the signal-to-noise ratio (SNR) between the input and output of a link and is defined as:

$$F = \frac{S_i/N_i}{S_O/N_O} = \frac{N_O}{GN_i} \tag{4.11}$$

where S_i and N_i are the input signal and noise powers; S_o and N_o are the output signal and noise powers; and G is the link gain discussed in the previous section. By definition, the input noise power is the noise power from a matched resistor, $N_i = kTB$, where k is Boltzmann's constant; T is the resistor temperature; and B is the signal bandwidth [10]. The output noise power can be expressed by:

$$N_o = GN_i + \eta B \tag{4.12}$$

where hB is the additive noise introduced by the link. Substituting $N_i = kTB$, we can express the noise figure as:

$$F = 1 + \frac{\eta}{GkT} \tag{4.13}$$

For the coherent AM optical link, the noise figure is

$$F_{cd} = 1 + \frac{4\alpha\eta_{cd}}{G_{cd}kT} \tag{4.14}$$

where h_{cd} and G_{cd} are given by (4.4) and (4.9), respectively. Similarly, for the direct detection optical link, the noise figure is

$$F_{dd} = 1 + \frac{\eta_{dd}}{G_{dd}kT} \tag{4.15}$$

where h_{dd} and G_{dd} are given by (4.7) and (4.10), respectively.

4.4 Demonstration of Phase Noise Cancellation

It was mentioned in Chapter 1 that the phase noise of semiconductor lasers can cause substantial performance degradation in coherent analog links. However, the use of WIRNA processing in a coherent heterodyne link can be effective at minimizing the impact of phase noise. In this section, we demonstrate phase noise cancellation in the coherent AM-WIRNA heterodyne link.

Figs. 4-10(a), (b), (c), and (d) show the RF signal spectrum at three different points of the coherent AM link. Fig. 4-10(a) shows the spectrum of the two-tone test signal at the RF input to the modulator.

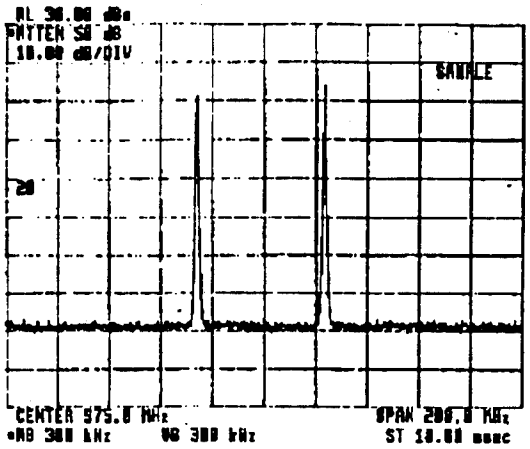

Fig. 4-10(a). Signal spectrum of the two-tone signal at the RF input to the modulator.

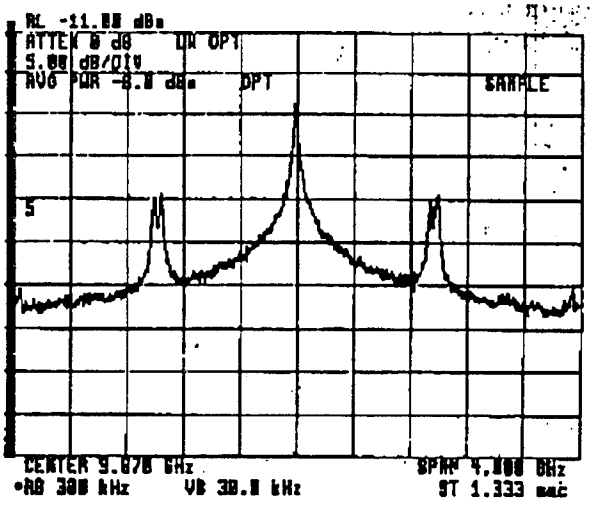

Fig. 4-10(b). Signal spectrum of the two-tone signal at the photodetector output.

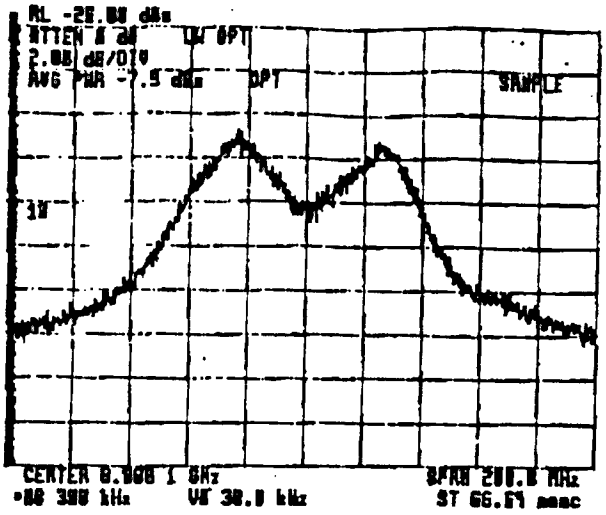

Fig. 4-10(c). Close-up of the spectrum of the two-tone signal at the output of the photodetector.

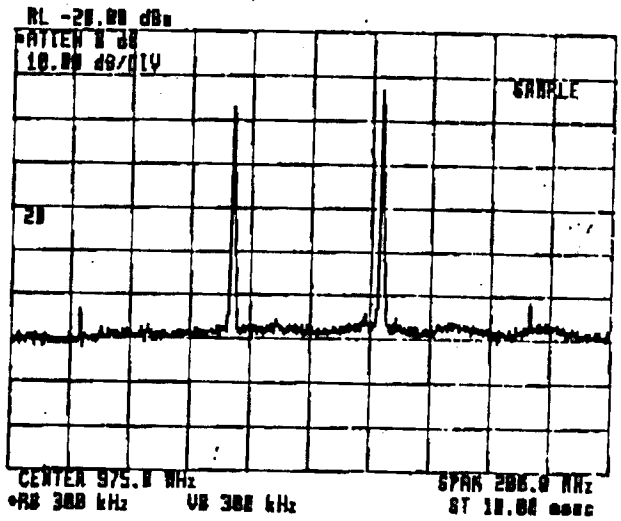

Fig. 4-10(d). Signal spectrum of the two-tone signal at the output of the AM-WIRNA receiver.

Fig. 4-10(b) shows the IF signal spectrum at the photodetector output. Note the IF of approximately 10 GHz with the two-tone signal present at its sidebands. Fig. 4-10(c) is an enlargement of the two-tone signal, showing that these signals have a full width at half maximum (FWHM) of approximately 20 MHz, corresponding to the combined linewidth of the transmitter and LO lasers. This clearly illustrates the spectrum-broadening effect of laser phase noise.

Fig. 4-10(d) shows the spectrum of the signals (together with the third order IMDs) at the output of the AM-WIRNA receiver. The linewidths of both signal tones are seen to be extremely small and similar to that of the input signals shown in Fig. 4-10(a). These figures illustrate the phase noise cancellation in the coherent AM-WIRNA link of Fig. 4-9(a).

4.5 Impact of System Parameters

To further investigate the usefulness of the coherent AM-WIRNA heterodyne link and understand its behavior, we study the impact of the various system parameters on the link dynamic range. Section 4.5.1 discusses the impact of the laser linewidth and IF filter bandwidth, followed by Section 4.5.2 demonstrating the impact of laser RIN. The impact of the received optical signal power is presented in Section 4.5.3, while Section 4.5.4 deals with the effect of the LO power on the dynamic range.

4.5.1 Linewidth and the IF Bandwidth

The SFDR measurements as a function of the laser linewidth using three different IF filter bandwidths are shown in Fig. 4-11. To vary the linewidth beyond 20 MHz, we directly modulated the DFB laser with a noise source so that the spectral linewidth was broadened by laser chirping [11]. We measured the laser relative intensity noise (RIN) for each case used. As shown in Section 4.5.2, for the range of RIN values in this experiment (-153 to -130 dB/Hz), the SFDR is independent of RIN at these power levels; this makes linewidth the only important variable in this section.

From Fig. 4-11, it is observed that for IF bandwidths of 3 and 4 GHz, the SFDR is almost constant at 84 dB•$Hz^{2/3}$ and 82 dB•$Hz^{2/3}$, respectively, for linewidths from 10 to 300 MHz. For an IF bandwidth of 2 GHz, the SFDR is at least 3 dB less. As the linewidth is increased beyond 300 MHz, all three bandwidth cases show a considerable drop in the SFDR, with the 2 GHz case having the most rapid decrease, and the 4 GHz, the least.

The explanation of the foregoing experimental results is as follows. Laser phase noise (which is associated with wide laser linewidths) causes the received signal spectrum to widen. If the IF filter cuts off part of the signal spectrum, this results in phase noise-to-amplitude noise conversion which causes a deterioration of the link performance. The signals used in this experiment are sinusoids at 0.9 and 1 GHz; therefore, it is clear why

the link with an IF bandwidth of 2 GHz has the worst SFDR -- for any finite linewidth, a part of the signal spectrum will always be rejected by the IF filter. As the linewidth increases, a larger and larger part of the signal power will be rejected by the bandpass filter causing signal distortion and phase noise-to-amplitude noise conversion, resulting in a poorer SFDR.

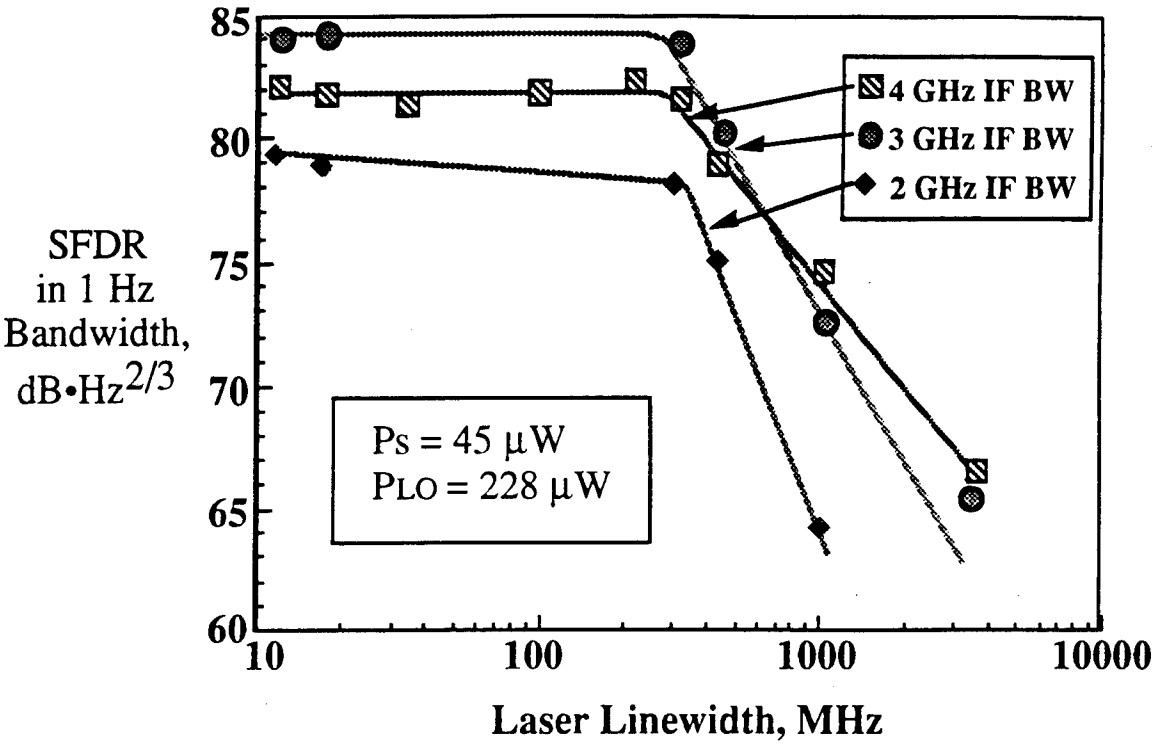

Fig. 4-11. Experimentally measured impact of the laser linewidth and the IF bandwidth on the spurious-free dynamic range of the coherent AM link [12].

For the 3 and 4 GHz bandwidth cases, when the linewidths are less than 300 MHz, the IF bandwidth is much wider than the signal spectral width, so that only a negligible part of the phase noise-widened signal spectrum is cut off. This causes the link to be linewidth-insensitive; i.e., the SFDR is essentially independent of the laser linewidth. However, similar to the 2 GHz case, when the linewidth is increased to the point when considerable amount of the signal power is cut off, the SFDR deteriorates. For both the 3 and 4 GHz cases, this occurs for linewidths greater than 300 MHz.

The disadvantage of a wider IF bandwidth is that it collects more additive noise, which translates to a higher noise floor, and therefore, to a lower SFDR. This is supported by Fig. 4-11: the 4 GHz IF bandwidth link has a poorer SFDR than the link with a 3 GHz IF bandwidth, for linewidths less than 300 MHz. The choice of IF

bandwidth is therefore very important: A narrow IF filter increases the amount of phase noise-to-amplitude noise conversion while a wide IF filter collects more additive noise. For example, in Fig. 4-11, when the linewidth is 700 MHz or more, the link with a 4 GHz IF bandwidth outperforms the link with a 3 GHz IF bandwidth. This is because there is much more phase-to-amplitude noise degradation in the 3 GHz case than the 4 GHz case, and for this situation, the degradation due to phase noise-to-amplitude noise conversion is more significant than the degradation caused by additive noise.

An important conclusion of this section is that as long as the bandpass filter is designed to be wide enough to pass the phase noise-widened spectrum of the signal, the coherent AM-WIRNA link is insensitive to laser linewidth and to any changes in the linewidth that may be brought about by temperature and drive current fluctuations. The SFDR can be maximized by having the smallest possible IF bandwidth that is wide enough to avoid cutting off a considerable amount of signal power while minimizing the additive noise collected.

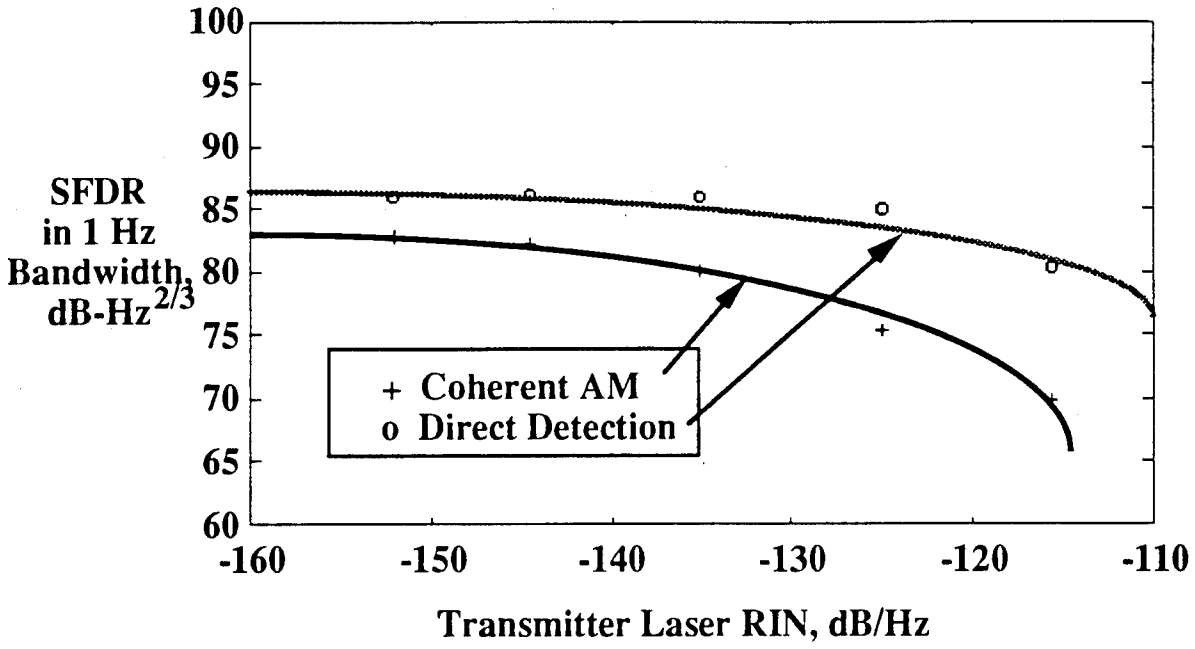

Fig. 4-12. Experimental results of the impact of laser RIN on the coherent AM link. The laser parameters are listed in Table 4-2.

4.5.2 Relative Intensity Noise (RIN)

To investigate the impact of laser RIN on link performance, it is desirable to vary the RIN of a laser while holding other laser parameters (i.e., output power, linewidth)

constant. However, a given laser has an intrinsic RIN at a given output power level. Therefore, in our measurements, we have synthetically increased the RIN of the transmitter DFB laser by inputting a noise source to the RF input of the EOM but maintaining the other system parameters like received optical signal power (by using a variable attenuator as shown in Fig. 4-1) and linewidth (by modulating the EOM instead of the laser), constant. By varying the noise source's power level, different RIN values can be obtained. The corresponding plot showing the impact of the transmitter laser RIN on the dynamic range of the coherent AM link is displayed in Fig. 4-12, and the system parameters are listed in Table 4-2.

Table 4-2. Laser Parameters for SFDR vs. RIN Measurements

	Transmitter Laser for both links	**LO Laser**
Received Optical Power	45 μW	228 μW
Laser Linewidth	13 MHz	43 kHz

Note that the coherent AM link is more sensitive to RIN than the direct detection system. For the direct detection system, the SFDR is almost constant for the RIN values we are considering. It is only when RIN drops to -116 dB/Hz that a degradation is observed. For coherent systems, the SFDR remains unchanged from its value at RIN = -152 dB/Hz only until RIN = -145 dB/Hz. Beyond that, the worsening effect of laser RIN on the system performance is clear. This is expected for a coherent system employing a single photodetector receiver since RIN is approximately proportional to the square of the LO optical power.

4.5.3 Received Signal Power

Using the variable optical attenuator shown in Fig. 4-1, we varied the received optical signal power for both coherent AM and direct detection links. The SFDR measurements of the coherent AM-WIRNA heterodyne link as a function of the received optical signal power are shown in Fig. 4-13, and the system parameters are listed in Table

4-3. The SFDR measurements for a similar externally modulated direct detection link are also shown for comparison. The maximum received optical power (signal plus LO) at the photodetector is limited largely due to the optical modulator losses, and also by the optical output power of our DFB laser used as the transmitter and the tunable semiconductor laser as the LO laser. However, these modest powers are sufficient for a proof-of-concept experiment on the merits of this coherent AM link.

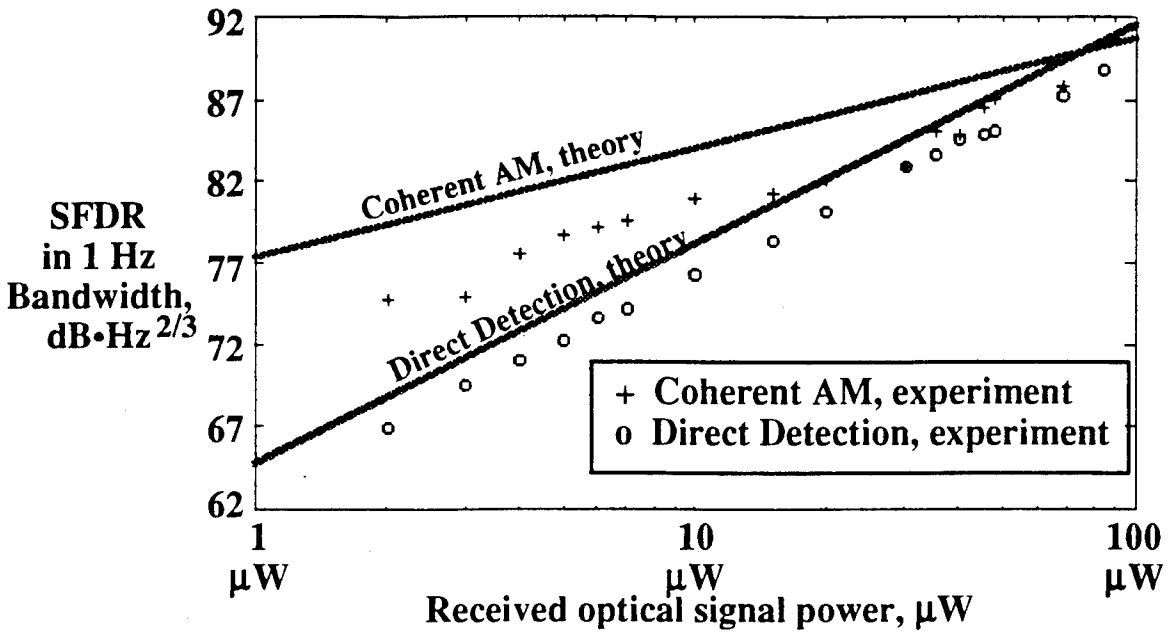

Fig. 4-13. Spurious-free dynamic range versus received optical signal power for the coherent AM and direct detection links. The laser parameters are listed in Table 4-3.

Table 4-3. Laser Parameters for SFDR vs. Received Signal Power Measurements

	Transmitter Laser for both links	**LO Laser**
Received Optical Power	variable	228 μW
Laser Linewidth	7.9 MHz	19.2 kHz
Laser RIN	-153.8 dB/Hz	-148.7 dB/Hz

Fig. 4-13 also contains theoretical SFDR estimates obtained using Eqs. (4.2) and (4.6); the estimates take into account the RIN of both lasers, the receiver amplifier noise, the laser linewidths, and the finite optical power of the LO laser.

Fig. 4-13 shows that the coherent AM link has a higher SFDR (by up to 10 dB) than the corresponding direct detection link when the received optical signal power is less than 85 μW. This is because the direct detection link is thermal noise-limited at these power levels while the coherent AM link is closer to being shot noise-limited. As the received optical signal power increases beyond 85 μW, both types of receivers approach the shot noise-limited regime. In this case, the direct detection link has a higher dynamic range than the coherent AM link [7]. This is shown by the theoretical curves in Fig. 4-13. This cross-over optical power point between the coherent AM and direct detection links can be increased using an LO laser with a higher output power (we are currently limited to an optical LO power at the photodetector of 228 μW by our tunable laser).

Table 4-4. SFDR penalty due to the SLD imperfections.

Received Optical Signal Power, (μW)	SFDR penalty due to SLD (dB)
50.0	0.5
27.5	1.1
17.6	1.5
10.0	2.3
6.2	3.0
3.9	3.8

Fig. 4-13 shows that the measurements agree very well with theory for the direct detection case, with a difference of only 1 dB. The experimental data for the coherent AM link differs from the theory by 2 to 4 dB. This is attributed partially to optical connector losses in the receiver (up to 1 dB) and fluctuations and instabilities in the output of the LO laser (a penalty of about 1 dB). The latter is due to polarization changes and tuning required to maintain the IF at 10 GHz. However, the main reason for the difference is the third order distortion introduced by the square law detector (SLD) at the link output. The SLD introduces third order distortion in the output signal resulting in a lower SFDR than that predicted by theory. By varying the input RF power into the SLD (so that only the nonlinearities produced by the SLD, as the RF input to it changes, can be studied), we verified that the additional distortion is caused mainly by the SLD.

Since the RF input power to the SLD changes as the received optical signal power changes, third order nonlinearities produced by the SLD affect the measured link SFDR. Table 4-4 on the previous page shows the additional SFDR penalty due to the SLD as a function of the received optical signal power that corresponds to the RF power we input to the SLD. Inspection of Table 4-4 reveals that the SFDR penalty due to the SLD corresponds to most of the discrepancy between the theoretical and experimental results.

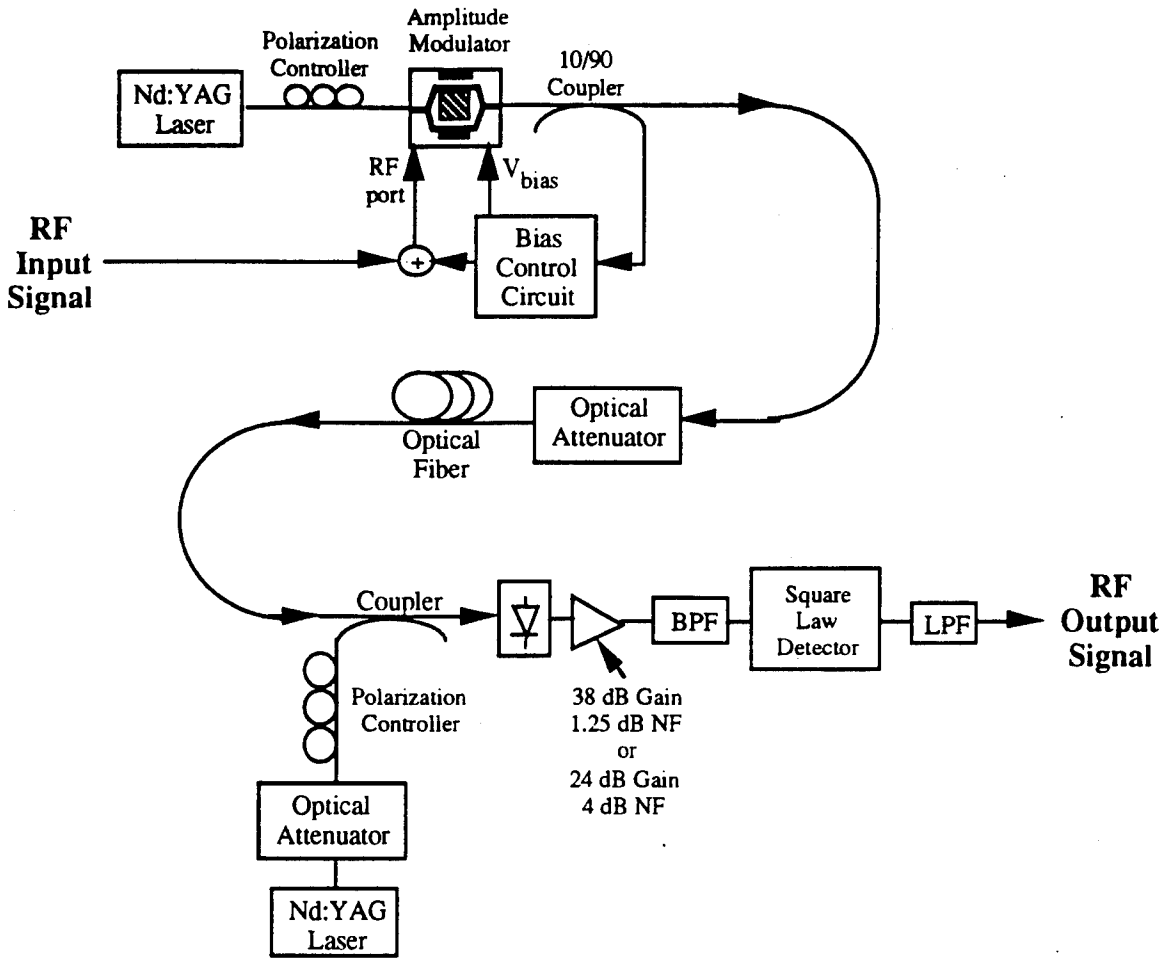

Fig. 4-14. Set-up used for the measurement of the system performance of the coherent AM link using Nd:YAG lasers.

4.5.4. Laser Local Oscillator (LO) power

The dynamic range of the coherent AM link shown in Fig. 4-9(a) is limited by the low output power of the DFB and TSL lasers used. Since high power semiconductor lasers are currently being developed, we decided to investigate what dynamic range could

be achieved with higher received optical signal and LO powers. For these measurements we replaced the DFB and TSL lasers with high power Nd:YAG lasers.

The measurement set-up we used for this experiment is shown in Fig. 4-14. Optical attenuators are used to vary the received optical signal and LO powers for the SFDR measurements. An AFC loop is not necessary for this case since the Nd:YAG lasers have very stable output optical frequencies.

Fig. 4-15 shows experimentally measured SFDR of the coherent AM link as a function of the received optical signal power for LO powers ranging from 100 μW to 1 mW. The maximum total received optical power is currently limited by the photodetector we have. Results indicate that a 10 dB increase in the LO power, from 100 μW to 1 mW corresponded to a 10 dB or more increase in the SFDR. Through these measurements, we have also shown that a coherent AM link using high power lasers is capable of achieving a dynamic range of 101 dB-$Hz^{2/3}$. We are confident that we could get an even higher SFDR with increased optical power for both transmitter and LO lasers, but we are currently limited to a total received optical power of 1 mW by the saturation of the photodetector and RF pre-amplifier we were using.

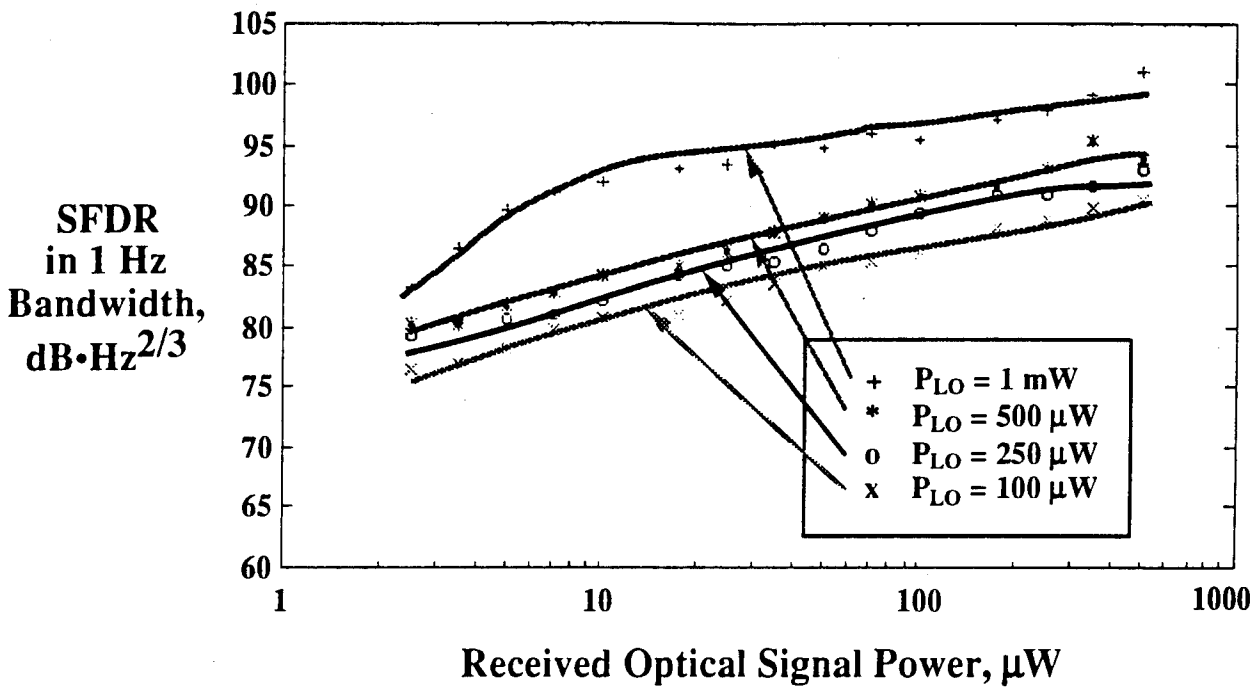

Fig. 4-15. Spurious-free dynamic range versus received optical signal power for different local oscillator powers. RIN of both lasers = -164 dB/Hz.

4.6 Link Gain and Noise Figure [12]

We investigated the gain and noise figure of the coherent AM and direct detection links shown in Figs. 4-9(a) and 4-9(b), respectively, by measuring the output signal and noise power for a +15 dBm input signal. Since we are interested in the performance of the *optical* link, we did not take into account the effect of any link pre- and post-amplifiers. The total link gain and noise figure can, of course, be greatly improved by using low-noise amplifiers before the link, and high-gain amplifiers after the link [8, Chapter 6 of this report].

The dependence of the gain and noise figure on the laser linewidth, IF bandwidth, and RIN is similar to the dynamic range results; hence, we do not provide separate plots for these parameters. It is, however, important to determine how the gain and noise figure change with the received optical signal power since this knowledge provides us with typical values of both optical links' gain and noise figure.

Table 4-5. Laser Parameters for the Link Gain and Noise Figure vs. Received Signal Power Measurements

	Transmitter Laser for both links	**LO Laser**
Received Optical Power	variable	228 μW
Laser Linewidth	7.9 MHz	19.2 kHz
Laser RIN	-153.8 dB/Hz	-148.7 dB/Hz

The experimental measurements and theoretical values of the link gain and noise figure of the coherent AM-WIRNA heterodyne and direct detection links as a function of the received optical signal power are shown in Fig. 4-16(a) and Fig. 4-16(b), respectively, and the laser parameters for these measurements are listed in Table 4-5. For most cases, the experimental values agree well with the theoretical results. Because optical links tend to have very low gain (in this case, negative gain), their noise figures are fairly high; this is clearly seen from Eq. (4.13). Fig. 4-16(b) shows that the noise figure for the coherent link is always greater than that for the direct detection link. This is primarily due to the fact

that the gain of the coherent AM link is much smaller than that of the direct detection link because of the conversion loss encountered in the square law detector.

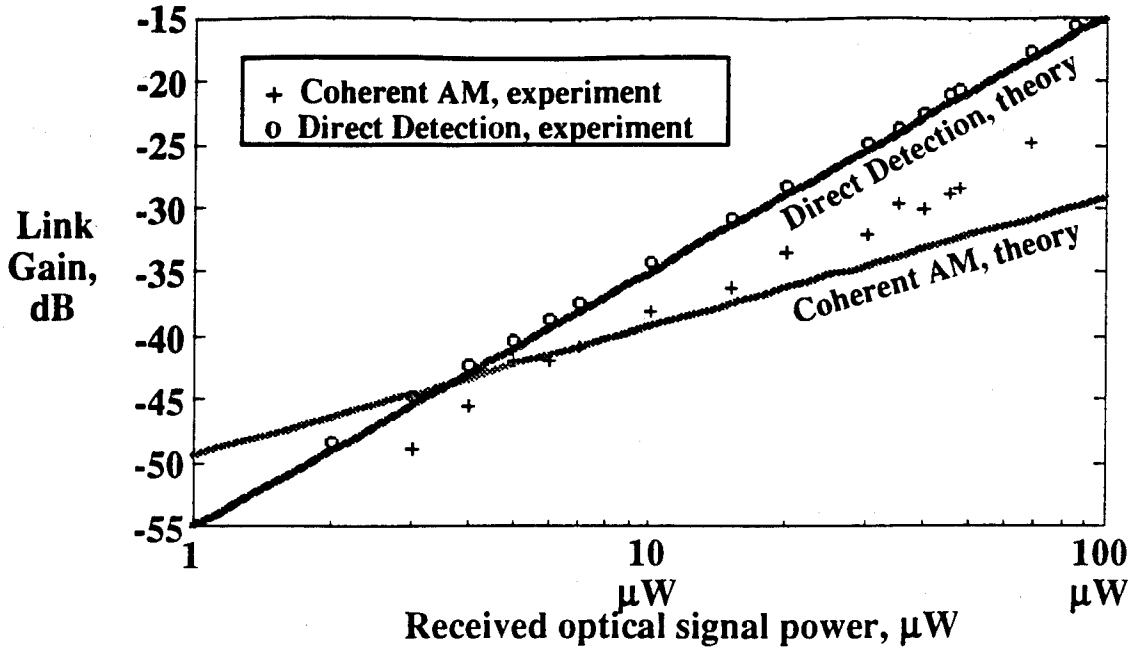

Fig. 4-16(a). Link gain versus received optical signal power for the coherent AM and direct detection links. The laser parameters are listed in Table 4-5.

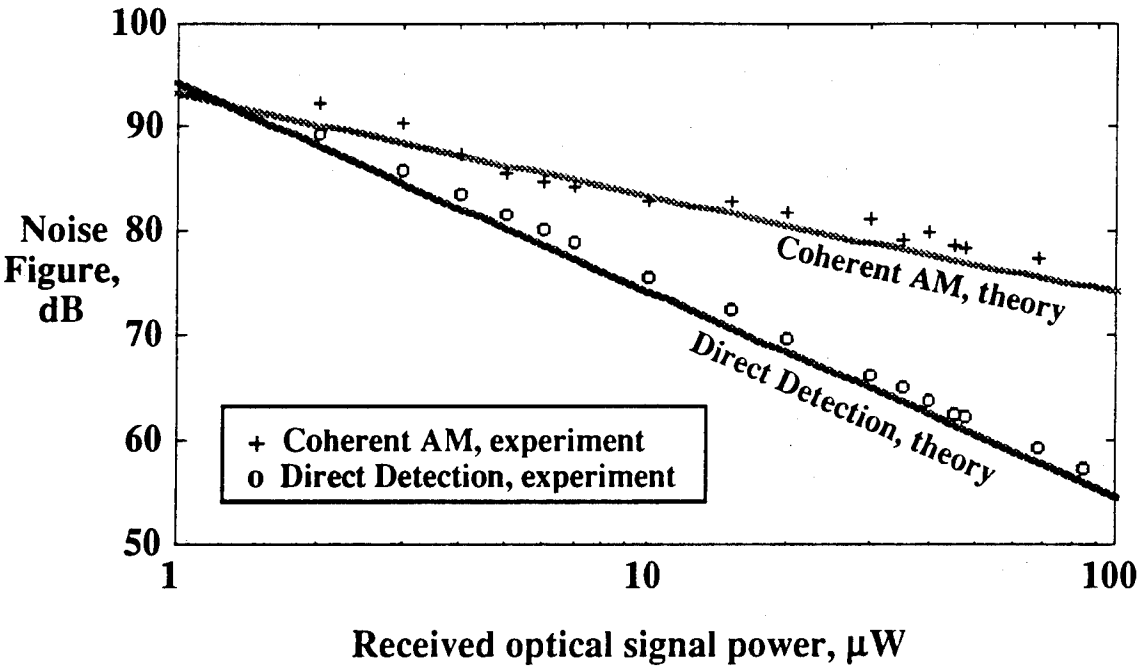

Fig. 4-16(b). Noise figure versus received optical signal power for the coherent AM and direct detection links. The laser parameters are listed in Table 4-5.

Fig. 4-16(a) shows that for received optical signal power P_S greater than 4 μW, the gain of the direct detection link is greater than that of the coherent AM link. This is because the gain is proportional to the square of the received optical signal power P_S for the direct detection case while for the coherent AM link, the gain is proportional to P_S only. For direct detection, the experimental values agree very well with the theoretical results. For the coherent AM link, there is up to a 5 dB difference between the theoretical and experimental results for P_S less than 4 μW. This discrepancy is primarily due to the variations in the conversion efficiency of the square law detector for different RF powers, especially for very low levels (similar to that discussed in Section 4.5.3). The difference between the theoretical and experimental results may also be due to the instabilities and fluctuations in the LO laser (a penalty of about 1 dB, as discussed in Section 4.5.3). Also, at low power levels the output becomes very noisy, making it very difficult to make accurate measurements.

4.7 Link Loss Measurements: Coherent Versus Direct Detection

In this section, we present measurements of the SFDR against link loss. Link loss can easily be converted into the number of destinations or splits for distribution systems and into transmission distance for point-to-point links. So, if one wants to build a system with a prescribed number of splits or transmission distance, the plot of SFDR versus link loss shows the best configuration.

Let us compare the SFDR versus link loss performance of the coherent AM-WIRNA heterodyne and direct detection links shown in Figs. 4-9(a) and 4-9(b), respectively; the experimental measurements are presented in Fig. 4-17.

Inspection of Fig. 4-17 shows that for low loss links (less than 5 dB link loss), the direct detection link gives the better dynamic range since it is shot noise-limited at this region. For link loss less than 7 dB, the coherent AM-WIRNA heterodyne link is RIN-limited as evidenced by the flat curve. The impact of RIN is very pronounced for a single-photodetector coherent receiver. This penalty causes the coherent AM link to have a lower SFDR.

For link loss greater than 7 dB, the coherent AM link outperforms the direct detection link, because in this region, the coherent AM link has a better receiver sensitivity due to the presence of a LO laser. The coherent AM link is now shot noise-limited while the direct detection link is thermal noise-limited. Thus, this section shows that coherent AM links are good for lossy links.

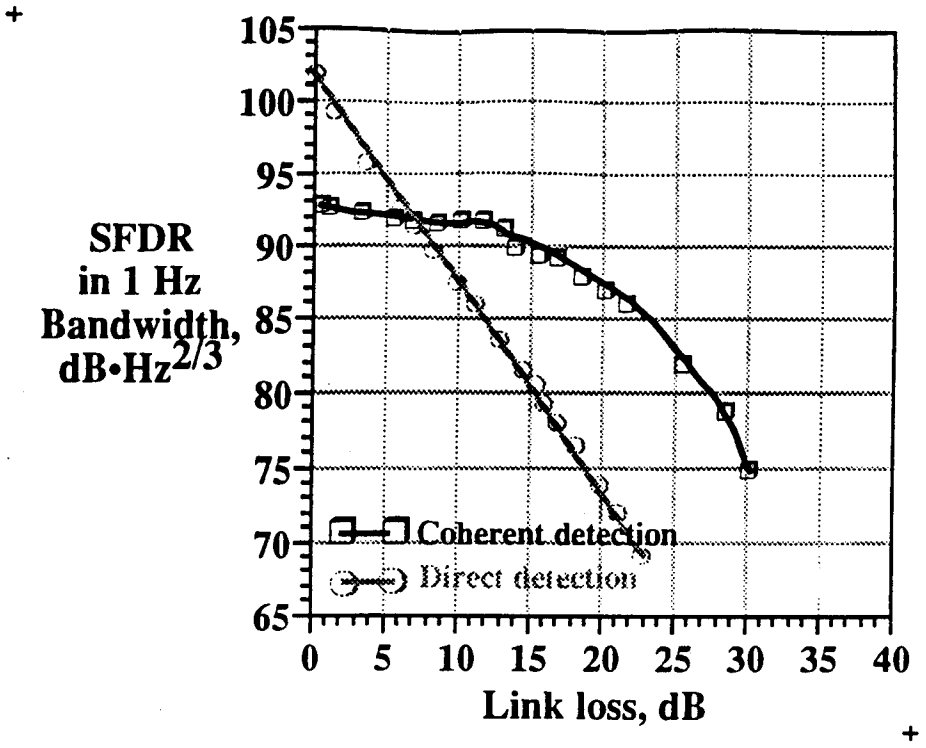

Fig. 4-17. Spurious-free dynamic range vs. the link loss for the direct detection and coherent AM links. P_{LO} = 0.5 mW, transmitter laser power = P_{TR} = 2 mW.

With the development of optical amplifiers, the performance of both coherent AM and direct detection links are expected to improve, enabling both to handle higher link losses. This will be the topic of the next chapter.

4.8 References

[1] N. Walker, and G. Walker, "Polarization Control for Coherent Communications," IEEE/OSA *Journal of Lightwave Technology*, vol. LT-8, no. 3, pp. 438-458, March 1990.

[2] L. G. Kazovsky, P. Meissner, and E. Patzak, "ASK multiport optical homodyne receivers," IEEE/OSA *Journal of Lightwave Technology*, vol. LT-5, no. 2, pp. 770-791, June 1987.

[3] L. G. Kazovsky, R. Welter, A. F. Elfefaie, and W. Sessa, "Wide-linewidth phase diversity homodyne receivers," IEEE/OSA *Journal of Lightwave Technology*, vol. LT-6, no. 10, pp. 1527-1536, October 1988.

[4] M. Tabara, D. J. M. Sabido IX, T. K. Fong, and L. G. Kazovsky, "A Linewidth-insensitive Coherent AM Optical Link: A Comparison of Direct and External Modulation Formats," LEOS '93 Annual Meeting, San Jose, CA, November 1993, pp. 368-369.

[5] D. J. M. Sabido IX, T. K. Fong, R. F. Kalman, and L. G. Kazovsky, "Linewidth-Insensitive Coherent Optical Analog Links," *Optoelectronic Signal Processing for Phased Array Antennas III*, SPIE Vol. 1703, pp. 504-522, 1992.

[6] B. H. Kolner, and D. W. Dolfi, "Intermodulation distortion and compression in an integrated electrooptic modulator," *Appl. Opt.*, vol. 26, pp. 3676-3680, 1987.

[7] T. K. Fong, D. J. M. Sabido IX, M. Tabara, R. F. Kalman, and L. G. Kazovsky, "Linewidth-Insensitive Coherent AM Optical Links: Design, Performance and Potential Applications," IEEE/OSA *Journal of Lightwave Technology*, vol. LT-12, no. 3, pp. 526-534, March 1994.

[8] R. Simons, "Microwave Fiber Optic Links," *Optical Control of Microwave Devices*, chap. 5, Boston: Artech House, 1990, pp. 121-155.

[9] C. H. Cox, "Gain and Noise Figure in Analogue Fiber-Optic Links," *IEE Proceedings - J*, vol. 139, no. 4, pp. 238-242, August 1992.

[10] D. M. Pozar, *Microwave Engineering*, New York: Addison-Wesley, 1990, pp. 589-594.

[11] K. Petermann, *Laser Diode Modulation and Noise,* Norwell, Massachusetts: Kluwer Academic Publishers, 1988, pp. 198-200.

[12] D. J. M. Sabido IX, M. Tabara, T. K. Fong, R. F. Kalman, and L. G. Kazovsky, "Experimental Linewidth-Insensitive Coherent Analog Optical Link," IEEE/OSA *Journal of Lightwave Technology,* accepted for publication.

Appendix. List of Devices Used

Description	Vendor	Model No.
Optical Attenuator	JDS Fitel	MV471U-OOFAOOFA)
Angled Optical Connectors	Wave Optics	FC/A&PC
Transmitter DFB Laser	Fujitsu Electronics	FLD150F2KP
External Amplitude Modulator	Ramar Corp.	402-IM15-5
Manual Polarization Controllers	BT&D	MPC1000
10/90 Optical coupler	Gould Fiber Optics	1550-COS-10/90-02x02
1 GHz Photodetector	Fujitsu Electronics	FID13Z81PZ
Lock-in Amplifier	Stanford Research Syst.	SR830 DSP
Tunable Semiconductor Laser	Santec	TSL-600-1550
3 dB Optical Coupler	Gould Fiber Optics	Gould 1550-COS-50/50-02x02
Photodetector	Lasertron	QDEMW1-002
8 to 12 GHz Preamplifier	Miteq	AMF-4S-080120-15
Mixer for AFC loop	Avantek	DBX184L
8 to 12 GHz Amplifier	Miteq	AFS4-08001200-40-23P-4
Bandpass filter	Lark Eng'g	3B10000-4000-8AA
Square Law Detector	Miteq	MX2J130260
Lowpass Filter	Lark Eng'g	LSM 2000-10AA
0.5 to 2 GHz Preamplifier	Miteq	AFS3-00500200-15-10P-4
0.9 and 1 GHz Voltage Controlled Oscillators	Avantek	VTO-8090
Variable Gain Amplifier used for two-tone signal	Hewlett-Packard	HP8347A
Power Combiner	M/A Com	DMS 285
0.5 to 2 GHz Microwave Isolators	Trak Microwave	60A1101

Chapter Five

Optically Amplified Links

Optical amplifiers (OAs) can be used to improve the link performance by boosting the intensity of an optical signal. They can serve several purposes in the design of fiber-optic communication systems: for example, as in-line amplifiers, boosters of transmitter power, preamplifiers to the receiver, and compensators of distribution losses in broadcast networks. However, like any conventional electronic amplifier, OAs add noise to the amplified signal. Although erbium-doped fiber amplifiers (EDFAs) degrade system performance by generating amplified spontaneous emission (ASE) noise, they lengthen the transmission distance of point-to-point links and increase the potential number of destinations in a distribution system.

Previous work concentrated on the use of optical amplifiers in digital systems [1] and in direct detection (DD) analog links [2]. In this project, we investigated the impact of OAs on a coherent AM analog optical link. The use of both optical amplifier and coherent detection technologies in one link can offer a number of attractive features. The wavelength selectivity of coherent detection techniques allows more efficient use of the optical amplifier bandwidth and the excellent selectivity of the intermediate frequency (IF) filter offers improved rejection of optical noise over that of an optical filter.

This chapter is organized as follows: Section 5.1 contains a comparison between the semiconductor optical amplifier (SOA) and the erbium-doped fiber amplifier (EDFA). Section 5.2 contains the theoretical analyses of the performance of the links with optical amplifiers followed by Section 5.3 describing our experimental results showing the dependence of the SFDR on the received optical signal power. Finally, Section 5.4 contains the dynamic range versus link loss measurements for both coherent and direct detection links..

5.1 Semiconductor Optical Amplifiers Versus Erbium-Doped Fiber Amplifiers

There are basically two practical approaches to making optical amplifiers: laser-diode amplifiers/semiconductor optical amplifiers (SOA) and doped-fiber amplifiers [3]. For the latter, fibers doped with erbium -- the erbium-doped fiber amplifier (EDFA) --

has been the most successful. In this section, we characterize and compare these two types of optical amplifiers.

5.1.1 SOA Characterization Results

The SOA we used for our experiments is a BT&D SOA3100-1550, operating in the 1550 nm range of wavelengths. The SOA uses the same basic construction as the conventional Fabry-Perot semiconductor laser. The SOA devices are based on a 500 μm long buried heterostructure device made by the MOVPE process. The chip is anti-reflection coated on both facets with a residual reflectivity of less than 0.5%. It is this reduction in the facet reflectivity from its uncoated reflectivity which produces a near traveling wave amplifier [4].

The following set of figures shows the characteristics of the SOA. Fig. 5-1 shows the noise spectra of the SOA, with the optical signal center wavelength of 1532 nm and a 3 dB bandwidth of 47.2 nm. More detailed views of the noise spectrum for various SOA bias currents, with 1 dB/div in the vertical axis, are shown by the series of spectra in Fig. 5-2. These figures show that the SOA amplifier gain exhibits ripples, demonstrating the effects of residual facet reflectivities. Later, we will show that because of these ripples, the SOA interacts with the signal generating IMDs.

Fig. 5-3(a) shows the output optical power versus the input optical power of the SOA with various SOA bias currents, with Fig. 5-3b showing the corresponding gain versus input optical power curves. The latter demonstrates the gain saturation effect. The measured gain values are lower than specified since the wavelength we used was that of our transmitter laser at 1545 nm, where the gain is about 2 dB lower than at the peak/center wavelength, as shown in Fig. 5-1.

To measure the noise figure of the optical amplifier for a given optical input power P_{in}, we characterized the SOA using the HP Lightwave Signal Analyzer. The amplifier noise figure can be calculated as follows:

$$F = \frac{P_{in}\left(RIN_{out} - RIN_{in}\right)}{2h\nu} \tag{5.1}$$

where RIN_{in} is RIN measured at the amplifier input and RIN_{out} is the RIN measured at the amplifier output. Measurements reveal the noise figure of the SOA to be 11.7 dB.

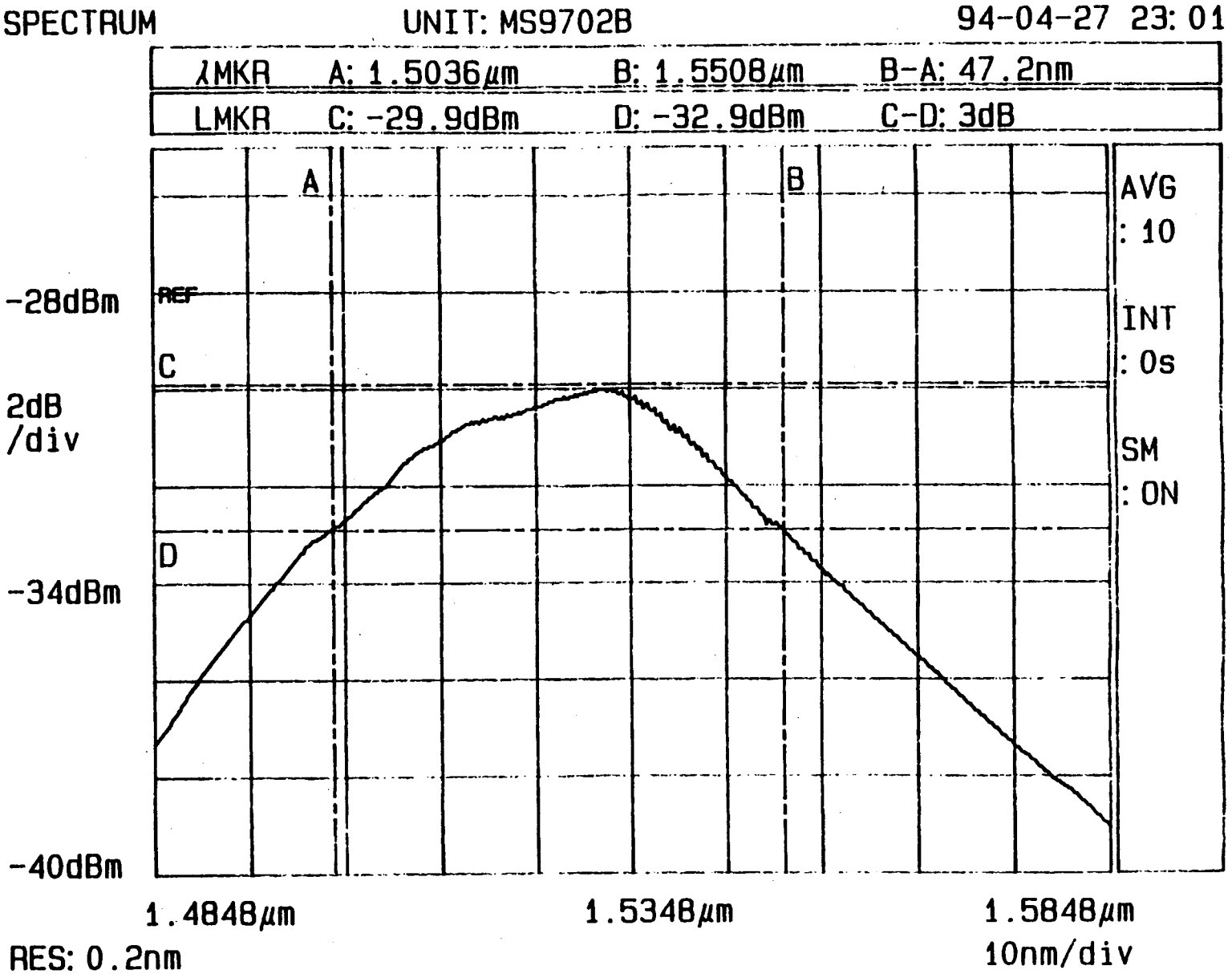

Fig. 5-1. SOA Fluorescence spectra showing its 3 dB bandwidth.

A154213

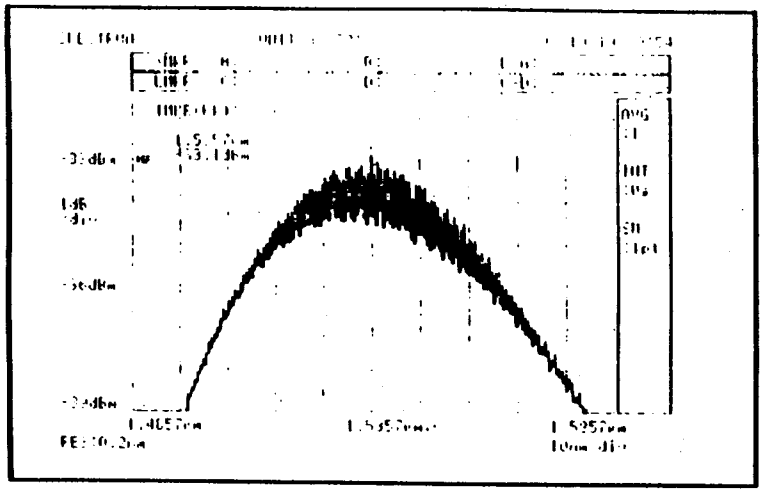

@ 50mA

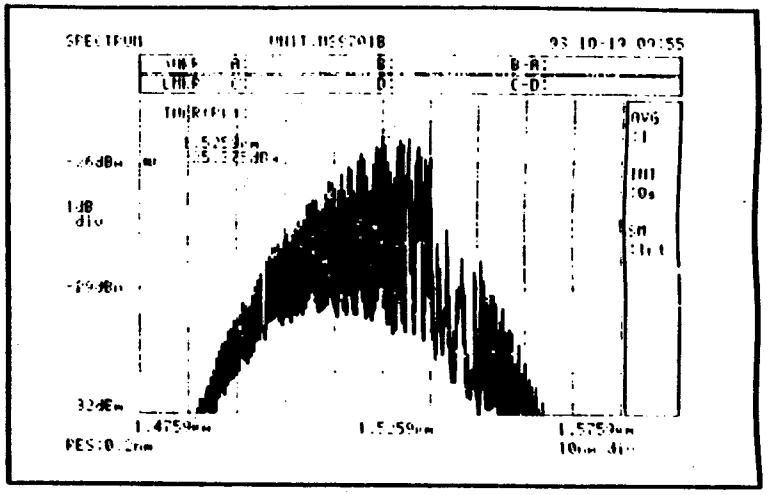

@ 75mA

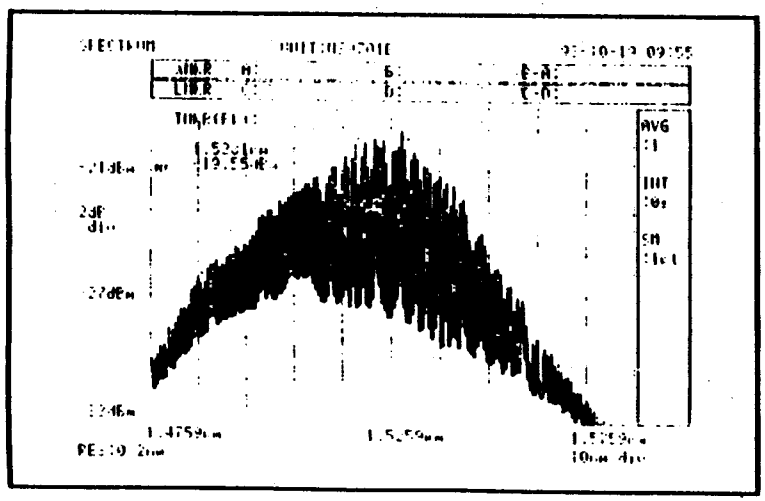

@ 100mA

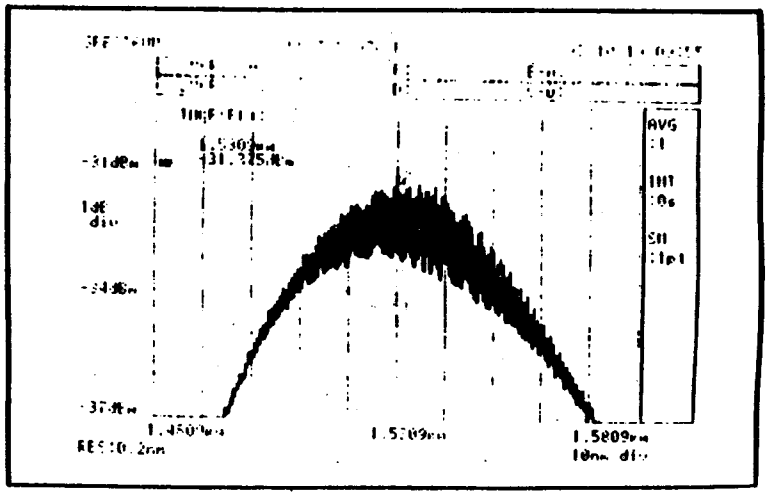

2.50dB ripple point @ 55mA

Fig. 5-2. Detailed SOA Fluorescence spectra for different values of SOA bias current.

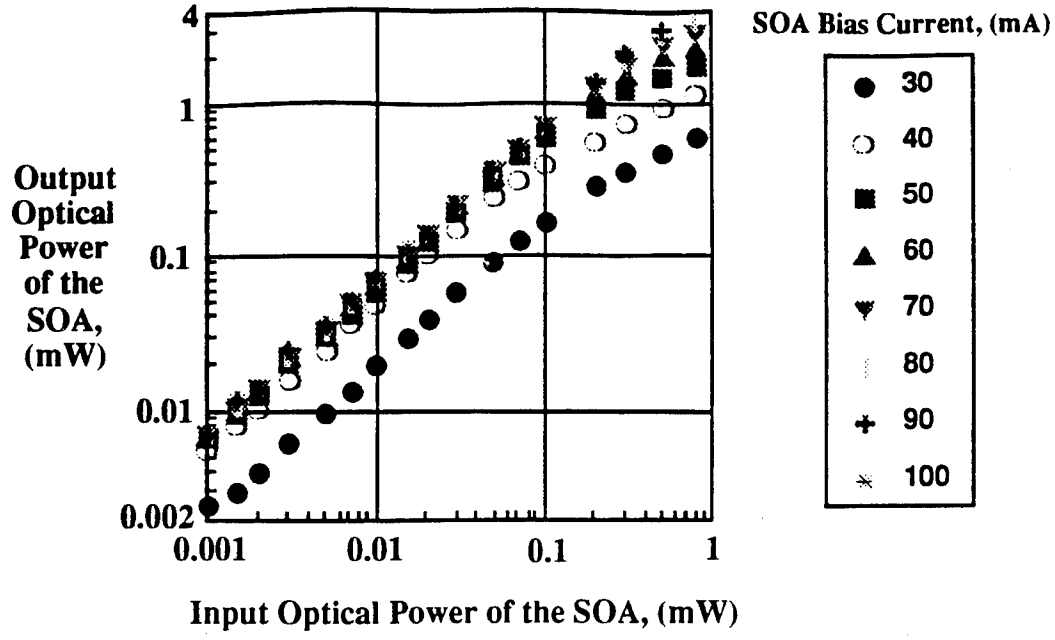

Fig 5-3(a). Output vs. input optical power characteristic of the SOA used in our experiments.

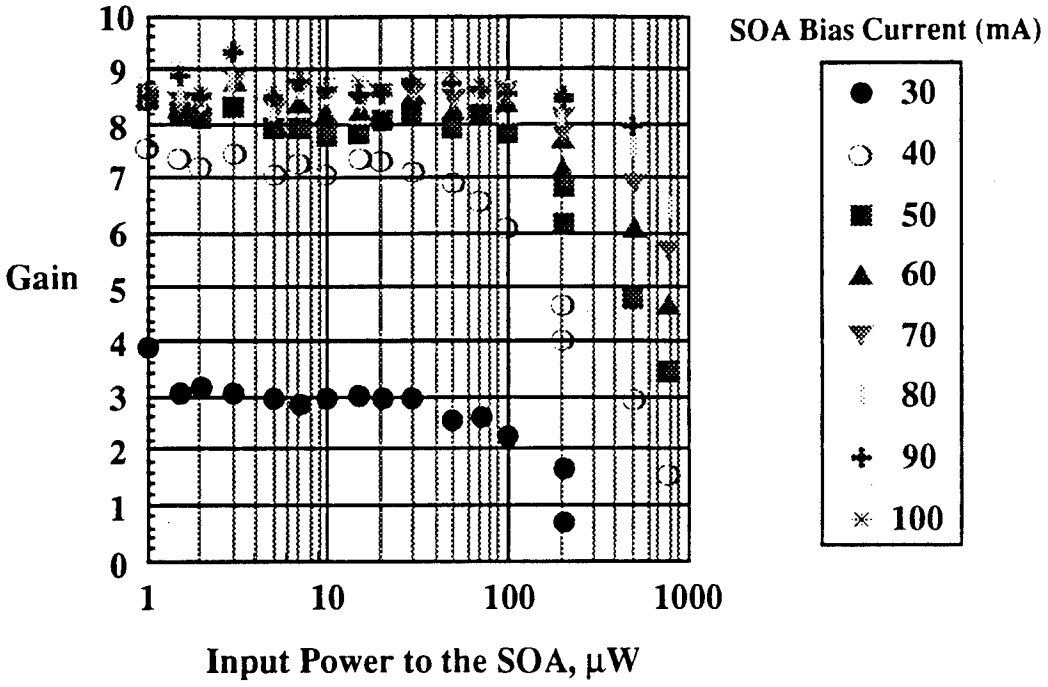

Fig. 5-3(b). Gain vs. input optical power characteristic of the SOA used in our experiments.

5.1.2 EDFA Characterization Results

The EDFA we used in our experiments is a Furukawa Electric ErFA1030. Fig. 5-4 shows the EDFA configuration. The erbium-doped fiber is pumped in a backward pumping configuration by a 1480 nm high power semiconductor laser via a WDM coupler. In-line isolators are located in the input and output ports of the amplifier to suppress optical feedback and reduce system noise.

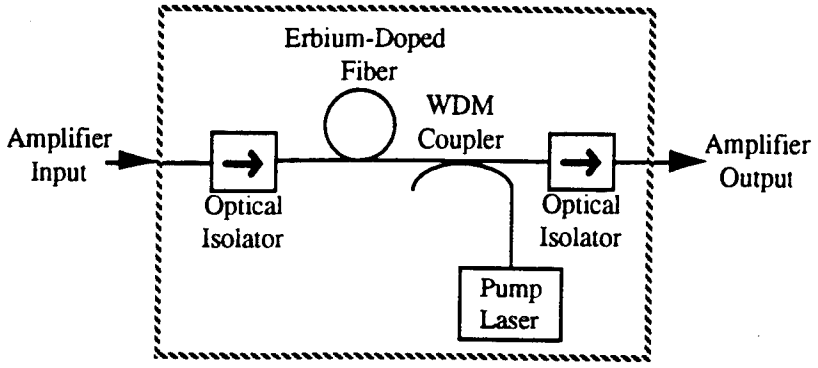

Fig. 5-4. Configuration of the erbium-doped fiber amplifier used in the experiments.

Fig. 5-5 shows the noise spectra of this EDFA, with the optical signal center wavelength of 1552 nm (disregarding the peak at 1532 nm) and a 3 dB bandwidth of about 35 nm.

Fig. 5-6(a) shows the output optical power versus the input optical power of the EDFA with various pump laser currents, with Fig. 5-6(b) showing the corresponding gain versus input optical power curves. The latter demonstrates the gain saturation effect.

Using the same method as described in the previous section, the noise figure of the EDFA was determined to be 10 dB.

5.1.3 Comparison between their characteristics

From the results of the two previous sections and also from our observations during experiments, we summarize the characteristics of these two optical amplifiers in Table 5-1.

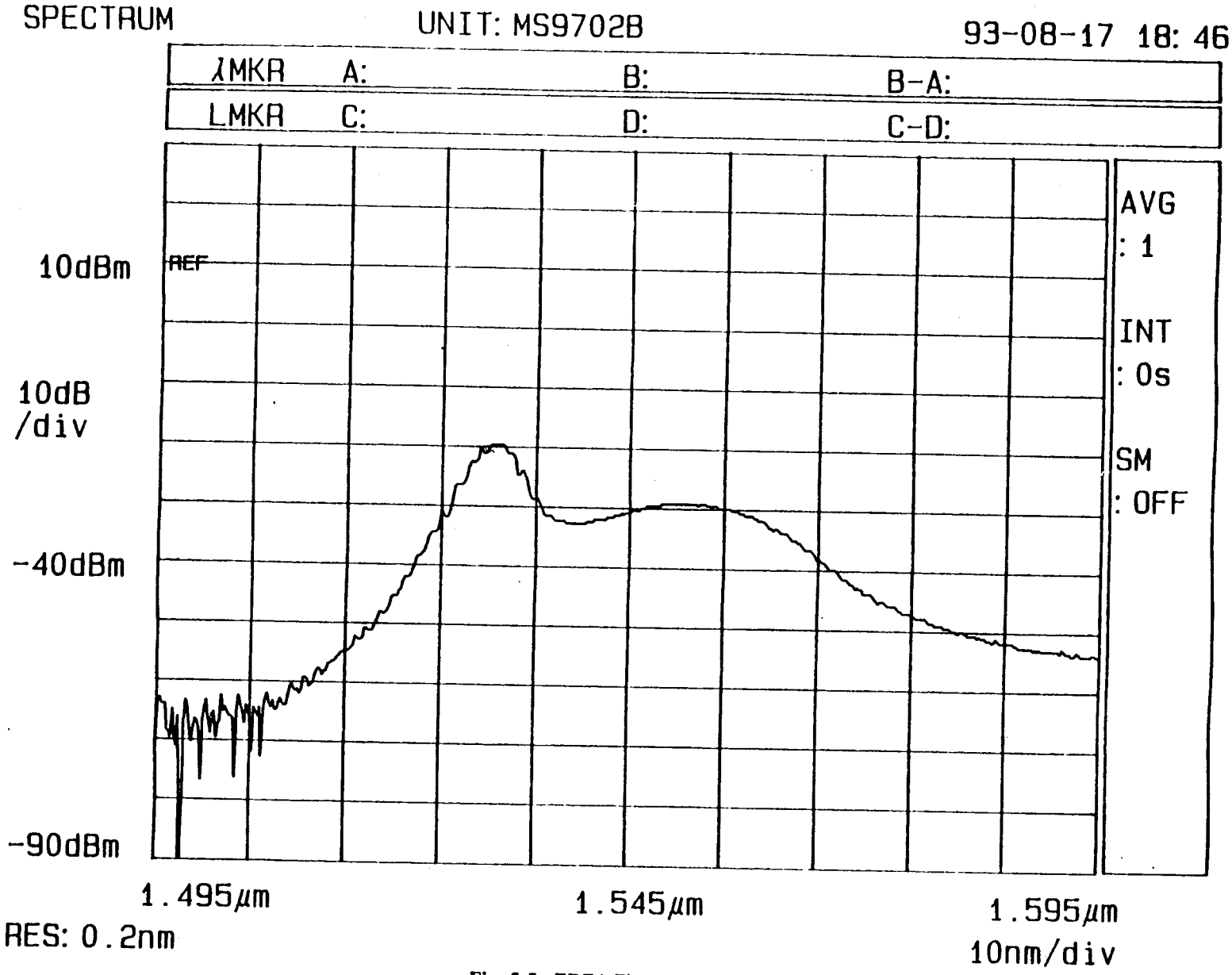

Fig. 5-5. EDFA Fluorescence spectra.

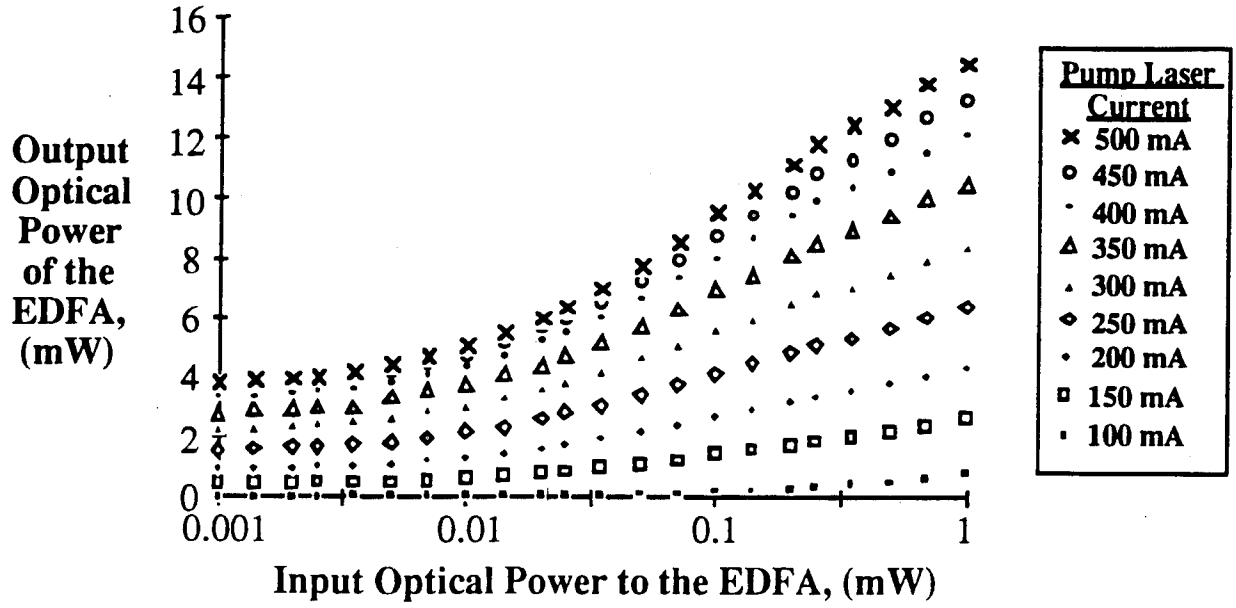

Fig. 5-6(a). Output versus input optical power characteristic of the EDFA shown in Fig. 5-4.

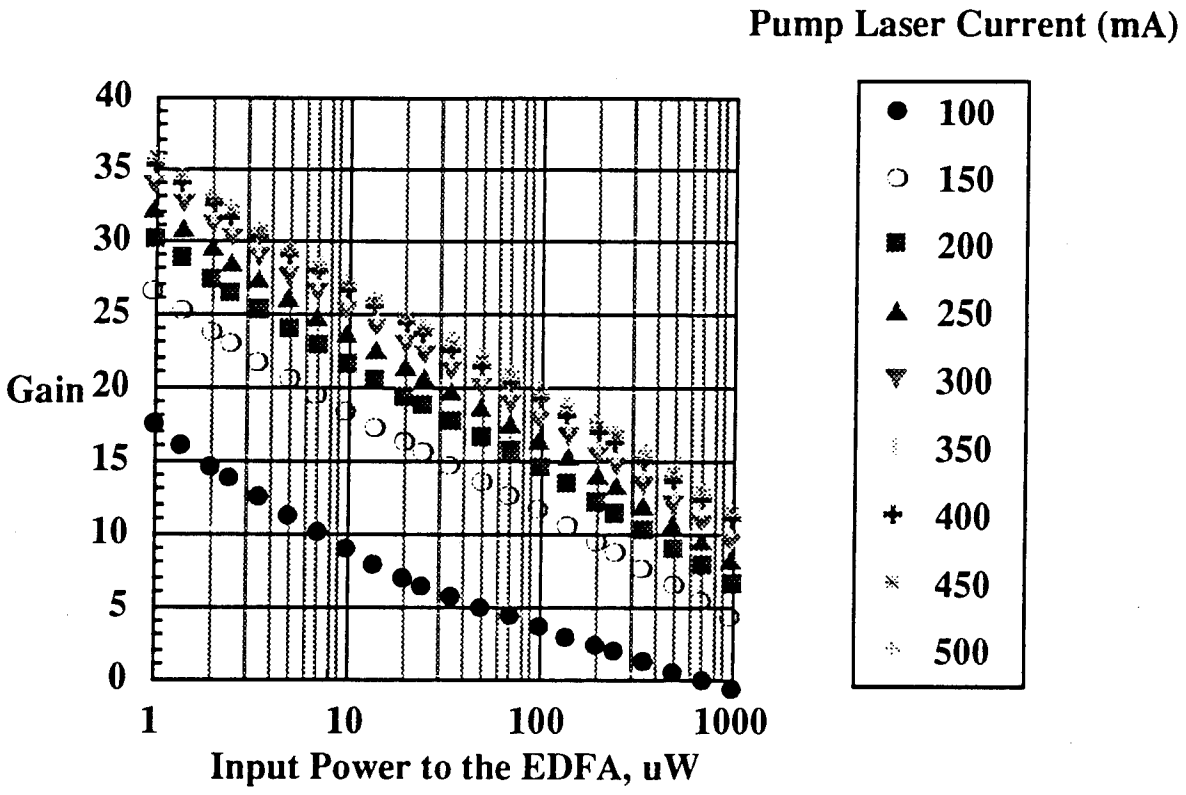

Fig. 5-6(b). Gain vs. input optical power characteristic of the EDFA shown in Fig. 5-4.

Table 5-1. Comparison Between an SOA and an EDFA.

	Semiconductor Optical Amplifier	Erbium-Doped Fiber Amplifier
3 dB Bandwidth, nm	47.2	35
Saturation Output Power, mW	4	14
Maximum Gain, dB	9	35
Noise Figure, dB	11.7	10
Polarization Sensitivity	4.5 dB difference between TE and TM modes	insensitive
Facet Reflectivity Problem	Critical	None
Resonance Peak	None	Present at 1532 nm
Coupling Losses	Higher than EDFA	Negligible
Temperature Sensitivity	Requires a temperature controller	Insensitive (except the pump laser)
Wavelength Ranges	800, 1300, 1550 nm	1550 nm 1300 nm (?)
Intregratability	Possible	Difficult

Table 5-1 can explain why at present, EDFAs are more attractive: due to their higher output power, larger gain, lower noise figure, polarization and temperature-insensitivity, and lower or negligible coupling losses. SOAs are still under consideration and in the future, the interest may switch from EDFAs to SOAs, especially since researchers are working at reducing the facet reflectivities and at obtaining higher output powers and gain. SOAs also have the potential to be integrated with other optical and electrical devices, and they easily work with various wavelength ranges.

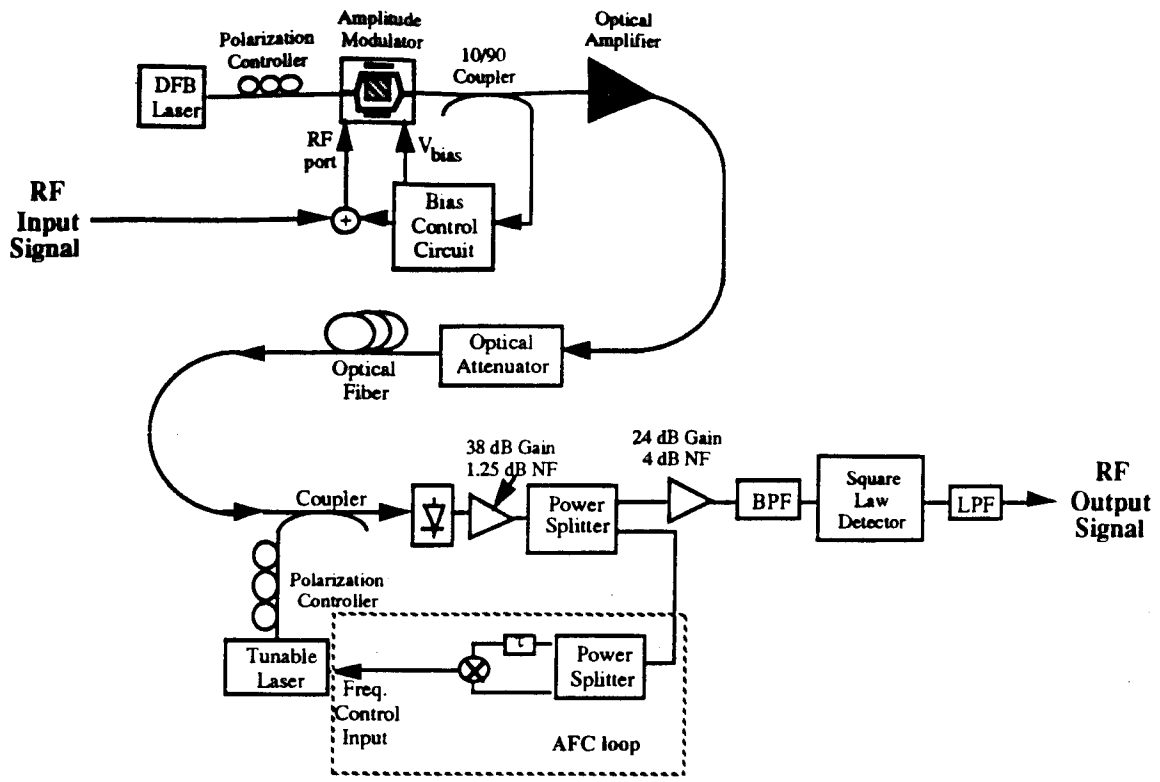

Fig. 5-7. The block diagram of an externally modulated coherent AM link using an optical amplifier.

5.1.4 Link Performance Comparison: Experimental Results

The experimental set-up used to compare the performance between an SOA and an EDFA in a coherent AM link is shown in Fig. 5-7. For one set of measurements we used the SOA in the link, and for another set we used the EDFA. The SFDR of these two links as a function of the received optical signal power is shown in Fig. 5-8.

Results show that the link using the EDFA exhibited a higher SFDR (by up to 5 dB) than the corresponding coherent AM link using the SOA. The reason for the poorer performance for the SOA link is primarily due to ripples in the SOA spectra, caused by the residual facet reflectivities. Because of these ripples, the nonlinear gain response of the SOA interacts with the signal, generating its own IMDs and thus, giving a worse SFDR than the EDFA link.

It is fair to conclude that for coherent AM links, a better dynamic range is achieved using an EDFA. Work is still needed to reduce the facet reflectivities of SOAs. In the succeeding sections, we will focus on investigating the performance, properties and behavior of coherent AM links using an EDFA. We begin with Section 5.2 giving a

theoretical overview of the impact of optical amplifiers on coherent links and comparing the results with direct detection links.

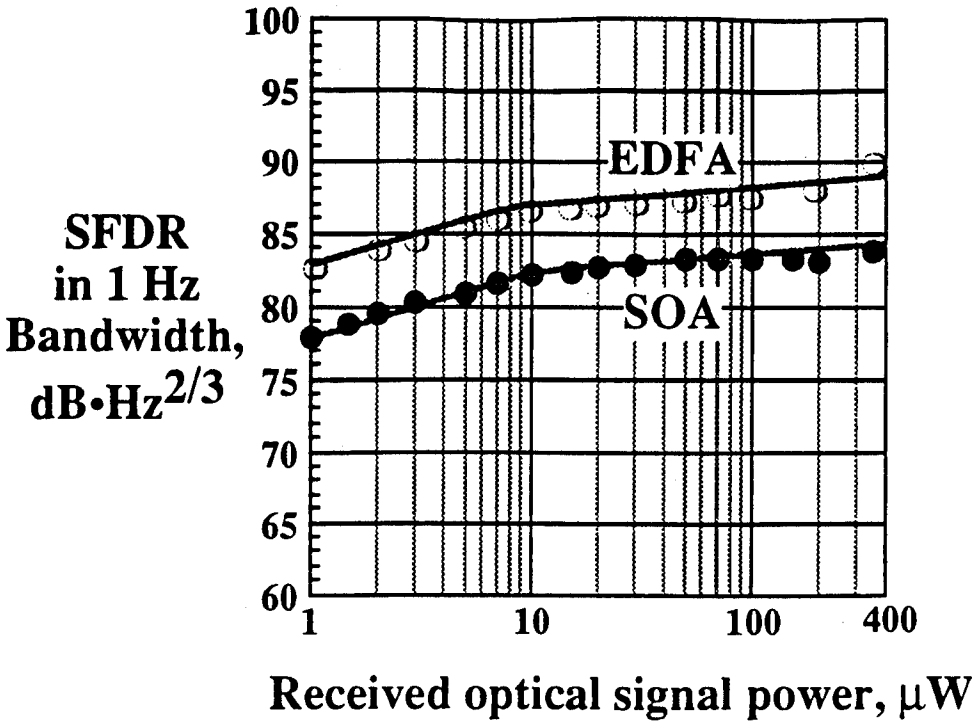

Fig. 5-8. Spurious-free dynamic range vs. receiver optical power for the coherent AM link with an SOA and an EDFA.

5.2 Theoretical Analysis

An optical amplifier is added to a coherent AM link to form an externally modulated optically amplified coherent AM link shown in Fig. 5-9. The received optical signal is amplified directly before mixing with the local oscillator laser (LO) output field. The IF filter removes excess ASE noise before the square law detector. The definitions of the mathematical symbols used in this analysis are listed in Table 5-2. The output SNR of the link is given by:

$$SNR = \frac{4m^2R^4G^2P_s^2P_{LO}^2}{8R^2GP_sP_{LO}\eta B + \eta^2 B(2B_{IF} - B)} \tag{5.2}$$

where

$$\eta = \eta_{th} + 2qR(GP_s + P_{LO}) + 2R^2GP_sP_{LO}10^{RIN/10} + 4R^2G(G-1)P_{LO}n_{sp}h\nu. \tag{5.3}$$

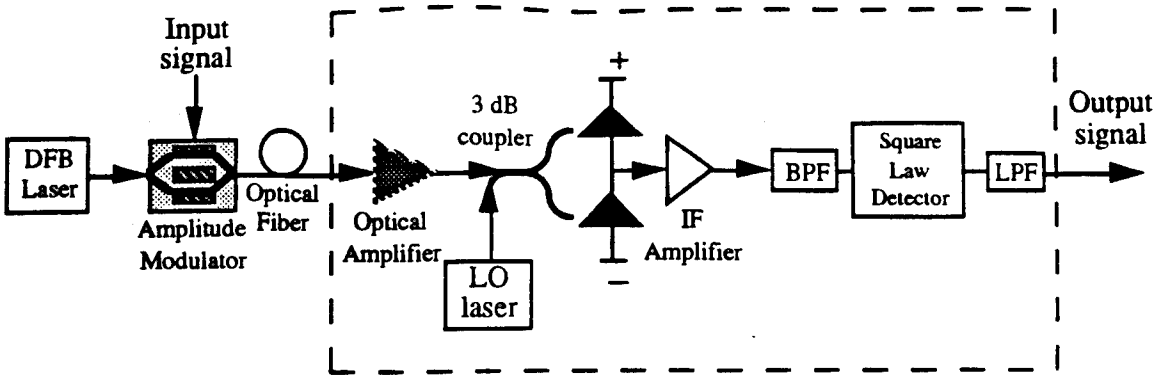

Fig. 5-9. The block diagram of an externally modulated optically amplified coherent AM link.

Table 5-2. Definitions and numerical values of system parameters.

B	Signal bandwidth
B_o	= 30 nm, Optical bandwidth
B_{IF}	= 2B, Electrical IF bandwidth
G	= 15 dB, Optical gain
hn	= 1.28×10^{-19} J, Photon energy
m	Modulation index
n_{sp}	= 1, Spontaneous emission factor
h_{th}	= 330 pA^2/Hz, Thermal noise
P_s	Received optical power
P_{LO}	= 10 dBm, Local oscillator power
q	= 1.602×10^{-19} C, Electronic charge
R	= 1.25 A/W, Responsivity of the photodetector
RIN	Laser relative intensity noise (dB/Hz)

The last term in Eq. (5.3) represents the LO-ASE beat noise. An advantage of coherent detection with amplification is that the LO power is, in general, sufficient to ensure that the receiver is truly LO-ASE beat noise-limited, without recourse to a narrow-band optical filter to reduce ASE-ASE beat noise.

The SFDR for this link is given by:

$$SFDR = 4\left[\frac{4R^4G^2P_s^2P_{LO}^2}{8R^2GP_sP_{LO}\eta B + \eta^2 B(2B_{IF} - B)}\right]^{2/3} \tag{5.4}$$

In Fig. 5-10, the SFDRs are plotted against the received optical power for this link and three other links: a coherent AM link and direct detection links with and without an optical preamplifier. The numerical values of the system parameters are listed in Table 5-2. For small received optical power (P_S < 1mW), the amplified coherent AM link performs better than the conventional direct detection link because the gain of the optical preamplifier and the strong LO power lead to shot noise-limited performance while the conventional direct detection link is thermal noise-limited. As the optical power increases, the conventional link approaches the shot noise limit. In this regime, the conventional link performs better because the amplifier coherent link has a worse receiver sensitivity (due to the ASE noise of the optical amplifier and due to the extra processing of the coherent detection technique). The shot noise-limited SFDR for these links are listed in Table 5-3.

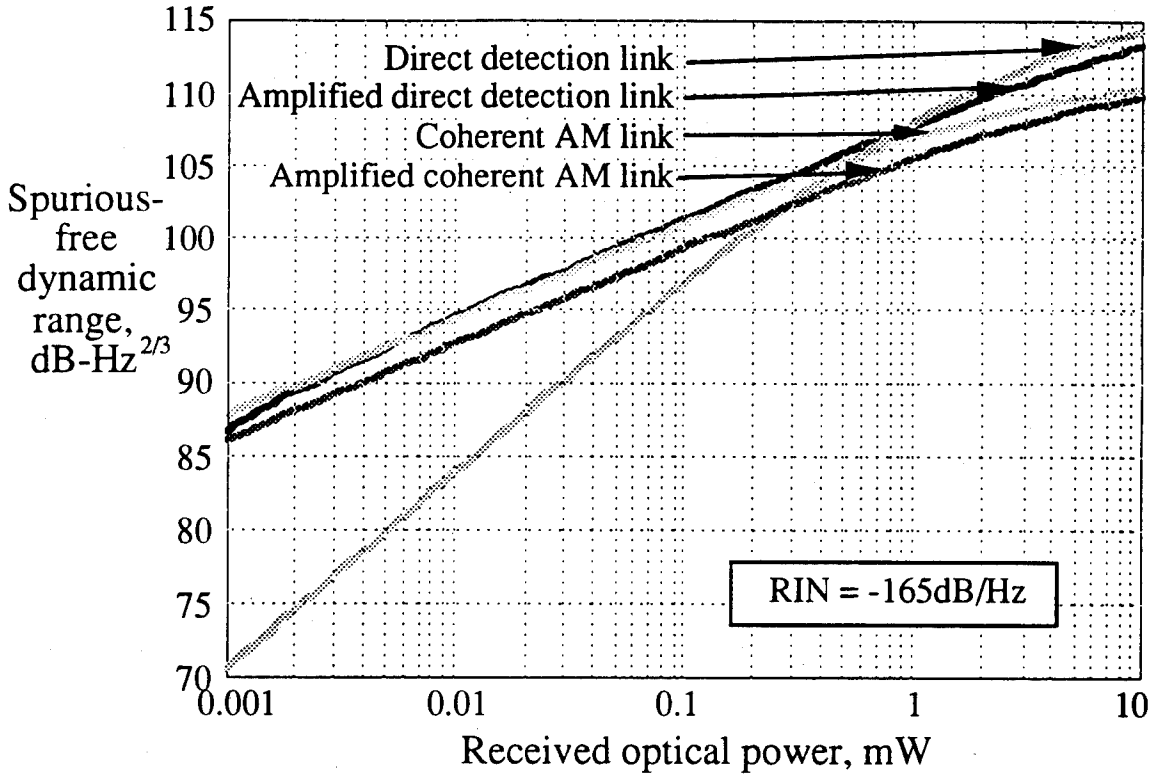

Fig. 5-10. Spurious-free dynamic range vs. receiver optical power for the direct detection and coherent AM links with and without an optical preamplifier.

Table 5-3. Shot noise-limited and RIN-limited spurious-free dynamic ranges for the direct detection and coherent AM links with and without an optical amplifier.

	Shot noise-limited *SFDR* ($dB\text{-}Hz^{2/3}$)	RIN-limited *SFDR* ($dB\text{-}Hz^{2/3}$)
Direct detection link	$4\left(\frac{RP_s}{2q}\right)^{2/3}$	$\frac{4}{(RIN)^{2/3}}$
Amplified direct detection link	$4\left(\frac{RP_s}{4q}\right)^{2/3}$	$\frac{4}{(RIN)^{2/3}}$
Coherent AM link	$4\left(\frac{RP_s}{4q}\right)^{2/3}$	$\frac{4}{(4RIN)^{2/3}}$
Amplified coherent AM link	$4\left(\frac{RP_s}{8q}\right)^{2/3}$	$\frac{4}{(4RIN)^{2/3}}$

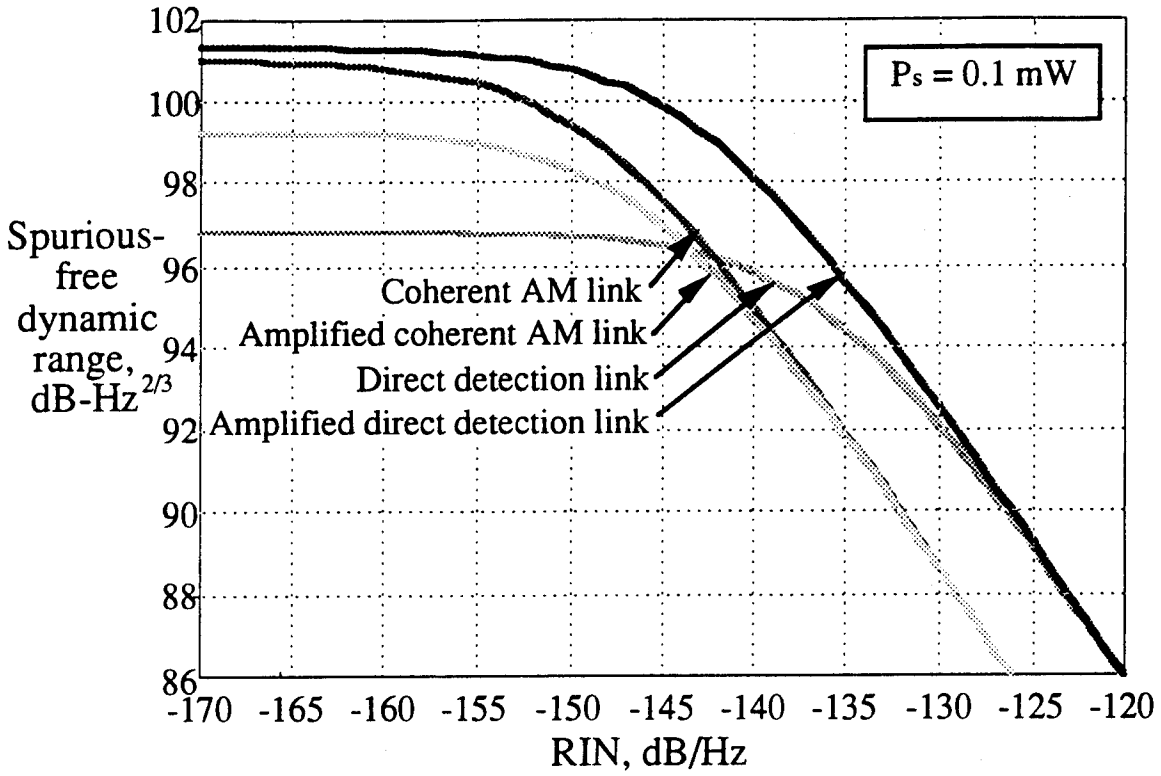

Fig. 5-11. Spurious-free dynamic range vs. RIN for the direct detection and coherent AM links with and without an optical amplifier.

Because an optical amplifier adds ASE noise to the signal, the performance of the amplified coherent link is degraded as compared to the coherent link. The minimum noise figure for an ideal amplifier is 3 dB (corresponds to $n_{sp} = 1$). The 3 dB noise figure stems from the fact that not only the real ASE spectrum but also the image ASE spectrum is

down-converted by the LO and folded into the IF band. It is possible, in principle, to eliminate the image LO-ASE beat noise using of optical filtering or image-rejection techniques; then, the amplified coherent link should achieve the same shot noise-limited SFDR as the coherent link and amplified direct detection link.

The relative intensity noise (RIN) can degrade the performance of all four links. In Fig. 5-11, the SFDRs are plotted against the RIN. It can be seen that all links behave similarly. For the amplified coherent link, when RIN starts to dominate the system noise (RIN worse than -150 dB/Hz), the link's performance approaches that of the unamplified coherent AM link. Comparing with the direct detection links, RIN starts to affect the system's performance of the coherent links at a lower RIN level. The RIN-limited SFDR of coherent links is 4 dB worse than that of direct detection links; this penalty is due to the squaring operation in the coherent AM receiver. The performance of the coherent AM receivers would be degraded further if a single photodetector receiver were used instead of the balanced receiver shown in Fig. 5-9.

5.3 Experimental Results: Impact of Received Optical Power

This section deals with the performance of four experimental optical links we constructed: (a) a conventional direct detection link, (b) an amplified direct detection link, (c) a coherent AM link, and (d) an amplified coherent AM link. The block diagrams of the experimental externally modulated direct detection and coherent AM links which we constructed and investigated are shown in Fig. 5-12. Similar to the previous theoretical section, we investigated four analog links: (a) a direct detection link without any optical amplifiers, Fig. 5-12(a); (b) a direct detection link with an optical amplifier, Fig. 5-12(a); (c) a coherent link without any optical amplifiers, Fig. 5-12(b); and (d) a coherent link with an optical amplifier, Fig. 5-12(b).

Using the variable optical attenuator shown in Fig. 5-12, we varied the received optical power for the coherent and direct detection links. The SFDR measurements of (a) direct detection, (b) optically amplified direct detection, (c) coherent detection, and (d) optically amplified coherent detection analog optical links, are shown in Fig. 5-13.

Fig. 5-13 shows that the optically amplified direct detection link and coherent links (with and without an optical amplifier) have a higher SFDR, by up to 4 dB, 7 dB, and 9 dB, respectively, than the corresponding direct detection link, when the received optical power is less than 10 mW. This is because the direct detection link is thermal noise-limited at these power levels while both coherent links are closer to being shot noise-limited. As the received optical power increases beyond 10 mW, the direct

detection link is not in the thermal noise-limited regime anymore and gives a higher dynamic range than both coherent links. The direct detection link gives the best performance as the received optical power increases beyond 80 mW. This is expected as the links approach shot noise-limited operation.

Both coherent links have similar behavior for the range of received optical power values examined, with the optically amplified coherent AM link having a 1 to 2 dB lower SFDR due to the large noise figure of the optical amplifier. As shown in Eq. (5.3), this penalty results from the ASE noise generated by the amplifier. As the received optical power increases beyond 10 mW, the SFDR of the coherent links starts to saturate, mostly due to the RIN of the lasers.

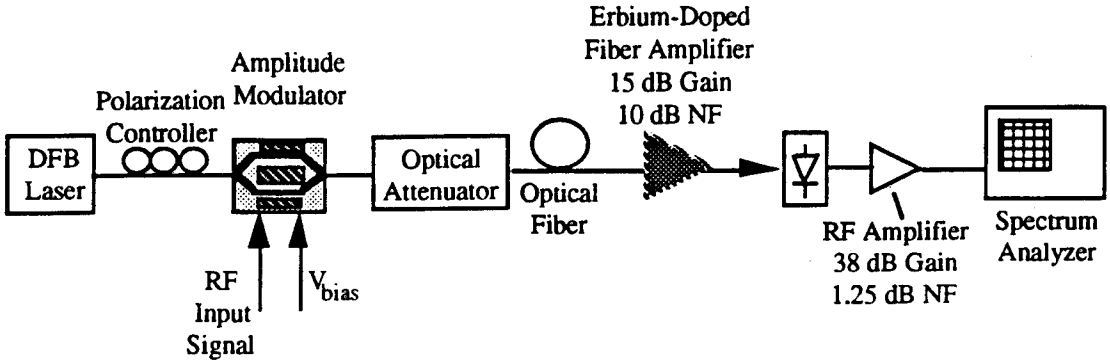

Fig. 5-12(a). The block diagram of the experimental externally modulated optical amplified direct detection link.

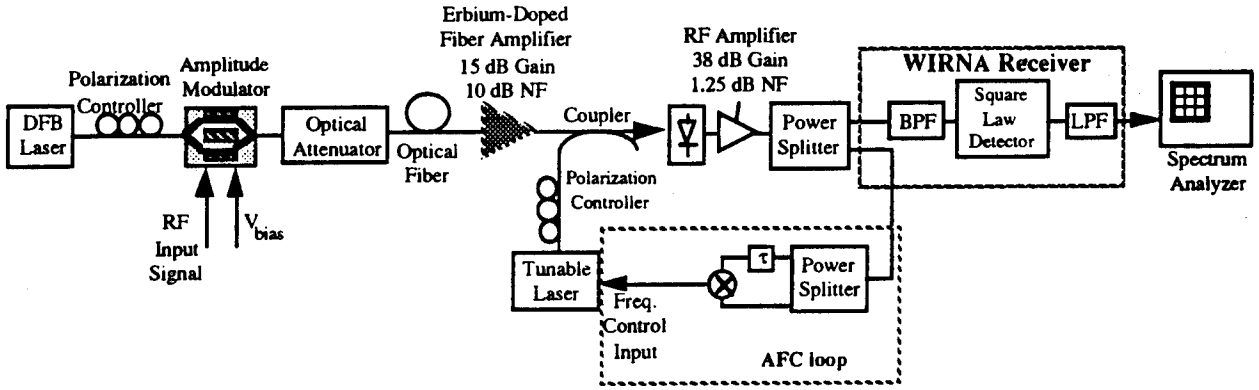

Fig. 5-12(b). The block diagram of the experimental externally modulated optically amplified coherent AM link.

For very small received optical powers, the optically amplified direct detection link has a lower SFDR than both coherent links. However, as the optical power increases to about 10 mW, the optically amplified direct detection link outperforms the coherent

links and gives the best SFDR out of the four links. Beyond 100 mW, the direct detection link has the best performance.

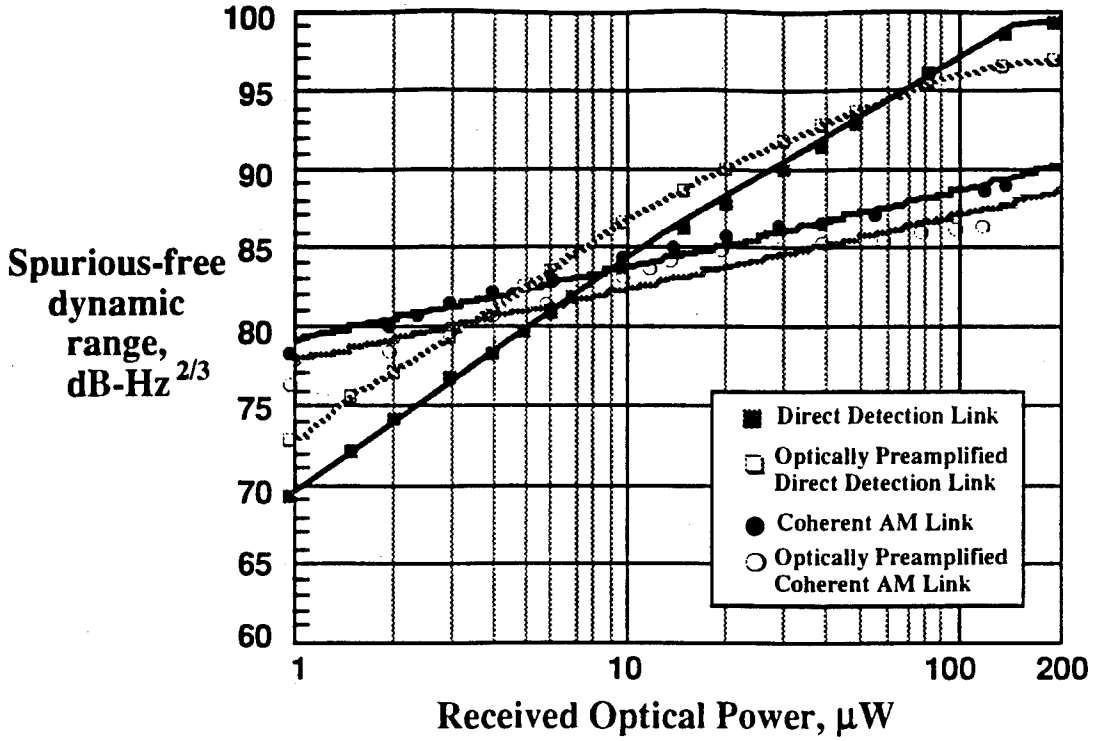

Fig. 5-13. Spurious-free dynamic range versus received optical power for coherent and direct detection links with and without optical amplifiers.

5.4 Dynamic Range Versus Link Loss Measurements

We have studied the major types of analog links: direct and coherent detection; with and without optical amplifiers (OA); and with OAs at different positions. Our goal is to answer the following question: what is the best analog link in terms of the spurious-free dynamic range (SFDR). The answer to this question is discussed below.

In this section, we continue the results initially presented in Section 4.7 and present measurements of the SFDR against the link loss for optically amplified links. Link loss can easily be converted into the number of destinations or splits for distribution systems and into transmission distance for point-to-point links. So, if one wants to build a system with a prescribed number of splits or transmission distance, the plot of SFDR versus link loss shows the best configuration.

With the development of optical amplifiers, the performance of both coherent and DD links is expected to improve, enabling both to handle higher link losses. Optical

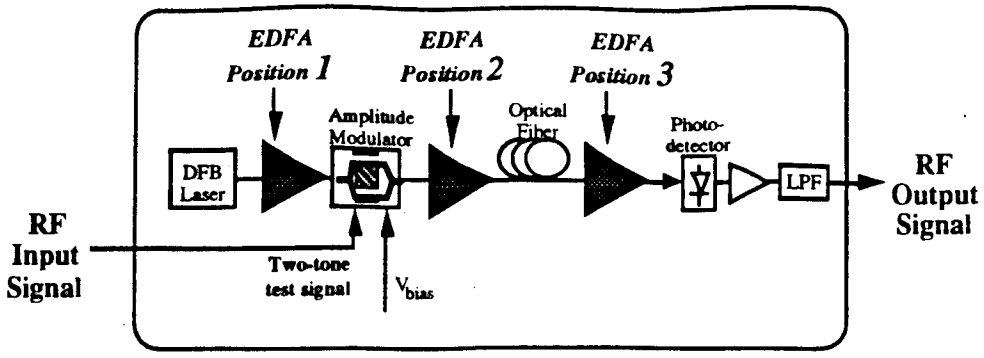

Fig. 5-14(a). Block diagram of the direct detection link showing the possible positions for an optical amplifier.

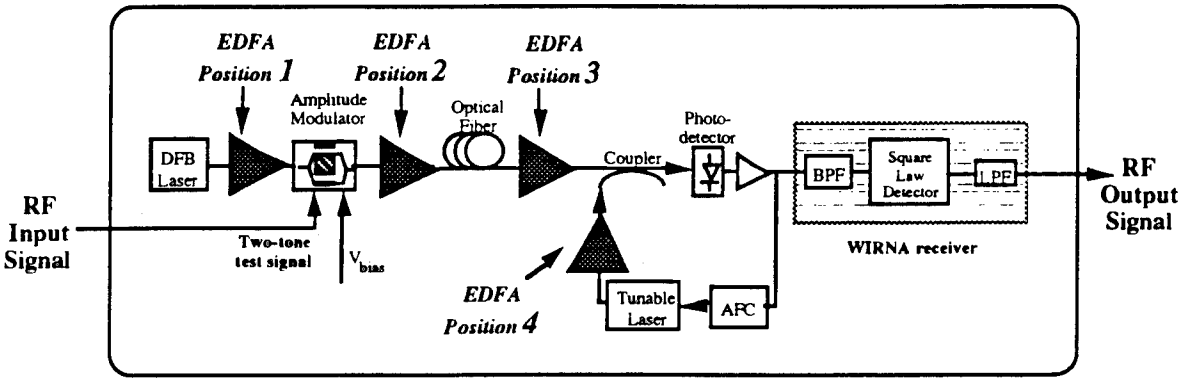

Fig. 5-14(b). Block diagram of the coherent AM link showing the possible positions for an optical amplifier.

amplifiers can be placed in the following positions in DD and coherent AM links (see Fig. 5-14):

(1) EDFA after the transmitter laser, to boost the signal power going into the electro-optic modulator (EOM);

(2) EDFA after the EOM, to amplify the signal going out into the transmission fiber; and

(3) EDFA before the optical receiver as a preamplifier, to amplify the signal at the receiver.

For the coherent link, there is one additional position:

(4) EDFA after the LO laser, to amplify the optical output of the semiconductor LO laser.

Fig. 5-15(a) and Fig. 5-15(b) show the SFDR versus link loss measurements for the DD and coherent AM links, respectively. In some link configurations, we could not measure the SFDR for link loss close to or at 1 mW since the photodetector we are using at our receiver saturates for optical powers above 1 mW. For both DD and coherent AM links, with an EDFA before or after the EOM, we increase the optical power going into the fiber; this enables the links to handle larger losses. Because of the loss in the modulator, the link with an EDFA after the EOM has a higher power into the fiber and can handle greater link loss than the links with the EDFA before the EOM.

The effect of the approximately 10 dB loss in the EOM is clearly seen in the DD case; the separation between the two curves, for the link with the EDFA before and after the EOM, is 10 dB. This phenomenon is not quite obvious in the coherent AM link, since the performance of the link is affected by other effects such as the RIN of the lasers and the much larger effect of the signal-ASE and ASE-ASE beat noises.

The main difference between the DD and the coherent AM links' curves is the flattening in the low loss region for the coherent case because of the impact of RIN for the single photodetector receiver. But overall, an EDFA still extends the link loss margin that can be handled by the coherent AM link.

For both DD and coherent links, the EDFA in the receiver gives poor SFDR performance because of the signal-ASE and ASE-ASE noises being the dominant noise terms. This is due to the fact that when the input power to the EDFA is smaller, the impact of the amplifier's ASE noise is stronger. Also, more ASE noise is collected at the receiver as compared to the cases when the EDFA is before and after the EOM, since for the latter cases the link loss attenuates the ASE noise while for the former all the ASE noise generated goes into the receiver.

Similar reasons explain the performance of the coherent AM link with the EDFA after the LO laser: the signal-ASE, LO-ASE, and ASE-ASE noises deteriorate the system performance significantly; all the ASE noise generated is collected by the photodetector since the EDFA is located at the receiver. When the EDFA is in the receiver, the performance is slightly better since the input power to the EDFA is larger when the EDFA is after the LO laser.

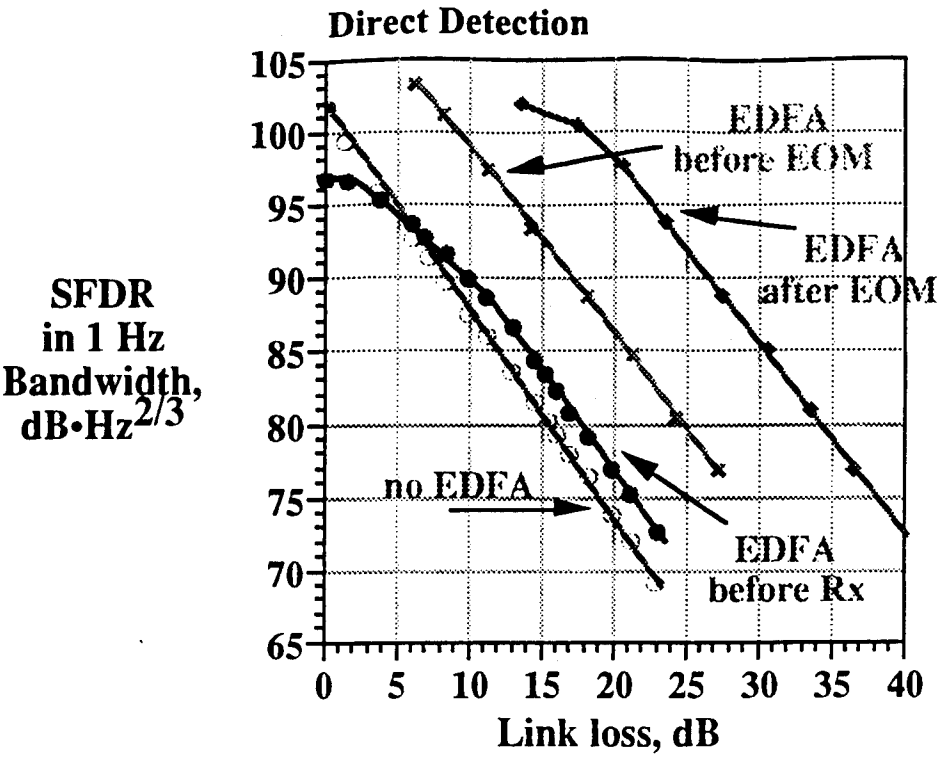

(a)

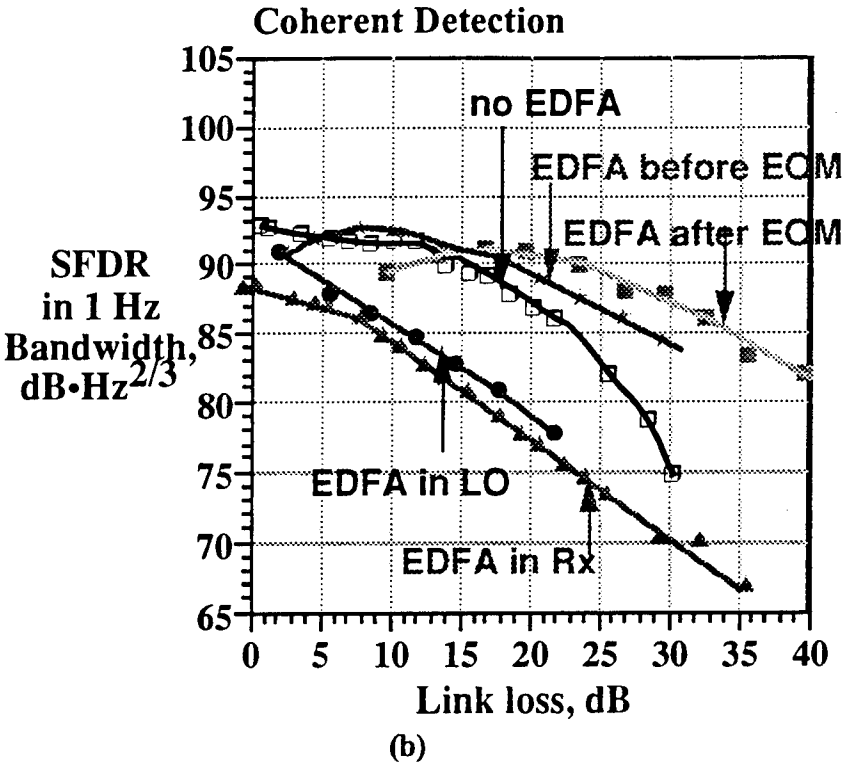

(b)

Fig. 5-15. Spurious-free dynamic range vs. the link loss for (a) the direct detection link, and (b) the coherent AM link, with an optical amplifier at different positions.

To summarize the results presented in Fig. 5-15, let us compare the performance of the best four links for specific ranges of link loss. The results are replotted in Fig. 5-16 and stated in Table 5-4. For medium loss (link loss between 10 to 25 dB), the DD links perform better because of the stronger impact of RIN on the coherent AM link. However, the coherent AM link outperforms the DD link for high loss (loss greater than 28 dB) links due to the better sensitivity of the coherent receiver caused by the presence of an LO laser.

Table 5-4. Summary: Best Link Design.

If the Link Loss, L, is:	The Best Link (in terms of SFDR) is:
0 dB < L < 7 dB	Direct Detection, no EDFA
7 dB < L < 13 dB	Direct Detection, EDFA before EOM
13 dB < L < 28 dB	Direct Detection, EDFA after EOM
L > 28 dB	Coherent Detection, EDFA after EOM

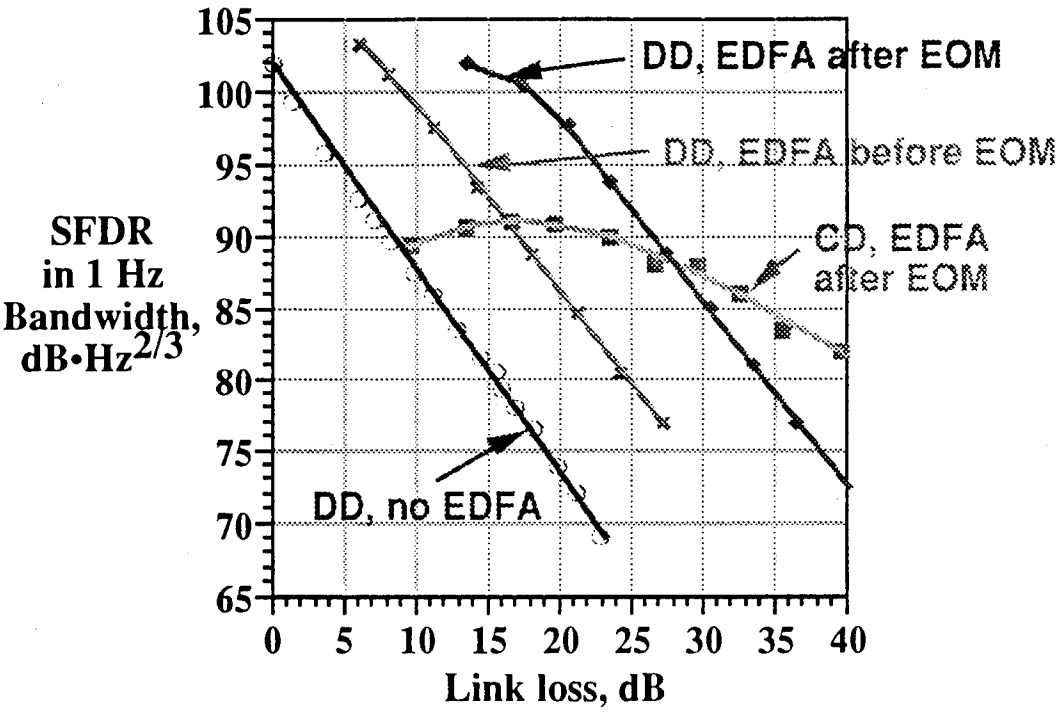

Fig. 5-16. Spurious-free dynamic range vs. the link loss: comparison of four of the best links.

5.5 References

[1] S. Ryu and Y. Horiuchi, "Use of an Optical Amplifier in a Coherent Receiver," IEEE *Photonics Tech. Letters*, vol. 3, no. 7, pp. 663-665, July 1991.

[2] K. E. Alameh and R. A. Minasian, "Optimization of Fiber Amplifier SCM Lightwave Video Systems Using Direct and External Modulation," IEEE/OSA *J. Lightwave Technol.*, vol. 11, no. 1, pp. 76-81, January 1993.

[3] P. E. Green Jr., *Fiber Optic Networks*, New Jersey: Prentice-Hall, Inc., 1993, p. 220.

[4] BT&D Technologies SOA1100 and SOA3100 Semiconductor Optical Amplifier Application Note.

Chapter Six

Improving the Link Performance

The previous chapters on coherent AM links focused on the properties of this link with regards to various system parameters and noise terms, and also the impact of using an optical amplifier. We have shown numerous experimental investigations to demonstrate the link properties and as proofs-of-concept. In these experiments, the dynamic range values which we obtained were usually limited by the equipment we had available. The performance of both coherent AM and direct detection links can be significantly improved by auxiliary subsystems and/or by using better optical and electrical devices. A discussion of these improvements and how they could be obtained is the focus of this chapter.

From its definition in Chapter 2, there are three ways to increase the link dynamic range [1]: (1) increase the received optical power; (2) lower the noise; and, (3) lower the nonlinearities generated in the link. In Section 6.1, we discuss the use of high power lasers as a way to increase the received optical power; followed by lower RIN lasers in Section 6.2 as one means of lowering the noise. Numerous ways of improving the electro-optic modulator (EOM) response to lower the nonlinearities generated in the link are presented in Section 6.3. Section 6.4 deals with the advantage of using a balanced or dual-detector receiver for the coherent AM link. In short, a dual-detector receiver has the combined effect of increasing the received optical power and lowering the noise. Section 6.5 contains a discussion on improving the link gain and noise figure. Finally, in Section 6.6 we present our experimental investigations on the dynamic range improvements brought about by using a cascaded linearized modulator structure and Nd:YAG lasers, which have higher power and lower RIN than conventional semiconductor lasers.

6.1 High-Power Lasers

The dynamic range, link gain, and noise figure improve, to varying degrees, with increasing optical power. For example, a 10 dB increase in the received optical signal power would increase the dynamic range by 6.7 dB and the link gain by 20 dB; and the noise figure would decrease by 10 dB. Thus, using higher power lasers for both the

transmitter and local oscillator can result in significant improvements in the link performance.

6.2 Lower Relative Intensity Noise (RIN) Lasers

As shown in Section 4.5.2, for larger optical LO and signal powers, laser relative intensity noise (RIN) causes degradation in the performance of the coherent AM link. This is expected for a coherent AM link employing a single-photodetector receiver as that of Fig. 4-9(a), since the impact of RIN is approximately proportional to the square of the received signal and LO optical powers. It would therefore be advantageous to use lower RIN lasers. As will be shown in Section 6.6, the use of lower RIN lasers may improve the dynamic range by up to 10 dB.

6.3 Improving the Electro-Optic Modulator Response

At high frequencies, externally modulated links tend to have a higher dynamic range and lower noise figure than directly modulated links [2, 3]. However, the dynamic range of externally modulated links are usually limited by the sinusoidal L-versus-V response (output Light-versus-drive Voltage) of the electro-optic modulator (EOM). Therefore, significant improvements in the dynamic range can be obtained by modifying the structure of the modulator so that it is more linear in the required region of operation.

There have been several schemes proposed in the literature for linearizing the response of an EOM such as

(a) electronic linearization - feedforward and predistortion linearization;
(b) polarization mixing;
(c) using a parallel modulator structure;
(d) modified directional coupler; and,
(e) using a cascade structure of modulators.

Several experiments have been conducted and their improvements are shown in Table 6-1.

Table 6-1. Comparison between the improvements from the various EOM linearization schemes.

	Maximum Reduction in 3rd order distortion	Maximum Dynamic Range Improvement	References
Electronic Feedforward	25 dB	> 8.4 dB	4
Electronic Predistortion	16 dB 16.4 dB	5.4 dB 5.5 dB	5 6
Polarization Mixing	14 dB 21	4.7 dB 7 dB	7 8
Parallel Modulator	20 dB	> 7 dB	9
Modified Directional Coupler	30 dB 33 dB	> 10 dB 11 dB	10 11
Cascaded Modulators	20 dB **34 dB**	7 dB **11.4 dB**	12 **This study**

We conducted our own experiments using the modulator in [13]; the results of which will be presented in Section 6.6.

6.4 Balanced or Dual-Detector Receiver

Similar to a digital link, the laser RIN problem of the coherent AM link can be minimized by using a balanced receiver [14]. Balanced receivers can eliminate most of the laser relative intensity noise in the receiver, and thus increase the coherent AM link's dynamic range. In addition, all of the signal and local oscillator powers are used effectively since no part of the optical signal is rejected, making it easier to operate in the shot-noise limit [15]. For example, when the received optical signal power is 10 mW, the LO power 10 mW, the RIN of both lasers is -150 dB/Hz, and the SFDR is 91 dB•$Hz^{2/3}$ for a single-photodetector receiver and is 102 dB•$Hz^{2/3}$ for a balanced receiver.

We will now present our theoretical investigation of the improvement in dynamic range by a dual-detector receiver for coherent analog optical links.

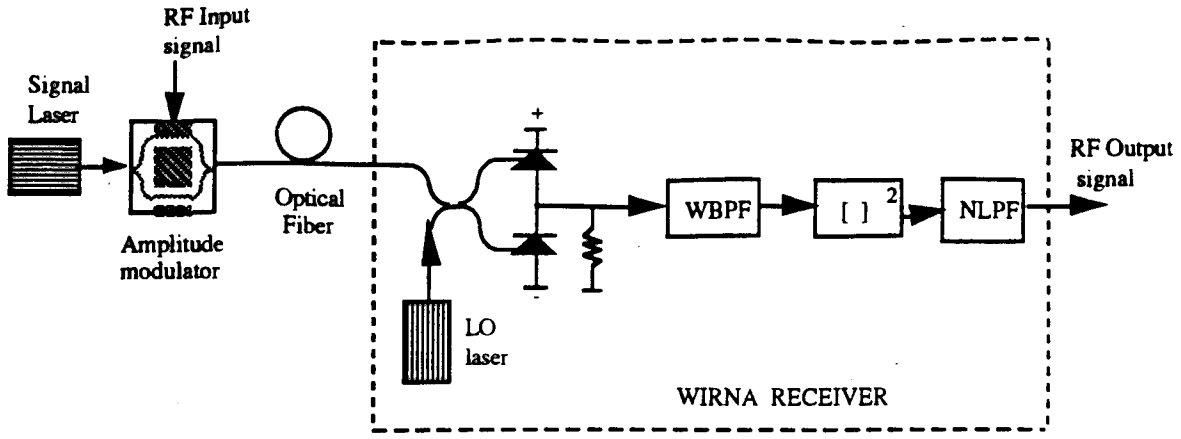

Fig. 6-1. Block diagram of coherent AM-WIRNA using a dual-detector receiver.

A coherent AM analog optical link using a dual-detector receiver is shown in Fig. 6-1. In the single-detector configuration, one of the coupler ports of the 3 dB coupler is not used and half of the optical power is lost. Assuming the two branches of the dual-detector receiver are perfectly balanced, the IF signals in the two photocurrents, i_1 and i_2, are 180 degrees out-of-phase. However, the LO RIN will be in phase. When the two photocurrents are subtracted, the IF signal power is increased while the LO RIN is attenuated. In this case, the combined additive noise density, h_d, at the output of the dual-detector is (see Table 4-1 for symbol definitions):

$$\eta_d = \eta_{th} + 2qR(P_s + P_{LO}) + 2R^2 P_s P_{LO} 10^{RIN/10} \tag{6.1}$$

The last term in (6.1) represents the RIN generated by the signal-times-LO product that is not attenuated in the balanced receiver. The spurious-free dynamic range for the dual-detector link is expressed as:

$$SFDR \approx 4\Gamma_{\phi}^{2/3}\left[\frac{A^4}{4A^2\eta_d B_2 + \eta_d^2 B_2(4B_1 - B_2)}\right]^{2/3} \tag{6.2}$$

where A and Gf are given by Eqs. (4.3) and (4.5), respectively. In Fig. 6-2, the dynamic range is plotted against the received optical power for a direct detection link and the two coherent AM links employing single- and dual-detector receivers. As the optical power increases, RIN starts to dominate and limits the dynamic range. In Fig. 6-2, we can see that the coherent AM links are more susceptible to RIN than the direct detection link. This is due to the strong LO power for the coherent AM links. Since the RIN power is

proportional to the optical power, the dynamic range would be limited to a value restricted by RIN. The RIN-limited SFDR for the three links are listed in Table 6-2 where a is the ratio of P_S and P_{LO} in dB. Fig. 6-2 indicates that using a dual-detector receiver in a coherent AM link improves the link dynamic range by up to 12 dB.

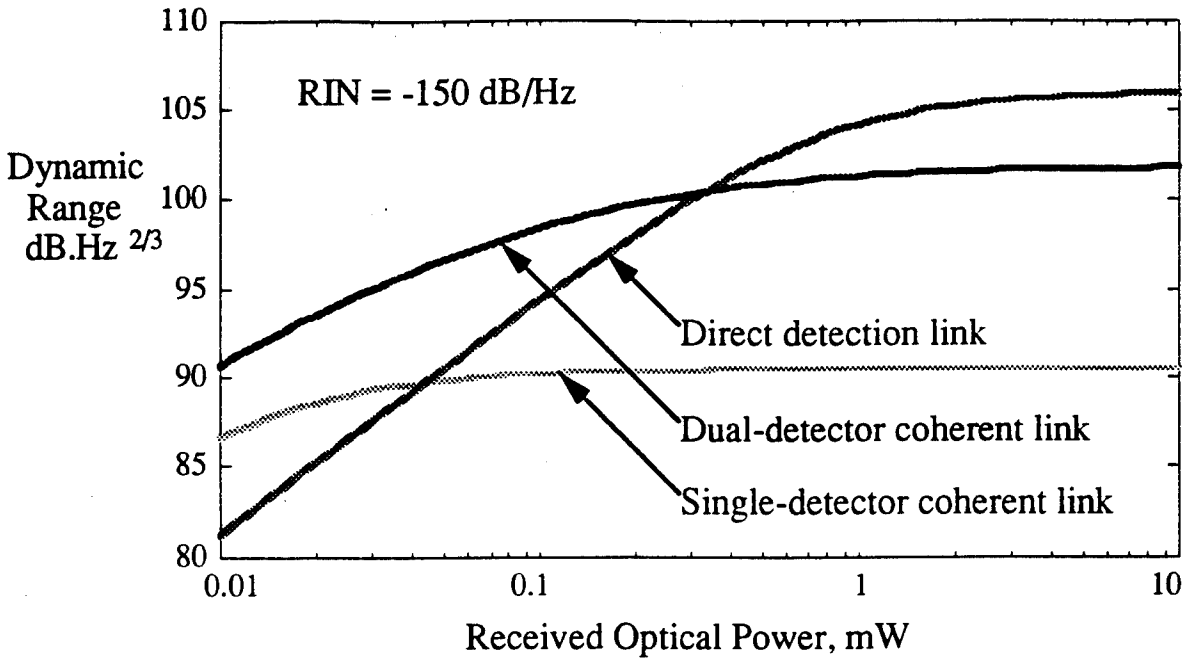

Fig. 6-2. Dynamic range vs. received optical power for coherent AM links and a direct detection link, for RIN = - 150 dB/Hz and $P_{LO} = P_S$+20 dB.

Table 6-2: RIN-limited SFDR.

Analog optical links	RIN-limited SFDR (dB·Hz$^{2/3}$)
Direct detection link	$6-\frac{2}{3}RIN$
Coherent AM link with single-detector	$4-\frac{2}{3}(\alpha+RIN)$
Coherent AM link with dual-detector	$2-\frac{2}{3}RIN$

6.5 Improving the Link Gain and Noise Figure

The obvious solution to improve the gain and noise figure of optical links would be to use high gain and low noise electronic amplifiers before and after the link. Let us look into this in more detail. In general, RF amplifiers can be added before and after the optical link (as shown in Fig. 6-3).

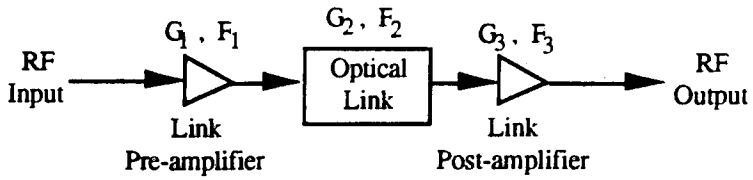

Fig. 6-3. Optical link with a pre-amplifier and a post-amplifier.

The overall gain G of this amplifier- optical link - amplifier system is given by:

$$G = G_1 G_2 G_3 \tag{6.3}$$

where G_2 is the optical link gain, and G_1 and G_3 are the preamplifier and post-amplifier gains, respectively. G_2 depends on the efficiencies of the electrical-to-optical and optical-to-electrical conversions.

The total noise figure for the system shown in Fig. 6-3 can be determined using the following expression:

$$F = F_1 + \frac{F_2 - 1}{G_1} + \frac{F_3 - 1}{G_1 G_2} \tag{6.4}$$

where F_2 is the optical link noise figure, and F_1 and F_3 are the preamplifier and post-amplifier noise figures, respectively.

For the case of optical links $G_1 G_2 \ll 1$ so that,

$$F \approx \frac{F_3 - 1}{G_1 G_2} \tag{6.5}$$

Expressing the terms in dB,

$$F \approx F_3 - G_1 - G_2 = F_3 - G + G_3 , \quad [\text{dB}] \tag{6.6}$$

This means that the noise figure can be minimized (a) using a high gain pre-amplifier G_1; (b) increasing the optical power (corresponds to increasing G_2); and (c) minimizing the noise figure, F_3, and gain, G_3, of the link post-amplifier. The sum of the noise figure and RF transfer ratio for the optical link is approximately constant:

$$F + G \approx F'_3 + G_3 = constant \tag{6.7}$$

Therefore, it is possible to construct a system having both desirable features of high gain and low noise figure.

Other ways of improving the link gain and noise figure include: using better components like EOM with lower losses [16], as well as the use of impedance matching at both the transmitter and receiver ends of the link (to minimize RF reflection losses) [17, 18] could also result in a link with a higher gain and lower noise figure.

6.6 Experiments with a Linearized Modulator, High Power, and Lower RIN Lasers

In this section, we present our experimental investigations of the effect of using a linearized modulator, high power and lower RIN lasers on the performance of the coherent AM link. We show that significant improvements in the dynamic range can be achieved by using better devices as discussed in the previous sections. We were limited to those devices we had in our laboratory; such as the Nd:YAG lasers and the photodetector that saturates at 1 mW of optical power. Even though this was the case, we were able to demonstrate that with these better devices we achieved the highest spurious-free dynamic range reported to date for a coherent AM link.

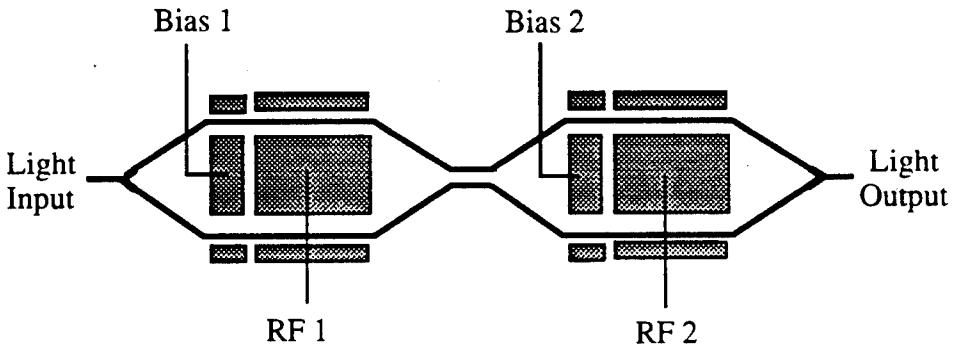

Fig. 6-4. Schematic representation of the Crystal Technology, Inc. linearized modulator.

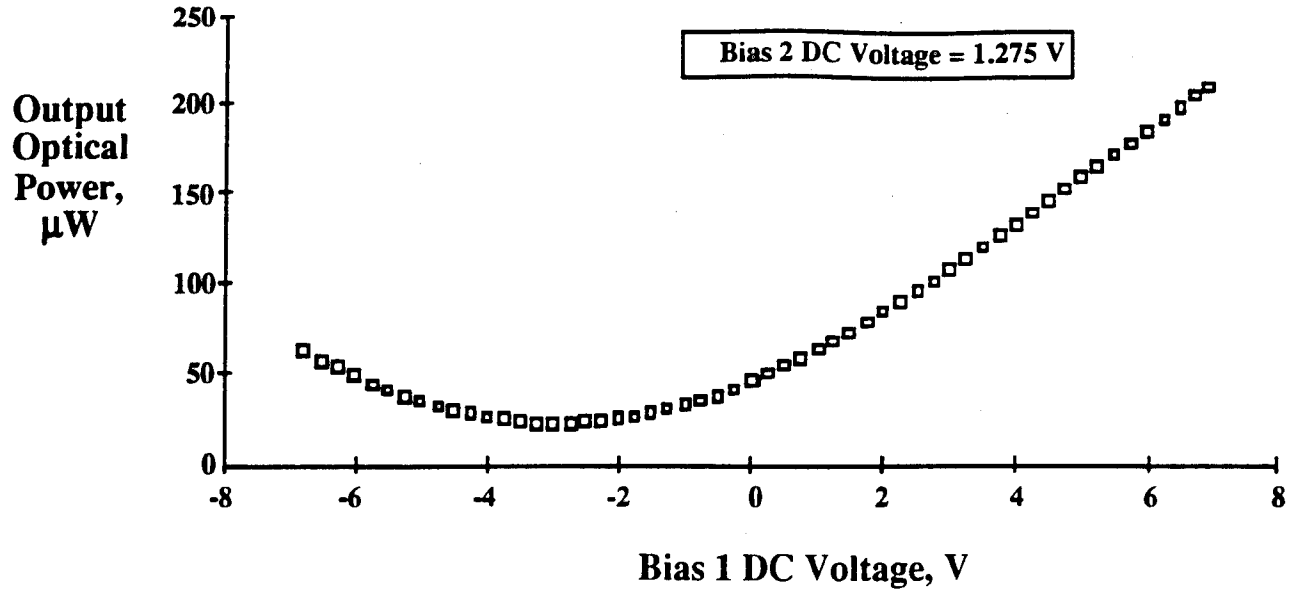

Fig. 6-5(a). Output optical power vs. bias 1 voltage transfer characteristic of the CTI linearized modulator; bias 2 is fixed at 1.275 V.

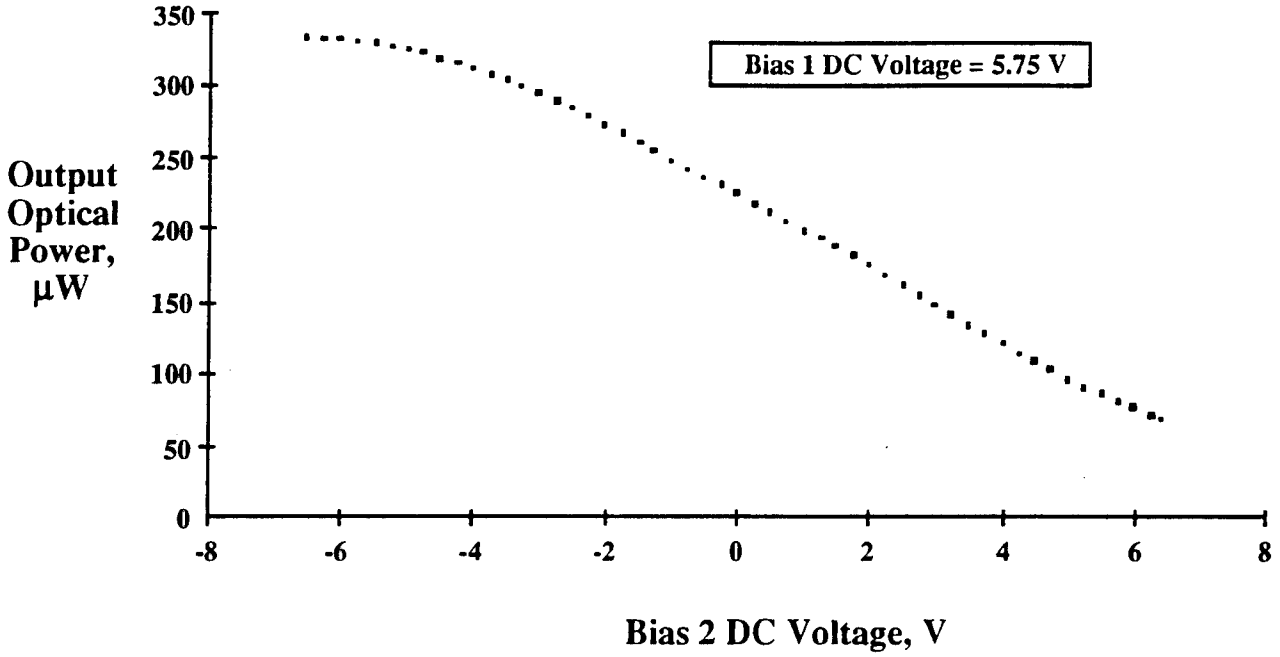

Fig. 6-5(b). Output optical power vs. bias 2 voltage transfer characteristic of the CTI linearized modulator; bias 1 is fixed at 5.75 V.

6.6.1 Description of the Modulator

In Section 6.3, we showed that significant improvements in the dynamic range can be obtained by modifying the structure of the modulator such that it is more linear in the required region of operation. We investigated the impact of a linearized modulator on the SFDR of the coherent AM link. The linearized modulator was lent to us by Crystal Technology, Inc. (CTI). The modulator's principle of operation is described in [13].

A schematic representation of the CTI linearized modulator is shown in Fig. 6-4. The modulator is completely passive; no electronic predistortion, feedback, or feedforward techniques are used. The linearization takes place entirely on the optical chip. The linearized modulator is actually a cascade of two modulators: the second modulator compensates for the nonlinearities introduced by the first modulator. Linearization is achieved by properly biasing both modulators and tuning the relative amplitude and phase of the two RF electrodes to suppress the second and third order harmonics and intermodulation products (IMP) [19].

We measured the transfer curves (output optical power versus bias voltage) of the linearized modulator. Since this modulator has two bias voltage ports, we obtained two transfer curves: one with the bias 2 voltage fixed and the bias 1 voltage varying, and vice versa. The results are shown in Figs. 6-5(a) and 6-5(b). The fixed voltages used are the bias voltages yielding the optimum linearization. Note from the figures that these voltages occur in the most linear region of the transfer curves.

6.6.2 System Description

The experimental set-up to measure the effect of the linearized EOM, higher optical power and lower RIN lasers on the performance of the coherent AM link is shown in Fig. 6-6. Nd:YAG lasers having a RIN of -164 dB/Hz and output power of +10 dBm (in the fiber) are used for both the transmitter and LO lasers.

The RF input signal is split two ways via a power divider and fed into the RF ports of the EOM. Using different attenuations and cable lengths, the relative amplitude and phase of the two RF input signals to each port can be adjusted such that the nonlinearities are minimized [19]. The following is the tuning procedure we discovered to obtain optimal linearization:

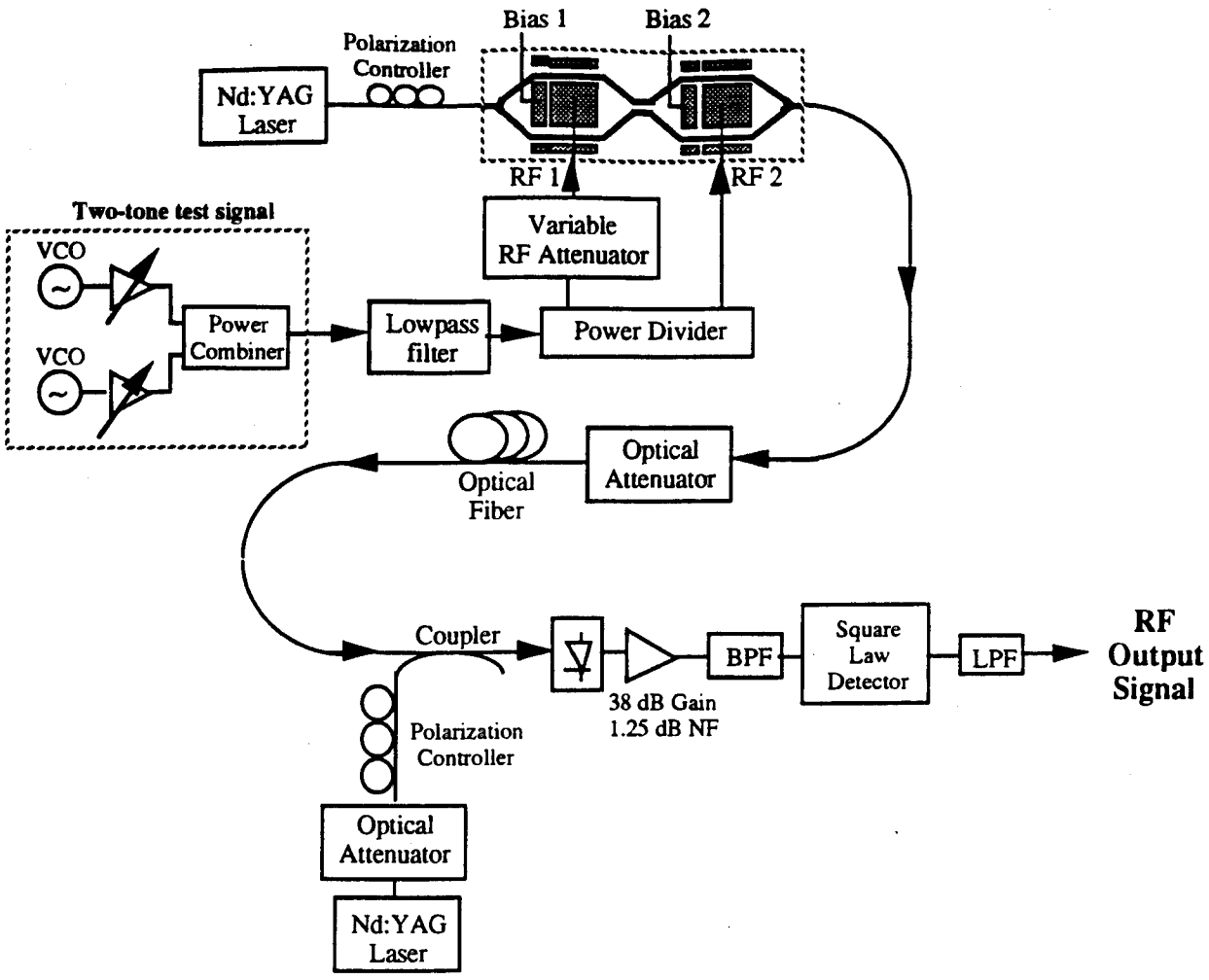

Fig. 6-6. Block diagram of the coherent AM link using a CTI linearized modulator and Nd:YAG lasers.

(1) Connect the RF input signal to RF port 1 only; terminate RF port 2.

(2) Adjust bias 1 and bias 2 for minimum second harmonic generation at the link output.

(3) Connect the RF input signal to RF port 2 (both RF ports are now connected).

(4) Adjust the attenuation in the RF 1 branch, while keeping the RF signal path lengths the same, for minimum third order harmonics and IMPs at the link output.

(5) Adjust bias 1 and bias 2 for minimum second harmonic generation at the link output.

(6) Repeat steps (4) and (5) until the minimum nonlinearities is observed at the link output.

(7) Measure the dynamic range.

6.6.3 Experimental Measurements

The SFDR versus link loss measurements are shown in Fig. 6-7. For comparison, also shown in the figure are the SFDR measurements for the set-up shown in Fig. 4-1(a) and presented in Section 4.6. For link losses greater than 15 dB, there is at least 12 dB improvement due to a more powerful LO laser and a linearized modulator. The improvement due to the lower RIN is negligible in this high loss region since the received optical powers are small. The improvement due to the linearized modulator is about 11.3 dB corresponding to 34 dB third harmonic suppression. This agrees well with the specifications given by Crystal Technology.

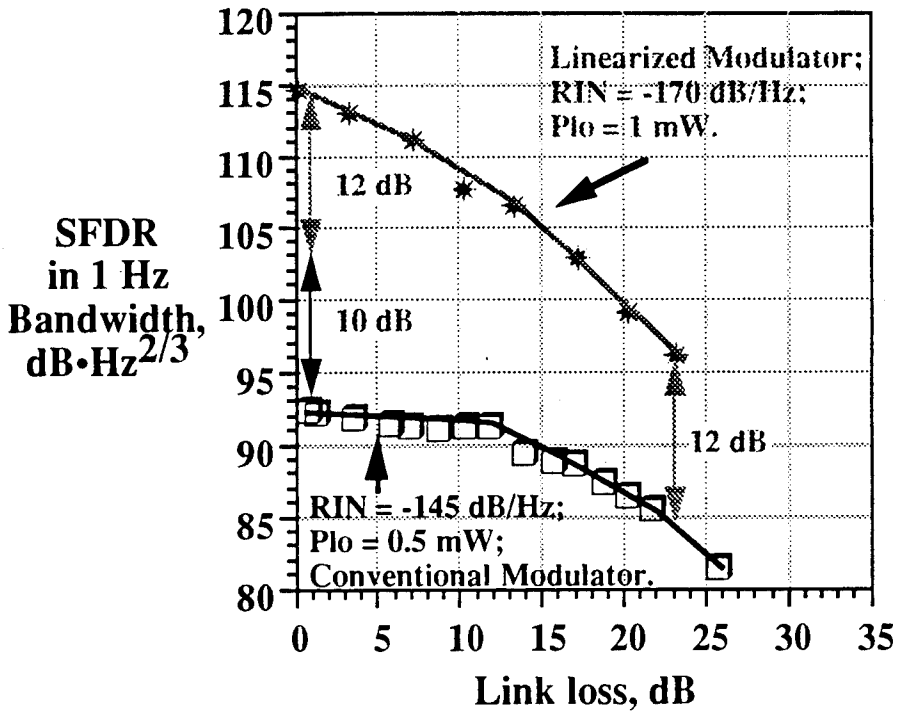

Fig. 6-7. Spurious-free dynamic range vs. the link loss for the coherent AM link using a CTI linearized modulator and Nd:YAG lasers.

At lower link losses, down to 0 dB, as much as 10 dB additional improvement is brought about by a lower RIN in both LO and transmitter lasers.

Our experiments provide strong evidence that the dynamic range of coherent AM links can be improved by using better devices. The SFDR of 115 dB·$Hz^{2/3}$ we obtained is the best dynamic range ever attained with a coherent analog link; it was obtained using modest optical powers of 1 mW LO and 0.5 mW received optical signal, and this was because we were limited by the saturation of our photodetector for higher optical powers. We are confident that even higher SFDR values can be obtained using much better devices. In addition, we have experimentally obtained up to 34 dB reduction in third-order IMD, the largest reported for any modulator linearization scheme for any type of analog optical link.

Although these measurements were conducted using Nd:YAG lasers, which have very narrow linewidths and high power, our link is capable of using semiconductor lasers with high optical output power and considerable linewidths. We have shown earlier that by proper design, the coherent AM link can be made linewidth-insensitive. Certain laboratories have research efforts underway for producing very high power semiconductor lasers. The results shown here provide a proof-of-concept demonstration on what dynamic ranges can be obtained with high optical power.

6.7 References

[1] M. L. Farwell, W. S. C. Chang, and D. R. Huber, "Increased Linear Dynamic Range by Low Biasing the Mach-Zehnder Modulator," *IEEE Photonics Technology Letters,* vol. 5, no. 7, pp. 779-782, July 1993.

[2] C. E. Cox, G. E. Betts, and L. M. Johnson, "An analytic and experimental comparison of direct and external modulation in analog fiber-optic links," *IEEE Trans. MTT*, vol. 38, no. 5, pp. 501-509, May 1990.

[3] G. E. Betts, L. M. Johnson, and C. H. Cox III, "High-dynamic-range, low-noise analog optical links using external modulators: analysis and demonstration," *High Frequency Analog Fiber Optic Systems,* SPIE Vol. 1371, pp. 252-257, 1990.

[4] R. M. De Ridder, and K. Korotky, "Feedforward Compensation of Integrated Optic Modulator Distortion," *Technical Digest of the Optical Fiber Communication Conference*, p. 78, paper WH5, February 1990.

[5] Y. Trisno, L. K. Chen, and D. Huber, "A Linearized External Modulator for Analog Applications," *SPIE Proc. on High Frequency Analog Fiber Optic Systems* (San Jose, CA), SPIE Vol. 1371, pp. 8-12, September 1990.

[6] R. B. Childs, and V. A. O'Bryne, "Multichannel AM Video Transmission Using a High-Power Nd:YAG Laser and Linearized External Modulator," *IEEE J. Selected Areas in Communications,* vol. 8, no. 7, pp. 1369-1376, September 1990.

[7] L. M. Johnson, and H. V. Roussell, "Linearization of an Interferometric Modulator at Microwave Frequencies by Polarization Mixing," *IEEE Photonics Technology Letters,* vol. 2, no. 11, pp. 810-811, November 1990.

[8] L. M. Johnson, and H. V. Roussell, "Reduction in Intermodulation distortion in interferometric Optical Modulators," *Optics Letters,* vol. 13, no. 10, pp. 928-930, October 1988.

[9] J. L. Brooks, G. S. Maurer, and R. A. Becker, "Implementation and Evaluation of a Dual Parallel Linearization System for AM-SCM Video Transmission," *IEEE/OSA J. Lightwave Technology,* vol. 11, no. 1, pp. 34-41, January 1993.

[10] M. L. Farwell, Z. Q. Lin, E. Wooten, and W. S. C. Chang, "An Electrooptic Intensity Modulator with Improved Linearity," *IEEE Photonics Technology Letters,* vol. 3, no. 9, pp. 792-795, September 1991.

[11] J. H. Schaffner, *et. al,* "Spur-Free Dynamic Range Measurements of a Fiber Optic Link with Traveling Wave Linearized Directional Coupler Modulators," *IEEE Photonics Technology Letters,* vol. 6, no. 2, pp. 273-275, February 1994.

[12] Y. Wang-Boulic, "A Linearized Optical Modulator for Reducing Third-Order Intermodulation Distortion," *IEEE/OSA J. Lightwave Technology,* vol. 10, no. 8, pp. 1066-1070, August 1992.

[13] H. Skeie, and R. V. Johnson, "Linearization of Electro-Optic Modulators by a Cascade Coupling of Phase Modulating Electrodes," *SPIE Proc. on Integrated Optical Circuits* (Boston, MA), SPIE Vol. 1583, pp. 153- 164, Sept. 1991.

[14] G. L. Abbas, V. W. S. Chan, and T. K. Yee, "A Dual-Detector Optical Heterodyne Receiver for Local Oscillator Noise Suppression," *J. Lightwave Technol.*, vol. LT-3, no. 5, pp. 1110-1122, October 1985.

[15] G. P. Agrawal, "Coherent Lightwave System," *Fiber-Optic Communication Systems*, New York: John Wiley & Sons, Inc., 1992, pp. 226-271.

[16] G. E. Betts, C. H. Cox III, and K. G. Ray, "20 GHz Optical Analog Links Using an External Modulator," *IEEE Photonics Technol. Letters*, vol. 2, no. 12, pp. 923-925, December 1990.

[17] C. H. Cox, III, "Analog Fiber-Optic Links with Intrinsic Gain," *Microwave Journal*, vol. 35, no. 9, pp. 90-99, Sept. 1992.

[18] S. Wanuga, E. I. Ackerman, D. Kasemset, D. W. Hogue, and S. R. Chinn, "A Low Loss L-Band Microwave Fiber-Optic Link for Control of a T/R Module," *Integrated Optics and Optoelectronics II*, SPIE Vol. 1374, pp. 97-106, 1990.

[19] Crystal Technology, Inc. OGW 1x2 1500 nm Linearized Modulator Application Note, Palo Alto, CA.

Chapter Seven

AM Links: Conclusions

7.1 Summary

The studies of amplitude-modulated optical links conducted within this part has provided a comprehensive survey of techniques in improving the performance of current analog optical links [1, 2, 3]. These studies also led to the recommendations for several optical experiments to be constructed in order to adequately demonstrate the features and advantages of certain advanced analog links.

We have studied theoretically four types of amplitude-modulated optical links:

- homodyne AM-WIRNA links:
  - (a) 2-port homodyne link;
  - (b) K-port homodyne link; and
  - (c) 2K-port homodyne link;
- heterodyne AM-WIRNA links;
- optically amplified direct detection links;
- optically amplified heterodyne AM-WIRNA links.

We have successfully built and tested the following links operating at 2 GHz:

- a conventional direct detection link;
- a heterodyne AM-WIRNA link;
- a direct detection link with a semiconductor amplifier;
- a direct detection link with an erbium-doped fiber amplifier;
- a heterodyne AM-WIRNA link with a semiconductor amplifier;
- a heterodyne AM-WIRNA link with an erbium-doped fiber amplifier;

For low received optical power (< 100 μW), optical amplification, coherent detection, or both can be used to improve the dynamic range of the links. However, for high received optical power (>1 mW), the conventional direct detection link gives the best

performance. The shot noise-limited SFDR of the conventional direct detection link is 2 dB higher than that of the amplified direct detection and coherent AM link; this is due the 3 dB noise figure of the optical amplifier in the amplified link and the extra signal processing in the coherent receiver for the coherent AM link. We have also shown that the coherent AM links are more sensitive to RIN than the direct detection links. The RIN-limited SFDR of the coherent AM links is 4 dB worse than that of the direct detection links.

Through the construction, measurement and analysis of the four experimental links, we were able to make a performance evaluation of practical optical links using optical amplification, coherent detection, and both techniques, using readily available optical and microwave components. Our experimental results follow the same behavioral trend as that predicted by theoretical models we constructed. Both theory and experiment present cross-over points between the four links' dynamic range performance, and agree that these are due to noise terms like thermal noise, shot noise, RIN, signal-ASE noise, ASE-ASE beat noise, and LO-ASE beat noise becoming dominant as the received optical power changes. However, our measurements only show modest improvements when using an optical amplifier and coherent detection techniques.

7.2 Recommendations for Future Work

In Chapter 3, we have discussed the advantages of using balanced receivers. Since balanced receivers reject common mode signals, the second harmonic components in the homodyne links and the common mode noises, such as the LO RIN, are suppressed. It is very important to suppress the LO RIN because of the high optical power requirement of analog optical links. In addition, these receivers allow more efficient utilization of the received optical power. Balanced receivers are commercially available for about $20K. With these receivers, we would be able to improve the performance by more than 3 dB.

In this project, we have experimentally demonstrated the feasibility of coherent heterodyne links. It is difficult to obtain RF components for an arbitrarily high IF. A finite IF can cause a small penalty to the receiver sensitivity. As discussed in Chapter 3, homodyne links are also useful for analog applications. However, homodyne links, in general, require more complex optical processing and in some cases, custom-made components are required.

7.3 References

[1] T. K. Fong, D. J. M. Sabido, R. F. Kalman and M. Tabara, and L. G. Kazovsky, "Linewidth-Insensitive Coherent AM Optical Links: Design, Performance, and Potential Applications," *J. Lightwave Technol.*, vol. LT-12, no. 3, pp. 526-534, Mar. 1994.

[2] D. J. M. Sabido, M. Tabara, T. K. Fong, R. F. Kalman and L. G. Kazovsky "Experimental Linewidth-Insensitive Coherent Analog Optical Link," *J. Lightwave Technol.*. accepted for publication.

[3] T. K. Fong, D. J. M. Sabido, and M. Tabara, and L. G. Kazovsky, "Dynamic range of externally modulated analog optical links," *Optoelectronic Signal Processing for Phase Array Antennas IV*, SPIE's OE/LASE'94, Los Angeles, vol. 2155, pp. 229-240, January 1994.

PART 3:

ANGLE MODULATED LINKS

Chapter Eight

Coherent FM and PM Links

8.1 Potential Dynamic Range Improvement Using Angle Modulation

Angle modulation is well-known to offer potential performance advantages over amplitude modulation in analog links. These advantages are exploited in commercial FM radio and video. There are a number of reasons to believe that angle modulation could be useful in optical systems. Wideband angle modulation provides improved signal-to-noise ratio at the expense of increased transmission bandwidth. Because optical fiber offers a very large potential transmission bandwidth, optical transmission systems are well-suited to handle expanded bandwidth signals.

Angle modulation can be achieved in analog links using either direct or external modulation. The frequency of semiconductor laser diodes can be directly modulated by a varying input current, which changes the index of refraction of the laser gain medium. Using multi-section lasers, the optical frequency can be varied independently of the optical power. External angle modulation is based on optical phase modulators, which are essentially ideally linear, in contrast to the highly nonlinear characteristics of Mach Zehnder amplitude modulators. The linearity of optical phase modulators can be exploited to both PM and FM systems to achieve large spurious-free dynamic range (SFDR - see Section 2.1.1.2).

Coherent detection provides both amplitude and phase information about the detected optical field, and it is thus well-suited to the detection of angle modulated signals. However, because angle modulated links carry their information in the optical phase, they are intrinsically sensitive to the laser phase noise in coherent detection links. In Section 8.2, we present an analysis of the SFDR, RF power transfer ratio, and noise figure of coherent PM and FM links. In Section 8.3, we compare their performance to that of AM coherent and AM direct detection links. Section 8.4 contains references.

8.2 Coherent PM and FM Links

8.2.1 Link Descriptions

An externally modulated PM coherent link is shown in Fig. 8-1. The input signal is phase modulated on an optical carrier. At the receiver the signal is combined with the LO laser light using a 3 dB directional coupler and detected. It is then amplified at the IF, limited, put through a delay line filter, envelope detected, and integrated.

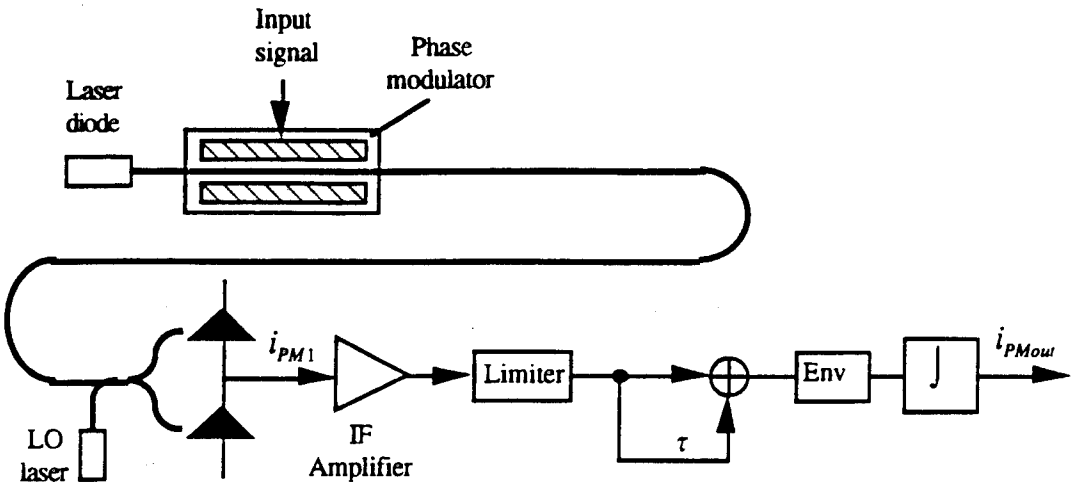

Fig. 8-1. Externally modulated coherent PM link

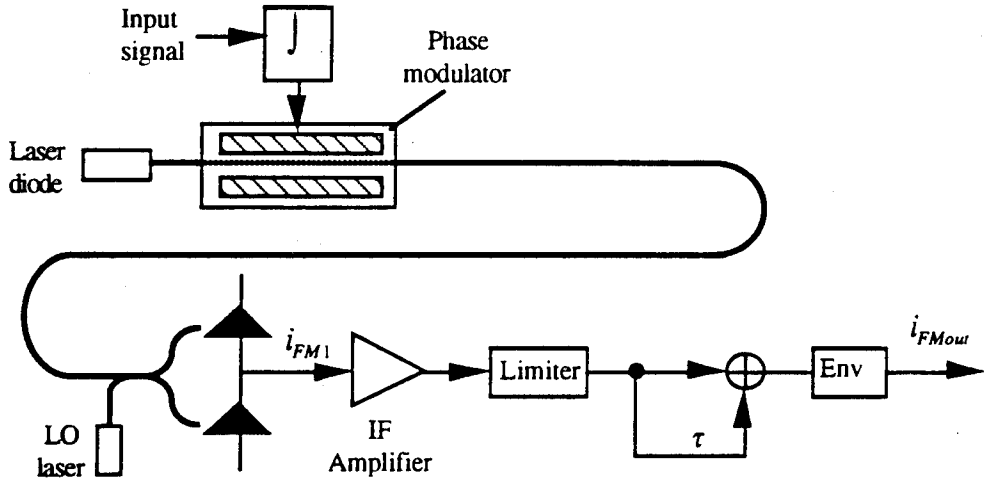

Fig. 8-2(a). Externally modulated coherent FM link

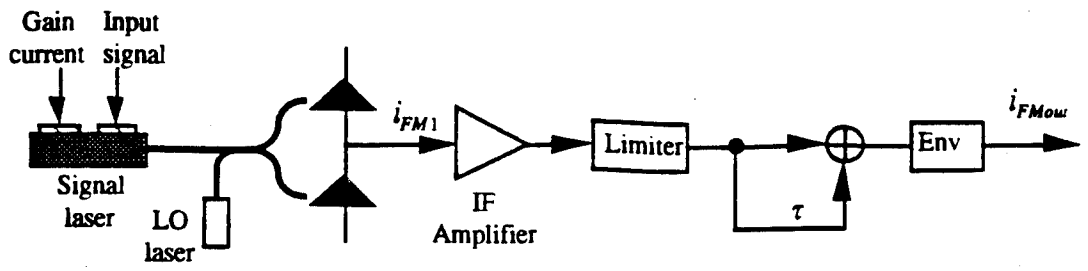

Fig. 8-2(b). Directly modulated coherent FM link

Externally modulated and directly modulated coherent FM links are shown in Figs. 8-2(a) and (b), respectively. In Fig. 8-2(a), the input signal is integrated before being applied to a phase modulator. In Fig. 8-2(b), the input signal is applied to the grating section of a semiconductor laser diode, generating optical FM. The FM receiver is identical to the PM receiver, except that there is no integrator before the output.

In all cases, there is filtering implied in the baseband and IF amplifiers. For the purposes of our analysis, we assume that the amplifier bandwidths are sufficiently broad to pass signals undistorted, including signals with bandwidths broadened by phase noise. In the coherent systems, balanced receivers are utilized to both increase the collected signal power and suppress part of the laser relative intensity noise (RIN) [1].

8.2.2 Impact of Laser Linewidth, RIN, and Receiver Noise

The output signal-to-noise ratios (SNRs) for the PM and FM links are derived in Appendix C.1.1 and are given by

$$SNR_{PM} = \varphi_\Delta^2 \frac{4R^2P_SP_{LO}\langle x^2(t)\rangle}{4R^2P_SP_{LO}\langle(\varphi_{nS}-\varphi_{nLO})^2\rangle + \frac{1}{4}b(RP_S)^2\langle n_{RS\,bp}^2\rangle + \frac{1}{4}b(RP_{LO})^2\langle n_{RLO\,bp}^2\rangle + \langle n_{D\,bp}^2\rangle}$$

$$= \varphi_\Delta^2 SNR_{PMo} \tag{8.1}$$

$$SNR_{FM} = \left(\frac{\omega_\Delta}{B}\right)^2 \frac{4B^2R^2P_SP_{LO}\langle x^2(t)\rangle}{4R^2P_SP_{LO}\langle(\dot\varphi_{ns}-\dot\varphi_{nLO})^2\rangle + \frac{1}{4}b(RP_S)^2\langle \dot n_{RS\,bp}^2\rangle + \frac{1}{4}b(RP_{LO})^2\langle \dot n_{RLO\,bp}^2\rangle + \langle \dot n_{D\,bp}^2\rangle}$$

$$= \left(\frac{\omega_\Delta}{B}\right)^2 SNR_{FMo} \tag{8.2}$$

where R is the responsivity of the photodetectors, B is the bandwidth of the baseband signal $x(t)$, and b is the photodetector matching factor, which is defined in Appendix A.2.5. P_S is the received optical power, P_{LO} is the local oscillator power, and $\langle x^2(t) \rangle$ is the average power of the two-tone applied signal, which is normalized to one. The normalized SNRs SNR_{PMo} and SNR_{FMo} are the SNRs for each of the links for a unity modulation index; note that the modulation indices may exceed unity. The various noise expressions in Eqs. (8.1) and (8.2), which correspond to phase noise, RIN due to the signal laser, RIN due to the local oscillator laser, and receiver noise, are evaluated in Appendix A.2.

The SNR expression SNR_{FMo} is accurate for both directly modulated and externally modulated FM links. As shown in Appendix C.1, the form of the transmitted optical signal is identical for both, which is the reason that a single SNR expression has been given.

Eqs. (8.1) and (8.2) indicate that the SNR increases monotonically with the modulation index. The maximum useful modulation index is limited by intermodulation distortion associated with nonlinear effects. In the next section, we derive expressions for the maximum useful modulation index and the associated spurious-free dynamic range.

8.2.3 Spurious-Free Dynamic Range (SFDR)

In this section, we derive the spurious-free dynamic range (SFDR) for a link with a single channel. This derivation is fully general for any link with an SFDR limited by third-order nonlinearitics, which is the case in our analog angle modulated links assuming that the transmitter sections are perfectly linear. The output current expressions of Appendix C.1 can be written in the form

$$i_{out}(t) = s\left\{rx(t) + b_3\left[rx(t)\right]^3\right\} + n_{tot}(t) \tag{8.3}$$

where r is the modulation index, s is the signal amplitude, b_3 is the coefficient describing the third-order nonlinearity, and $n_{tot}(t)$ is the total noise. The nonlinearity for the PM link is of a slightly different form and is discussed below. Table 8-1 gives r and b_3 for the two links. In Section 8.2.2, we showed that generic SNR expressions for the various links can be written as

$$SNR = r^2 \frac{s^2\langle x^2(t)\rangle}{\langle n_{wt}^2(t)\rangle} = r^2 SNR_o \tag{8.4}$$

Table 8-1. Modulation index r and nonlinear coefficient b_3 for the various links.

	PM	FM
r	φ_Δ	ω_Δ/B
b_3	$-1/6(pf_{max}/2f_{IF})^2$	$-1/6(B/4f_{IF})^2$

The key performance measure of an analog link is the spurious-free dynamic range (SFDR), defined as the ratio of the maximum signal power to the minimum signal power the link can transport. At high modulation depths, the third order nonlinearity results in significant intermodulation products falling within the signal band. From Section 2.1.1.2, the SFDR is the SNR at which the intermodulation power is equal to the noise power. We assume a normalized test signal of the form

$$x(t) = \alpha_1 \cos(\omega_1 t + \varphi_1) + \alpha_2 \cos(\omega_2 t + \varphi_2) \tag{8.5}$$

where $\alpha_1^2 + \alpha_2^2 = 1$, giving $\langle x^2(t)\rangle = 0.5$; and φ_1 and φ_2 are arbitrary constant phases. For less than one octave of bandwidth, the maximum intermodulation power falling within the band is

$$\langle i_{NL3}^2 \rangle = \frac{9}{128} s^2 b_3^2 r^6 \tag{8.6}$$

where the only important terms falling within the signal band are those at $2\omega_1 - \omega_2$ and $2\omega_2 - \omega_1$. This occurs for $\alpha_1 = \alpha_2 = 1/\sqrt{2}$. Setting the intermodulation power equal to the noise power, we find that the maximum useful modulation depth is given by

$$r^2 = \left(\frac{64}{9} \frac{1}{b_3^2 SNR_o} \right)^{1/3} \tag{8.7}$$

Because the SFDR is defined as the SNR at the maximum useful modulation depth, Eq. (8.7) is substituted into Eq. (8.4) to give the SFDR,

$$SFDR = \left[\frac{8SNR_o}{3|b_3|}\right]^{2/3} \tag{8.8}$$

From Eq. (C.12) of Appendix C.1, the total intermodulation power for an FM link is easily obtainable by substituting in Eq. (8.5). For a PM link with the test signal of Eq. (8.5), the total intermodulation power is given by

$$\left\langle i_{NL3}^2 \right\rangle = \frac{K^2}{2}\left[\frac{\varphi_\Delta^3}{6}\frac{3}{4}\left(\frac{1}{4f_{IF}}\right)^2\right]^2\left[\left(\alpha_1^2\alpha_2\frac{\omega_1^2\omega_2}{2\omega_1-\omega_2}\right)^2+\left(\alpha_2^2\alpha_1\frac{\omega_2^2\omega_1}{2\omega_2-\omega_1}\right)^2\right] \tag{8.9}$$

It can be shown that the worst case (i.e., maximum $\left\langle i_{NL3}^2 \right\rangle$) occurs for $\alpha_1 = \alpha_2 = 1/\sqrt{2}$ and $\omega_1 = \omega_2 = 2\pi f_{max}$, where f_{max} is the maximum signal frequency; for a one octave signal bandwidth, $f_{max} = 2B$.

The corresponding values of b_3 is given in Table 8-1. Using these values of b_3, the SFDRs of the coherent PM and FM links are then given by Eq. (8.8).

The SFDR expressions given in this section for coherent FM links are based upon the assumption that the nonlinearity which limits link performance is generated by the discriminator filter, not the transmitter. The validity of this assumption for externally modulated FM links is discussed in Appendix C.1.2. For directly modulated FM links, the linearity of the FM response of semiconductor laser diodes is device-dependent and also not well documented in the literature, and as a result we assume that the assumption is also valid for these links. The SFDR results in Section 8.3 for directly modulated and externally modulated FM links are therefore identical.

8.2.4 RF Power Transfer Ratio and Noise Figure

The RF power transfer ratios and noise figures of the coherent PM and FM links are defined and derived in Appendix C.1.2. The RF power transfer ratio for an externally modulated FM link is

$$G_{opt\,(ext.\,FM)} = \frac{S_o}{S_i} = \left(\frac{1}{4f_{IF}}\right)^2 4r^2 P_S P_{LO}\left(\frac{\pi}{V_\pi RC}\right)^2 R_S^2 L_{nl} \tag{8.10}$$

For the externally modulated coherent PM link, the RF power transfer ratio is

$$G_{opt\,(ext.\,PM)} = \left(\frac{1}{4f_{IF}}\right)^2 4r^2 P_S P_{LO} \left(\frac{\pi}{V_\pi RC}\right)^2 R_S^2 L_{nl} \tag{8.11}$$

which is identical to that of the externally modulated coherent FM link.

For the directly modulated coherent FM link, the RF power transfer ratio is

$$G_{opt\,(dir.\,FM)} = \left(\frac{500\pi\gamma}{f_{IF}}\right)^2 4r^2 P_S P_{LO} L_{nl} \tag{8.12}$$

The parameters in the above equations are defined in Table 8-3 and in Appendix C.1.2.

The derivation of noise figure is straightforward using the formula

$$F_{(link)} = 1 + \frac{noise\ power\ at\ link\ output}{G_{(link)} kTB} \tag{8.13}$$

We give below the output noise powers for the coherent PM and FM links. The noise figure is then obtained directly from Eq. (8.13).

The noise power at the output of the externally modulated coherent FM link is

$$\eta_{(ext.\,FM)} = R_S \left(\frac{1}{4f_{IF}}\right)^2 \left[4r^2 P_S P_{LO} [4\pi \Delta\upsilon B] + \frac{(2\pi)^2}{3} \left(4qr(P_S + P_{LO}) + \frac{4kT}{R_S} \right) \left(f_{\max}^3 - f_{\min}^3 \right) \right] \tag{8.14}$$

The noise power at the output of the directly modulated coherent FM link is

$$\eta_{(dir.\,FM)} = R_S \left(\frac{1}{4f_{IF}}\right)^2 \left[4r^2 P_S P_{LO} [4\pi \Delta\upsilon B] + \frac{(2\pi)^2}{3} \left(4qr(P_S + P_{LO}) + \frac{4kT}{R_S} \right) \left(f_{\max}^3 - f_{\min}^3 \right) \right] \tag{8.15}$$

which is identical to the output noise power for the externally modulated coherent FM link.

The noise power at the output of the externally modulated coherent PM link is

$$\eta_{(ext.\,PM)} = R_S \left(\frac{1}{4f_{IF}RC}\right)^2 \left[4r^2 P_S P_{LO} \left[\frac{\Delta\upsilon}{\pi} \left(\frac{1}{f_{\min}} - \frac{1}{f_{\max}} \right) \right] + \left(4qr(P_S + P_{LO}) + \frac{4kT}{R_S} \right) B \right]$$

(8.16)

Again, the parameters in the above equations are defined in Table 8-3 and in Appendix C.1.2.

8.3 Results and Discussion

In this section, we evaluate the SFDR, RF power transfer ratio, and noise figure of coherent PM and FM links and compare their performance to that of AM coherent and AM direct detection links. Note that the theoretical values for the AM links in this section will slightly overestimate the attainable SFDR shown in Chapter 4 due to the fact that amplifier noise figures and other experimental link imperfections have been ignored.

8.3.1 SFDR Comparison

We are now in a position to evaluate the SFDR of the coherent PM and FM links for a variety of parameter values, and to compare their performance to that of coherent AM and DD links. Note that the plots for coherent FM refer to both directly modulated and externally modulated FM links. The main system parameters include received optical power*, LO power, RIN, laser linewidth, signal bandwidth, and receiver intermediate frequency. In the examples considered, the signal occupies a one octave of bandwidth from 1 - 2 GHz.

We consider only combinations of laser parameters corresponding to two lasers typically used in optical communication systems: a diode-pumped Nd:YAG laser and a distributed feedback (DFB) laser diode. Diode-pumped Nd:YAG lasers exhibit low relaxation oscillation frequencies and narrow linewidths, whereas DFB laser diodes exhibit high relaxation oscillation frequencies and wider linewidths. In the following calculations, we will assume the two sets of laser parameters shown in Table 8-2. We will also assume, for the coherent links, that the local oscillator exhibits the same RIN and linewidth characteristics as the signal laser for each case. The DFB laser parameters are typical of a number of commercial lasers (e.g., Toshiba model TOLD335S-AH1, Fujitsu model FLD150F2KP) as are the Nd:YAG parameters (Lightwave Electronics Series 122,

* For the coherent AM and DD links, the received optical power is normalized to take into account the intrinsic loss due to the biasing of the external amplitude modulator at the half-power transmission point. This is for the purposes of a fair comparison to the angle modulated links.

Amoco Laser Company model ALC 1320-25EHS). The quantities in Table 8-2 are defined in Appendix A.2.

Table 8-2. Laser parameters used in numerical calculations

	DFB Laser Diode	Nd:YAG Laser
Linewidth $\Delta\nu$	10 MHz	5 kHz
RIN PSD η_R	-155 dB/Hz	-110 dB/Hz
RIN roll-off freq. f_R	3 GHz	200 kHz

Throughout our analysis, we assume a receiver front-end thermal noise power of 3.31 x 10^{-22} A^2/Hz, corresponding to a 50 Ω resistor at room temperature. This assumption is further discussed in Section 8.3.3. We also assume that the two photodiodes in each balanced receiver are well-matched, so the photodetector matching factor b for each link is 0.01 (b is defined in Appendix A.2.5).

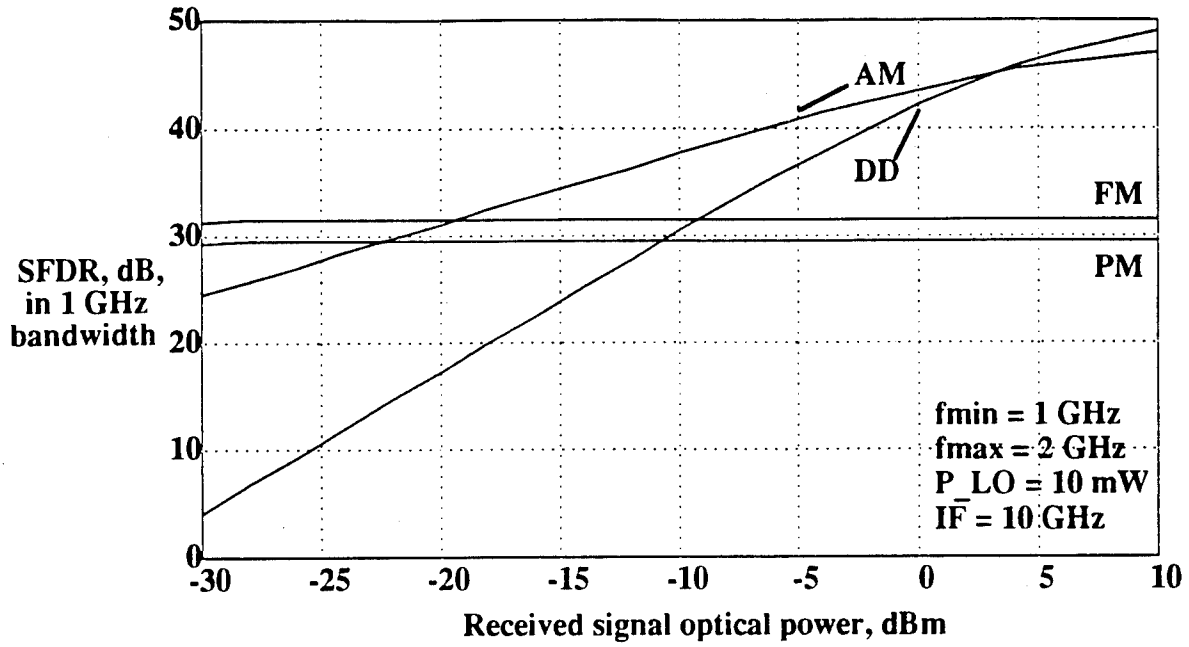

Fig. 8-3. SFDRs of DD, AM, PM, and FM links plotted against received signal optical power for a DFB laser with parameters in Table 8-2.

Fig. 8-3 compares the SFDR of the various links vs. normalized transmitted signal optical power (P_S) for the DFB laser considered. At signal power levels less than 1 mW, the SFDR of the DD link is dominated by receiver thermal noise, and its curve has a slope

of 4/3. Above 1 mW, shot noise and RIN become significant. In the RIN-limited regime, the DD link SFDR is independent of signal power. At low signal levels, the coherent AM link SFDR is dominated by LO shot noise (slope of 2/3), and shows a marked advantage over the DD link. At higher power levels, the coherent AM link has an intrinsic disadvantage with respect to the DD link due to the extra baseband RIN and shot noise encountered in a heterodyne receiver. At very low signal power levels (< -30 dBm), the SFDR of the PM and FM links is dominated by LO shot noise. However, above -30 dBm, phase noise is dominant and the SFDR is essentially independent of signal power level for both the PM and FM links.

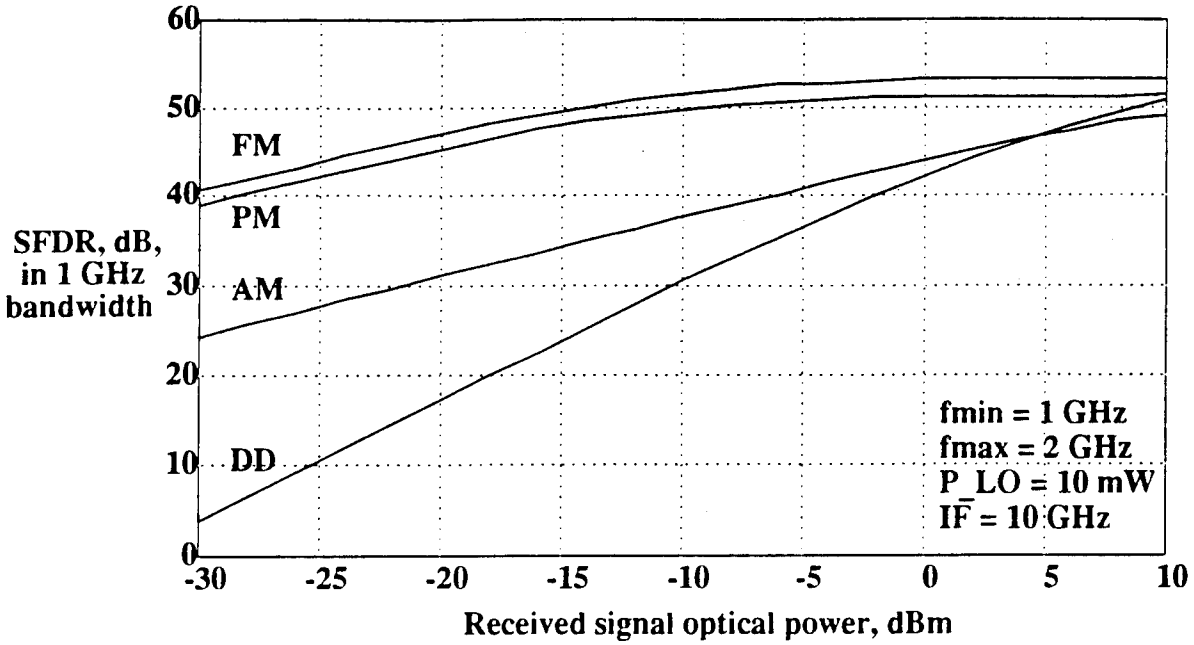

Fig. 8-4. SFDRs of DD, AM, PM, and FM links plotted against received signal optical power for an Nd:YAG laser with parameters in Table 8-2.

In Fig. 8-4, SFDR is plotted vs. P_S for the Nd:YAG laser parameters in Table 8-2. At low signal power levels, the behavior of the DD and AM links is identical to that with the laser diode. However, at high power levels, the low RIN of the Nd:YAG laser results in a higher SFDR for both the AM and DD links. The PM and FM links exhibit substantial improvements in performance compared to the laser diode case, due almost entirely to the decreased phase noise of the Nd:YAG laser. The PM and FM links exhibit larger SFDRs than the DD link up to a signal power level of 10 dBm.

Fig. 8-5 shows a plot of SFDR vs. laser linewidth for the PM and FM links for P_S values of -30 dBm, -15 dBm, and 0 dBm. We have chosen the RIN level and the RIN roll-

off frequency to be representative of the laser diode in Table 8-2. The signal and local oscillator lasers are both assumed to have linewidths equal to the linewidth value at each point on the plot. Due to the inherent immunity of PM and FM links to RIN, the curves for the Nd:YAG RIN parameters will be nearly identical. At low received power levels, the linewidth has little impact, since the noise is dominated by thermal noise. At high received power levels, the impact of phase noise on the PM and FM links is severe, with the SFDR being reduced by 7 dB for every factor of 10 increase in the linewidth. At signal power levels of -30 dBm, -15 dBm, and 0 dBm, the phase noise becomes dominant over all other noises for linewidths of 5 MHz, 200 kHz, and 5 kHz, respectively.

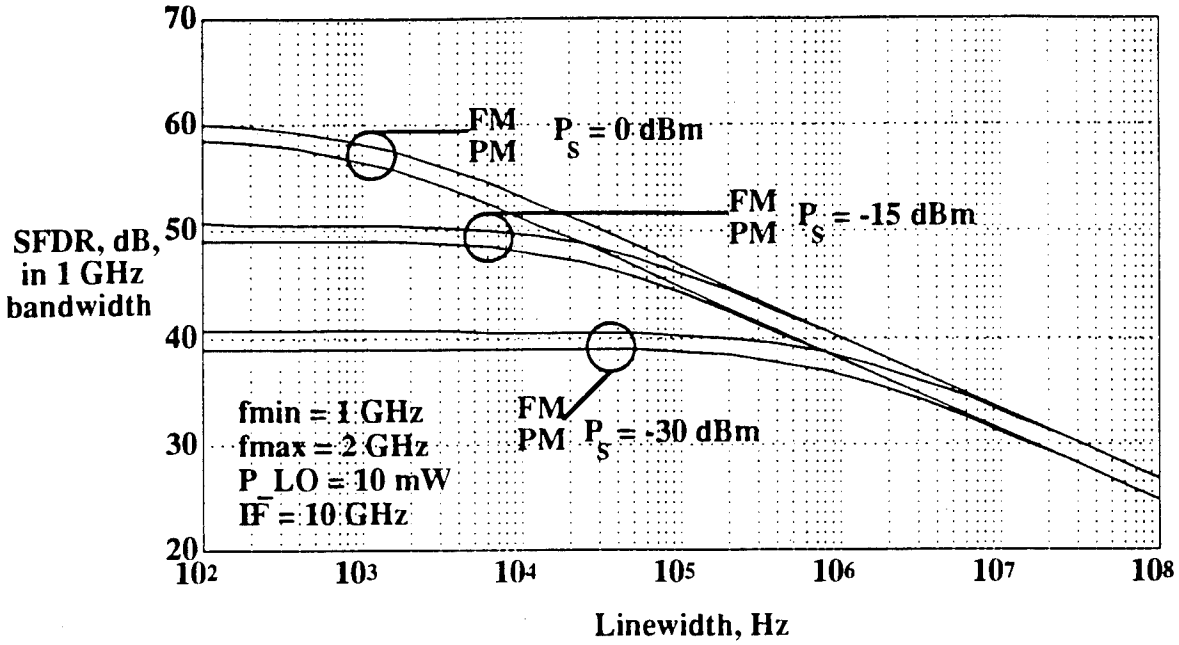

Fig. 8-5. SFDRs of PM and FM links plotted versus linewidth for received signal power levels of 0 dBm, -15 dBm, and -30 dBm.

Fig. 8-6 shows the SFDR of the PM and FM links vs. the intermediate frequency (IF). The two sets of curves correspond to the two lasers considered (see Table 8-2). For a signal bandwidth of 1 GHz, increasing the IF from 5 GHz to 25 GHz increases the SFDR by approximately 10 dB for all four cases shown. The increase in SFDR is due to two causes: (1) the improved linearity of the frequency discriminator (which is utilized in both the PM and FM links), and (2) the reduced RIN at frequencies above the RIN roll-off frequency (see Appendix A.2.4). The reduction in RIN due to roll-off plays a much more significant role in links using single-photodetector receivers than in links using balanced receivers; for the cases shown, essentially all of the improvement in SFDR is due

to the improved discriminator linearity. In these calculations, we have again assumed that the receiver thermal noise PSD is independent of the IF, as explained at the beginning of this section.

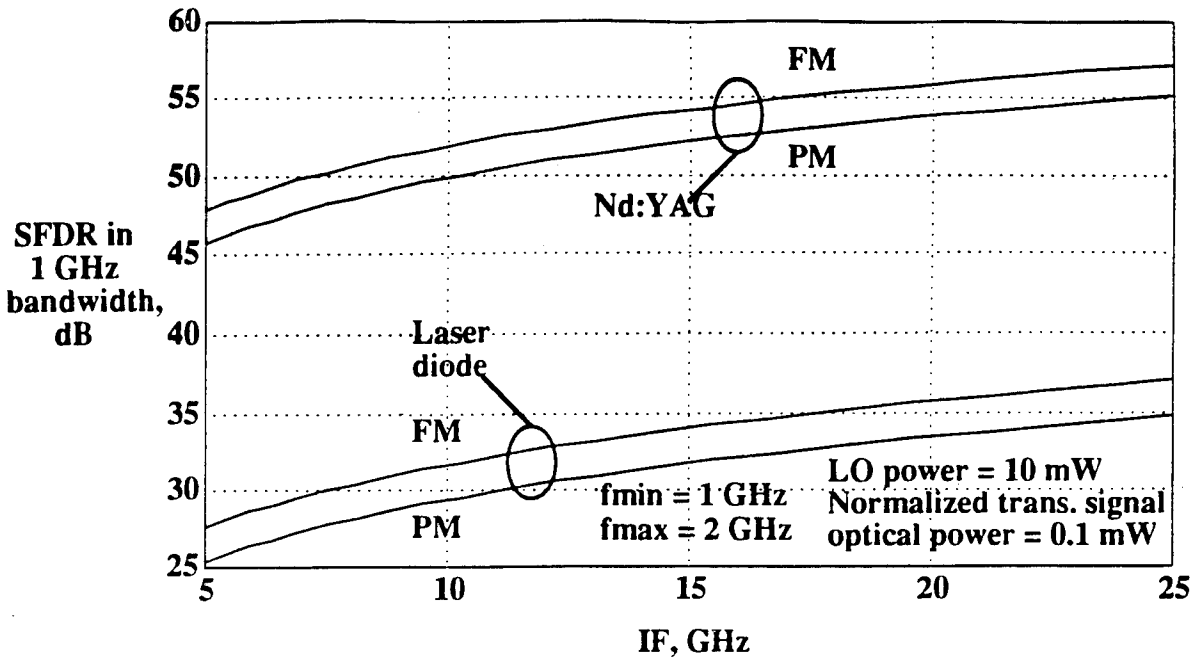

Fig. 8-6. SFDRs of PM and FM links plotted versus IF for the two different sets of laser parameters. The received signal optical power is set at 0.1 mW.

At low received signal power levels (P_s < 100 mW), coherent links exhibit notable SFDR advantages over direct-detection links. This is expected because the local oscillator "pulls" the detected signal up to higher levels, and thus allows operation in the shot noise limit for LO power levels in the milliwatt range or higher.

For PM and FM links at low power levels, the shot and thermal noise dominate phase noise effects and the PM and FM links exhibit superior performance to AM and DD links. For laser linewidths of 10 MHz, the phase noise dominates link performance for P_s > -30 dBm. For laser linewidths of 5 kHz, the phase noise dominates link performance for P_s > 0 dBm. Figs. 8-3 to 8-5 show that, for the performance of the PM and FM links to exceed that of a DD link at a received power level of 0 dBm, the combined linewidth of the signal and LO lasers must be < 100 kHz. In the PM and FM links, a balanced receiver suppresses the self-homodyne RIN terms, as is the case in AM links. However, because there is no signal information in the envelope of PM and FM signals, these systems can use a limiter to suppress heterodyne RIN, and PM and FM links can thus be made completely insensitive to RIN.

8.3.2 RF Power Transfer Ratio and Noise Figure Comparison

Table 8-3 shows the values of component parameters which we used in the numerical computation of link RF power transfer ratios and noise figures. The parameters were chosen to be representative of realistic system components.

Table 8-3. Parameter values used in numerical computation of RF power transfer ratios and noise figures.

Parameter	Assumed Value	Parameter	Assumed Value
LO power P_{LO}	10 mW	Mod. voltage V_π	15 V
RIN	-155 dB/Hz	HIPM index β	1
Relaxation osc. freq.	2 GHz	RC time constant	1.21E-9 s
Laser linewidth $\Delta\upsilon$	10 kHz or 1 MHz	Source imped. R_S	50 Ω
Signal bandwidth B	1 GHz	Conversion loss α	6 dB
Min. sig. freq. f_{min}	1 GHz	Nonlinear loss L_{nl}	6 dB
Max. sig. freq. f_{max}	2 GHz	Int. freq. f_{IF}	10 GHz
Laser FM resp. γ	1 GHz/mA	Responsivity r	0.8

The RF power transfer ratios (PTRs) of the angle-modulated links for the parameter values in Table 8-3 are compared to those of the direct detection link in Fig. 8-7; these RF PTRs measure the efficiency of the links without any amplification. As a result, the RF PTR indicates the amount of amplification which is required for the link output power to equal the link input power. The values of RF PTR in Fig. 8-7 do not take into account excess losses in the link, nor do they count the power required to drive the gain section of the laser in the direct FM case. This explains why actual RF gain is possible in the direct FM case for sufficiently high optical powers. The main point of Fig. 8-7 is that the directly modulated FM link has far lower RF loss due to the high conversion efficiency (on the order of 1 GHz/mA) of input RF current to optical frequency deviation. This efficiency is far better than that of the externally modulated direct detection or angle modulated links. The RF loss of the direct detection link is 10 to 20 dB less than that of the externally modulated PM and FM links due to the large losses of the integrator and discriminator in the PM and FM links. Table 8-1 and Fig. 8-6 make clear that an increase in the receiver intermediate frequency improves the linearity of the

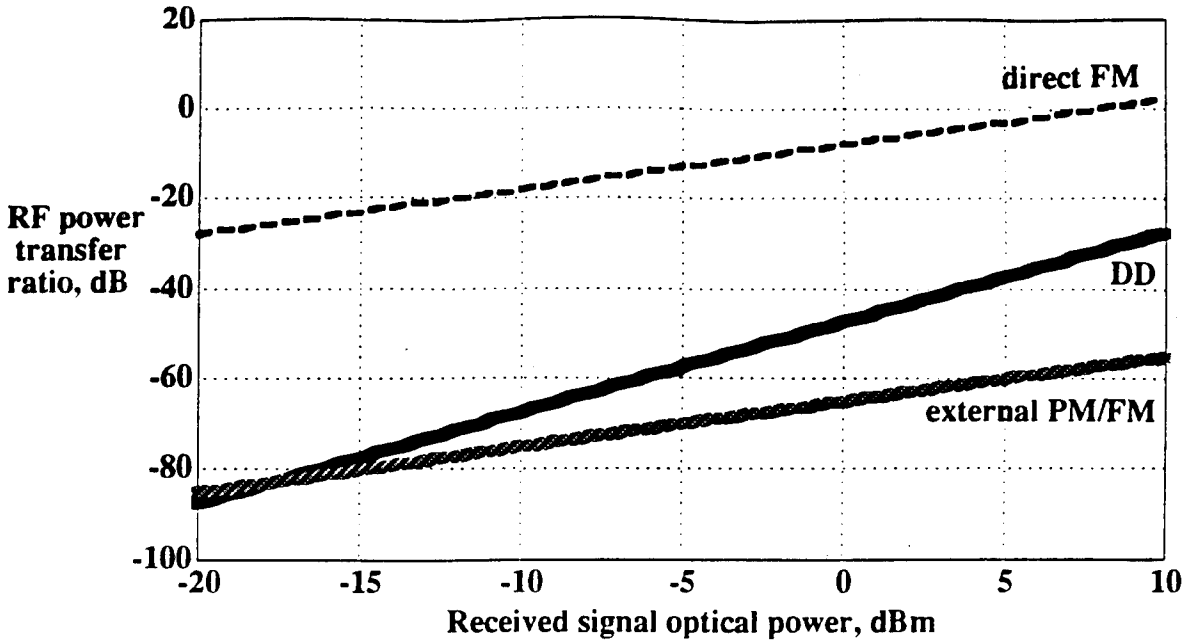

Fig. 8-7. RF power transfer ratios of a directly modulated FM link, externally modulated PM and FM links, and a direct detection link plotted versus received signal optical power for the parameter values in Table 8-3.

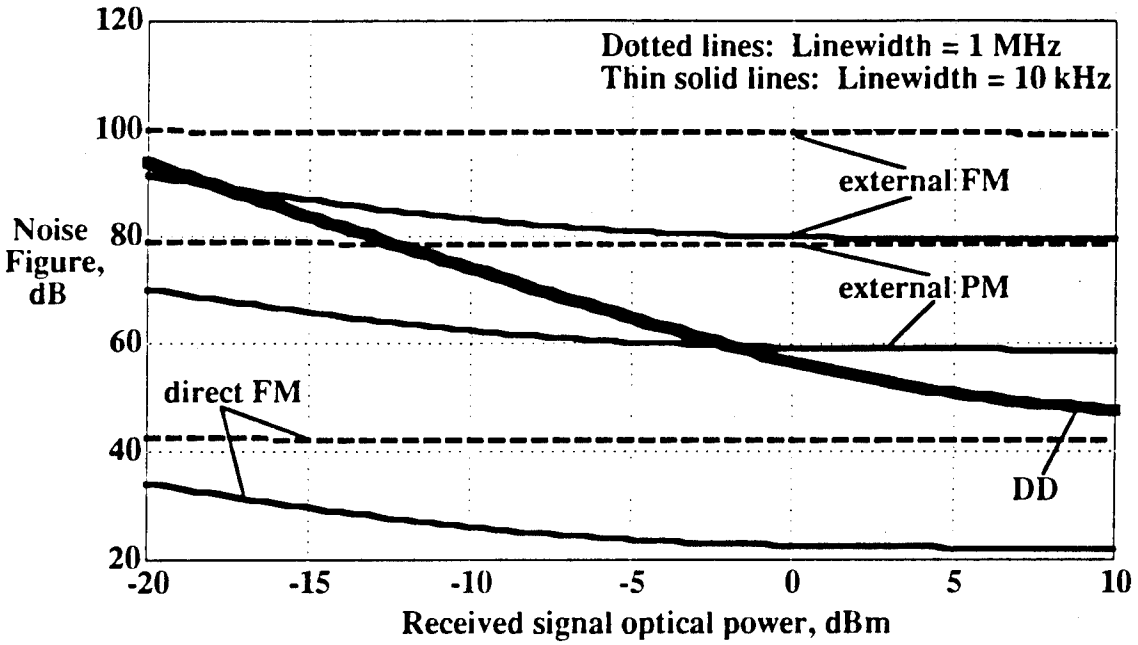

Fig. 8-8. Noise figures of a directly modulated FM link, externally modulated PM and FM links, and a direct detection link plotted versus received signal optical power for the parameter values in Table 8-3 and two different values of laser linewidth.

discriminator in angle modulated links and hence their SFDR, but at the cost of greater RF loss in the link.

The noise figures of the four links are compared in Fig. 8-8, again for the parameters in Table 8-3. The values of noise figure are extremely high since there is no amplification in any of the links and since phase noise, RIN, and receiver noises are generated in the link. These noise figures will clearly be significantly reduced through the use of suitable low-noise amplifiers in the link (from Eq. (C-24) in Appendix C.1.2). The main trends of note in Fig. 8-8 are the reduction of noise figure with increasing optical power and with decreasing linewidth. In the direct detection link, this trend is strongly evident since the receiver thermal noise is independent of optical power. In the angle modulated links, the output SNR does not depend on optical power if the linewidth is the dominant noise in the link, which explains the constant link noise figures for a linewidth of 1 MHz.

8.3.3 Implementation Considerations

In this section, we discuss some limitations of the system models used and practical considerations based on the characteristics of real components. In Section 8.3.3.1, we consider optical frequency modulation. In Section 8.3.3.2, we consider operation at high intermediate frequencies.

8.3.3.1 Optical Frequency Modulation

There are two major methods of generating FM optical signals: direct modulation of a laser diode and using an external modulator. In direct modulation, FM is obtained by modulating the current applied to a laser diode. Ideally, such a laser has a linear frequency versus current characteristic and does not exhibit spurious amplitude modulation. Multi-section DFB and DBR lasers come closest to achieving these objectives. However, some degree of spurious amplitude modulation is observed in all directly modulated lasers. Such amplitude modulation is suppressed in the systems analyzed through the use of a limiter, which also serves to reduce the impact of laser RIN.

In our nonlinearity analysis, we have assumed that the nonlinearities of the FM system are dominated by the nonlinear transfer characteristic of the discriminator filter. In an actual system, it is not clear that the nonlinearity of the frequency versus current characteristic of the laser will be insignificant compared to the nonlinearity of the

discriminator. In principle, nonlinearities in the frequency vs. current characteristic can be compensated for in the discriminator filter. However, it is unattractive to have to customize the discriminator filter characteristic for a given laser. This suggests that the development of lasers with a highly stable and linear (or at least a reproducible) frequency versus current characteristic is desirable if high dynamic range FM links are to be obtained.

The use an external phase modulator with an integrator at its input is known as indirect FM [2]. The optical phase modulator is a nearly ideal, linear modulator. An ideal integrator has an amplitude transmission inversely proportional to frequency, a constant group delay, and linear phase [3]. Nonlinearities will tend to arise in the transmitter from a nonideal integrator. We have modeled our integrator as a lowpass filter with a single-pole rolloff, which for frequencies much larger than the 3 dB bandwidth is very close to an ideal integrator. The cost of this highly linear integration is RF loss, which must be compensated for using amplification after integration. Also, due to the limited phase swing of external phase modulators (and hence the limited achievable frequency deviation, as discussed in Appendix C.1.3), a larger input power must be expended using an external modulator than direct modulation of a laser diode.

8.3.3.2 Operation at High Intermediate Frequencies

The improved linearity and RIN suppression achieved in the PM and FM links is associated with operation at a high IF. There are, however, practical limitations to the IF based on available component technology. Using commonly available microwave components, IFs in the 10 - 20 GHz range are practical. Substantially higher IFs may be difficult or expensive to achieve. Additionally, in principle, receivers operating at lower frequencies can use higher input impedances to achieve lower thermal noise power spectral densities (PSDs) than those operating at high frequencies [4]. However, to utilize standard microwave amplifiers with input impedances of 50 W, it is convenient to use photodiodes with an output impedance of 50 W. There are a number of commercial photodiodes with 3 dB frequencies of > 20 GHz which provide a 50 W output impedance (e.g., BT&D model no. PDC4310). We assume that such a photodiode is utilized in the systems we have analyzed.

The increased SFDR associated with increasing the IF is due primarily to the improved linearity of the delay-line discriminator at high frequencies (a secondary effect is a reduction in RIN). This SFDR improvement will only be evident, however, if adequate amplification is provided in the receiver to compensate for the increased loss due

to the small slope of the discriminator frequency response. At some point, other nonlinear effects may become dominant, and increasing the IF will not necessarily lead to further increases in the SFDR.

8.4 References

[1] G. L. Abbas, V. W. S. Chan, and T. K. Yee, "A dual-detector optical heterodyne receiver for local oscillator noise suppression," *IEEE J. Lightwave Technol.*, vol. LT-3, no. 5, pp. 1110 - 1122, 1987.

[2] E. H. Armstrong, "A method of reducing disturbances in radio signaling by a system of frequency modulation," *Proc. IRE*, vol. 24, pp. 689-740, 1936.

[3] D. J. Fitzmartin, E. J. Balboni, and R. G. Gels, "Wide-band analog frequency modulation of optic signals using indirect techniques," *Proc. of the SPIE*, vol. 1371, pp. 78-86, 1990.

[4] N. Takachio and K. Iwashita, "A novel resonance-type optical receiver for high-speed optical heterodyne transmission systems," *IEEE J. Lightwave Technol.*, vol. 7, no. 9, pp. 1371-1378, 1989.

Chapter Nine

Reference Transport Links: Interferometric Approach

In this chapter, we consider reference transport as a means of transmitter phase noise cancellation (PNC) in angle-modulated analog links. In Section 9.1, we introduce the reference transport concept and describe our motivation for investigating it. In Section 9.2, we describe conventional approaches and why they do not work for coherent angle-modulated analog links. We then present our novel approach to deal with the PNC problem, which utilizes interferometric links. In Section 9.3, we describe our novel approach to optical frequency shifting through sideband generation using electro-optic external modulation and other possible approaches. In Section 9.4, we describe angle modulated heterodyne interferometric links, which are based upon the novel approach of section 9.3, and give SNRs, SFDRs, RF power transfer ratios, and noise figures for both phase and frequency modulation. In Section 9.5, we describe angle modulated homodyne interferometric links and give SNRs, SFDRs, RF power transfer ratios, and noise figures for both phase and frequency modulation. In Section 9.6, we compare the SFDRs, RF power transfer ratios, and noise figures of the links in Sections 9.4 and 9.5 with those of intensity-modulated direct detection (IMDD) and coherent angle-modulated links. In Section 9.7, we describe and give results for a proof-of-concept HIPM link built in our laboratory. Section 9.8 contains references.

9.1 Introduction: Reference Transport Links

As seen in Chapter 8, laser phase noise is the primary factor limiting the SFDR of coherent angle-modulated analog links, particularly those using semiconductor lasers. Techniques to reduce or eliminate the impact of phase noise are, as a result, of great interest for these links. Reference transport techniques for PNC modulate only part of the source laser power while transporting the remainder to the receiver. That power is used as a reference to cancel the phase noise of the transmitter. Such systems can be realized in a variety of ways which may bear little resemblance to each other.

In basic reference transport systems, the power from the source laser is split before modulation. The light in one of these arms is modulated with the signal, while the

light on the second arm is sent to the receiver through an auxiliary path and used as the local oscillator (Fig. 9-1). An auxiliary path can be realized in a variety of ways, including a separate fiber or an orthogonal polarization in a single fiber [1]. The optical portion of this system is essentially an interferometer. In order to obtain the desired performance, the phase of the optical carrier in the reference arm must be related to that in the signal arm. This means that the optical lengths of the two arms must be matched to within a fraction of the coherence length of the source laser; for laser diodes with linewidths on the order of 100 MHz, this requires matching path lengths to within less than 1 m. Note that this kind of approach cannot be used for coherent links, since the phase noise of the local oscillator (LO) laser cannot be canceled.

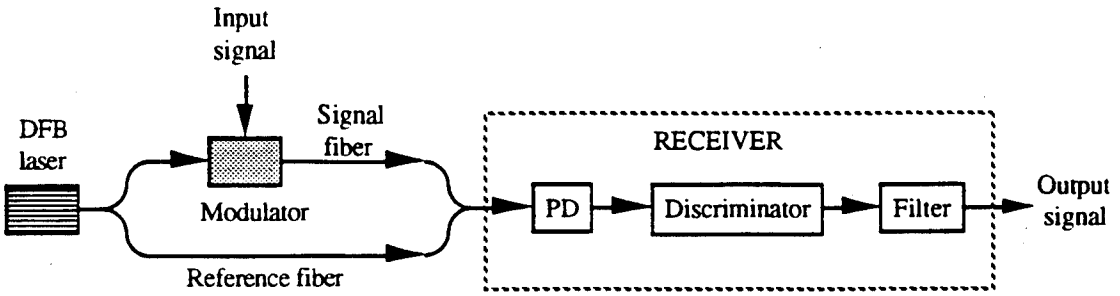

Fig. 9-1. A basic reference transport system employing an additional fiber to deliver the local oscillator signal to the receiver.

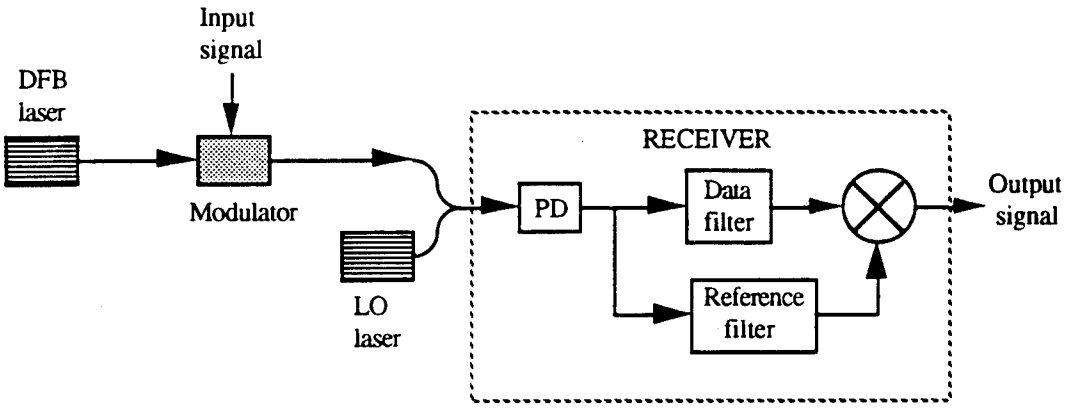

Fig. 9-2. Reference transport system utilizing an unmodulated carrier as a reference.

A more sophisticated reference transport system [2] is shown in Fig. 9-2. It has no auxiliary path and a second laser can be used as the LO. The operation of this system depends on the presence of a strong unmodulated carrier term embedded in the received signal spectrum. In the receiver, the unmodulated carrier is separated from the modulated

signal spectrum and used as a reference, allowing cancellation of phase noise. This technique is applicable when there is appreciable power in the carrier and when the signal sidebands are well separated from the carrier.

Reference transport links like that of Fig. 9-2 have been used successfully in narrowband phase-modulated analog links [2, 3]. This is because the small modulation index (<< 1) of narrowband phase-modulated signals allows the signal to be expanded as so:

$$\begin{aligned}\cos(\omega t + \varphi[x(t)]) &= \cos(\omega t)\cos(\varphi[x(t)]) - \sin(\omega t)\sin(\varphi[x(t)]) \\ &\approx \cos(\omega t) - \left(\varphi[x(t)] - \frac{(\varphi[x(t)])^3}{3!} + \ldots\right)\sin(\omega t)\end{aligned} \tag{9.1}$$

Eq. (9.1) shows that the signal sideband $\varphi[x(t)]\sin(\omega t)$, which is an AM signal, can be filtered out and demodulated just as in the heterodyne AM-WIRNA link. In this case, the signal will be distorted by third-order intermodulation distortion (IMD) products of exactly the same form as in AM-WIRNA. The SFDR performance and bandwidth requirements of narrowband angle-modulated links, as a result, are identical to those of AM-WIRNA.

As described in Chapter 1, a modulation index of at least 1 is required for angle-modulated links to show a significant SNR improvement over AM links. To detect the resulting wideband signal, a delay-line discriminator which mixes the signal and a delayed version of itself (shown in Figs. 9-7 and 9-8) is required. This discriminator behaves differently from a heterodyne AM demodulator. During this project we have investigated the feasibility of reference transport for wideband angle-modulated links.

9.2 Reference Transport in Analog Links

In Sections 9.2.1 and 9.2.2, we describe why conventional reference transport techniques cannot be applied to analog angle-modulated links. In Section 9.2.3, we consider how reference transport techniques can be applied to these links.

9.2.1 Reference Transport in Links Using Direct FM

A link using direct FM is shown in Fig. 8-2(b), and the link analysis is given in Appendix C.1.1. The signal entering the discriminator, omitting white noise terms, is proportional to $\cos\left(\omega t + \omega_\Delta \int_t x(t')dt' + \Delta\upsilon(t)\right)$. This can be written in the form

$$\cos\left(\omega t + \int_t \left(\omega_\Delta x(t') + \frac{d}{dt'}\Delta\upsilon(t')\right)dt'\right) \tag{9.2}$$

The results of Appendix A.2.3 indicate that the derivative of the laser phase noise process is white noise. As a result, laser phase noise in links using direct FM is equivalent to white noise in the original applied RF signal; this noise is clearly not removable using electronic processing at the receiver.

The above statement is validated by the following brief discussion of the residual carrier approach of Fig. 9-2. Fig. 9-3 shows the frequency spectrum of an FM signal corrupted by phase noise.

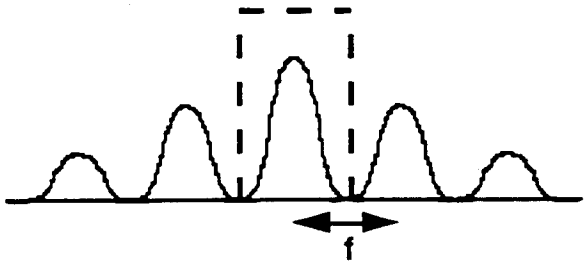

Fig. 9-3. Frequency spectrum of an FM signal corrupted by phase noise.

The dashed lines show the frequency response of an idealized reference filter. After the filtered carrier component is mixed with the corrupted FM signal, an FM signal is recovered which is corrupted only by the tails of the phase noise which lay outside the reference filter bandwidth. After detection, the power spectrum of the detected signal is then corrupted by $S_\Phi(\omega)S_{HPF}(\omega)S_D(\omega)$, where $S_\Phi(\omega)$ and $S_D(\omega)$ are the power spectra of the phase noise and the discriminator, respectively. $S_{HPF}(\omega)$ is ideally equal to 0 from DC to a frequency equal to half the width of the reference filter and 1 for all other frequencies. Since the derivative of the laser phase noise process is white noise, the detected signal is corrupted by white noise with a "hole" at DC. It is impossible for this

hole to extend to the signal frequency band unless the reference filter is of width greater than twice the maximum signal frequency; the detected signal will then be severely distorted, since the reference filter will then pass frequency components other than the carrier.

9.2.2 Reference Transport in Links Using External PM or FM

Externally modulated coherent links using PM and FM are shown in Figs. 8-1 and 8-2(a), respectively. The FM photocurrent for these links is of an identical form to Eq. (9.2), and hence the residual carrier method of section 9.2.1 will not work. The PM photocurrent is of the form $\cos\left(\omega t + \varphi_{\Delta} x(t) + \Delta\upsilon(t)\right)$. Though this looks slightly different from Eq. (9.2), the laser phase noise in links using external PM is equivalent to noise in the original applied RF signal with power spectral density given in Eq. (A.18) of Appendix A.2.3. As a result, the arguments of section 9.2.1 again apply.

It is certainly possible to cancel phase noise in externally modulated links by using a two-fiber approach such as that in Fig. 9-1. The problem with this method is that since there is no LO laser, the detected photocurrent is at baseband. This is acceptable for digital systems using phase-shift-keying (PSK) [4]. Analog links using FM or PM, however, use discriminators which must operate at an IF frequency much larger than the maximum signal frequency. Any reference transport approach which will succeed for analog angle-modulated links, therefore, must generate an angle-modulated signal at an IF before demodulation without using an LO laser.

9.2.3 Our Novel Approach: Interferometric Links

The name "interferometric links" refers to the novel class of reference transport links which (a) cancel phase noise by splitting power from the transmitter laser and transporting this reference with the optical signal to the receiver, in a single fiber or in separate fibers; and (b) generate an angle-modulated signal at an IF before demodulation without using an LO laser. There are two types of interferometric links. A heterodyne interferometric link is shown in Fig. 9-4. In this link, references separated from the transmitter laser frequency by the desired IF are generated using optical single-sideband frequency shifting or sideband generation. The received photocurrent is then at the desired IF, and demodulation can take place immediately after IF amplification.

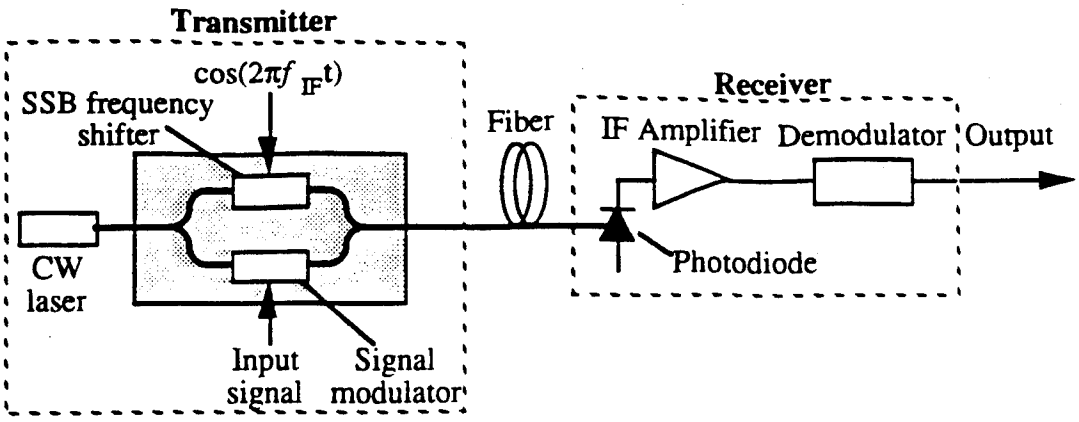

Fig. 9-4. Heterodyne interferometric link using optical single-sideband frequency shifter.

A homodyne interferometric link is shown in Fig. 9-5. In this link, the received photocurrent is at baseband, which means that the desired IF signal must be generated electrically (using mixers). An idealized homodyne interferometric link is analogous to an idealized heterodyne interferometric link in that both require single-sideband frequency shifters, one at microwave frequencies and the other at optical frequencies.

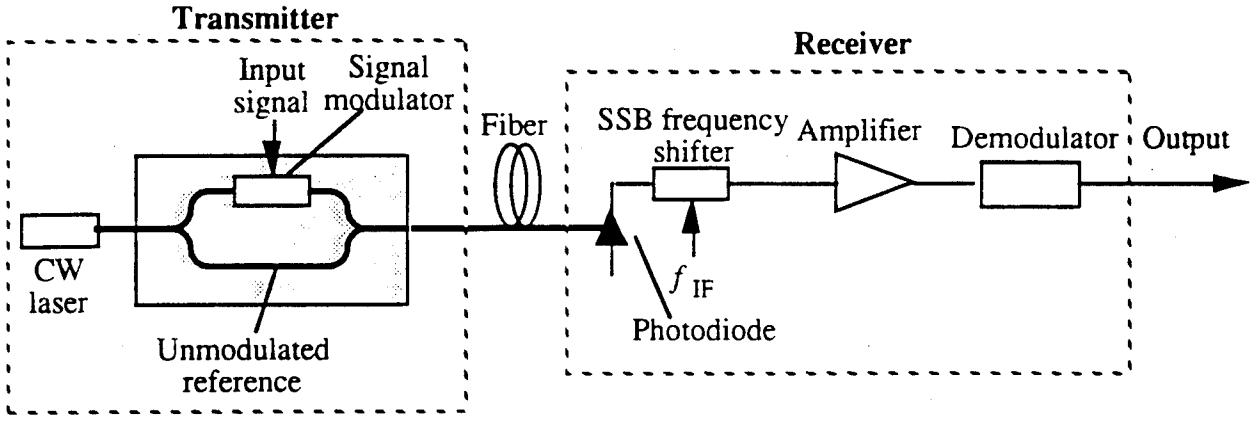

Fig. 9-5. Homodyne interferometric link using microwave single-sideband frequency shifter.

9.3 Optical Frequency Shifting in Heterodyne Interferometric Links

The ideal optical frequency shifter for use in a heterodyne interferometric link is lossless and transfers the input optical power fully to an optical frequency separated from the original frequency by the desired IF without generation of spurious components.

In Section 9.3.1, we briefly describe the state-of-the-art in true single-sideband (SSB) optical frequency shifters. In Section 9.3.2, we present a novel electro-optic sideband generator which can generate the desired reference with relatively low loss for desired IFs well above 10 GHz.

9.3.1 Single-Sideband Optical Frequency Shifters

SSB optical frequency shifting for interferometric links can be performed using acousto-optic or magneto-optic modulation of the reference. In both cases, acoustic or magnetic waves are propagated in a material which will generate the desired phase grating, which has maxima spaced by a distance corresponding to the desired IF frequency. After passing through the material, the input reference field is split into several diffraction orders, each separated from the input reference by some multiple of the IF. The nice feature of these approaches is that true single-sideband frequency shifting by the IF occurs for the first diffraction order. The problems, however, are numerous. There is tremendous loss of more than 20 dB due to the low conversion efficiency of the first diffracted order of the grating. It is very difficult to integrate such an optical frequency shifter into a rugged, compact form, and there will be significant additional loss due to coupling of the first diffracted order into a fiber. Though magneto-optic shifters have been demonstrated which operate at above 10 GHz [5], acousto-optic shifters are limited to IFs of a few GHz by acoustic attenuation and transducer fabrication limitations [6].

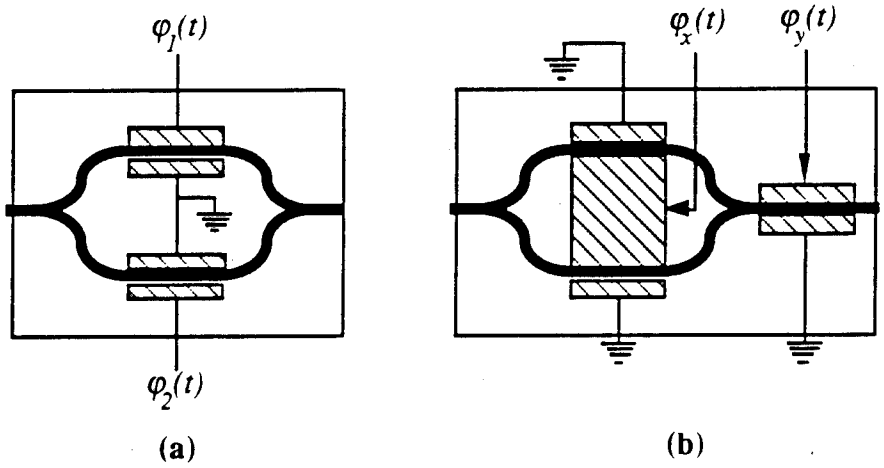

Fig. 9-6. Two implementations of an electro-optic quasi-SSB frequency shifter.

9.3.2 A Novel Approach: Sideband Generation Using External Modulation

We present a novel electro-optic modulation technique which can be used in the reference leg to generate a phase-modulated signal which has significant components at the desired IF above and below the laser optical frequency. This method can generate an angle-modulated signal at an IF at the receiver with a small penalty relative to ideal SSB frequency shifting and is well-suited to monolithic integration with other electro-optic devices. We refer to it as quasi-SSB frequency shifting. The signal modulator could be any sort of external modulator, but it is only sensible to use external PM or FM.

Fig. 9-6 shows two functionally identical implementations of the quasi-SSB frequency shifter. In Fig. 9-6(a), the modulator legs are phase modulated by quadrature CW RF signals at the desired shifting frequency. The DC optical phase bias between the legs must be $p/2$, which is the same bias required in a typical MZ amplitude modulator. In Fig. 9-6(b), the frequency shifter is implemented using a MZ amplitude modulator followed by a phase modulator (the order of the two sections is irrelevant). For $\varphi_1(t) = \beta\cos(\omega_{IF}t) + \frac{\varphi_b}{2}$ and $\varphi_2(t) = \beta\sin(\omega_{IF}t) - \frac{\varphi_b}{2}$, the output field phasor for a bias phase of $p/2$ is easily shown to be

$$E_{out}(t) = E_{in}(t)J_1(\beta)\exp(i\omega_{IF}t) + \frac{E_{in}(t)}{\sqrt{2}}\left[J_0(\beta) + J_2(\beta)\cos(2\omega_{IF}t) + \ldots\right] \quad (9.3)$$

where $E_{in}(t)$ is the input optical field phasor. The first term is the desired SSB frequency-shifted optical field, while the other terms are the unshifted carrier and higher-order terms. If ω_{IF} is much larger than the modulating signal bandwidth (which must be the case in any angle-modulated analog system), the undesired cross terms between the signal and the output of the frequency shifter can be filtered out in the post-detection electronics. The implementation in Fig. 9-6(b), which is used in the experiment in Section 9.7, is equivalent to that in Fig. 9-6(a) for $\varphi_x(t) = \frac{1}{2}(\varphi_1(t) - \varphi_2(t))$ and $\varphi_y(t) = \frac{1}{2}(\varphi_1(t) + \varphi_2(t))$.

9.4 Heterodyne Interferometric Links

In this section, we present heterodyne interferometric links using phase modulation (HIPM) and frequency modulation (HIFM). We give their performance measures, including SNR, SFDR, RF power transfer ratio, and noise figure. We then briefly discuss implementation details for this type of link.

9.4.1 Link Description

The heterodyne interferometric link is shown in Fig. 9-7. The transmitter consists of a CW laser and a novel three-leg modulator. The modulator is an integrated version of the electro-optic sideband generator of Section 9.3.2, with one leg driven by the signal and the other two legs driven by quadrature CW RF signals at a frequency w_{IF} and optically phase shifted by $p/2$ from each other. After traversing a fiber-optic link, the signal is detected at the receiver. The optical signals of the second and third legs of the modulator mix with the signal at the detector and result in a series of single-sideband signals at multiples of w_{IF}. Following IF amplification and filtering, the signal is limited. It is then put through a delay-line filter, an envelope detector, and an integrator; these three components function in tandem as a phase demodulator. We refer to the entire system as an HIPM link. An HIFM link has only one difference, which is that the integrator precedes the signal leg of the phase modulator rather than following the envelope detector.

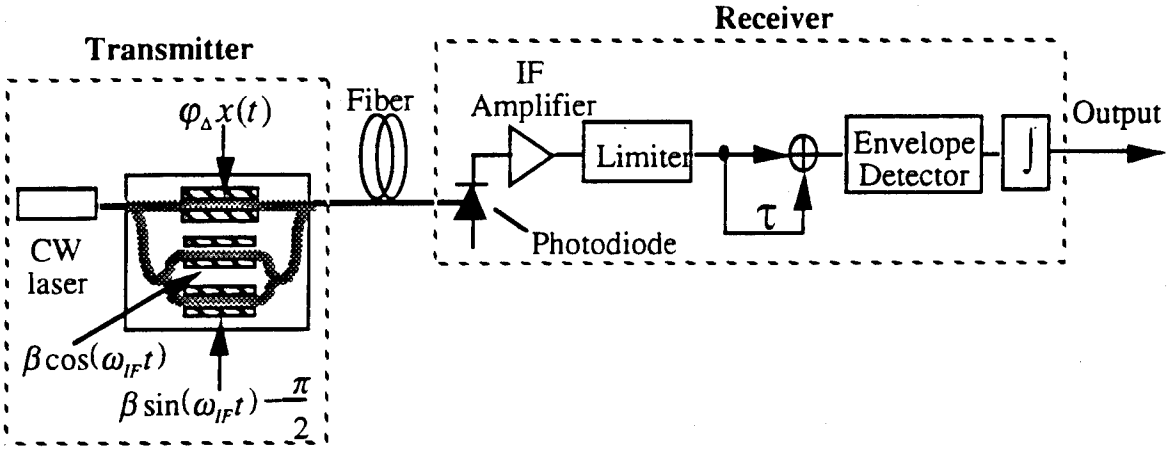

Fig. 9-7. Phase-modulated implementation of HIPM link with novel electro-optic modulator.

9.4.2 Signal-to-Noise Ratio (SNR)

The derivation of the HIPM and HIFM link SNRs are given in Appendix C.2.1. The expressions are

$$SNR_{HIPM} = \varphi_{\Delta}^2 \left[\left(\frac{4RPJ_1(\beta)}{9} \right)^2 \frac{\langle x^2(t) \rangle}{\langle n_{shot\,bp}^2 \rangle + \langle n_{thermal\,bp}^2 \rangle + \left(\frac{RP}{3} \right)^2 \left(1 + \frac{2}{3} J_0(\beta) \right)^2 \langle n_{RIN\,bp}^2 \rangle} \right] \tag{9.4}$$

$$SNR_{HIFM} = \left(\frac{\omega_{\Delta}}{B} \right)^2 \left[\left(\frac{4RPJ_1(\beta)}{9} \right)^2 \frac{B^2 \langle x^2(t) \rangle}{\langle i_{shot\,bp}^2 \rangle + \langle i_{thermal\,bp}^2 \rangle + \left(\frac{RP}{3} \right)^2 \left(1 + \frac{2}{3} J_0(\beta) \right)^2 \langle i_{RIN\,bp}^2 \rangle} \right] \tag{9.5}$$

where φ_{Δ} is the HIPM modulation index, $\frac{\omega_{\Delta}}{B}$ is the HIFM modulation index (traditional FM modulation index scaled by 2π), R is the photodiode responsivity, P is the laser optical power assuming that link and modulator excess loss are compensated by amplification in the link, B is the signal bandwidth, $\langle x^2(t) \rangle$ is the power of the applied signal (assumed equal to 1), and β is the amplitude of the applied IF sinusoids. The noise terms in the denominators are defined in Appendix A.2.

9.4.3 Spurious-free Dynamic Range (SFDR)

The SFDR of both links can be expressed by

$$SFDR = \left[\frac{8SNR_o}{3|b_3|} \right]^{2/3} \tag{9.6}$$

where SNR_o is defined as the terms in square brackets in Eqs. (9.4) and (9.5) and $|b_3|$, the third-order nonlinearity coefficient, is $\frac{1}{6}\left(\frac{\pi f_{max}}{2f_{IF}} \right)^2$ for the HIPM link and $\frac{1}{6}\left(\frac{B}{4f_{IF}} \right)^2$ for the HIFM link.

9.4.4 RF Power Transfer Ratio and Noise Figure

The derivation of RF power transfer ratio and noise figure for the HIPM and HIFM links is given in Appendix C.2.2. The expressions are

$$G_{opt(HIPM)} = G_{opt(HIFM)} = \left(\frac{1}{4f_{IF}}\right)^2 \frac{16}{81} R^2 P^2 J_1^2(\beta) \left(\frac{\pi}{V_\pi R_{\text{int}} C_{\text{int}}}\right)^2 R_S^2 L_{nl} \qquad (9.7)$$

where R_{int} and C_{int} are parameters of the integrating lowpass filter, R_S is the receiver impedance, and L_{nl} is the nonlinear loss of the limiter and the envelope detector.

The noise figures of the HIPM and HIFM links are given by

$$F_{(link)} = 1 + \frac{noise\ power\ at\ link\ output}{G_{(link)} kTB} \qquad (9.8)$$

where kTB represents the thermal noise power at the link input. The noise powers at the link output are given in Appendix C.2.2.

9.5 Homodyne Interferometric Angle Modulated Links

In this section, we present homodyne interferometric links using phase modulation (HPM) and frequency modulation (HFM). We give their performance measures, including SNR, SFDR, RF power transfer ratio, and noise figure. We then briefly discuss implementation details for this type of link.

9.5.1 Link Description

The homodyne interferometric link is shown in Fig. 9-8. The objective of the homodyne interferometric link, as described in Section 9.2.3, is to generate a photocurrent at a desired intermediate frequency before the IF amplifier by using microwave components to perform the necessary frequency shifting. This objective is achieved as follows. The output of a CW laser is modulated using a Mach Zehnder modulator with two outputs. A two-output modulator is usually constructed with a built-in 3-dB coupler directly preceding the outputs. The dc bias phase between the two legs, j_b, is arbitrary. The two outputs of the Mach Zehnder modulator are put through another 3-

dB coupler and a 90∞ optical hybrid before detection at the receiver. At the receiver, the two detected currents are mixed up to an IF by quadrature signals, added, and put through an identical receiver to that of the heterodyne interferometric link. We refer to the entire system as an HPM link. An HFM link has only one difference, which is that the integrator precedes the signal leg of the phase modulator rather than following the envelope detector.

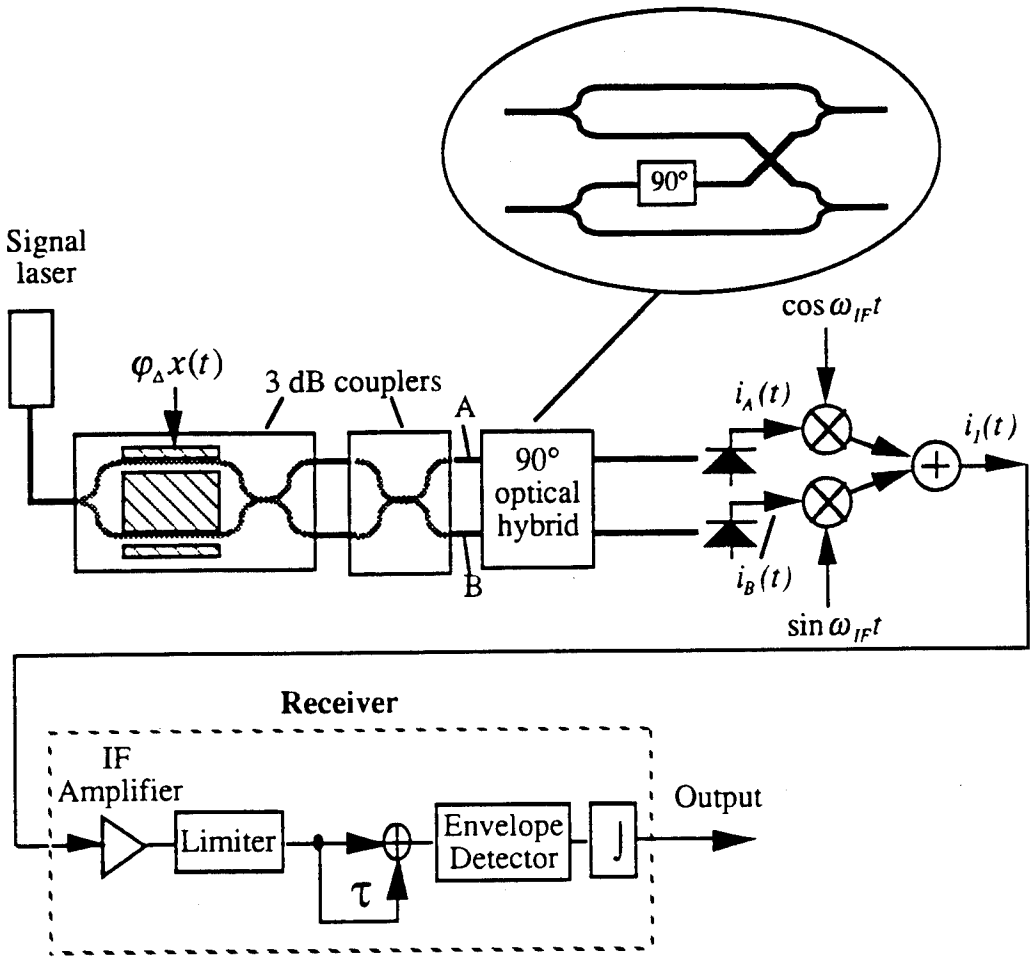

Fig. 9-8. Homodyne interferometric phase modulated link.

9.5.2 Signal-to-Noise Ratio (SNR)

The derivation of the HPM and HFM link SNRs are given in Appendix C.3.1. The expressions are

$$SNR_{HPM} = \varphi_{\Delta}^2 \left[\left(\frac{RP}{4} \right)^2 \frac{\langle x^2(t) \rangle}{\langle i_{recA\ bb}^2 \rangle + \langle i_{recB\ bb}^2 \rangle + \left(\frac{RP}{4} \right)^2 \langle i_{RIN\ bb}^2 \rangle} \right] \tag{9.9}$$

$$SNR_{HFM} = \left(\frac{\omega_{\Delta}}{B} \right)^2 \left[\left(\frac{RP}{4} \right)^2 \frac{B^2 \langle x^2(t) \rangle}{\langle i_{recA\ bb}^2 \rangle + \langle i_{recB\ bb}^2 \rangle + \left(\frac{RP}{4} \right)^2 \langle i_{RIN\ bb}^2 \rangle} \right] \tag{9.10}$$

where φ_{Δ} is the HPM modulation index, $\frac{\omega_{\Delta}}{B}$ is the HFM modulation index (traditional FM modulation index scaled by 2π), R is the photodiode responsivity, P is the laser optical power assuming that link and modulator excess loss are compensated by amplification in the link, B is the signal bandwidth, and $\langle x^2(t) \rangle$ is the power of the applied signal (assumed equal to 1). The noise terms in the denominators are defined in Appendix A.2 and Appendix C.3.1.

9.5.3 Spurious-free Dynamic Range (SFDR)

The SFDR of both links can be expressed by

$$SFDR = \left[\frac{8SNR_o}{3|b_3|} \right]^{2/3} \tag{9.11}$$

where SNR_o is defined as the terms in square brackets in Eqs. (9.9) and (9.10) and $|b_3|$, the third-order nonlinearity coefficient, is $\frac{1}{6}\left(\frac{\pi f_{\max}}{2 f_{IF}} \right)^2$ for the HPM link and $\frac{1}{6}\left(\frac{B}{4 f_{IF}} \right)^2$ for the HFM link.

9.5.4 RF Power Transfer Ratio and Noise Figure

The derivation of RF power transfer ratio and noise figure for the HPM and HFM links is given in Appendix C.3.2. The expressions are

$$G_{opt(HPM)} = G_{opt(HFM)} = \left(\frac{1}{4f_{IF}}\right)^2 \frac{1}{16} r^2 P_S^2 \left(\frac{\pi}{V_\pi RC}\right)^2 R_S^2 L_{nl} \alpha \qquad (9.12)$$

where R and C are parameters of the integrating lowpass filter, R_S is the receiver impedance, and L_{nl} is the nonlinear loss of the limiter and the envelope detector.

The noise figures of the HPM and HFM links are given by

$$F_{(link)} = 1 + \frac{noise\ power\ at\ link\ output}{G_{(link)} kTB} \qquad (9.13)$$

where kTB represents the thermal noise power at the link input. The noise powers at the link output are given in Appendix C.3.2.

9.6 Comparison of Interferometric Angle Modulated Links

In this section, we compare the performance of the interferometric angle modulated links as measured by SFDR (Section 9.6.1), RF power transfer ratio, and noise figure (Section 9.6.2). We discuss implementation considerations for interferometric angle modulated links in Section 9.6.3.

9.6.1 SFDR Comparison

Fig. 9-9 compares the SFDRs of the heterodyne interferometric links, the homodyne interferometric links, and a direct detection link for a laser RIN of -155 dB/Hz. The value of linewidth has no bearing on this plot due to the reference transport in the interferometric links. Since the reference of the interferometric links is split from the transmitter laser instead of from a separate local oscillator laser, the SFDR of interferometric links is also limited by thermal noise at optical powers below 1 mW. The improved discriminator linearity due to the high intermediate frequency compensates for the intrinsic losses of the interferometric modulator structures (three-leg modulator for heterodyne, optical hybrid for homodyne). The potential SFDR advantages for heterodyne and homodyne interferometric links at low powers are about 6 dB and 2 dB, respectively. As the received signal optical power* increases above 1 mW, the

* For the interferometric and DD links, the received optical power is normalized to take into account the intrinsic loss due to the biasing or other intrinsic losses of the external modulators. This is for the purposes of a fair comparison to the coherent angle modulated links.

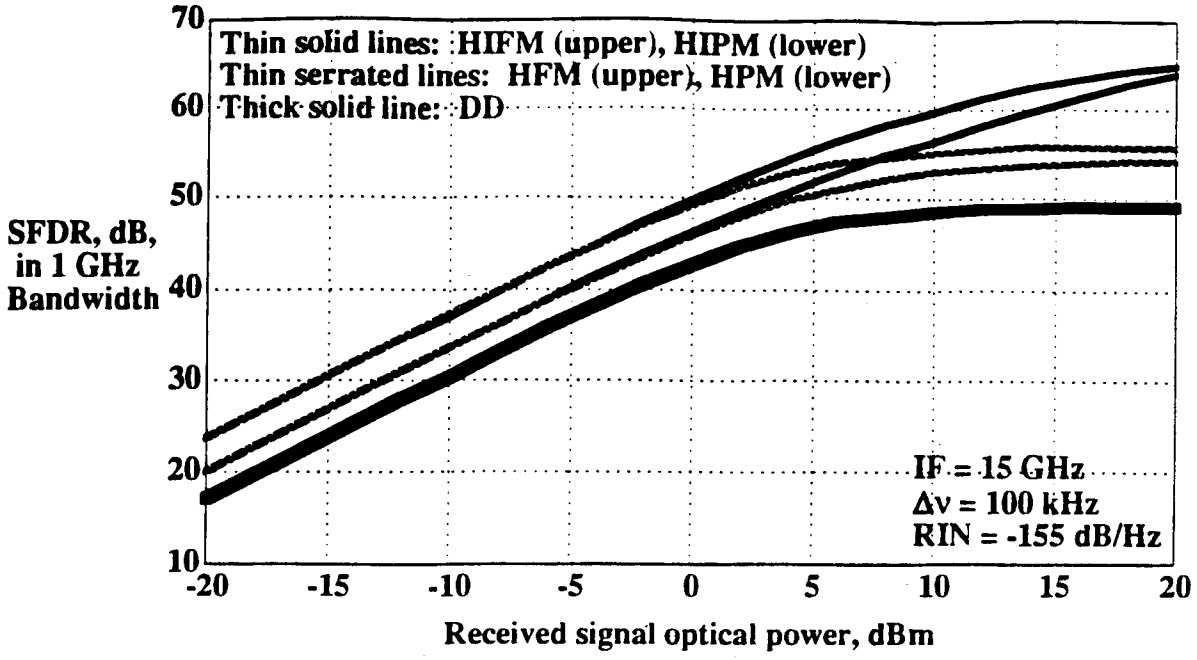

Fig. 9-9. SFDRs of HIFM, HIPM, HFM, HPM, and DD links plotted versus received signal optical power for laser RIN of -155 dB/Hz and a laser linewidth of 100 kHz.

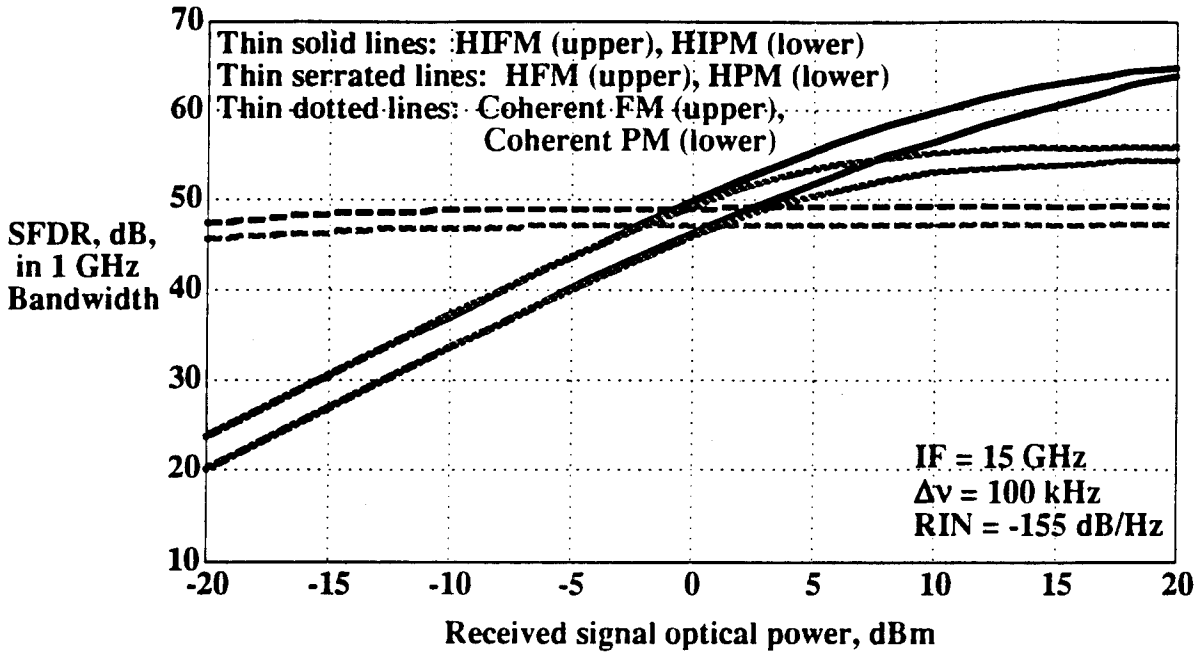

Fig. 9-10. SFDRs of HIFM, HIPM, HFM, HPM, coherent FM, and coherent PM links plotted versus received signal optical power for a laser RIN of -155 dB/Hz and a laser linewidth of 100 kHz.

heterodyne interferometric links begin to outperform the DD and homodyne interferometric links. This is because the heterodyne links are impacted by bandpass RIN, which is suppressed at frequencies far above the laser relaxation resonance frequency. The homodyne links are impacted by baseband RIN and gain little relative to the DD link. Another trend in Fig. 9-9 is that the advantage of the FM links over the PM links tends to decrease at optical powers above 1 mW. For powers below 1 mW, the FM links outperform the PM links because the higher frequencies of the 1 GHz to 2 GHz signal are suppressed by the integrator in the FM transmitter. Since the delay-line discriminator is more linear for lower signal frequencies, the SFDR of the FM links is higher than that of the PM links. For powers above 1 mW, the impact of the laser RIN affects the FM links more than the PM links because the signal frequencies are not at baseband, causing a noise augmentation effect (relative to PM) during demodulation. The HIFM link shows an 11 dB SFDR advantage over the DD link at a 10 mW optical power.

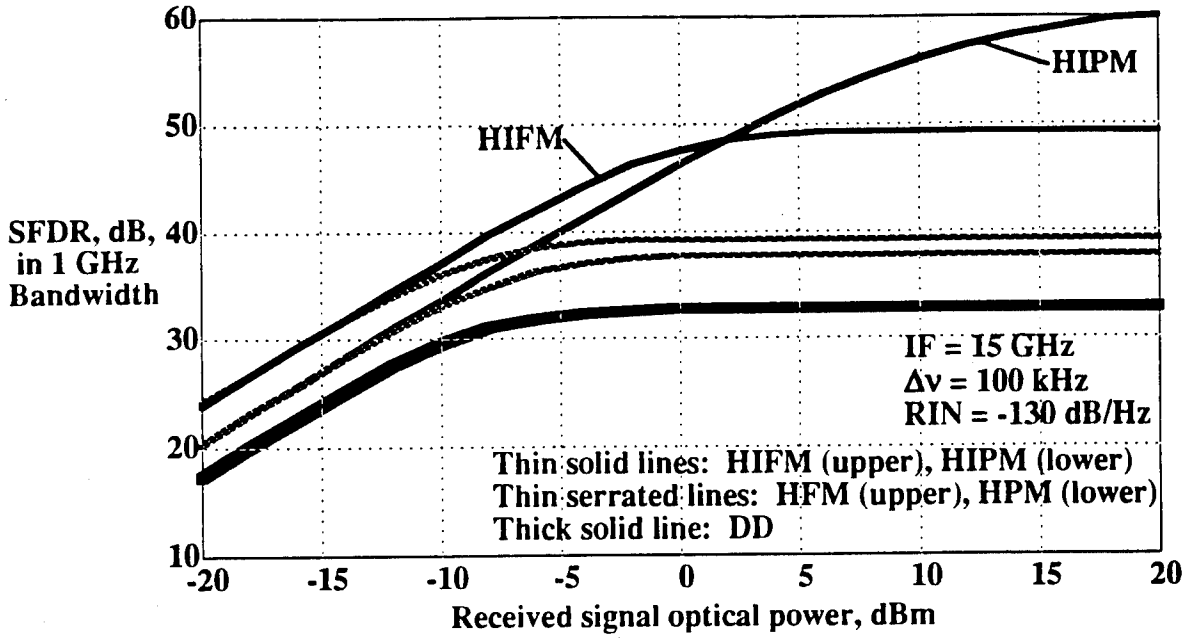

Fig. 9-11. SFDRs of HIFM, HIPM, HFM, HPM, and DD links plotted versus received signal optical power for a laser RIN of -130 dB/Hz and a laser linewidth of 100 kHz.

Fig. 9-10 shows the SFDRs of the interferometric links and the coherent angle modulated links plotted versus received signal optical power for a laser RIN of -155 dB/Hz and a laser linewidth of 100 kHz. For this value of linewidth, the SFDRs of the coherent links are essentially constant over the entire range of optical powers, since the laser linewidth is the dominant source of noise. The coherent FM link exhibits an 11 dB

SFDR advantage over the HIFM link at 100 μW optical power. The interferometric links begin to outperform the coherent links at optical powers in the 1 to 2 mW range, with the HIFM link showing a 10 dB SFDR advantage over the coherent FM link at 10 mW optical power.

Fig. 9-11 shows the significantly larger SFDR improvements made possible by the heterodyne interferometric links for a laser RIN of -130 dB/Hz. In this case, the HIPM link outperforms the HIFM link for optical powers larger than about 2 mW, for the same reason cited in the description of Fig. 9-9. At an optical power of 10 mW, the HIPM link exhibits a 23 dB SFDR advantage over the DD link.

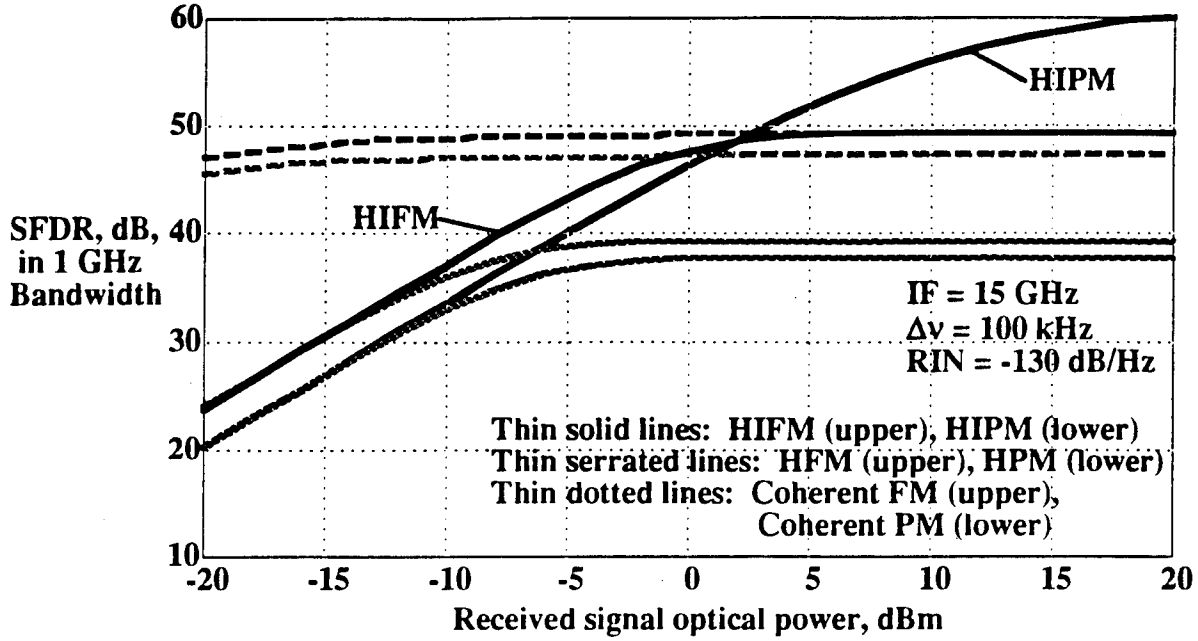

Fig. 9-12. SFDRs of HIFM, HIPM, HFM, HPM, coherent FM, and coherent PM links plotted versus received signal optical power for a laser RIN of -130 dB/Hz and a laser linewidth of 100 kHz.

Fig. 9-12 shows the improved performance of the coherent angle modulated links relative to the interferometric links for a laser RIN of -130 dB/Hz. The improvement is due to the use of balanced receivers in conjunction with limiters in the coherent angle modulated links, which render them essentially immune to laser RIN. In this case, only the HIPM link outperforms the coherent FM link, and then only for optical powers greater than 2 mW.

9.6.2 RF Power Transfer Ratio and Noise Figure Comparison

Fig. 9-13 shows the RF power transfer ratios (PTRs) of the interferometric links, the coherent angle modulated links, and the DD link plotted versus received signal optical power for the parameters listed in Table 9-1.

Table 9-1. Parameter values used in numerical computation of RF power transfer ratios and noise figures.

Parameter	Assumed Value	Parameter	Assumed Value
LO power P_{LO}	10 mW	Mod. voltage V_π	15 V
RIN	-155 dB/Hz	HIPM index β	1
Relaxation osc. freq.	2 GHz	RC time constant	1.21E-9 s
Laser linewidth $\Delta\upsilon$	10 kHz or 1 MHz	Source imped. R_S	50 Ω
Signal bandwidth B	1 GHz	Conversion loss α	6 dB
Min. sig. freq. f_{min}	1 GHz	Nonlinear loss L_{nl}	6 dB
Max. sig. freq. f_{max}	2 GHz	Int. freq. f_{IF}	10 GHz
Laser FM resp. γ	1 GHz/mA	Responsivity r	0.8

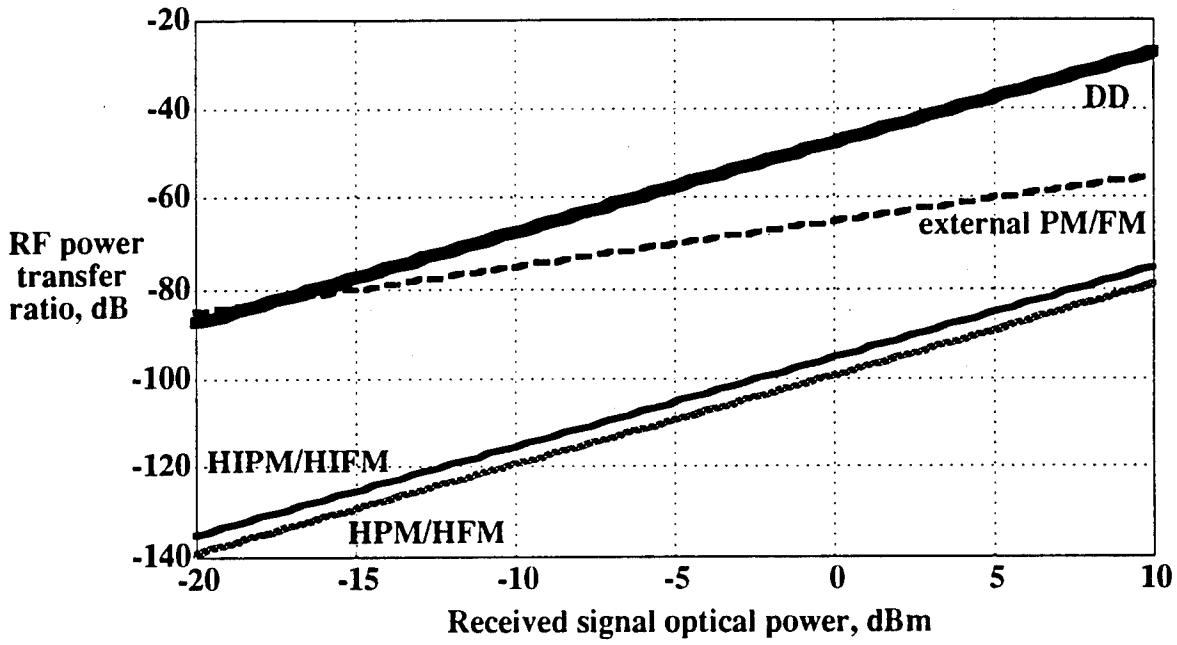

Fig. 9-13. RF power transfer ratios of HIFM, HIPM, HFM, HPM, coherent FM, coherent PM, and DD links plotted versus received signal optical power for the parameters listed in Table 9-1.

Fig. 9-13 shows that the interferometric links, in addition to having the same integrator and discriminator losses as the externally modulated coherent angle modulated links, also lose power due to the losses in the conversion process needed to obtain receiver signals at the desired intermediate frequencies. These losses come from imperfect optical frequency shifting and intrinsic modulator losses in the heterodyne links and from optical hybrid and mixer losses in the homodyne links. As a result, extra amplification is required in the interferometric links to compensate for these losses.

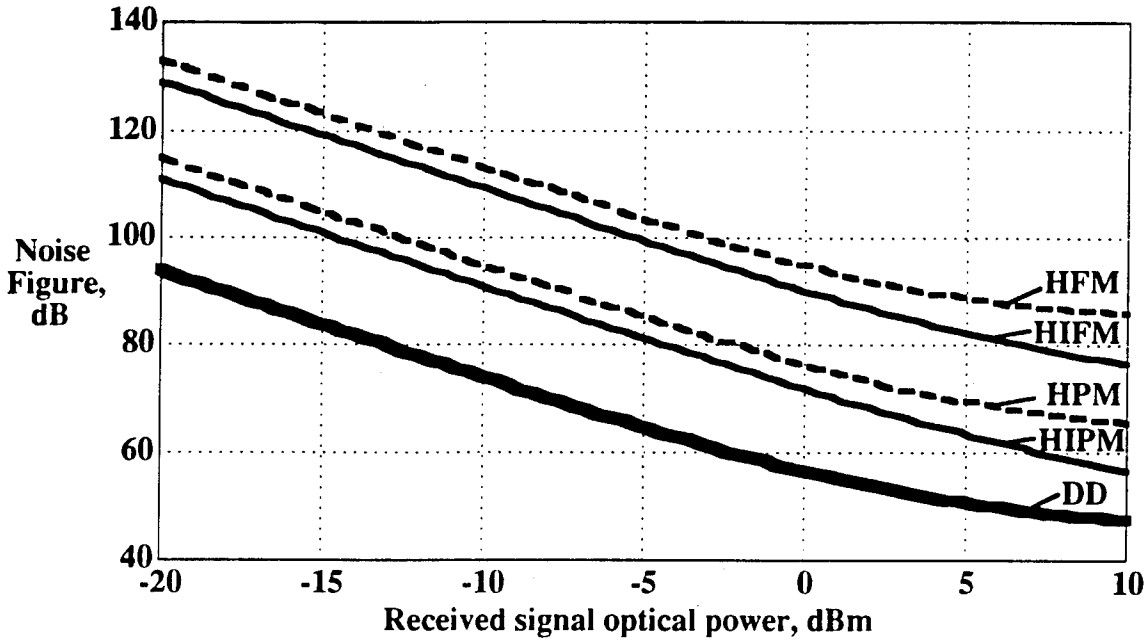

Fig. 9-14. Noise figures of HIFM, HIPM, HFM, and HPM links plotted versus received signal optical power for the parameters listed in Table 9-1.

Fig. 9-14 shows the noise figures of the interferometric links and the DD link plotted versus received signal optical power for the parameters listed in Table 9-1. The noise figures of the coherent angle modulated links are not included in this plot because those noise figures are obviously linewidth dependent. These noise figures are for the basic links without amplification, which is why the values are so high. With adequate low noise amplification, the noise figures can be greatly reduced. Fig. 9-14 indicates that more noise is generated in the FM links than in the PM links. This is because the signal frequencies are far from baseband, leading to noise augmentation during FM demodulation instead of noise suppression.

9.6.3 Implementation Considerations

In this section, we briefly consider some implementation details of heterodyne and homodyne interferometric links. For simplicity, details will be listed and addressed in order.

Maximum available external modulation depth and RF loss: This is addressed in Appendix C.1.3.

Choice of IF frequency: As stated in Chapter 8, it is possible using commercially available components to build modulators and receivers which operate for frequencies in the 10 GHz to 20 GHz range. The benefits of a high IF are more linear discriminator operation and greater RIN suppression. The disadvantages of a high IF are larger discriminator loss, higher thermal noise, and greater receiver cost and complexity.

Bias phase: There can be an arbitrary bias phase between the signal arm and the reference arms in the modulators for either the heterodyne or homodyne links. This bias phase is slowly varying relative to the signal and will not impact discriminator operation.

Modulator splitting coefficients in the heterodyne links: It is important that the spurious IF terms be eliminated through the appropriate choice of β, amplitude of the applied IF sinusoids. It is possible to determine a β for which the signal loss is insignificant provided that the loss in the two arms of the modulator corresponding to the IF sinusoids are nearly equal. This condition holds in regular Mach-Zehnder amplitude modulators and should not be difficult to achieve in a three-legged integrated device. Note that the splitting loss in the signal arm need not be the same as the loss in the two IF arms.

Quadrature of IF sinusoids in the heterodyne links: If the RF sinusoids are off of quadrature by an angle θ, the ratio of signal to distortion due to this goes as $\cot^2 \theta$. For a θ of 1 degree, this gives a signal to distortion ratio of 35 dB. Given that the wavelength of a 10 GHz signal is 3 cm, it is easily possible using delay lines in integrated form to achieve a θ of far less than one degree, if necessary. Including these delay lines in the modulator will not significantly increase its complexity or its size.

Construction of an optical hybrid in the homodyne links: An optical hybrid is difficult to build due to the precise optical phase shift required over a wide range of optical

frequencies. This requirement can be met over signal bands of several GHz using special polarization-dependent phase-shifting techniques. However, these techniques require bulk optics which must be continuously aligned as the optical frequency of the laser changes. The loss, size, and inconvenience of such hybrids has made the construction of all homodyne optical systems very difficult [7].

Mixers as frequency shifters in the homodyne links: The nonlinear loss of mixers arises from the imperfect sideband generation of these microwave devices. The spurious nonlinearities of mixers are difficult to predict and to model, but they will have a potentially significant impact on the homodyne links, particularly for the frequency shifting of wide bands of frequencies.

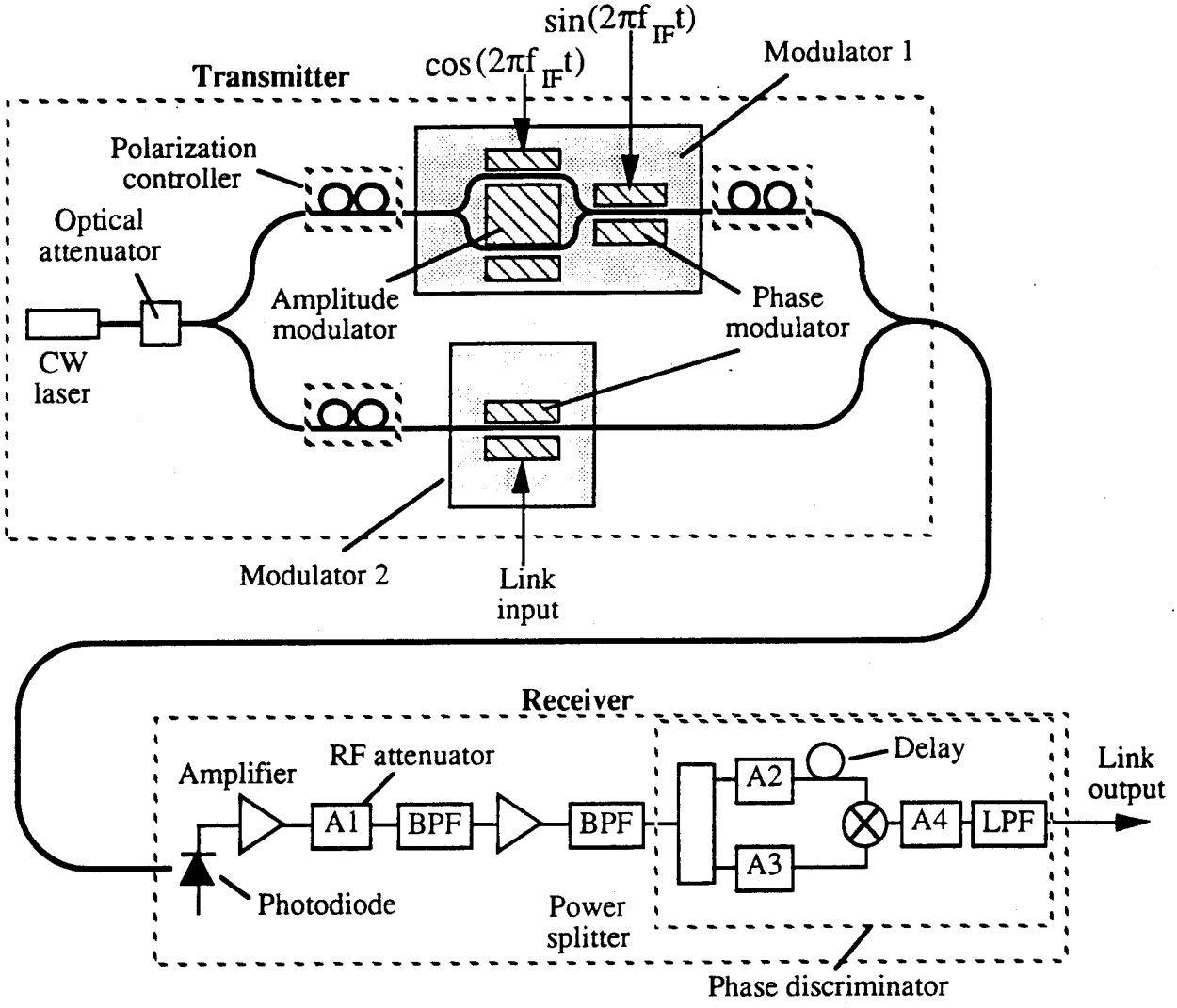

Fig. 9-15. Block diagram of experimental HIPM link.

9.7 HIPM Link: Experiment

This section presents preliminary results from the proof-of-concept experimental HIPM link which we have constructed in our laboratory [8]. Fig. 9-15 shows a simplified block diagram of the experimental link. The optical source consists of a CW Nd:YAG laser followed by an optical attenuator. The three-leg HIPM modulator is implemented using combination amplitude/phase modulators with 1 GHz 3 dB bandwidths which were available in our laboratory. The two sections of modulator 1 are driven with sinusoidal IF signals (at 650 MHz, in this implementation) in quadrature; modulator 2 is driven by the signal to be transmitted. The AM section of modulator 1 was biased where MZ modulators are typically biased, at $V_p/2$ below the maximum transmission point. After detection, the electrical signal is amplified, bandpass filtered, and sent through a phase discriminator. The discriminator consists of an RF power splitter, two delay lines of different length, a mixer, and an integrator (single pole lowpass filter). The length difference between the two delay lines was set to one quarter of the IF RF wavelength.

For an applied signal made up of sinusoids with frequencies f_{min} and f_{max}, we measured the two-tone third-order IMP levels at frequencies $2f_{min} - f_{max}$ and $2f_{max} - f_{min}$ at the link output using an RF spectrum analyzer. The theoretical ratios of the IMP power levels, $\langle i_{IMP}^2 \rangle$, to the signal power levels, $\langle i_s^2 \rangle$, for the AM direct detection link and the HIPM link are given by

$$\left[\frac{\langle i_{IMP}^2 \rangle}{\langle i_s^2 \rangle}\right]_{AM} = \frac{\varphi_\Delta^4}{64} \tag{9.14}$$

$$\left[\frac{\langle i_{IMP}^2 \rangle}{\langle i_s^2 \rangle}\right]_{HIPM} = \left(\frac{2\pi f_{max}}{4 f_{IF}}\right)^4 \frac{\varphi_\Delta^4}{64} \tag{9.15}$$

where φ_Δ is the modulation depth. These equations come directly from the results in Section 8.2.3. The AM direct detection link IMP measurements were made by removing modulator 1, modulating the AM port of modulator 2, and measuring the IMP levels after detection.

Fig. 9-16 compares the measured ratios of third-order IMP levels to signal levels vs. modulation depth of modulator 2 in radians of the HIPM and AM direct detection links. The two applied tones have frequencies f_{min} = 95 MHz and f_{max} = 105 MHz.

Our HIPM link demonstrated IMP levels that are consistently lower than those of an externally modulated AM direct detection link for the same modulation depths. The corresponding SFDR improvement in dB equals one-third of the IMP suppression in dB (see Eqs. (8.6)-(8.8)).

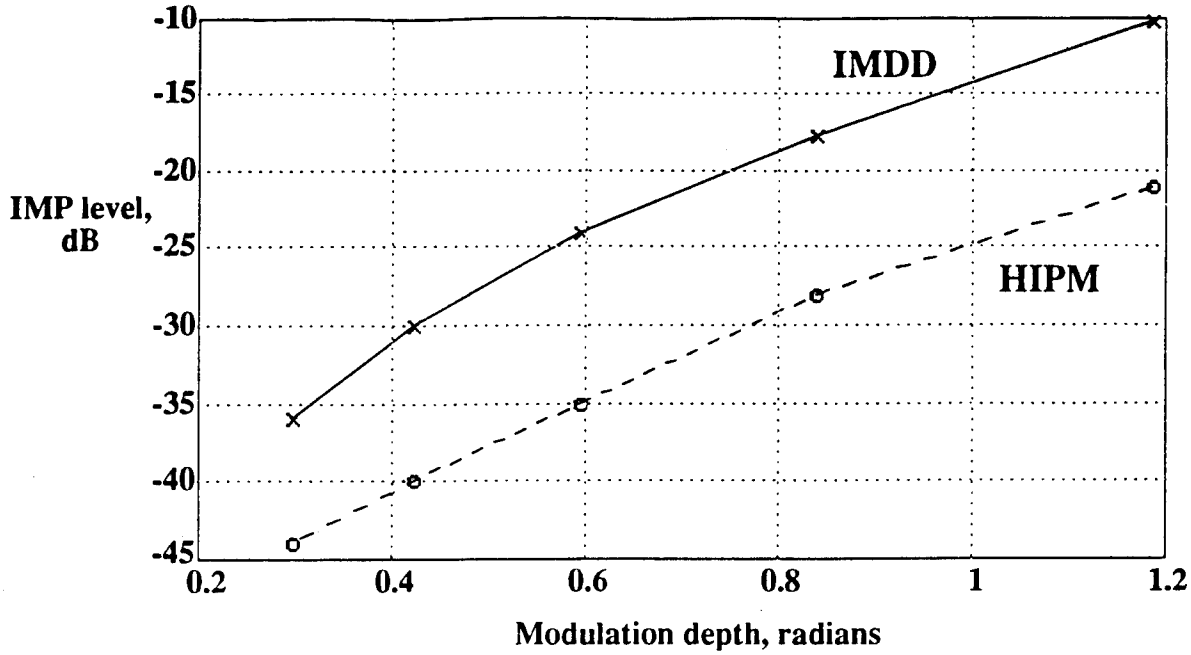

Fig. 9-16. Intermodulation product level vs. modulation depth for HIPM (o) and IMDD (x) links; f_{min} = 95 MHz and f_{max} = 105 MHz.

We investigated nonideal receiver component characteristics, such as amplifier, mixer, and discriminator nonlinearities, by altering the values of the RF attenuators in the receiver (A1 - A4), shown in Fig. 9-15. Fig. 9-17 shows the ratio of the HIPM link IMP levels to the AM direct detection link IMP levels vs. of modulation depth for two receiver configurations. For this case, f_{min} = 47.5 MHz and f_{max} = 52.5 MHz. Configuration 1 corresponds to A1 = 6 dB, A2 = 3 dB, A3 = 6 dB, and A4 = 6 dB. Configuration 2 corresponds to A1 = 10 dB, A2 = 0 dB, A3 = 6 dB, and A4 = 6 dB. The HIPM link demonstrates as much as 23 dB IMP suppression, which corresponds to 7.7 dB SFDR improvement. However, the HIPM link third-order nonlinear coefficient $(2\pi f_s / 4f_{IF})^4$ gives a theoretical two-tone third-order IMP suppression of 44 dB. Clearly, the link performance is limited by nonideal receiver component characteristics, and not by the intrinsic link nonlinearity predicted using Eq. (9.15). Fig. 9-17 shows that the IMP levels at various modulation depths can be varied over a large range by changing the position and value of RF attenuators in the receiver. This effect cannot be explained

by considering ideal receiver component characteristics, but can be caused by a number of nonideal factors including mixer nonlinearities, nonideal discriminator and filter characteristics, and amplifier nonlinearities.

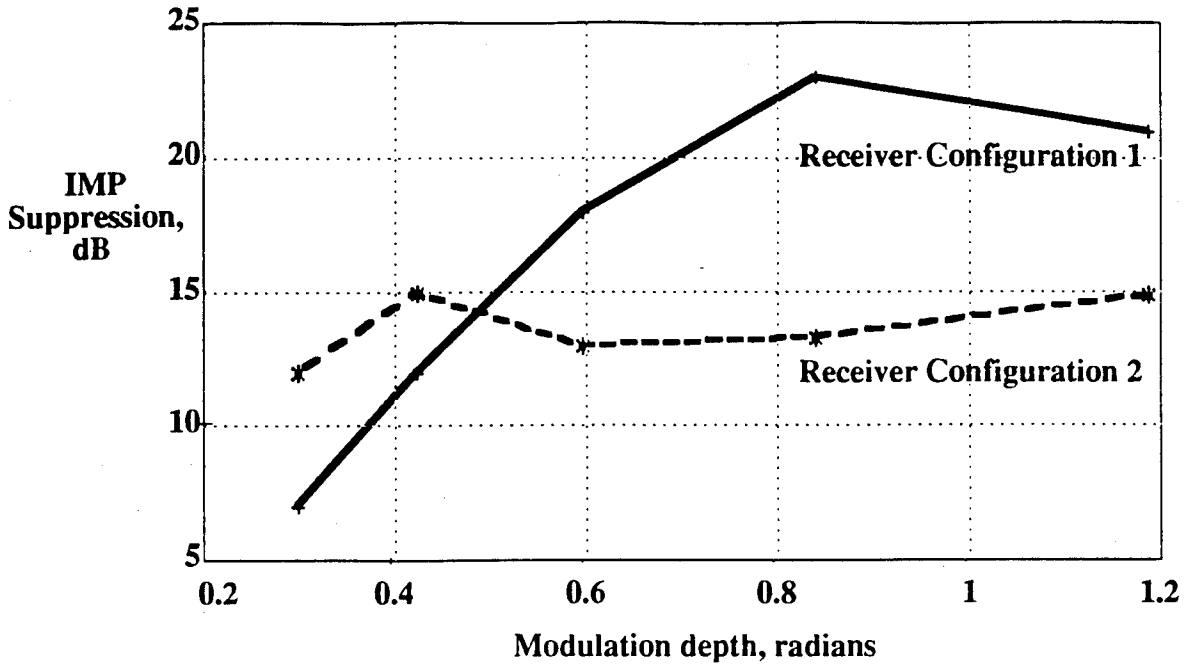

Fig. 9-17. Intermodulation distortion suppression of the HIPM link over an IMDD link for receiver configuration 1 (A1 = 6 dB, A2 = 3 dB, A3 = 6 dB, A4 = 6 dB) and receiver configuration 2 (A1 = 10 dB, A2 = 0 dB, A3 = 6 dB, A4 = 6 dB). f_{min} = 47.5 MHz and f_{max} = 52.5 MHz.

Even though our receiver could be significantly improved through the use of better components, the best third-order IMP suppression that we demonstrated is comparable to that in optimized implementations of linearized IMDD links [9]. This result suggests that the HIPM link may be a promising alternative to conventional linearized AM direct detection links for achieving high SFDR.

9.8 References

[1] S. Betti et al., "Phase noise and polarization state insensitive optical coherent systems," *IEEE J. Lightwave Technol.*, vol. 8, no. 5, pp. 756-767, 1990.

[2] R. Gross, R. Olshansky, and M. Schmidt, "Coherent FM-SCM system using DFB lasers and a phase noise cancellation circuit," *IEEE Photon. Technol. Lett.*, vol. 2, no. 1, pp. 66-68, 1990.

[3] PCO Inc., "Coherent fiber optic links," Final Report, Contract no. F30603-86-C-0004, 1989.

[4] K. Tamura et al., "Phase-noise canceled differential phase shift keying (PNC-DPSK) for coherent optical communication systems," *IEEE J. Lightwave Technol.*, vol. 8, no. 2, pp. 190-201, 1990.

[5] Y. Pu and C. Tsai, "Wideband integrated magnetooptic frequency shifter and modulator at X-band," *Proc. of the IEEE 1992 Ultrasonics Symposium*, pp. 161-164, 1992 (Tuscon, AZ).

[6] C. S. Tsai, "Integrated acoustooptic circuits and applications," *IEEE Trans. Ultrasonics, Ferroel., and Freq. Control*, vol. 39, no. 5, pp. 529-554, 1992.

[7] P. J. Lin, "Impact of pathlength difference on phase diversity ASK homodyne receivers using a 90 degrees hybrid," *Proc. of the SPIE - Multigigabit Fiber Communications*, pp. 410-419, 1992 (Boston, MA).

[8] R. F. Kalman and L. G. Kazovsky, "Demonstration of an analog heterodyne interferometric phase-modulated (HIPM) link," accepted for publication in *IEEE Photon. Technol. Lett.*.

[9] M. Nazarathy et al., "Progress in externally modulated AM CATV transmission systems," *IEEE J. Lightwave Technol.*, vol. 11, no. 1, pp. 82-105, 1993.

Optically Amplified Interferometric Links

In this chapter, we consider the use of optical amplifiers to increase the available optical power in interferometric links using semiconductor lasers and to compensate for link losses in real systems. In Section 10.1, we describe the interferometric link which we will model in this chapter. In Section 10.2, we present its SFDR. In Section 10.3, we provide results and discussion for antenna remoting applications.

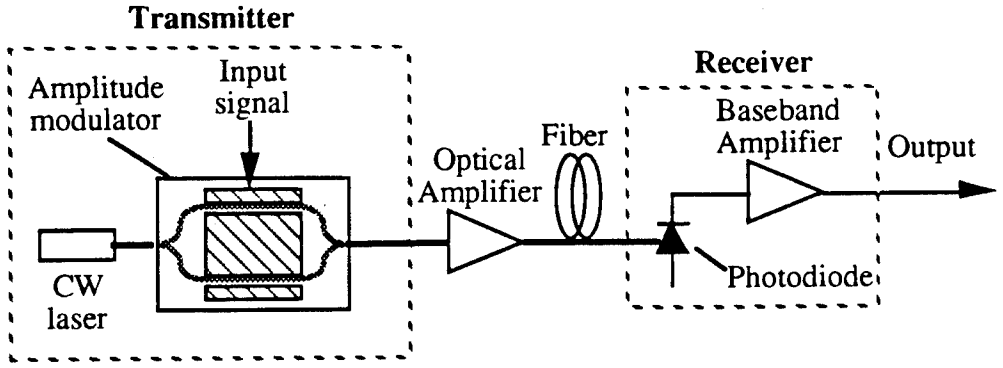

Fig. 10-1(a). Generic optically amplified direct detection link.

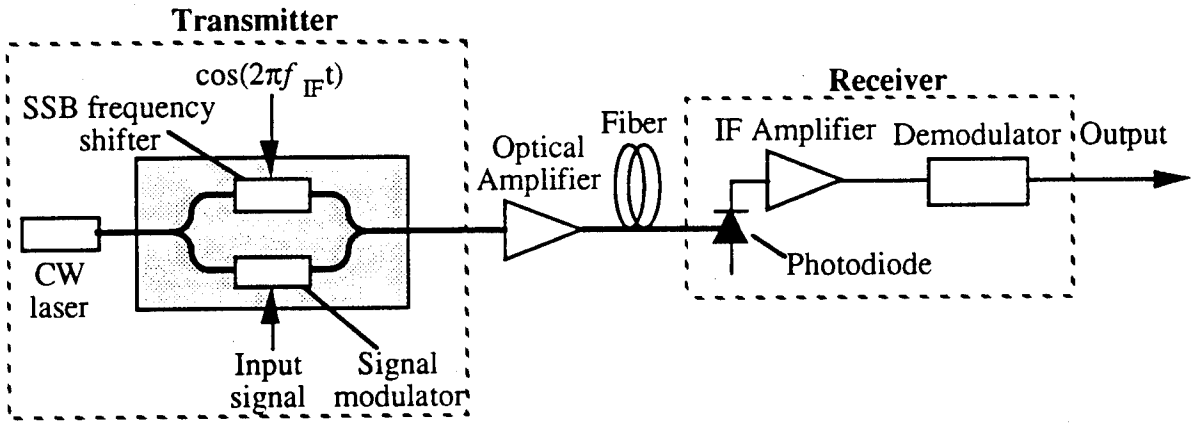

Fig. 10-1(b). Generic optically amplified heterodyne interferometric link.

10.1 Link Description

Block diagrams of a conventional direct detection (DD) link and a generic heterodyne interferometric link are shown in Figs. 10-1(a) and 10-1(b), respectively. In the DD case, the signal voltage is applied to a standard Mach-Zehnder (MZ) modulator, which modulates the optical field output of the CW laser. The modulator output is optically amplified, received, and amplified at baseband. Note that in this chapter, we will be primarily interested in the operation of these links at laser powers greater than -10 dBm* since, as described in Chapter 9, interferometric links offer the potential for SFDR improvement over DD and coherent links at high powers. Since the spontaneous-spontaneous beat noise due to optical amplification is not significant for high powers, the insertion of an optical filter will not have a noticeable impact on interferometric or DD link performance. In the heterodyne interferometric link, the transmitter optical power is split between a reference path and a signal path. The optical frequency of the reference is shifted by an amount f_{IF} using a single sideband (SSB) frequency shifter. The optical signals are coupled into a single fiber and are optically amplified.

10.2 SFDR

In this section, we derive the SNRs at the outputs of the heterodyne interferometric and DD links, and from there the corresponding SFDRs. Section 10.2.1 gives SFDR expressions for a generic heterodyne interferometric link. Section 10.2.2 gives the specific SFDR expressions for the specific implementation of the heterodyne interferometric link described in Section 9.4.1.

10.2.1 SFDR of a Generic Optically Amplified Interferometric Link

The received photocurrent after the photodiode in a generic optically amplified heterodyne interferometric (OAHI) link is given by

$$i_{OAHI}(t) = R\left|\sqrt{P_{opt}GL(1+n_{RIN}(t))}\left(\sqrt{L_{sig}L_{xsig}}\exp i\left[\omega_{opt}t+\varphi_{sig}\{x(t)\}+\varphi_p(t)+\varphi_b\right]+\right.\right.$$
$$\left.\left.\sqrt{L_{ref}L_{xref}}\exp i\left[\left(\omega_{opt}+\omega_{IF}\right)t+\varphi_p(t)\right]\right)+\sqrt{L}\left(n_{OA\hat{s}}(t)+n_{OA\hat{o}}(t)\right)\right|^2+n_{sh}(t)+n_{th}(t) \tag{10.1}$$

* Note that we refer to laser power instead of received optical power. Link losses and modulator losses are taken into account in all numerical results presented in this chapter.

where R is the photodiode responsivity, P_{opt} is the output optical power of the laser, G is the power gain of the optical amplifier, L is the total link loss, $n_{RIN}(t)$ is the laser relative intensity noise (RIN) process, L_{sig} is the ratio between the power entering the signal modulator and the laser power assuming ideal splitting (0.5 for even splitting), L_{xsig} is the excess loss of the signal modulator, w_{opt} is the angular optical frequency, $j_{sig}\{x(t)\}$ is the phase term due to the applied signal voltage $x(t)$ (corresponding to either PM or FM), $j_p(t)$ is the laser phase noise process, j_b is an arbitrary and slowly varying phase between the signal and reference legs, L_{ref} is the ratio between the power entering the frequency shifter and the laser power assuming ideal splitting, L_{xref} is the excess loss of the frequency shifter, w_{IF} is the desired angular intermediate frequency, $n_{OA\hat{s}}(t)$ and $n_{OA\hat{o}}(t)$ are due to the amplified spontaneous emission (ASE) of the optical amplifier in the signal polarization and orthogonal to the signal polarization, respectively, $n_{sh}(t)$ is due to the shot noise, and $n_{th}(t)$ is due to the receiver thermal noise.

Note that the phase noise process is eliminated through mixing at the photodiode, assuming that the lengths of the modulator legs are matched to within a fraction of the laser coherence length. This is easy to achieve in a monolithic modulator structure but may be difficult in a separate fiber configuration. After amplification, the signal is detected using either phase or frequency discrimination.

After mathematical manipulation, the output currents for the DD link (which is simply the current after the photodiode) and for the heterodyne interferometric link can be derived. The DD output current is derived exactly as in Chapter 2 with slight modifications due to the presence of an optical amplifier. Note that we neglect high-order noise terms and signal-cross-noise terms except for those due to the optical amplifier since analog links have high SNRs and small modulation depths. The result is (with parameters repeated from Eq. (10.1) having the same meanings)

$$i_{DD\,out}(t) \cong R\frac{P_{opt}}{2}GLL_{xsig}\left[mx(t) - \frac{m^3}{6}x^3(t) + n_{RIN\,bb}(t)\right] + RL\sqrt{2P_{opt}GL_{xsig}}\,n_{OA\hat{s}\,bp}(t) + RL\left|n_{OA\hat{s}\,bp}(t)\right|^2 + RL\left|n_{OA\hat{o}\,bp}(t)\right|^2 + n_{D\,bb}(t) \tag{10.2}$$

m is the amplitude modulation depth and $n_D(t)$ refers to the sum of shot and thermal noise. The subscript bb indicates baseband noise, which refers to noise which is added to the signal band after the signal has been converted to baseband. The subscript bp indicates bandpass noise, which refers to noise which is added to the signal band when

it is located on a high-frequency carrier. The second term is a signal-spontaneous noise cross term, and the third and fourth terms are spontaneous-spontaneous cross terms in the two orthogonal polarizations.

The OAHI PM and FM output currents are derived similarly to the coherent PM and FM output currents in Appendix C.1.1. The results are

$$i_{OAHI\ PM\ out}(t) \cong K\{2RP_{opt}GL\sqrt{L_{sig}L_{xsig}L_{ref}L_{xref}}\left[\varphi_\Delta x(t) - \frac{\varphi_\Delta^{\,3}}{6}\left(\frac{1}{4f_{IF}}\right)^2\int \dot{x}^3(t)dt\right] + n_{D\,bp}(t) + RP_{opt}GLL_{sig}L_{xsig}n_{RIN\,bp}(t) + RL\left(\sqrt{2P_{opt}G}\left(\sqrt{L_{sig}L_{xsig}} + \sqrt{L_{ref}L_{xref}}\right)n_{OA\hat{s}\,bp}(t) + n_{sp\text{-}sp\,bp}(t)\right)\} \tag{10.3}$$

$$i_{OAHI\ FM\ out}(t) \cong T\{2RP_{opt}GL\sqrt{L_{sig}L_{xsig}L_{ref}L_{xref}}\left[\omega_\Delta x(t) - \frac{\omega_\Delta^{\,3}}{6}\left(\frac{1}{4f_{IF}}\right)^2 x^3(t)\right] + \dot{n}_{D\,bp}(t) + RP_{opt}GLL_{sig}L_{xsig}\dot{n}_{RIN\,bp}(t) + RL\left(\sqrt{2P_{opt}G}\left(\sqrt{L_{sig}L_{xsig}} + \sqrt{L_{ref}L_{xref}}\right)\dot{n}_{OA\hat{s}\,bp}(t) + \dot{n}_{sp\text{-}sp\,bp}(t)\right)\} \tag{10.4}$$

where K and T are scaling factors dependent on the amount of RF amplification and T has dimensions of seconds.

$$n_{sp\text{-}sp\,bp}(t) = \left|n_{OA\hat{s}\,bp}(t)\right|^2 + \left|n_{OA\hat{o}\,bp}(t)\right|^2 \tag{10.5}$$

The third-order nonlinearity terms arise due to the imperfect linearity of the delay-line phase discriminator. Second-order nonlinearity terms, which are not shown above, can be ignored assuming that the signal bandwidth is restricted to a single octave. The additional terms in Eqs. (10.3) and (10.4) which do not fall into the form presented in Appendices C.1.1 and C.2.1 are the three final terms, which are the signal-spontaneous (s-sp), reference-spontaneous (r-sp), and spontaneous-spontaneous (sp-sp) beat noise contributions to the output currents. Sinusoidal components which reduce the s-sp and r-sp powers in the link output SNR expressions by a factor of 2 have been replaced by a scaling factor of $\frac{1}{\sqrt{2}}$ for simplicity. Note that the s-sp and r-sp noises do not add coherently, only on a power basis. The arbitrary slowly-varying bias phase has no impact on discriminator operation.

For these three links, the corresponding signal-to-noise ratios are given by

$$SNR_{DD} = m^2 \frac{\left(RP_{opt}GLL_{xsig}\right)^2 \left\langle x^2(t)\right\rangle}{\left(4\left\langle n_{D\,bb}^2\right\rangle + \left(RP_{opt}GLL_{xsig}\right)^2 \left\langle n_{RIN\,bb}^2\right\rangle + (2RL)^2 \left\langle n_{sp-sp\,bp}^2\right\rangle + 8(RL)^2 P_{opt}GL_{xsig}\left\langle n_{OA\hat{s}\,bp}^2\right\rangle\right)} \tag{10.6}$$

$$SNR_{OAHI\,PM} = \varphi_\Delta^2 \frac{\left(2RP_{opt}GL\right)^2 L_{sig}L_{xsig}L_{ref}L_{xref}\left\langle x^2(t)\right\rangle}{\left(\left\langle n_{D\,bp}^2\right\rangle + \left(RP_{opt}GLL_{sig}L_{xsig}\right)^2 \left\langle n_{RIN\,bp}^2\right\rangle + (RL)^2 \left\langle n_{sp-sp\,bp}^2\right\rangle + 2(RL)^2 P_{opt}G\left(L_{sig}L_{xsig}\left\langle n_{OA\hat{s}\,bp}^2\right\rangle + L_{ref}L_{xref}\left\langle n_{OA\hat{o}\,bp}^2\right\rangle\right)\right)} \tag{10.7}$$

$$SNR_{OAHI\,FM} = \left(\frac{\omega_\Delta}{B}\right)^2 \frac{\left(2RP_{opt}GLB\right)^2 L_{sig}L_{xsig}L_{ref}L_{xref}\left\langle x^2(t)\right\rangle}{\left(\left\langle \dot{n}_{D\,bp}^2\right\rangle + \left(RP_{opt}GLL_{sig}L_{xsig}\right)^2 \left\langle \dot{n}_{RIN\,bp}^2\right\rangle + (RL)^2 \left\langle \dot{n}_{sp-sp\,bp}^2\right\rangle + 2(RL)^2 P_{opt}G\left(L_{sig}L_{xsig}\left\langle \dot{n}_{OA\hat{s}\,bp}^2\right\rangle + L_{ref}L_{xref}\left\langle \dot{n}_{OA\hat{o}\,bp}^2\right\rangle\right)\right)} \tag{10.8}$$

where B is the bandwidth of the baseband signal $x(t)$. The various noise expressions in Eqs. (10.6) - (10.8), not including the optical amplifier noise terms, are evaluated in Appendix A.2. The optical amplifier noise expressions are presented in Appendix A.3. Eqs. (10.6) - (10.8) indicate that the SNR increases monotonically with modulation index. The maximum useful modulation index is limited by intermodulation distortion associated with nonlinear effects. From here, the SFDR is easily derived as in Section 8.2.3. The SFDRs of the HIPM, HIFM, and DD links are given by

$$SFDR = \left[\frac{8SNR_o}{3|b_3|}\right]^{2/3} \tag{10.9}$$

where

$$SNR = r^2 SNR_o \tag{10.10}$$

Eq. (10.10) is in the same form as Eqs. (10.2) - (10.4), where r is the modulation index (m for IMDD link, φ_Δ for the HIPM link, and $\frac{\omega_\Delta}{B}$ for the HIFM link) and SNR_o is the signal-to-noise ratio for unity modulation index. b_3 is the third-order nonlinearity

coefficient for each link and is given by $-\frac{1}{6}$ for the IMDD link, $-\frac{1}{6}\left(\frac{\pi f_{max}}{2f_{IF}}\right)^2$ for the HIPM link, and $-\frac{1}{6}\left(\frac{B}{4f_{IF}}\right)^2$ for the HIFM link. For an IF frequency much larger than the maximum signal frequency or the signal bandwidth, the third-order nonlinearity of each of the interferometric links is significantly suppressed, which enables the use of a larger modulation index.

10.2.2 SFDRs of the Optically Amplified HIPM and HIFM Links

The SFDRs of the HIPM and HIFM links have been given in Section 10.2.1, with the exception of the loss parameter values in Eqs. (10.7) and (10.8). For the implementation of Fig. 9-7, the loss parameters are given by $L_{sig}=\frac{1}{9}$, $L_{ref}=\frac{4}{9}$, $L_{xsig}=10^{-0.6}$, and $L_{xref}=10^{-0.6}J_1(\beta)$. The $10^{-0.6}$ terms assume a 6 dB modulator excess loss, and the $J_1(\beta)$ term refers to an additional loss due to the unshifted and higher-order terms in Eq. (9.3). It is important to choose β not only to maximize L_{xref}, but also to reduce the spurious carrier term at the IF generated at the photodiode through the mixing of the different terms in Eq. (9.3). The amplitude of this term is proportional to

$$J_0(\beta)J_1(\beta)-J_2(\beta)J_3(\beta)+J_4(\beta)J_5(\beta)-\ \ldots \tag{10.11}$$

Both of these requirements are satisfied for values of β near 2.2, which is very close to the β of 1.84 which maximizes L_{xref}.

10.3 Results and Discussion

In this section, we evaluate the SFDRs of the optically amplified HIPM, HIFM, and DD links for antenna remoting applications. Among the important parameters considered are signal power, saturation and noise in optical amplification, laser RIN, link and modulator excess loss, signal bandwidth, and receiver intermediate frequency (IF).

The parameters which are common to all of the subsequent plots are included in Table 10-1. These have been chosen to be realistic for presently or soon-to-be available commercial devices. The RIN parameters are chosen to be typical of high-quality laser diodes without requiring special modulation characteristics or expense. A linewidth value

has not been specified since all three links to be considered in this section are linewidth-insensitive.

Table 10-1. Parameter values assumed in the plots in this section.

Parameter	Assumed Value	Parameter	Assumed Value
Max. output power of opt. amp.	100 mW	Modulator excess loss	6 dB
Gain of opt. amp.	15 dB	Int. freq.	15 GHz
n_{sp} of opt. amp.	1	Responsivity	0.8
Laser wavelength	1.3 μm	IF filter bandwidth	10 GHz
RIN	-155 dB/Hz	RIN roll-off freq.	2 GHz

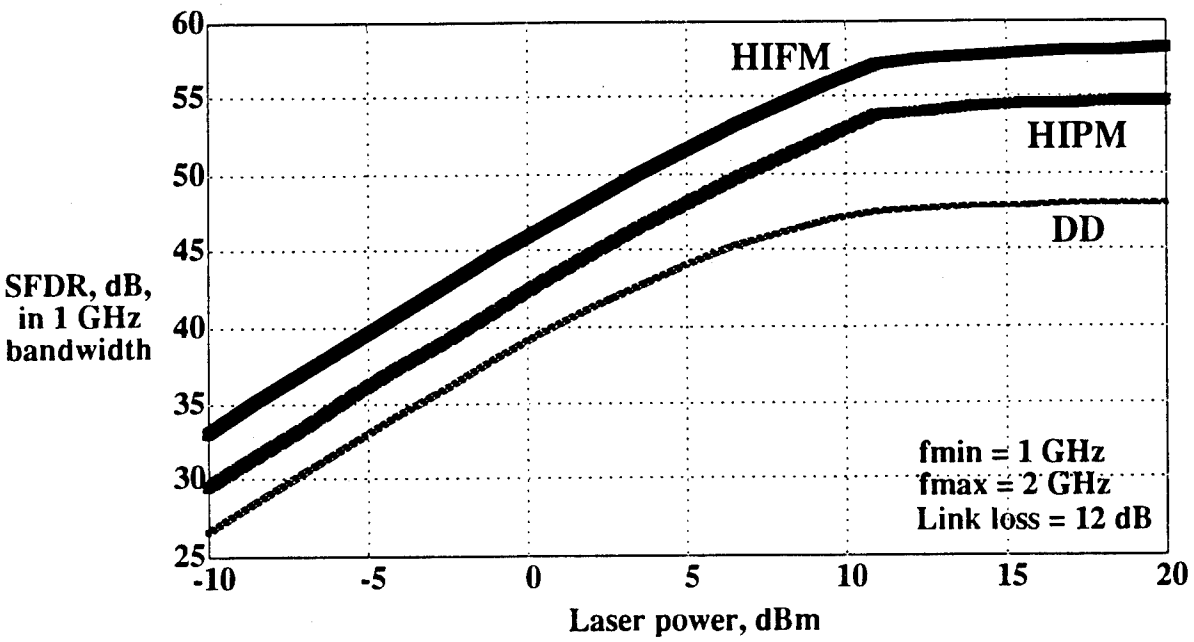

Fig. 10-2. SFDRs of the HIFM, HIPM, and DD links plotted versus transmitter optical power for antenna remoting and the parameters in Table 10-1.

Fig. 10-2 compares the SFDR of the three links vs. transmitter laser power (in the fiber) for the antenna remoting application and a 12 dB link loss. The HIFM and HIPM links exhibit 6 dB and 3 dB advantages, respectively, over the DD link at low laser powers. This advantage comes primarily from the improved linearity of the interferometric links, as is evidenced by the values of the third-order nonlinearity parameter b_3 in Section 10.2.1. The SFDR advantage of the HIFM and HIPM links increases to 10 dB and 7 dB for laser powers above 10 mW. This increase is due to the

partial immunity to RIN of the interferometric links, which results from limiting prior to discrimination combined with operation at a high IF. The advantage increases for higher RIN but does not increase in the above plot for laser powers above 10 mW, because signal-spontaneous (plus reference-spontaneous in the interferometric links) beat noise becomes the dominant noise affecting all three links. The slope discontinuity in the interferometric link graphs at about 10 mW is due to the 100 mW maximum output power of the optical amplifier. Though saturation only causes the SFDR to level off for interferometric links, its existence in DD links can generate significant additional nonlinearities, which can cause the DD SFDR to be penalized relative to that shown in the plot for laser powers greater than about 10 mW. The SFDR difference of about 3 dB between the HIFM and HIPM links results from a combination of effects. The displacement from baseband of the signal band eliminates the SFDR advantage which one would expect in FM links due to noise suppression. However, the integrator before the modulator in the HIFM link serves to predistort the signal by weighting the lower frequencies more heavily. This means that the sinusoidal discriminator characteristic (of maximum slope at f_{IF} and of zero slope at 0 and $2f_{IF}$) appears more linear to the HIFM signal than to the HIPM signal. The SFDR of the HIFM link is above 50 dB, a desirable goal for antenna remoting systems, for laser powers above about 2 mW and a 12 dB link loss. This figure is not attained by the DD link for any laser power.

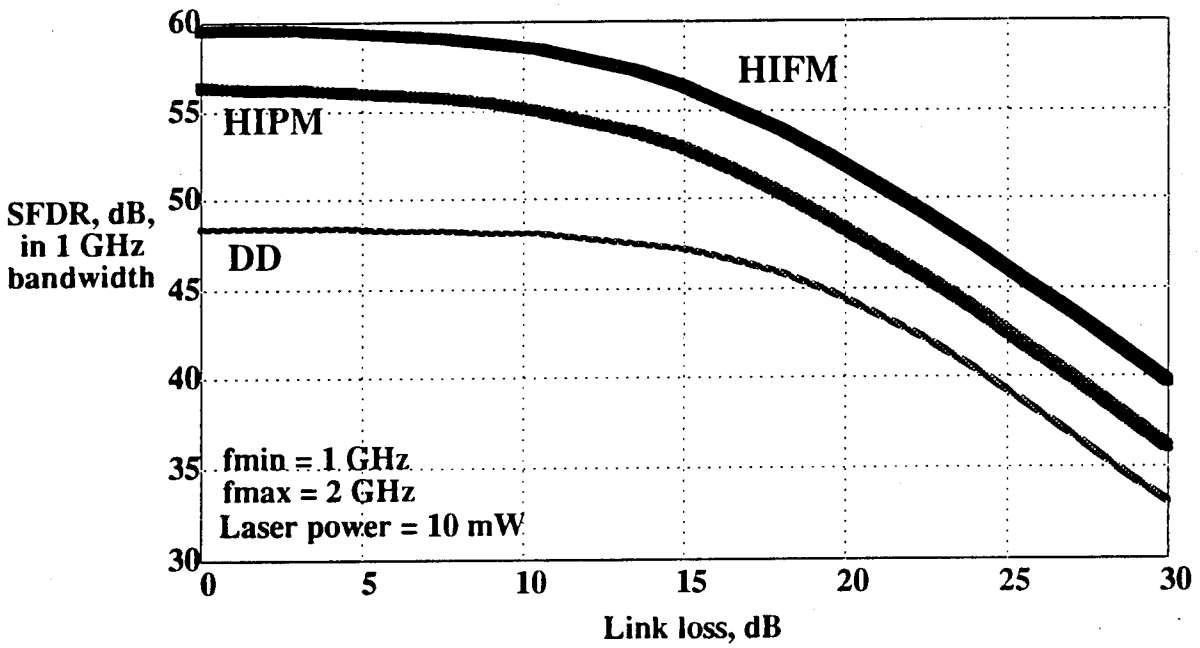

Fig. 10-3. SFDRs of the HIFM, HIPM, and DD links plotted versus link loss for antenna remoting and the parameters in Table 10-1.

Fig. 10-3 compares the SFDRs of the three links vs. fiber link loss for the antenna remoting application and a 10 mW laser power. Link loss can be due to splitting loss in a distribution system or to fiber attenuation and connector losses. This plot is nearly equivalent to Fig. 10-2 with high link losses corresponding to low laser powers and vice versa. This correspondence will only hold, however, for optical amplifier placement at the transmitter so that link loss will simultaneously suppress both the laser power and the amplified spontaneous emission. For a 10 mW laser power, the HIFM link meets the 50 dB SFDR criterion for link losses below 22 dB, while the DD link does not reach 50 dB SFDR for any value of link loss. As a result, it is again clear that optically amplified interferometric links show the potential to outperform optically amplified direct detection links in antenna remoting systems with realistic link and modulator losses taken into account.

Discriminator Linearization

In this chapter, we briefly discuss a simple method for discriminator linearization which can improve link SFDR. In Section 11.1, we describe the linearization method. In Section 11.2, we discuss the results.

11.1 Discriminator Linearization

The SFDR of angle modulated analog links is limited by the nonlinearities of the discriminator filter. Through the addition of extra discriminator arms, the discriminator transfer function can be linearized and the SFDR can thus be improved. Assume that the transfer function of the filter discriminator can be expanded as a polynomial in the vicinity of the intermediate frequency (IF):

$$H_D(\omega) = A\sum_{n=0}^{\infty} a_n(\omega - \omega_{IF})^n \tag{11.1}$$

where A is a constant. We found in Section 8.2.3 that $a_2 = 0$ and $a_3 = -\frac{1}{6}\left(\frac{\pi f_{max}}{2f_{IF}}\right)^2$ for the two-leg delay-line discriminator, which we refer to as a 2nd-order delay-line filter (DLF).

In an N-th order DLF, the input signal is split into N arms. The signal in the nth arm is delayed $(n\text{-}1)t$, multiplied by a complex weight, w_n, and recombined with the other arms. Such filters can be constructed using microstrip delay lines and phase shifters, and have a transfer function which can be expressed as

$$H_N(\omega) = A\sum_{n=0}^{N-1} w_n \exp[-i\omega n\tau] \tag{11.2}$$

where A is some complex constant. The second-order DLF has $w_1 = w_2 = 1$ and a transfer characteristic given by

$$H_2(\omega) = A\cos(\omega\tau/2) \tag{11.3}$$

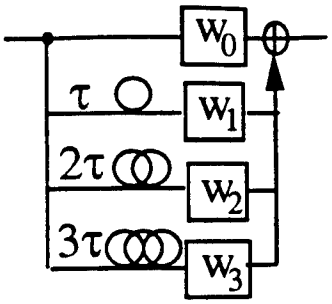

Fig. 11-1. Generic four-leg delay-line filter

A fourth-order DLF, shown in Fig. 11-1, has $w_0 = w_3 = 1/27$ and $w_1 = w_2 = 1$. Such a filter has a transfer function given by

$$H_4(\omega) = A\left[\cos(\omega\tau/2) - \frac{1}{27}\cos(3\omega\tau/2)\right] \tag{11.4}$$

For these weights, we find that $a_2 = a_3 = 0$, and hence fifth-order nonlinear terms are dominant with an a_5 which is a complicated expression with a large number of terms (generated using the method of Appendix C.1.1). For this filter, intermodulation products of interest are generated at $2f_1 \pm f_2$, $2f_2 \pm f_1$, $3f_1 \pm 2f_2$, and $3f_2 \pm 2f_1$. For closely spaced modulating frequencies, all of the difference-frequency products will fall within the signal band and will thus impact link SFDR.

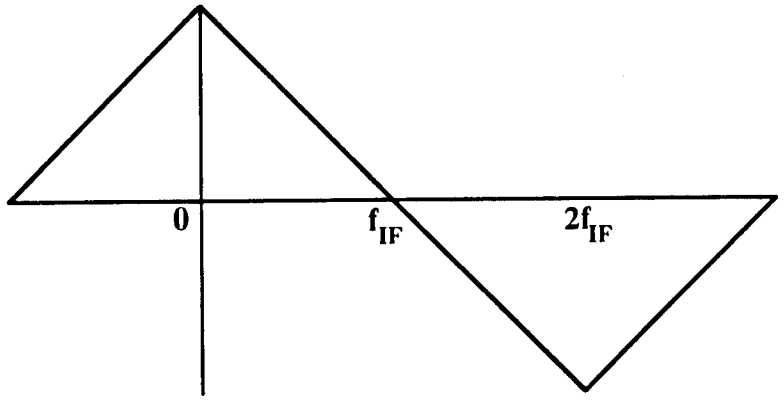

Fig. 11-2. Idealized discriminator transfer characteristic.

11.2 Results and Discussion

We begin this section with a comparison of the discriminator transfer functions using the linearization method of Section 11.1, which simply chooses weights which cancel out the third-order nonlinearity, and a truncation of the conventional Fourier series of the idealized transfer function. The Fourier series truncation, instead of using $w_0 = w_3 = -1/27$ to cancel out the third-order nonlinearity of the second-order DLF, uses $w_1 = w_2 = b_1$ and $w_0 = w_3 = b_2$, where b_1 and b_2 are the first two coefficients of the Fourier cosine expansion of the idealized discriminator transfer characteristic shown in Fig. 11-2 (in this case, there are no sine terms in the expansion). b_1 and b_2 are given by $\frac{16}{\pi^2}\sin^2\left(\frac{\pi}{4}\right)$ and $\frac{16}{9\pi^2}\sin^2\left(\frac{3\pi}{4}\right)$, respectively.

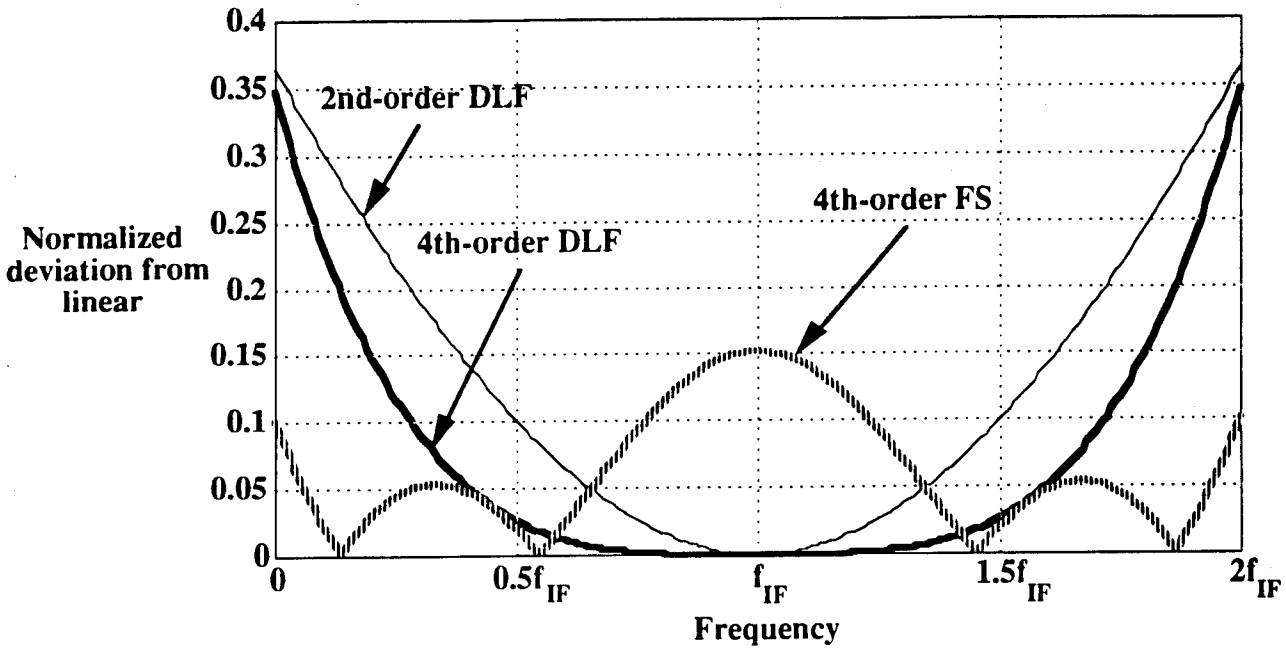

Fig. 11-3. Normalized deviations from the idealized transfer characteristic of Fig. 11-2 for the 2nd-order DLF, the 4th-order DLF, and the 4th-order FS filters.

Fig. 11-3 shows a comparison of the transfer characteristics produced by our linearization method and by the Fourier expansion method. The normalized deviations from linearity are the differences between the linear characteristic of Fig. 11-2 and the characteristics of the individual filters, normalized by the values of the linear characteristic. It is clear that for an intermediate frequency much larger than the signal

frequencies and for simple DLFs with only four legs, the method presented in Section 11.1 performs better than the Fourier expansion method. This result is important, since due to the difficulty of implementing the long delays required for DLFs with many legs, it is important to keep the linearized DLF as simple as possible.

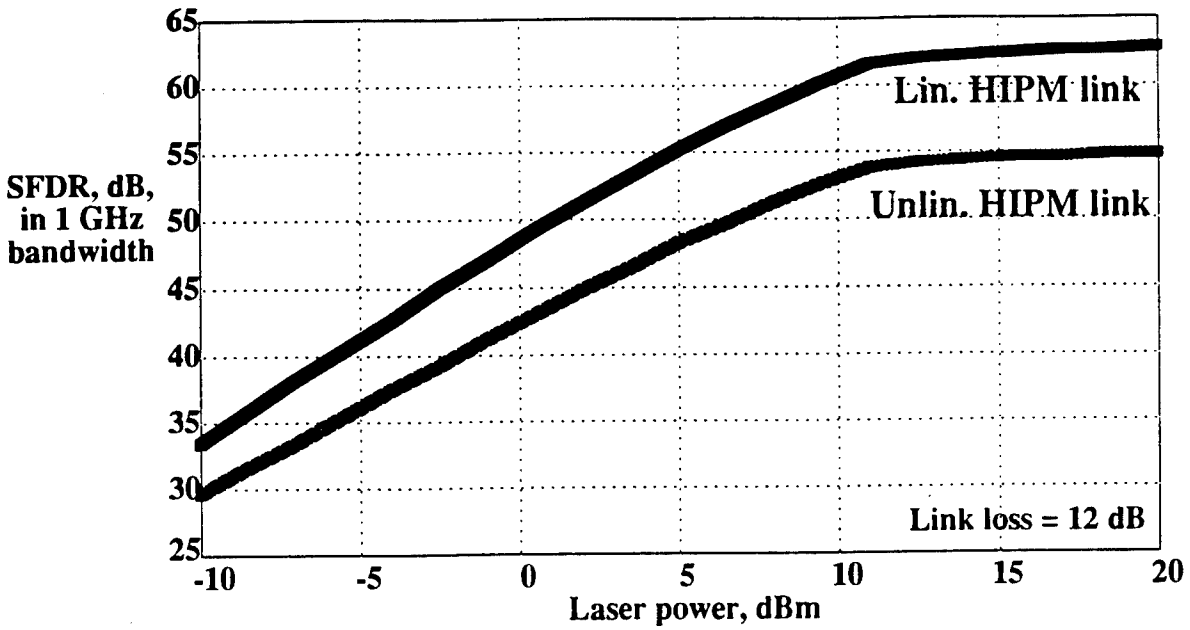

Fig. 11-4. SFDRs of linearized and unlinearized HIPM link plotted versus transmitter optical power for antenna remoting parameters in Table 10-1.

Fig. 11-4 compares the SFDRs of a linearized HIPM link using a four-leg delay-line filter with that of an unlinearized HIPM link vs. laser power for a link loss of 12 dB. The advantage for a -10 dBm laser power is 3 dB and increases steadily until the saturation point at 10 mW, at which the advantage remains constant at 8 dB. This is because as the SNR for an interferometric link increases with power, the optimum modulation index which equates the noise and nonlinearity powers decreases. Hence, at high laser powers the relative increase in optimum modulation index for a given decrease in nonlinearity power will be larger, leading to a larger improvement in SFDR. These SFDR advantages due to linearization are comparable to those attained in our laboratory for externally modulated IMDD links.

The linearity improvements for any of the other angle modulated links are similar, since the discriminator structures are identical for all angle modulated links which we have considered.

Subcarrier Multiplexing in Angle Modulated Links

In this chapter, we consider the use of subcarrier multiplexing (SCM) as a means of transmitting many narrowband channels using a single transceiver. In Section 12.1, we derive the SFDR of an analog link using SCM. In Section 12.2, we present SFDR requirements for applications including conventional analog video (both AM and FM) and digital video. These requirements are presented alongside requirements for antenna remoting for purposes of comparison. In Section 12.3, we discuss results for both coherent and interferometric SCM links. Section 12.4 contains references.

12.1 SFDR in a Subcarrier Multiplexed (SCM) Link

In a subcarrier multiplexed (SCM) link, the total signal bandwidth B is broken into N channels, each with a bandwidth of B/N. To compute IMD power, we generalize the test signal of Eq. (8.5):

$$x(t) = \frac{1}{\sqrt{N}} \sum_{n=1}^{N} \cos(\omega_n t + \varphi_n) \tag{12.1}$$

where w_n falls within the band of the n-th channel. We assume that the phases in the various channels, j_n, are uncorrelated so that the input signal power is normalized to $\langle x^2(t) \rangle = 0.5$. The maximum number of third-order intermodulation products falling within the n-th channel band is [1]

$$M = \frac{n}{2}(N - n + 1) + \frac{1}{4}\left[(N-3)^2 - 5\right] \tag{12.2}$$

M achieves its maximum value for $n = N/2$ and its minimum value for $n = 1$. For $N > 10$, the minimum value of M is > 0.6 times its maximum value, and M is thus relatively insensitive to n.

The maximum total IMD power within a channel band is given by

$$\left\langle i_{NL3}^2 \right\rangle = \frac{9}{16}\frac{M}{N^3} s^2 b_3^2 r^6 \tag{12.3}$$

Solving for the maximum modulation depth as in Eq. (8.7) and using Eq. (8.4), we find that the SFDR for channel n is given by

$$SFDR = \left(\frac{8}{9}\frac{N^3}{M}\right)^{1/3}\left(\frac{SNR_o^{channel\ n}}{|b_3|}\right)^{2/3} \tag{12.4}$$

where $SNR_o^{channel\ n}$ is the SNR_o corresponding to channel n. For large N and taking $n = N/2$, we find that $M \cong 3N^2/8$ and

$$SFDR \cong \frac{4}{3} N^{1/3}\left(\frac{SNR_o^{channel\ n}}{|b_3|}\right)^{2/3} \tag{12.5}$$

If the total received optical power is fixed and the noise spectrum of the output current is independent of the channel frequency band, then the SFDR of an N channel system is given by

$$SFDR \cong \frac{4}{3} N^{-1/3}\left(\frac{SNR_o^{1\ channel}}{|b_3|}\right)^{2/3} \tag{12.6}$$

where $SNR_o^{1\ channel}$ is the SNR_o of a system transmitting a single channel only with the full received optical power. For the coherent PM and FM links, the noise spectrum is not white. Also, in the PM link the intermodulation distortion power is not uniformly distributed over the signal band, and the worst-case SFDR occurs at the midband channel frequency (the location of the most third-order intermodulation products). For the FM link, the worst-case SFDR occurs at the highest channel frequency for the desired application if linewidth causes negligible performance degradation. The worst-case SFDR occurs at the midband channel frequency if linewidth is the dominant source of performance degradation. For DD and coherent AM links, the worst-case SFDR usually occurs at the midband channel frequency. If the dominant noise is RIN and if the power spectral density of the RIN is rolling off in the SCM signal band (see Appendix A.2.4), then the worst-case SFDR may occur at the lowest channel frequency.

12.2 SCM Link Requirements

Table 12-1 shows the SFDR and channel bandwidth requirements for conventional AM and FM analog video (CATV), for digital video, and for antenna remoting. The SFDR requirements for AM CATV and antenna remoting are comparable, as are the requirements for FM CATV and SCM digital video. In this chapter, we compare the performance of angle-modulated links to that of DD and coherent AM links for these four applications. In all cases, the number of channels has been chosen to make the total signal bandwidth requirement (shown in Table 12-1) approximately equal for all applications.

Table 12-1. Parameters for different types of video and antenna remoting.

	AM CATV	FM CATV	SCM digital	Antenna remoting
SFDR	50 dB	17 dB	17 dB	55 dB
Channel Bandwidth	4 MHz	30 MHz	10 MHz	1 GHz
# of channels	100	25	80	1
Total Signal Bandwidth	600 MHz	1 GHz	1 GHz	1 GHz

12.3 Results and Discussion

In this section, we present SFDR results for SCM angle-modulated links and compare them to SCM DD and coherent AM links. Section 12.3.1 considers coherent angle-modulated links and Section 12.3.2 considers interferometric angle modulated links.

A reasonable guardband between SCM channels is taken into account in the computation of total signal bandwidth for each application in Table 12-1. The signal frequency range for each application is chosen for single-octave operation. We assume a sufficiently large number of channels ($N > 20$) in each SCM system for the multichannel SFDR expression given in Eq. (12.2) to be accurate. In all cases, the channel with the worst-case SFDR is used to define whether system performance is acceptable for a given application. The worst case for the FM link in this section combines the intermodulation product count of the midband channel frequency and the noise of the highest channel

frequency. This assumption provides a lower bound on SFDR of within 1 dB for the applications of interest.

Table 12-2. Laser linewidth requirements for coherent PM and FM links.

	Received optical power	Required Laser Linewidth PM	FM
AM CATV	1 mW	1 kHz	3 kHz
FM CATV	1 μW	150 MHz	350 MHz
SCM digital	1 μW	80 MHz	200 MHz
Antenna remoting	1 mW	2 kHz	4 kHz

Table 12-3. Laser RIN requirements for DD and coherent AM links.

	Received optical power	Required Laser RIN DD	AM
AM CATV	50 mW	-175 dB/Hz	max. only 45 dB
	100 mW	-167 dB/Hz	max. only 46 dB
FM CATV	20 μW	max. only 16 dB	-140 dB/Hz
	50 μW	-115 dB/Hz	-115 dB/Hz
SCM digital	20 μW	max. only 14 dB	-130 dB/Hz
	50 μW	-120 dB/Hz	-120 dB/Hz
Antenna remoting	50 mW	-170 dB/Hz	max. only 51 dB
	100 mW	-165 dB/Hz	max. only 51 dB

12.3.1 SCM Coherent Angle Modulated Links

Tables 12-2 and 12-3 show laser linewidth and RIN requirements for coherent angle-modulated, coherent AM, and DD links for the four applications shown in Table 12-1. This data was obtained assuming a receiver intermediate frequency of 10 GHz and a local oscillator laser power of 10 mW.

For AM CATV systems, an SFDR of 50 dB is required in a bandwidth of 4 MHz [2]. At a received optical power (P_S) of 1 mW, this requires a linewidth of < 1 kHz in the PM system and a linewidth of < 3 kHz in the FM system. Even at a P_S of 10 mW, such a dynamic range is unachievable in the DD and AM systems without modulator linearization.

In antenna remoting systems, a dynamic range of 55 dB in a 1 GHz bandwidth, or 115 dB-$Hz^{2/3}$, is representative of system requirements. In the absence of linearization techniques, this requires a linewidth of < 2 kHz for a PM system or a linewidth of < 4 kHz in an FM system for a P_S of 1 mW. At this power level, this dynamic range requirement is unattainable in either the DD or the AM system. If P_S is increased to 50 mW, then the DD system can reach the required dynamic range for a RIN level of < -170 dB/Hz. Even for a P_S of 100 mW, the AM system is unable to meet the requirements without modulator linearization.

In an SCM digital system, an SFDR of 17 dB in a 10 MHz bandwidth is required [2]. At a P_S of 1 μW, this requires a linewidth of < 80 MHz in the PM system and a linewidth of < 200 MHz in the FM system. It can also be achieved in a DD system at a P_S of 50 μW. The coherent AM system can attain the required SFDR at a P_S of 20 μW. For these small optical powers, high values of RIN are necessary for RIN to dominate thermal noise .

In all four links considered, FM subcarriers can be utilized. Such systems require an SFDR of 17 dB to achieve acceptable video transmission for an FM subcarrier bandwidth of 30 MHz [3]. This can be achieved in a PM or an FM system at a P_S of 1 μW with linewidths of < 150 MHz and < 350 MHz, respectively. In the AM and DD systems, the smallest P_S for which the SFDR requirement can be achieved are 0.5 μW and 25 μW, respectively. The power requirements for FM CATV are lower than those for SCM digital because fewer channels can be transmitted in a 1 GHz signal band, leading to less intermodulation distortion.

12.3.2 SCM Interferometric Angle Modulated Links

Tables 12-4 and 12-5 show laser linewidth and RIN requirements for interferometric angle-modulated links for the four applications shown in Table 12-1. This data was obtained assuming a receiver intermediate frequency of 15 GHz.

For AM CATV and antenna remoting systems, the HIFM and HFM links can meet the SFDR requirements for a laser RIN of -160 dB/Hz and a received optical power of 5 mW in both cases. The HIPM and HPM links show higher resistance to laser RIN at

very high powers but require a 10 mW received optical power to meet the SFDR requirements in both cases. The performance of the interferometric links compares favorably to that of the DD and coherent AM links in the previous section due to the partial immunity of interferometric links to laser RIN (see Chapter 9).

Table 12-4. Laser RIN requirements for heterodyne interferometric links.

	Received optical power	Required Laser RIN HIPM	HIFM
AM CATV	5 mW	-130 dB/Hz	-145 dB/Hz
	10 mW	-120 dB/Hz	-140 dB/Hz
FM CATV	15 μW	max. only 16 dB	not even -100 dB/Hz
	50 μW	not even -100 dB/Hz	not even -100 dB/Hz
SCM digital	20 μW	max. only 16 dB	not even -100 dB/Hz
	50 μW	not even -100 dB/Hz	not even -100 dB/Hz
Antenna remoting	5 mW	max. only 54 dB	-145 dB/Hz
	10 mW	-125 dB/Hz	-140 dB/Hz

In SCM digital and FM video systems, the HIFM and HFM links can potentially achieve the desired SFDR performance for 15 μW received optical power. Though the HIPM link is the most resistant to laser RIN at high powers, it shows no advantage at these low powers. Nevertheless, at 50 μW received optical power, all four interferometric links can perform acceptably with essentially no RIN restriction. This result is similar to that for the DD and coherent AM links, though the RIN requirements are less stringent for the interferometric links.

Table 12-5. Laser RIN requirements for homodyne interferometric links.

	Received optical power	Required Laser RIN HPM	HFM
AM CATV	5 mW	-170 dB/Hz	-160 dB/Hz
	10 mW	-155 dB/Hz	-155 dB/Hz
FM CATV	15 μW	max. only 16 dB	-115 dB/Hz
	50 μW	-110 dB/Hz	-110 dB/Hz
SCM digital	20 μW	max. only 16 dB	-115 dB/Hz
	50 μW	-115 dB/Hz	-115 dB/Hz
Antenna remoting	5 mW	max only 53 dB	-160 dB/Hz
	10 mW	-160 dB/Hz	-155 dB/Hz

12.4 References

[1] M. T. Abuelmatti, "Carrier-to-intermodulation performance of multiple FM/FDM carriers through a GaAlAs heterojunction laser diode," *IEEE Trans. Commun.*, vol. COM-33, no. 3, pp. 246-248, 1985.

[2] R. B. Childs and V. A. O'Byrne, "Multi-channel AM video transmission using a high-power Nd:YAG laser and linearized external modulator," *IEEE J. Select. Areas in Commun.*, vol. 8, no. 7, pp. 1369 - 1376, 1990.

[3] T. E. Darcie, "Subcarrier multiplexing for lightwave networks and video distribution systems," *IEEE Journal of Sel. Areas in Commun.*, vol. 8, no. 7, pp. 1240-1248, 1990.

Chapter Thirteen

Angle Modulated Links: Conclusions

In this chapter, we summarize our work on angle modulated links during this project and recommend future work which builds directly on the work described in Chapters 8 through 12. Section 13.1 contains the summary and Section 13.2 contains the recommendations for future work.

13.1 Summary

Due to the large potential transmission bandwidth of optical fiber, optical transmission systems are well-suited to handle the expanded bandwidth of wideband angle modulated signals. Our investigation of angle modulated links during this project has been motivated by a desire to see the same signal-to-noise ratio (SNR) improvements in fiber systems that are exploited in commercial FM radio and video.

In Chapter 8, we presented the spurious-free dynamic ranges (SFDRs), RF power transfer ratios, and noise figures of coherent phase modulated (PM) and frequency modulated (FM) links using either direct modulation of the grating section current of a laser diode or external phase modulation. We found that coherent angle modulated systems are intrinsically sensitive to phase noise because their signal information is contained in the optical phase. For a combined transmitter laser and local oscillator laser linewidth of 20 MHz, phase noise is the dominant noise in PM and FM links for received optical power levels above -30 dBm, and limits the SFDR to 30 dB and 31 dB in a 1 GHz bandwidth for PM and FM links, respectively. For a combined linewidth of 10 kHz, phase noise dominates the noise characteristics for received optical power levels above -5 dBm, and limits the SFDR to 51 dB and 53 dB in a 1 GHz bandwidth for PM and FM links, respectively. Angle modulated links can exhibit substantial RIN insensitivity through the use of a limiter in the receiver and by operating at an IF well above the RIN roll-off frequency. The linearity of angle modulated links tends to improve for high IFs due to the improved linearity of the phase or frequency discriminator in the receiver.

We found that externally angle modulated coherent links are inherently more lossy than externally amplitude modulated links, due to the large losses of the integrator and

discriminator filters in these links. Extra amplification is required before these filters for these links to attain their SFDR potential. The directly frequency modulated coherent link, on the other hand, is less lossy than externally amplitude modulated links due to its high conversion efficiency of input RF power to optical frequency deviation. The difficulty with directly frequency modulated links is that it is difficult to guarantee a linear frequency versus current characteristic over many GHz in conjunction with a sufficiently low linewidth.

In Chapter 9, we considered reference transport as a means of transmitter phase noise cancellation (PNC) in angle modulated analog links. We found that reference transport in links using direct frequency modulation is not a useful means of PNC because laser phase noise in links using direct FM is equivalent to white noise in the original applied RF signal. We found that reference transport in externally angle modulated links requires frequency shifting of the reference to facilitate demodulation of the PM or FM signal. As a result, we analyzed a novel class of linewidth-insensitive analog links: interferometric angle modulated links. Linewidth insensitivity is attained through the transport of a reference derived from the transmitter laser in the same fiber as the optical field carrying the desired signal. The IF frequency shift required for demodulation of FM and PM signals is generated using a novel electro-optic quasi-single sideband (SSB) frequency shifter in heterodyne interferometric links and using mixers at the receiver in homodyne interferometric links.

We presented the SFDRs, RF power transfer ratios, and noise figures of heterodyne and homodyne interferometric PM and FM links. Since interferometric links are more linear than externally amplitude modulated links for high intermediate frequencies, the phase modulated interferometric links (HIPM and HPM) show about a 2 dB SFDR advantage over amplitude modulated links at low received optical powers. The frequency modulated interferometric links (HIFM and HFM) show a corresponding 5 dB SFDR advantage. As laser relative intensity noise (RIN) becomes dominant for received optical powers above 1 mW, the potential SFDR advantage of the interferometric links increases. At a received optical power of 10 mW, the HIFM link shows an 11 dB SFDR advantage over a direct detection link for a laser RIN of -155 dB/Hz. For a laser RIN of -130 dB/Hz, the HIPM link shows a 24 dB SFDR advantage over the direct detection link. Heterodyne interferometric links are partially insensitive to laser RIN because the signal information is in the optical phase. However, they are not completely insensitive to laser RIN due to the RIN of the optical reference. Homodyne interferometric links are less insensitive to laser RIN because baseband RIN is converted up to the intermediate frequency of the receiver.

Interferometric links are also significantly more lossy than externally amplitude modulated links. They share the lossy integrator and discriminator filters of the coherent angle modulated links and have additional optical losses due to the optical reference transport. As a result, significant amplification is again required for interferometric links to reach their SFDR potential.

We briefly describe a proof-of-concept experimental demonstration of an HIPM link to verify the potential of interferometric links. A 23 dB suppression of third-order nonlinearities (7.7 dB SFDR improvement) over that of a conventional direct detection link is obtained using an HIPM link with an intermediate frequency of 650 MHz and signal frequencies of 47.5 and 52.5 MHz. Data is presented which shows the significant impact of receiver nonidealities, indicating that the SFDR improvement can be nearly twice as large in a carefully optimized system.

In Chapter 10, we consider the use of optical amplifiers to increase the available optical power in interferometric links. We derive the SFDR expressions for optically amplified interferometric PM and FM links and show that for realistic antenna remoting system parameters (including modulator and link losses), the HIPM and HIFM links have the potential to improve link SFDRs by 6 dB and 9 dB, respectively, over an optically amplified direct detection link.

In Chapter 11, we consider a simple method for discriminator linearization to improve angle modulated link SFDR. Assuming the realistic antenna remoting system parameters of Chapter 10, a linearized HIPM link can potentially gain 7 dB of SFDR over an unlinearized HIPM link at a received optical power of 10 mW.

In Chapter 12, we consider the use of subcarrier multiplexing (SCM) as a means of transmitting many narrowband channels using a single transceiver. The derived results are used to find signal power, laser linewidth, and laser RIN requirements for analog video systems, SCM digital systems, and antenna remoting systems. For AM video and antenna remoting applications, low-linewidth sources such as Nd:YAG lasers are needed for PM and FM coherent systems. For these same applications, the amplitude modulated links need extremely high received optical powers and low RIN due to the high required CNRs. Even if optical amplifiers (OAs) are used in the amplitude modulated links, noise associated with the spontaneous emission of OAs and the received power limitations on the photodiode may prevent the fulfillment of the SFDR requirements in that link. For FM video and SCM digital applications, presently available semiconductor laser diodes can easily fulfill the requirements on the laser transmitter in the direct detection and the coherent systems. Interferometric links behave similarly to the direct detection and coherent AM links, with less stringent RIN requirements.

The fundamental conclusion which we draw from our work on angle modulated links is that coherent angle modulated links are promising for low received powers (< 1 mW) and low laser linewidths, while interferometric angle modulated links are promising for high received powers (> 1 mW). As a result, coherent angle modulated links are potentially useful in distribution and other high-loss links using solid-state Nd:YAG or low-linewidth (< 100 kHz) semiconductor lasers. Interferometric links do not have linewidth requirements but do require high-power semiconductor lasers and optical amplification. All externally angle modulated links are lossy in the RF domain and require more RF amplification than in externally amplitude modulated links.

13.2 Recommendations for Future Work

The future work discussed in this section pertains to externally angle modulated links. Future work pertaining to directly frequency modulated links is discussed in Chapter 15.

Because of the SFDR limitation due to laser linewidth and our interest in using semiconductor lasers in experimental work for this project, we chose to build a heterodyne interferometric link instead of an externally angle modulated (PM or FM) coherent link. In this section, we will therefore discuss possible improvements to the heterodyne interferometric link. This discussion is also relevant to externally angle modulated coherent links*.

13.2.1 Transmitter Design Considerations

Many of the important issues in transmitter design for heterodyne interferometric links are discussed in Section 9.6.3. The main conclusions are that amplification of the RF input signal must be done, particularly after integration in FM links, to attain the maximum possible phase deviation from the phase modulator, and that an integrated modulator must be built to minimize optical loss, to equalize modulator splitting coefficients, and to guarantee that the applied IF sinusoids are in quadrature.

The remaining issue is the design of the integrated modulator. Conventional high-speed modulators use $LiNbO_3$ to provide the optical phase shift and traveling-wave electrodes. Narrowband resonant RF design for the IF electrodes in the modulator will

* To build a coherent angle modulated link, we would use the optics section of the AM-WIRNA system with the Mach-Zehnder amplitude modulator replaced by a phase modulator. The receiver construction would be identical to that for the heterodyne interferometric link.

reduce drive power requirements. $LiNbO_3$ modulators are adequate for the signal and IF frequency parameters used in Chapter 9 (1 GHz to 2 GHz signal, 15 GHz IF). For future systems, nonlinear polymers may soon exhibit higher modulation speeds, lower drive voltages, and cheaper packaging costs than $LiNbO_3$.

13.2.2 Receiver Design Considerations

Theoretical predictions of HIPM link performance indicate that performance over AM direct detection links can be improved substantially. These performance predictions assume that the receiver components are "well behaved," i. e. receiver noise performance is dominated by front-end thermal noise, and link nonlinearities are dominated by the idealized shape of a delay line filter. However, in the proof-of-concept HIPM experiment we performed, receiver performance was dominated by nonideal receiver component characteristics. These nonidealities included amplifier and mixer nonlinearities, non-flat frequency responses of the various components, RF reflections between the various components causing ripples in the passband frequency characteristics, and excess noise associated with the amplifiers and mixers.

Research and development is required to build and demonstrate a high-performance receiver for angle modulated links. With such a receiver, the high dynamic ranges predicted by theory can be approached in a demonstration link.

One of the more fundamental decisions in receiver (and link) design is the choice of intermediate frequency (IF). Theoretical predictions indicate that the highest possible IF is desirable to achieve the most linear frequency discriminator response, and to allow the most suppression of RIN. However, there are practical limitations to IF choice based on electronic component and photodetector performance and availability at very high IFs. For IFs much above 40 GHz, component availability decreases substantially. In the development of a high-performance angle modulation receiver, such pragmatic issues are of great importance.

Other than the discriminator filter, all other components in the angle modulation receiver must exhibit very flat bandpass characteristics across the entire IF bandwidth. Amplifiers meeting this requirement must be identified; it is anticipated that it should be possible to find commercial amplifiers which meet the system requirements. These amplifiers must also exhibit sufficiently low nonlinearities and noise so that they do not degrade receiver performance. The issues of flat frequency response and low noise and nonlinearities also hold for the mixer used in the receiver. As is the case with amplifiers,

there is a tremendous variety of commercial mixers, and it should be possible to meet the system requirements with a standard part.

In connecting the various components in the receiver, reflections can arise. These reflections cause ripple across the frequency response of the chain of components in the receiver. In an angle modulated link, such frequency ripple can give rise to intermodulation distortion through phase-to-amplitude conversion. Proper receiver design requires the liberal use of RF attenuators and isolators to suppress these reflections.

A high-performance limiter is also required in the receiver. The limiter suppresses amplitude variation associated with RIN and any spurious optical amplitude modulation. Additionally, the limiter can be used to suppress some of the spurious amplitude modulation associated with non-flat frequency response of various receiver components.

PART 4:

PROJECT CONCLUSIONS

Chapter Fourteen

Summary and Comparison of Link Design

14.1 Comparison Between Amplitude and Angle Modulated Links

In this report, the main links which we have compared are the heterodyne coherent AM (WIRNA) link, the coherent angle modulated (FM or PM) link, the heterodyne interferometric (HIFM or HIPM) link, and the conventional direct detection (DD) link. Chapters 8 and 9 contain a full theoretical comparison of these links, while Chapters 4 through 6 contain an experimental comparison of the coherent AM link to the conventional DD link. In this section, we will reiterate our main conclusions.

Due to the high power local oscillator laser in coherent receivers, coherent links exhibit substantial immunity to thermal noise. For low received optical powers (< 100 μW to 1 mW), coherent AM links can outperform DD links. For high LO powers of approximately 10 mW and higher, the crossover point occurs at between 1 and 5 mW. Therefore, coherent AM links are most applicable for applications with low received power, such as broadcast and distribution systems.

Coherent angle modulated links are sensitive to laser phase noise. However, for laser linewidth values below 100 kHz (exhibited by solid-state Nd:YAG lasers and multi-quantum-well semiconductor lasers), these links can potentially outperform coherent AM and DD links for a received optical power of 1 mW. The farther the laser linewidth dips below 100 kHz, the greater the improvement in SFDR. Fig. 8-4 shows that for an Nd:YAG transmitter and local oscillator, coherent angle modulated links can outperform a DD link for received optical powers up to 10 mW for antenna remoting parameters. Assuming the use of semiconductor lasers, coherent angle modulated links remain most applicable for applications with low received power, such as broadcast and distribution systems.

Interferometric angle modulated links are insensitive to laser phase noise. They also do not have an LO laser, which means that they perform best at high received powers (like the DD link). Fig. 9-9 shows that interferometric links can potentially outperform DD links over the full range of received optical powers from 10 μW to 100 mW. Fig. 9-10 shows that, assuming a laser linewidth of 100 kHz, these links can potentially

outperform coherent angle modulated links only above 1 mW. Therefore, interferometric links remain most applicable for applications with high received power, such as cellular antenna to base station connection.

14.2 Potential Link Applications

In this section, we consider the suitability of coherent, interferometric, and direct detection links for two promising applications for optical analog links. Section 14.2.1 compares the suitability of coherent and direct detection links in broadcast and distribution networks. Section 14.2.2 compares the suitability of optically amplified interferometric and direct detection links in cellular base station to antenna connections, in which high power is required for the downlink.

14.2.1 Broadcast and Distribution Networks

One of the conclusions which we obtained from our theoretical and experimental work is that for low optical powers, coherent links give a higher dynamic range than the direct detection link, while for high optical powers, the direct detection link performs better. In this section, we discuss the implications of this conclusion for broadcast and distribution networks.

Many applications of optical communication require that information not only be transmitted but also distributed to a group of destinations. Distribution networks using only passive devices are attractive due to their lower cost and simple maintenance. An example of such application is the distribution of master oscillator signals to the elements of an optically controlled active phase array radar. Transmission distances are usually relatively short but the distribution capacity of the system is critical.

Three common topologies for distribution networks are the star, hub and bus. The star topology shown in Fig. 14-1 is frequently used and is considered here. In this topology, all destinations are connected through point-to-point links to a star coupler. The transmitter optical power P_i is divided equally among N destinations. For a passive star composed of directional couplers, the received optical power per subscriber can be written as:

$$P_S = \frac{P_i}{N}(1-\delta)^{\log_2 N} \tag{14.1}$$

where d accounts for the excess loss and P_i is the input power from the transmitter laser.

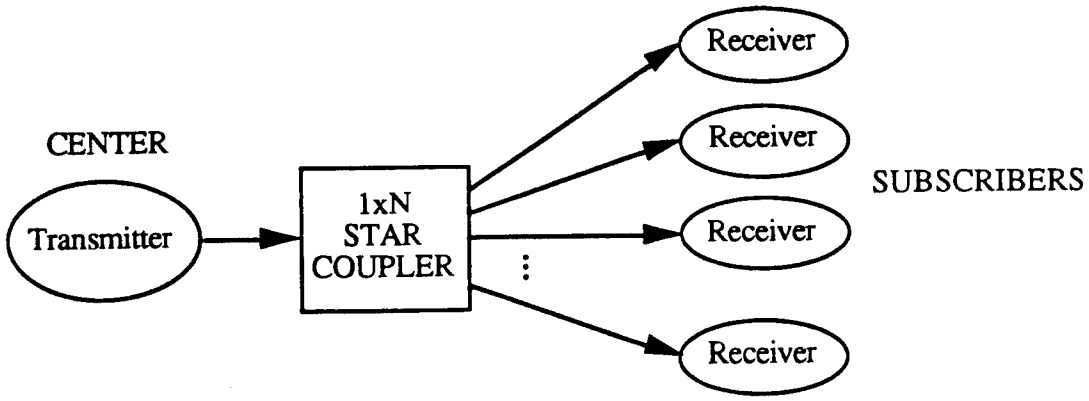

Fig. 14-1. A passive star topology.

14.2.1.1 Experimental Comparison of Coherent AM and DD Links

Using 3 dB couplers and the experimental set-up shown in Fig. 14-2, we measured the SFDR as a function of the number of destinations for both coherent AM and direct detection links. Since each coupler divides the optical power into two destinations, k cascaded couplers simulate the output for 2^k destinations. The star topology distribution system for 2, 4, 8 and 16 destinations were constructed with 3 dB couplers as shown in Figs. 14-3(a), (b), (c), and (d), respectively. We were limited to 16 destinations by the number of 3 dB couplers we had. Index-matching gel was used for the coupler FC/PC connectors to minimize the reflections.

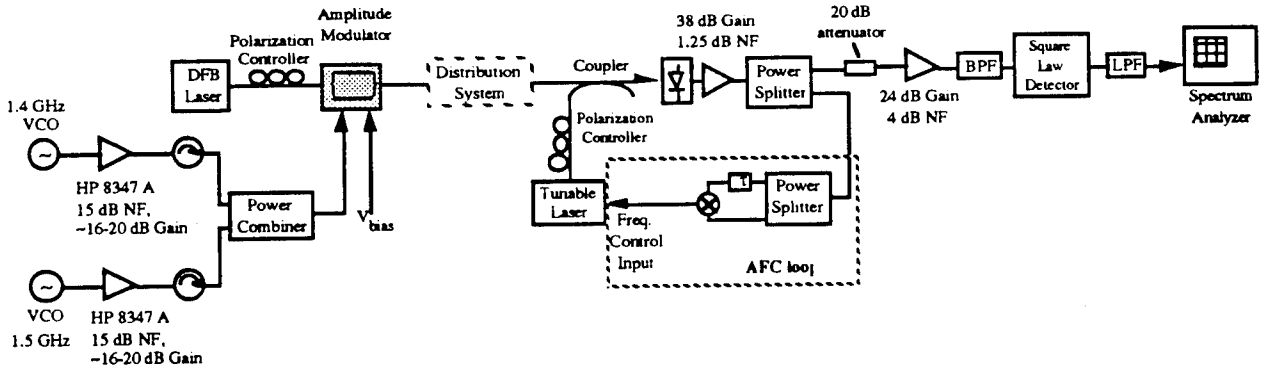

Fig. 14-2. Measurement set-up for the distribution system proof-of-concept experiment.

Table 14-1. System Parameters

DFB laser:	T = 22.5°C I = 80.02 mA P_s = 54.7 mW	LO laser:	Wavelength = 1544.95 nm I = 134.5 mA Tl = 24.334°C Te = 30°C P_{LO} = 204.1 mW

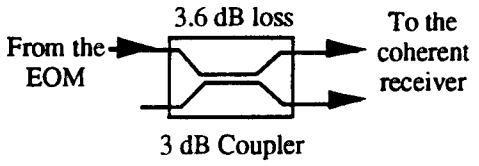

(a)

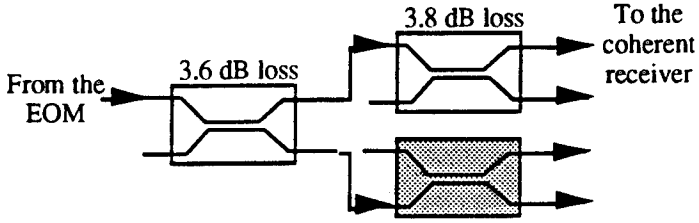

(b)

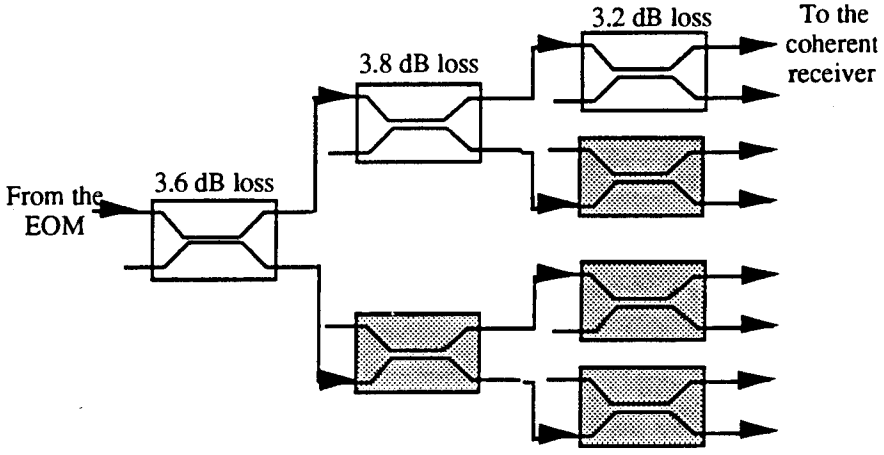

(c)

Fig. 14-3. Distribution system we used consisting of 3 dB couplers for: (a) 2 destinations, (b) 4 destinations, and (c) 8 destinations. Losses in each coupler are indicated. (Continued on the next page). The shaded elements were omitted since they were not needed for the measurement.

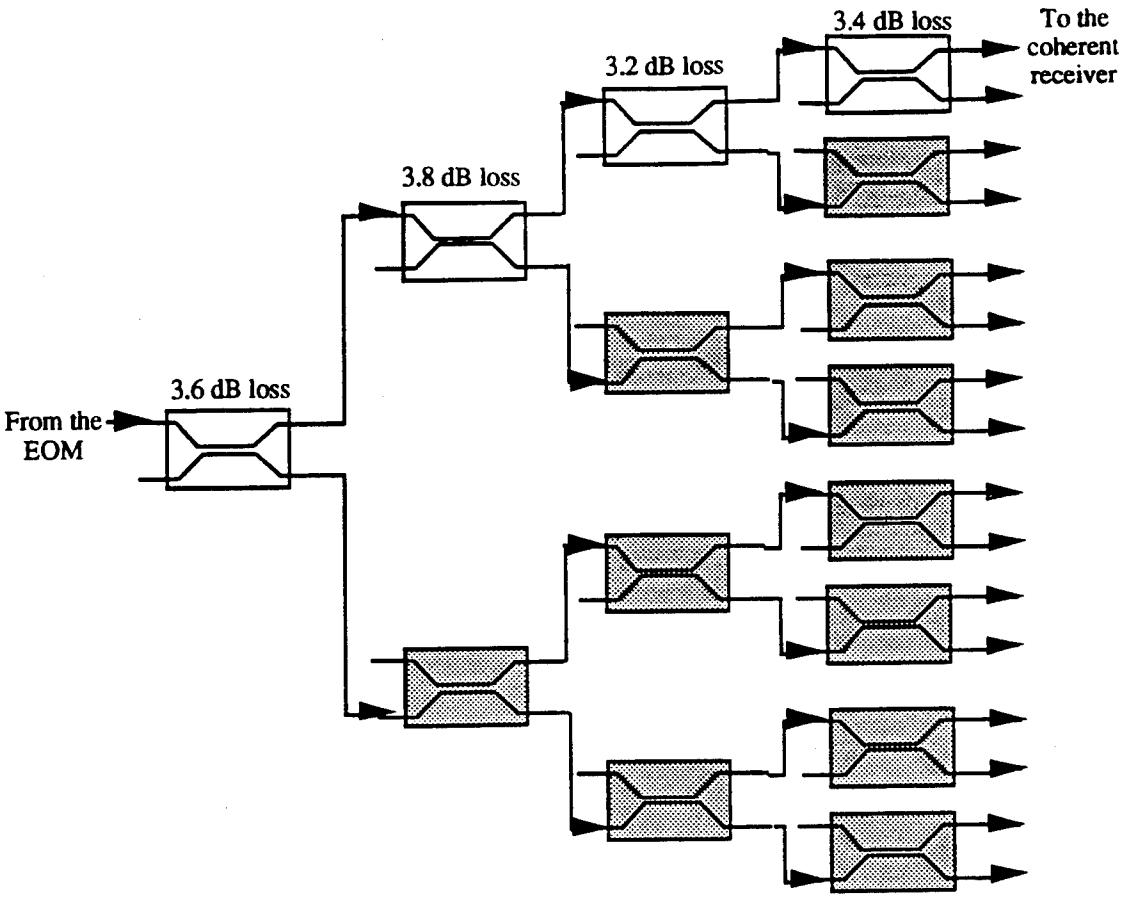

(d)

Fig. 14-3(d). Distribution system we used consisting of 3 dB couplers for 16 destinations. Losses in each coupler are indicated. The shaded elements were omitted since they were not needed for the measurement.

Fig. 14-4 shows the experimental measurements we obtained for the SFDR as a function of the number of destinations for the coherent AM and direct detection links. The system parameters are listed in Table 14-1.

Inspection of Fig. 14-4 shows that the coherent link performs better than the direct detection link except for systems with a small number (= 2) of destinations. Therefore, coherent AM links have the potential to be applied to distribution systems like phased array radar or broadcast of multiple video channels.

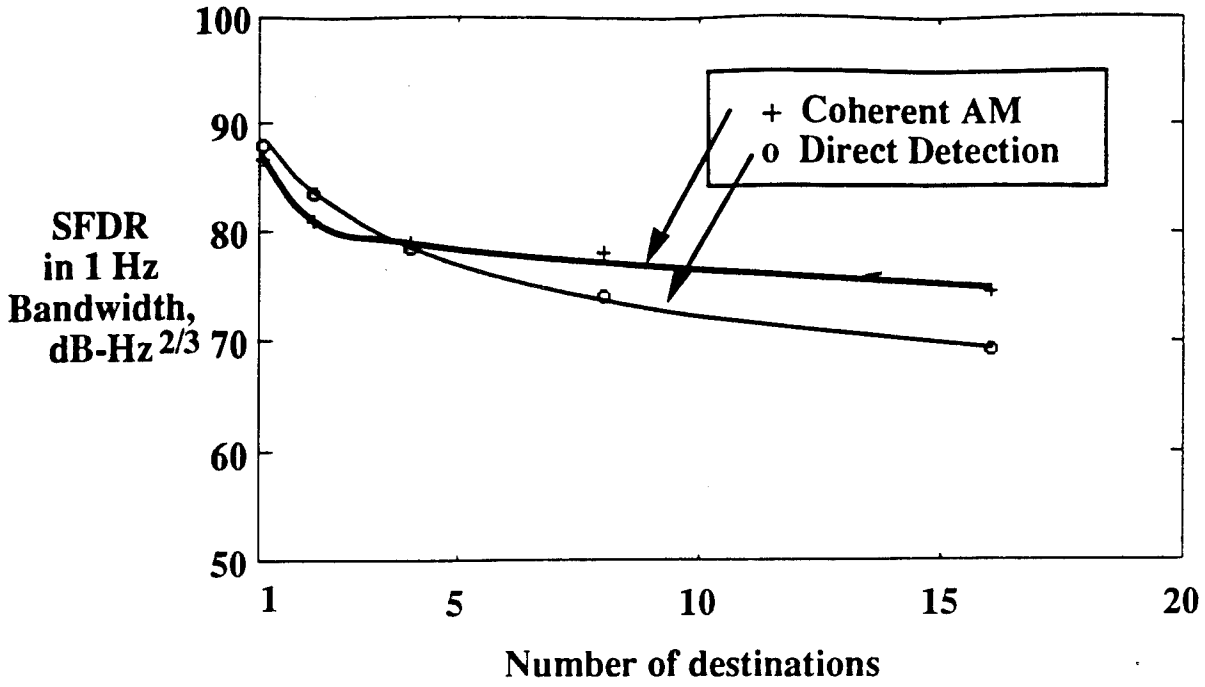

Fig. 14-4. SFDR versus the number of destinations for coherent AM and direct detection links.

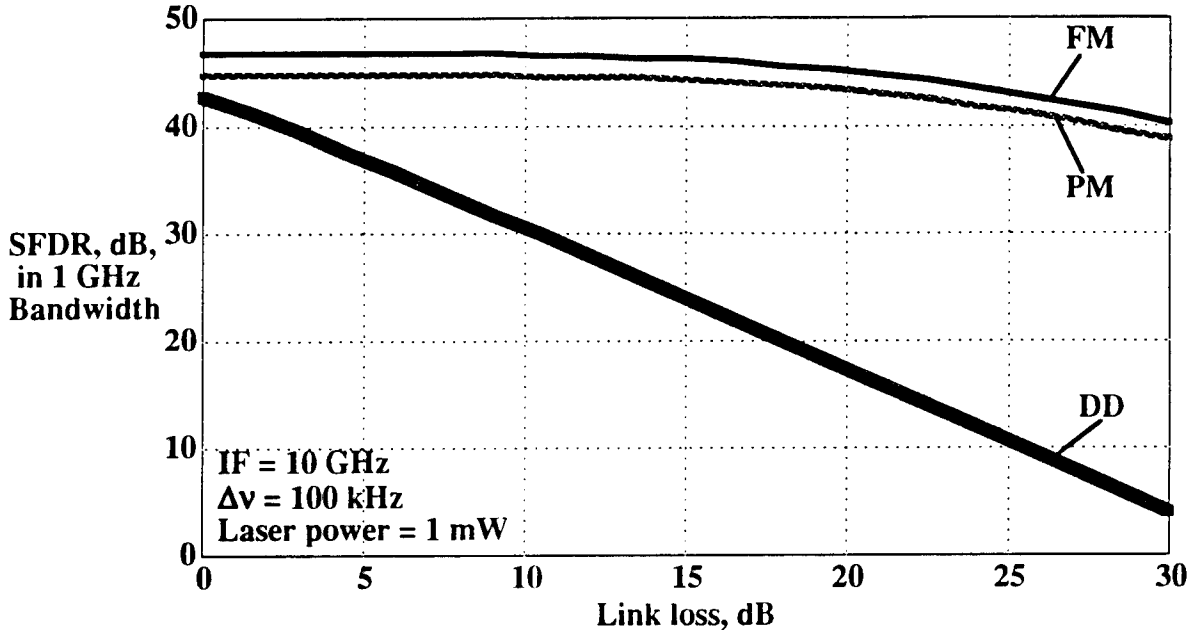

Fig. 14-5. SFDR versus link loss in dB for coherent angle modulated and direct detection links.

14.2.1.2 Comparison of Coherent Angle Modulated and DD Links

Fig. 14-5 shows a simple example of the significant gains that are potentially available through the use of coherent angle modulated links in distribution systems. For a laser power (neglecting modulator excess losses) of 1 mW, a linewidth of 100 kHz, and an LO power of 10 mW, the SFDR improvement is over 25 dB for a 20 dB link loss and over 35 dB for a 30 dB link loss. These gains are much larger than those of the coherent AM link over the DD link. As a result, coherent angle modulated links, though more complex than DD links, exhibit potential, especially for low-linewidth lasers, to significantly outperform DD and coherent AM links.

14.2.2 Cellular Base Station to Antenna Connections

Fig. 14-6 shows a potential configuration for the fiber connections between base station and antenna locations in antenna remoting and cellular systems. The optical power output of a CW semiconductor laser is split, with one path being routed to the interferometric link modulator and the other being routed directly to the antenna location. This eliminates the need for a separate laser at each antenna. The outbound RF signal from the base station is applied to the interferometric link modulator, and the output optical field is then amplified and sent to the antenna location for transmission to mobile users. Inbound RF signals from mobile users are applied to a modulator at the antenna location, and the output optical field is sent to the base station for processing and routing to the desired destination address. The SFDR requirements for the downlink (base station to antenna) are 40 - 50 dB for mobile users in indoor or uncongested outdoor environments but increase to greater than 70 dB for users in environments where there are occlusions or where jamming may be present [1]. For the uplink (antenna to base station), 40 - 50 dB SFDR is adequate since the signal has already passed through the noisy atmospheric link. These requirements are highly demanding, particularly for the L (1 - 2.6 GHz) microwave band to be used by futuristic beamforming antennas and SCM cellular systems.

One possible approach for the downlink is to use linearized laser diodes or high-power Nd:YAG lasers with linearized external modulator and direct detection. As the density of users in each service area (or microcell) and the bandwidth requirements of desired services increase, the linearization and packaging of optical components to satisfy the extremely high SFDR requirements will become increasingly difficult and expensive. Also, the power budget of the downlink will be limited by the unavoidable effects of

clipping due to output power saturation during optical amplification. These problems will be less severe for components needed to satisfy the lower SFDR requirements of the uplink. As a result, the uplink modulator in Fig. 8 could represent a linearized external modulator. The limited power (on the order of -10 dBm) available at the base station receiver for 10 dB link loss also makes the uplink well-suited for coherent angle-modulated links [2].

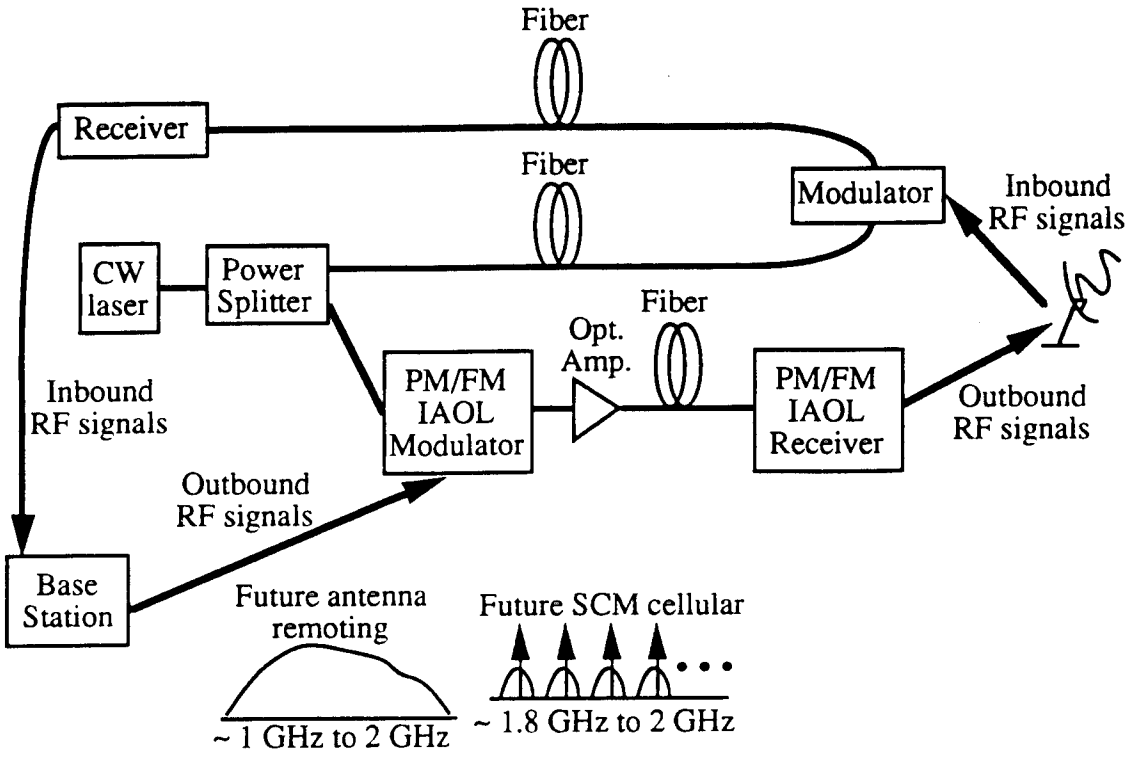

Fig. 14-6. Potential configuration for antenna remoting and cellular systems.

PM and FM heterodyne interferometric links (referred to as simply interferometric links for the remainder of this section) are interesting alternatives for future downlinks, in particular, and uplinks. The unlinearized PM and FM interferometric links offer the potential, as shown in Chapter 9, to significantly outperform unlinearized externally modulated DD links. The SFDR improvement attainable through simple filter linearization at the receiver is shown to be comparable to the improvement through external modulator linearization. The constant envelope of angle-modulated signals makes it possible to take advantage of the full available output power of the optical amplifier. The linewidth insensitivity of interferometric links enables the use of analog angle modulation without the simultaneous requirement of extremely low laser linewidth, which is a major difficulty in other angle-modulated analog

links [2]; as a result, semiconductor lasers are feasible alternatives for solid-state lasers in interferometric links. The construction of wideband receivers is already possible in the 25 GHz IF range, and future components will enable this to be increased further. Though RF amplification is required in all optical links, additional amplification is necessary in IAOLs to compensate for losses in the integrator and discriminator filter.

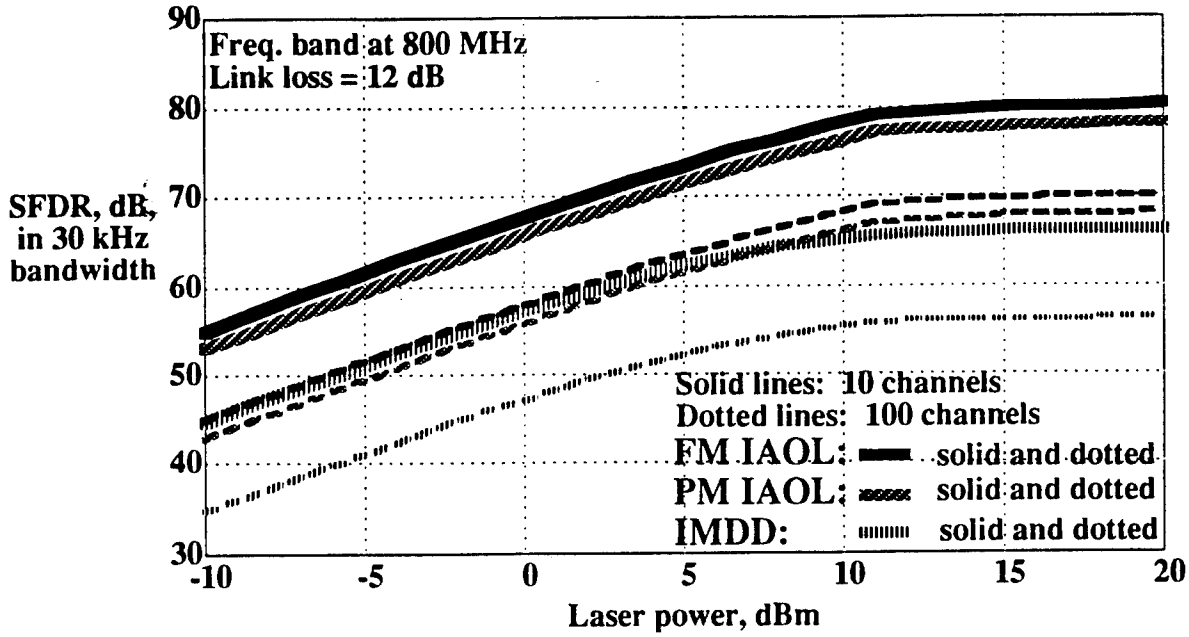

Fig. 14-7. SFDRs of the FM interferometric link, the PM interferometric link, and a DD link plotted versus laser power for SCM cellular voice channels (30 kHz) in the 800 MHz frequency band. Solid lines correspond to 10 channels and dotted lines correspond to 100 channels.

A potentially inexpensive approach for future downlink and uplink connections is to use high-power semiconductor lasers with external modulators (such as an interferometric link modulator) integrated into a compact transmitter module. Output optical powers of 100 mW at 1.51 μm [3] and over 1 W at other infrared wavelengths [4] have already been demonstrated using multiple quantum well devices. The choice of external modulation removes the need for lasers which must be highly linear and have uniform modulation response at multi-GHz frequencies. The recent availability of optical amplifiers at 1.3 μm will remove the problem of chromatic dispersion for fiber links longer than a couple of kilometers without causing fiber attenuation to become unmanageable; this is particularly important for angle-modulated systems such as the interferometric link. The potential SFDR advantages of interferometric links at high

powers make their use an interesting alternative, particularly for transmission of wideband signals at high subcarrier frequencies.

Fig. 14-7 compares the SFDRs of the three links vs. laser power for SCM cellular voice channels (30 kHz each) located at the 800 MHz cellular band for a link loss of 12 dB, which is representative of the loss in a 20 km fiber link at 1.3 μm including connector losses. The FM and PM interferometric links exhibit maximum SFDR advantages over the DD link's SFDR of 13 dB and 11 dB, respectively. For 10 channels, the FM interferometric link reaches the 70 dB SFDR required for transmission in occluded regions [1] for a laser power of 2 mW; for 100 channels, the FM interferometric link reaches 70 dB SFDR at slightly more than 10 mW. The DD link does not reach 70 dB SFDR in either case. Note that the SFDR difference between the 10 channel and 100 channel cases is, conveniently, 10 dB.

14.3 References

[1] W. I. Way, "Optical fiber-based microcellular systems: an overview," *IEICE Trans. Commun.*, vol. E76-B, no. 9, pp. 1091 - 1102, 1993.

[2] R. F. Kalman, J. C. Fan, and L. G. Kazovksy, "Dynamic range of coherent analog fiber-optic links," *IEEE J. Lightwave Technol.*, vol. 12, no. 7, 1994.

[3] T. Tanbun-ek at al., "High output power single longitudinal mode graded index separate confinement multiple quantum well InGaAs/InP distributed feedback (GRIN SCH MQW DFB) lasers," *IEEE Photon. Technol. Lett.*, vol. 2, no. 7, pp. 453 - 455, 1994.

[4] Farries, M. C. et al., "High power semiconductor lasers for lidar and sensing applications," *Proc. of the SPIE*, vol. 2088, pp. 55 - 58, 1994.

Chapter Fifteen

Recommendations for Future Work

In this chapter, we recommend directions for future work relating to analog fiber optic links. In Section 15.1, we discuss potential future work for directly frequency modulated analog links. In Section 15.2, we discuss the importance of the impact of fiber characteristics on analog links and potential future work in this area. Section 15.3 contains references.

15.1 Directly Frequency Modulated Analog Links

During our current project, we have shown that analog optical FM links can potentially achieve larger spurious-free dynamic range (SFDR) than AM links if laser linewidths are sufficiently small (below 100 kHz). Recently, there have been several demonstrations of semiconductor lasers with linewidths of 100 kHz and below [1-3]. These lasers can be directly frequency modulated and have been demonstrated to have output powers on the order of 10 mW. They are typically fabricated using strained multi-quantum well (MQW) materials and distributed feedback (DFB) or grating reflector configurations. Such devices remain in the research stage at present but should become more widely available during the next several years.

Though frequency-shift-keying (FSK), the digital counterpart of FM, has been widely investigated and demonstrated for use in optical communication systems, there have been only a few investigations of the use of optical FM in analog optical links. A notable exception is the combined theoretical and experimental work of GTE Labs and Stanford on a directly modulated FM system for subcarrier multiplexed (SCM) video transmission [4]. During the past two years at Stanford, we have developed theoretical models for predicting the performance of both directly and externally modulated FM coherent analog links, taking into account laser linewidth, laser relative intensity noise (RIN), receiver noise, and nonlinearities of the frequency discriminator.

A coherent FM link is shown in Fig. 15-1. The signal laser has at least two electrodes, where one is used to provide the gain and the other is used to vary the laser frequency. In the FM link, the payload signal is input to the electrode which controls the

frequency of the laser diode. At the receiver, the output of a local oscillator laser is combined with the signal and is heterodyned. The heterodyned current is then limited, put through a discriminator filter, and envelope detected.

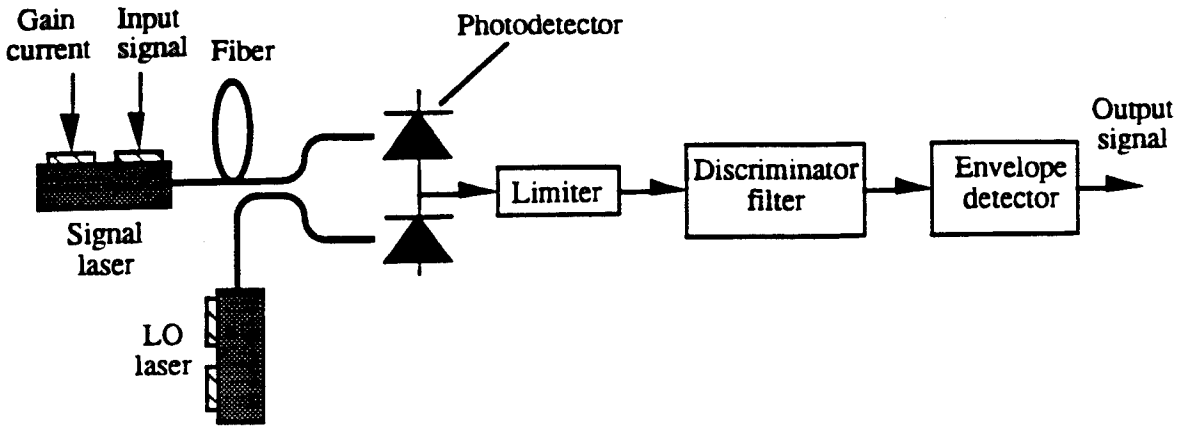

Fig. 15-1. FM link using direct modulation and a coherent optical receiver.

An interesting alternative to a coherent detection FM receiver is a direct detection FM receiver in which the photodetector is preceded by a optical filter (Fig. 15-2). If the FM optical spectrum falls on a linear slope of the filter transfer characteristic, the filter will differentiate the optical signal, and convert the frequency deviation to amplitude deviation. The optical filter thus performs the same function as the discriminator filter in a coherent receiver.

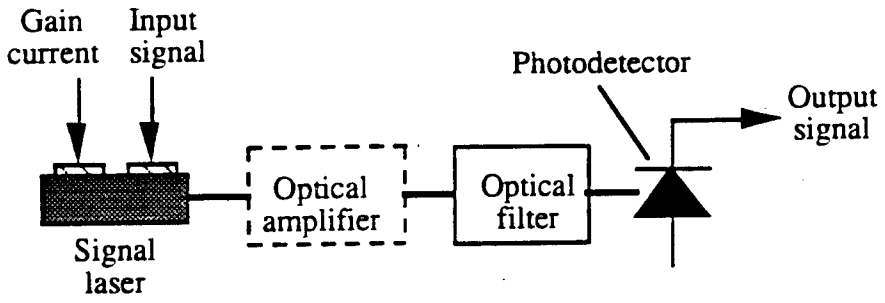

Fig. 15-2. FM link using an optical filter and a direct-detection receiver.

Motivated by the recent advances in laser technology and our encouraging theoretical results for FM links based on narrow-linewidth lasers, we recommend an experimental and theoretical investigation of FM analog links. The experimental investigation will involve the construction and characterization of an FM analog link using direct modulation of low-linewidth semiconductor lasers.

15.1.1 Theoretical Work

We recommend the theoretical investigation of the following facets of FM analog optical links: (a) the degree of nonlinearity of the laser frequency-vs.-current characteristic of semiconductor lasers and its impact on the dynamic range; (b) the nonuniformity of the laser FM response and its impact on the dynamic range; (c) the impact of laser RIN and linewidth; and (d) the impact of fiber imperfections, including dispersion and nonlinearities (see Section 15.2 for a discussion of fiber imperfections.) The theoretical investigation will be conducted for both coherent and direct-detection FM links.

When a current through the grating section of a DFB or DBR laser changes, its lasing frequency will change. The frequency change is a function of the carrier density in the active region and, for large SFDR, should be a linear function of the drive current irrespective of the modulating frequency. The actual linearity (or nonlinearity) of the laser frequency versus current characteristic is, however, unknown. It is important to model the laser frequency-vs.-current characteristic of actual laser diodes and compare it with measurable device parameters. It is important to assess the impact of this nonlinearity on link dynamic range.

The frequency modulation response of a laser diode is the dependence of the optical frequency deviation on the frequency of the applied modulating current. The FM response of laser diodes is not uniform as a result of the following effects: the nonlinear interaction of the carrier and photon populations, the finite carrier and photon lifetimes, nonlinear grating dispersion, and mode hopping. It is important to model the FM response of actual laser diodes and compare it with measurable device parameters. It is important to assess the impact of the nonideal laser response and nonlinearities of the discriminator filter in the receiver. It is important to model the impact of laser FM response on SFDR and will also consider means of equalizing the FM response.

The signal information in FM links is contained in the optical phase rather than in the optical intensity. Therefore, the impact of RIN on FM coherent links can be reduced by a limiter in the receiver and a balanced front end. It is important to investigate how well a practical limiter can suppress RIN, and how well-balanced the receiver must be in terms of matching the complex frequency response of the two photodetectors.

It is important to theoretically investigate the performance of a direct detection FM link. Specifically, it is important to investigate the linearity and SFDR of the link for

various types of optical filters. Additionally, it is important to investigate the impact of RIN on the direct detection FM link.

15.1.2 Experimental Work

We recommend the construction and characterization of an experimental FM link. We plan to use a directly modulated low-linewidth laser diode to produce a frequency modulated optical carrier. If a coherent optical receiver will be used, it will contain a local oscillator (LO) laser diode similar to that used at the transmitter (Fig. 15-1). If a direct-detection receiver will be used, the receiver will contain an optical filter instead of a local oscillator laser (Fig. 15-2).

It is important to characterize the transmitter laser diode. It is important to measure the linearity of the laser frequency versus current characteristic. The static linearity will be measured by varying the dc current at the input to the transmitter grating section and measuring the optical frequency of the output using an optical spectrum analyzer. The dynamic linearity of the laser is more difficult to quantify. One possible method is to demodulate the optical FM signal using either coherent detection with delay line discrimination or direct detection with an optical filter. If two microwave tones are used as the test signal, the output signal will display easily measurable nonlinear components. This is shown in Fig. 15-3 for coherent detection. The photocurrent spectrum is a downconverted copy of the laser FM spectrum, and the output spectrum contains the two test tones plus additional components stemming from the laser input. After characterization of the discriminator using a network analyzer, it may be possible to eliminate the effect of the known discriminator nonlinearities, enabling a more accurate characterization of the laser frequency versus current characteristic.

The FM response of a laser is the dependence of the laser frequency deviation on the modulation current frequency. It is important to characterize the FM response of the transmitter at various modulation depths. It is important to also measure the optical linewidth of the laser and the laser RIN.

If we use coherent detection, we will initially build a simple microwave two-branch delay-line filter and characterize the system performance using this filter in the receiver. It is important to then construct a four branch delay-line filter and use this filter in the link*. It is important to then evaluate the resulting SFDR improvement. If we use

* Our analysis has shown that a four-branch filter can eliminate third-order distortion, making fifth-order distortion the dominant nonlinearity and increasing the SFDR by 4 - 8 dB.

direct detection, It is important to use various optical filters (such as a fiber Fabry-Perot and a Mach-Zehnder) and characterize the system performance.

It is important to verify the predictions of our theoretical model for link SFDR as a function of laser linewidth, laser RIN, and signal optical power by measuring link SFDR using a two-tone input signal. It is important to measure the SFDR penalty due to laser nonlinearity and due to nonuniform laser FM response.

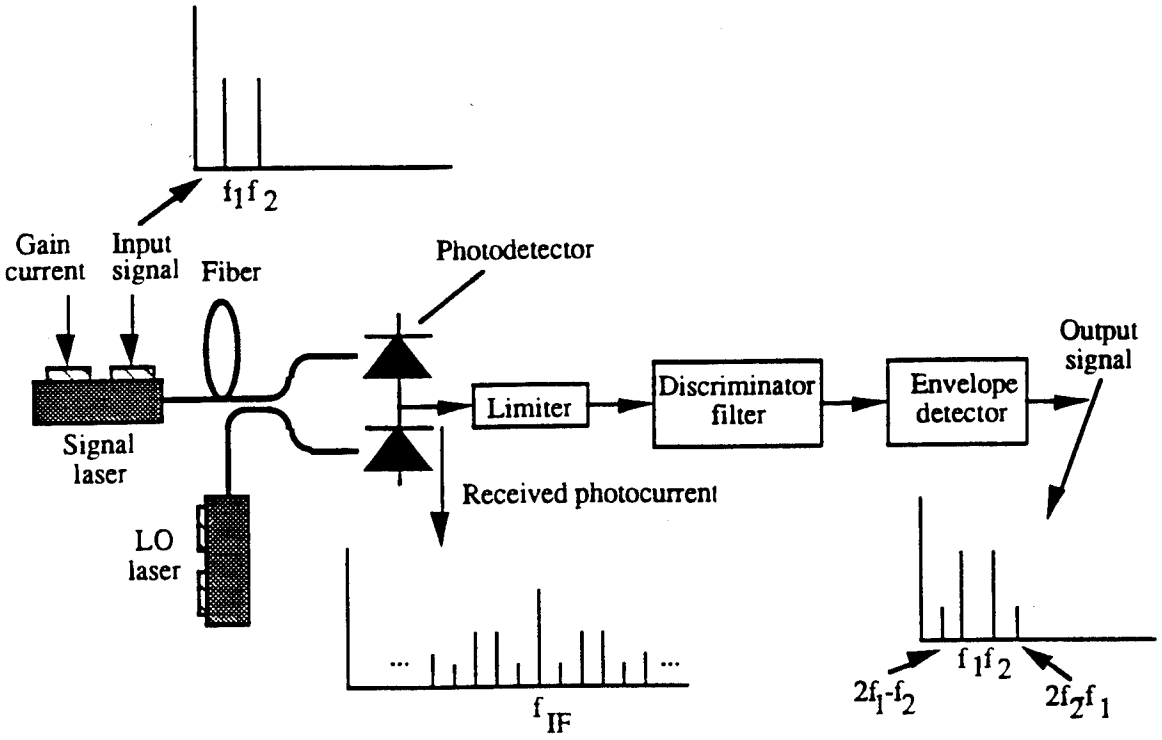

Fig. 15-3. Spectra of signals in an FM link using direct modulation and a coherent optical receiver.

15.2 Impact of Fiber Characteristics on Analog Links

The speed of light in an optical fiber is a function of the optical frequency, an effect known as dispersion. Dispersion may distort a signal propagating through the fiber. The distortion is proportional to the *optical* * signal bandwidth and may limit the dynamic range of analog optical links.

Due to the development of high-power and high-speed lasers and optical amplifiers, the optical power and bandwidth of the signal traveling along the fiber have increased significantly. Fiber characteristics can potentially limit the SFDR of analog

* *Optical* signal bandwidth is substantially larger than the bandwidth of the electrical signal transmitted.

links; fiber dispersion is especially important at high RF frequencies, and fiber nonlinearities is especially important at high optical powers.

For optically amplified analog links, there is an additional concern. In the course of amplification, optical amplifiers add spontaneous emission to the signal. Upon detection, this spontaneous emission results in a number of noise terms, including signal-spontaneous beat noise, spontaneous-spontaneous beat noise, and excess shot noise. For the high saturation power amplifiers now available, signal and spontaneous emission power levels may be quite high. The impact of optical fiber nonlinearities is of particular concern in such systems.

Four types of fiber nonlinearities can degrade the performance of optical fiber systems: (a) four wave mixing (FWM), (b) self and cross-phase modulation (SPM and XPM, respectively), (c) stimulated Brillouin scattering (SBS), and (d) stimulated Raman scattering (SRS). The four effects are briefly described below:

Four wave mixing (FWM): Four wave mixing is caused by the intensity-dependent refractive index of optical fiber. Two copropagating waves at different frequencies can mix together to generate two new waves at different frequencies. In WDM systems, this process can cause power losses, signal distortion in each channel, and interference with other channels. The interaction strength of FWM depends critically on the phase matching condition. Because of the dispersion properties of optical fibers, this process is important if the frequency separation between channels is small or if the system is operated near the zero-dispersion point.

Self and cross-phase modulation (SPM and XPM): The nonlinear index of refraction of the optical fiber may cause phase changes due to signal intensity fluctuations. In single channel transmission systems, it is called self-phase modulation (SPM). In WDM systems, cross-phase modulation (XPM) may convert intensity fluctuation in one channel to phase fluctuations in other channels. If the channel separation is large enough, no new frequencies are generated by these effects.

Stimulated Brillouin scattering (SBS): Stimulated Brillouin scattering is an interaction between incident light and acoustic phonons (sound waves) in the material. Due to energy and momentum conservation criteria, SBS in optical fibers will only generate backward propagating waves at downshifted frequencies (Stokes waves). SBS may cause crosstalk between counter-propagating waves or power losses due to reflection in unidirectional transmission systems. A signal wave and a Stokes wave will experience a

strong SBS interaction if the optical frequency separation is equal to the fiber acoustic resonance frequency (about 10-20 GHz). Because of the narrow interaction bandwidth of SBS (less than several hundreds of megahertz), the effect of SBS is especially important for narrow linewidth lasers.

Stimulated Raman scattering (SRS): Stimulated Raman scattering is an interaction between incident light and optical phonons, or molecular vibrations of the material. The effects of SRS are similar to those of SBS, except that SRS can cause an interaction between copropagating and counter-propagating waves. The SRS gain coefficient increases approximately linearly with frequency separation up to 15,000 GHz. This broad bandwidth means that it is impossible to avoid SRS by proper channel allocation. SRS may lead to signal power losses and crosstalk between channels. In WDM systems, power may be transferred from channels with higher frequencies to channels with lower frequencies. This interaction becomes stronger as the number of channels and the channel separation increase.

Fiber imperfections affect the system as follows:

(1) Fiber dispersion can limit the spurious-free dynamic range of an optical link even when the link loss budget has not been exceeded. The large bandwidth of wide-deviation FM signals may also increase the impact of dispersion.

(2) FWM is important in WDM applications. FWM generates a new frequency of light through power transfer from three existing frequencies. The wavelengths of most generated signals fall into the waveband of WDM signals; therefore, these signals become a source of interference.

(3) SPM induces a change of the refractive index of the transmission material proportional to the light intensity; this index change induces a phase shift in the light, which can directly affect PM or FM systems. For AM links, this phase modulation results in frequency chirping, which, together with fiber chromatic dispersion, may cause signal distortion.

(4) When two or more waves propagate in a nonlinear medium (like optical fiber at high power levels), the amplitude modulation of one wave will result in the phase modulation of the others through the same mechanism that leads to SPM. This effects is known as XPM. The impact of XPM can be large in WDM systems, particularly when there is a combination of AM and FM optical signals.

(5) At the onset of SBS, a portion of the optical input power will be scattered back, resulting in a limit on the transmittable optical power of amplifier-based systems. FM systems may be less susceptible to SBS due to the lower power spectral density of wideband FM signals and due to the lower received power requirements of FM signals.

(6) Due to fiber nonlinearities, the spontaneous emission of optical amplifiers modulates the phase of the transmitted signal and broadens its spectrum. This may cause additional signal distortion for optically amplified analog links.

15.2.1 Theoretical Work

We recommend the investigation of the impact of fiber imperfections (dispersion and nonlinearities) on the performance of analog optical links with and without optical amplifiers. It is important to quantify the relationship between the SFDR and fiber characteristics taking into account the impact of optical power, signal bandwidth, and optical amplifier characteristics.

It is important to develop an understanding of the impact of fiber dispersion and fiber nonlinearities on analog optical links employing both conventional single-mode fiber and dispersion-shifted fiber. It will then be possible to evaluate the SFDR, RF power transfer ratio, and noise figure in the presence of fiber imperfections, and to subsequently identify a transmission scheme minimizing the impact of fiber imperfections on analog optical links.

It is important to investigate the impact of fiber dispersion and nonlinearities on analog fiber-optic links using optical amplifiers by concentrating on the interaction between optical amplifier characteristics, fiber dispersion and nonlinearities, and how these phenomena will affect the SFDR, RF power transfer ratio and noise figure. It is important to consider the difference in the performance of systems using erbium-doped fiber amplifiers (EDFAs) and semiconductor optical amplifiers (SOAs). The gain of optical amplifiers can be saturated by high-level signals and spontaneous emission. Saturation leads to both gain reduction and the generation of intermodulation distortion. EDFAs have much slower gain dynamics than SOAs; the gain variations in EDFAs occur on time scales of 10 ms versus 1 ns for SOAs. The slower gain dynamics of EDFAs leads to substantially lower intermodulation distortion than SOAs, and thus, EDFAs are likely to lead to better link performance. SOAs have also been known to have a gain ripple due to nonideal antireflection coating. It is important to investigate the distortion generated by the gain ripple's interaction with laser frequency chirping, and to evaluate the

intermodulation distortion generated by the two types of amplifiers. It will then be possible to evaluate the upper limit to link performance imposed by the intrinsic amplifier and fiber characteristics. It is also important to investigate the optimum positioning of optical amplifiers to minimize the impact of fiber imperfections on optically amplified analog optical links.

It is important to identify and investigate the dominant nonlinearities for each analog system. It is expected that for single channel AM links, Brillouin scattering may be the dominant effect due to the large narrowband carrier term in AM systems. FM systems spread the signal power over a wider band of frequencies. Though this may increase the impact of dispersion on FM systems, the impact of fiber nonlinearities may be reduced for the same reason. In FM systems, self-phase modulation is expected to be the dominant effect due to the sensitivity of FM systems to phase perturbations. In multichannel systems, four wave mixing and cross-phase modulation may become more important.

It is important to investigate techniques for reducing the impact of nonlinearities* and to identify modulation and demodulation techniques that minimize the degradation of SFDR due to fiber imperfection.

15.2.2 Experimental Work

It is important to experimentally investigate the impact of fiber dispersion and nonlinearities on analog optical links with and without optical amplifiers. An example of an experiment to measure the impact of fiber dispersion on SFDR is shown in Fig. 15-4. The effects of fiber dispersion are investigated for (a) a directly modulated system and (b) an externally modulated system. It has been experimentally shown that the coupling of laser chirp and fiber dispersion causes serious degradation of the dynamic range by the second order nonlinearity [5]. By comparing the two systems for different modulation indexes and different fiber lengths as shown in Fig. 15-4, it is possible to identify the combined effects of laser chirp and fiber dispersion.

It is also important to experimentally investigate the interaction between optical amplifier characteristics, fiber dispersion and nonlinearities, and how these phenomena affect the dynamic range, RF power transfer ratio and noise figure of analog links. This can be done by building and characterizing the link shown in Fig. 15-4 using an erbium-doped fiber amplifier (EDFA) and a semiconductor optical amplifier (SOA), and

* For example, it has been experimentally demonstrated that phase modulation can be used to reduce the impact of Brillouin scattering on AM systems [9].

comparing their performance to quantify the relationship between the optical power, signal bandwidth, optical amplifier and fiber characteristics. It is important to determine the various noise terms generated by the amplifier spontaneous emission at the receiver, such as signal-spontaneous beat noise, spontaneous-spontaneous beat noise, and excess shot noise. It is also important to investigate the impact of the gain ripple found in SOAs, how amplifier gain saturation leads to both gain reduction and the generation of intermodulation distortion, and the optimum positioning of optical amplifiers to minimize the impact of fiber imperfections on optically amplified analog optical links.

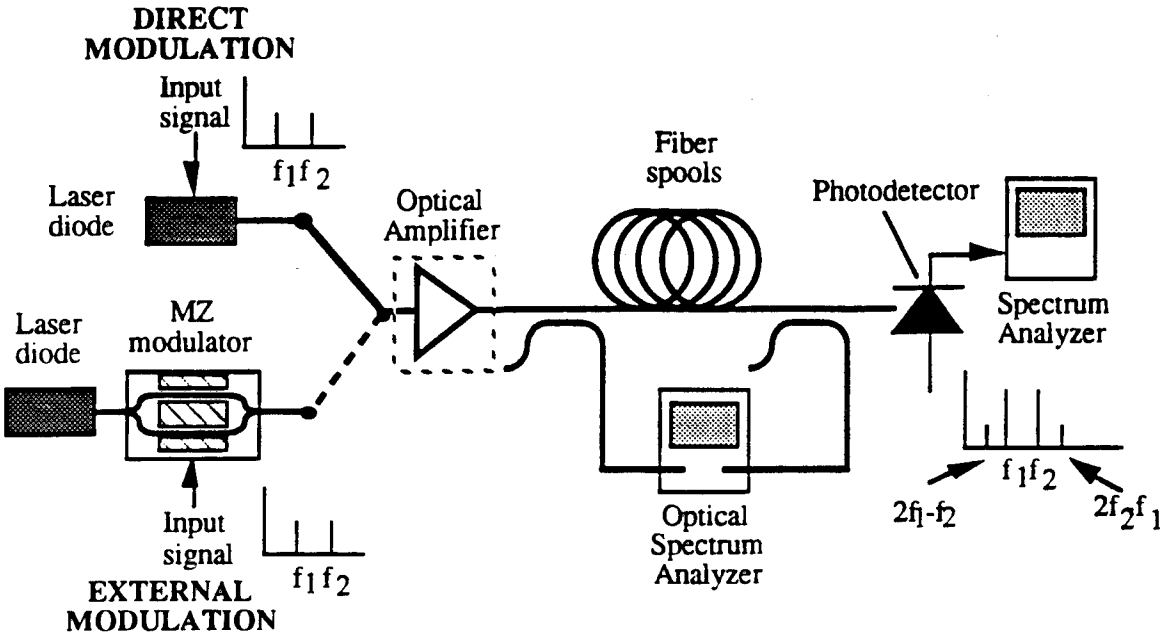

Fig. 15-4. Experimental set-up for measuring the impact of dispersion for a directly modulated system and an externally modulated system.

An example of an experiment to measure the impact of stimulated Brillouin scattering is shown in Fig. 15-5. The light from a transmitter laser travels through a long length of fiber consisting of multiple fiber spools spliced together. The light is then coherently detected and the detected signal is displayed on a spectrum analyzer. A directional coupler is included to allow the backscattered light due to Brillouin scattering to be measured.

As shown in both Figs. 15-4 and 15-5, we can apply two-tone test signals to measure the (a) spurious-free dynamic range, (b) intermodulation levels, (c) signal-to noise ratio, (d) RF power transfer ratio and (e) noise figure as a function of laser power and fiber length. With coherent detection, it will be possible to investigate the impact of

optical power fluctuations resulting from SBS on the dynamic range and to measure the backscatter as a function of optical power to quantify the impact of Brillouin scattering.

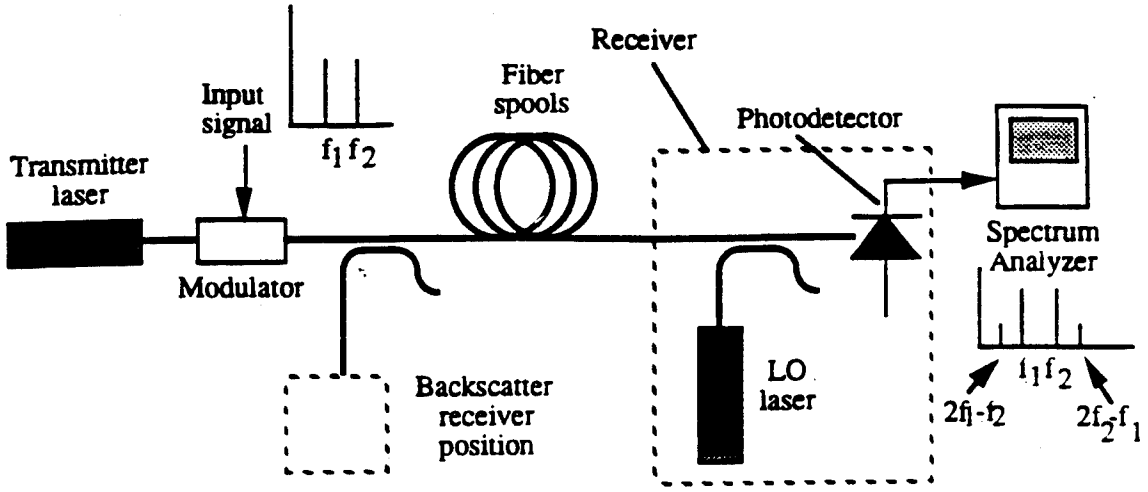

Fig. 15-5. Experimental set-up for measuring the impact of Brillouin scattering on spurious-free dynamic range.

15.3 References

[1] M. Okai et al., "Tunable DFB lasers with ultra-narrow spectral linewidth," *Electronics Lett.*, vol. 29, no. 4, pp. 349-351, 1993.

[2] H. Bissessur et al., "Very narrow-linewidth (70 kHz) 1.55 μm strained MQW DFB lasers," *Electronics Lett.*, vol. 28, no. 11, pp. 998-999, 1992.

[3] P. A. Andrekson et al., "High power semiconductor laser injection-locking at 1.3 μm," *IEEE/OSA Journal of Lightwave Technology*, vol. 10, no. 7, pp. 903-907, 1992.

[4] G. Fiksman, R. Gross, J. Fan, and L. Kazovsky, "Performance optimization of directly modulated FM-SCM systems with optical discriminator," *IEEE Photon. Tech. Lett.*, vol. 5, no. 7, pp. 845-848, 1993.

[5] E. E. Bergmann, C. Y. Kuo and S. Y. Huang, "Dispersion-Induced Composite Second-Order Distortion at 1.5 mm," *IEEE Photon. Tech. Lett.*, vol. 3, no. 1, pp. 59-61, January 1992.

PAGES 213 - 216 ARE INTENTIONALLY LEFT BLANK

PART 5:

APPENDICES

Appendix A

System Noises and Their Properties

A.1 Basic Noise Properties

In this section, we discuss the basic properties of noises which commonly affect analog optical links. These noises include receiver additive noise, laser relative intensity noise (RIN), laser phase noise, and amplified spontaneous emission (ASE) noise.

A.1.1 Additive Noise

Shot noise and thermal noise are the two fundamental noise mechanisms responsible for current fluctuations in all optical receivers even when the incident optical power P is constant. Of course, additional noise is generated if P is itself fluctuating because of relative intensity noise associated with the system. The photodiode current generated in response to a constant optical signal can be written as:

$$I(t) = I_p + i_t(t) + i_s(t) + i_r(t) \tag{A.1}$$

where $I_p = RP$ is the average current and $i_t(t)$, $i_s(t)$, $i_r(t)$ are current fluctuations related to thermal noise, shot noise and relative intensity noise, respectively.

A.1.1.1 Thermal noise

Random thermal motion of electrons in a resistor manifests as a fluctuating current even in the absence of an applied voltage. The load resistor in the front end of an optical receiver adds such fluctuations to the current generated by the photodiode. Mathematically, $i_t(t)$ is modeled as a stationary Gaussian random process with a spectral density that is frequency independent and is given by:

$$S_t(f) = \frac{4kT}{r}, \qquad \text{for } 0 < f < \infty \tag{A.2}$$

where k is the Boltzman constant, T is the absolute temperature, and r is the load resistor.

A.1.1.2 Shot noise

Shot noise is a manifestation of the fact that electric current consists of a stream of electrons that are generated at random times. Mathematically, the photocurrent fluctuation is a stationary random process with Possion statistics which in practice can be approximated by the Gaussian statistics with a spectral density given by:

$$S_s(f) = 2qI_p, \qquad \text{for } 0 < f < \infty \tag{A.3}$$

where q is the charge of an electron.

A.1.2 Relative Intensity Noise

In practice, light emitted by any transmitter exhibits power fluctuations. Such fluctuations are called relative intensity noise. An exact analysis of $i_r(t)$ is complicated, as it involves the calculation of photocurrent statistics which in turn depends on the intensity-noise statistics at the receiver. A simple approach is to assume the spectral density to be:

$$S_r(f) = R^2 P^2 10^{\frac{RIN}{10}}, \qquad \text{for } 0 < f < \infty \tag{A.4}$$

where the parameter *RIN*, in dB/Hz, is a measure of the noise level of the incident optical signal.

The above assumption is valid for modulation frequencies much lower than the laser relaxation resonance frequency. In Section A.2, we will describe the characteristics of laser RIN for modulation frequencies much larger than the relaxation resonance frequency.

A.1.3 Phase Noise

The spectral shape for semiconductor lasers can be approximated by the Lorenzian lineshape, i.e., the phase noise is dominated by white frequency noise. The single-sided PSD of *f(t)* is given by the following expression:

$$S_{\phi}(f) = \frac{\Delta\nu}{\pi f^2}, \qquad \text{for } 0 < f < \infty \tag{A.5}$$

where Dn is the FWHM linewidth.

A.1.4 Amplified Spontaneous Emission Noise

Spontaneous emission is a manifestation of the fact that photons are generated randomly in atoms by the movement of electrons from higher to lower energy states. As a result, even in the case of complete population inversion in the optical amplifier gain medium, noise is added to the amplified output signal. This noise, known as amplified spontaneous emission (ASE) noise, is uniformly present in any polarization and is white over the amplifier bandwidth, which is on the order of tens of nanometers. Mathematically, the fluctuation in the number of photons generated by a large number of atoms is, like shot noise, well approximated by Gaussian statistics. The single-sided PSD of each ASE component is

$$S_{ASE}(f) = (G-1)n_{sp}h\upsilon, \qquad \text{for } 0 < f < \infty \tag{A.6}$$

where $h\upsilon$ represents the energy of the spontaneously emitted photons and n_{sp} is the amplifier spontaneous emission factor. n_{sp} equals one for complete population inversion and is greater than one if inversion is incomplete.

A.2 Noise in Angle Modulated Links

In this section, we evaluate the noise expressions used throughout Part 3. Due to the receiver complexity of angle modulated links, we present not only the basic noise properties of the noises described in Section A.1, but also the properties of derivative noise processes and of baseband and bandpass noises.

A.2.1 Baseband and Bandpass Noise

In the following expressions, we encounter both bandpass noise terms around the IF and baseband noise. We will use the subscript *bp* to indicate bandpass noise, which is related to the unfiltered noise by

$$n_{bp}(t) = h_{bp}(t) * n(t) \tag{A.7}$$

where $h_{bp}(t)$ is the impulse response of the IF amplifier. We will use the subscript *bb* to indicate baseband noise, which is related to the unfiltered noise by

$$n_{bb}(t) = h_{bb}(t) * n(t) \tag{A.8}$$

where $h_{bb}(t)$ is the impulse response of the baseband circuitry.

A.2.2 Power Spectral Density of the Receiver Noise and its Derivative

The shot noise $n_{sh}(t)$ is white with a single-sided power spectral density (PSD) after *each* photodiode given by

$$G_{n_{sh}}(f) = \eta_{sh} = \begin{cases} eR(P_S + P_{LO}) & \text{(CD)} \\ 2eRP_S & \text{(DD)} \end{cases} \tag{A.9}$$

For coherent detection (CD), a balanced receiver is assumed. For direct detection (DD) as in interferometric links, a single photodetector is used.

The thermal noise $n_{th}(t)$ is also white with a single-sided PSD given by

$$G_{n_{th}}(f) = \eta_{th} = \frac{4kT}{R_r} \tag{A.10}$$

In the above expressions, P_S is the received signal optical power, P_{LO} is the received local oscillator optical power, e is the electron charge, k is Boltzmann's constant, T is the absolute temperature, and R_r is the effective receiver resistance. Assuming perfectly matched photodetectors, the sum of the shot and thermal noise, $n_D(t)$, has a

PSD given by $\eta_D = 2\eta_{sh} + \eta_{th}$. The root mean squared (RMS) power in $n_D(t)$ is thus given by

$$\left\langle n_{D\,bb}^2 \right\rangle = \eta_D B \tag{A.11}$$

$$\left\langle n_{D\,bp}^2 \right\rangle = 2\eta_D B \tag{A.12}$$

where B is the bandwidth of the baseband signal $x(t)$.

For the FM case, we must evaluate the PSD of $\dot{n}_D(t)$, which is given by

$$G_{\dot{n}_D}(f) = (2\pi f)^2 \eta_D \tag{A.13}$$

leading to

$$\left\langle \dot{n}_{D\,bp}^2 \right\rangle = \frac{(2\pi)^2}{3} \eta_D \left(f_2^3 - f_1^3 \right) \tag{A.14}$$

f_1 and f_2 are the lower and upper baseband signal frequency, respectively, and thus obey the relationship

$$B = f_2 - f_1 \tag{A.15}$$

A.2.3 Power Spectral Density of the Phase Noise and its Derivative

The PSD of the frequency noise $\dot{\varphi}_n(t)$ is given by [1]

$$G_{\dot{\varphi}_n}(f) = 4\pi\Delta\nu \tag{A.16}$$

which leads to

$$\left\langle \dot{\varphi}_n^2 \right\rangle = 4\pi\Delta\nu B \tag{A.17}$$

where Dn is the combined linewidth of the transmitter and local oscillator lasers. The PSD of the phase noise $\varphi_n(t)$ is given by

$$G_{\varphi_n}(f)=\frac{\Delta\nu}{\pi f^2} \tag{A.18}$$

which leads to

$$\left\langle \varphi_n^2 \right\rangle = \frac{\Delta\nu}{\pi}\left(\frac{1}{f_1}-\frac{1}{f_2}\right) \tag{A.19}$$

A.2.4 Power Spectral Density of the RIN and its Derivative

The PSD of the RIN is a complicated function of a number of laser parameters [2]. For the purpose of our analysis, we will describe the RIN PSD phenomenologically as

$$G_{n_R}(f)=\frac{\eta_R}{\left[1+(f/f_R)^2\right]^2}, \tag{A.20}$$

where η_R is an "average" low frequency RIN PSD and f_R is RIN roll-off frequency, which is related to the relaxation oscillation frequency of the laser. Through an appropriate choice of η_R and f_R, we can adequately model the impact of RIN on the analog links analyzed. Eq. (A.20) leads to

$$\left\langle n_R^2 \right\rangle = g_1(f_2)-g_1(f_1) \tag{A.21}$$

where

$$g_1(f)=\frac{\eta_R f_R}{2}\left[\tan^{-1}(f/f_R)+\frac{(f/f_R)}{1+(f/f_R)^2}\right] \tag{A.22}$$

For the bandpass RIN, we find

$$\left\langle n_{Rbp}^2 \right\rangle = g_1(f_{IF}+f_2)-g_1(f_{IF}+f_1)+g_1(f_{IF}-f_1)-g_1(f_{IF}-f_2) \tag{A.23}$$

In the FM SNR expression, we can evaluate $\left\langle \dot{n}_R^2 \right\rangle$ as

$$\left\langle \dot{n}_R^2 \right\rangle = g_2(f_{IF}+f_2)-g_2(f_{IF}+f_1)+g_2(f_{IF}-f_1)-g_2(f_{IF}-f_2) \tag{A.24}$$

where

$$g_2(f)=\frac{\eta_R f_R^3}{2}\left\{\tan^{-1}(f/f_R)-\frac{(f/f_R)}{1+(f/f_R)^2}\right\} \tag{A.25}$$

A.2.5 Photodetector Matching Factor

The photodetector matching factor b of the coherent PM link is defined as

$$b=\frac{\left\langle\left|[h_1(t)-h_2(t)]*n_R(t)\right|^2\right\rangle}{\left\langle n_R^2(t)\right\rangle} \tag{A.26}$$

where $h_1(t)$ and $h_2(t)$ are the impulse responses of the two photodetectors in the balanced receiver. For the coherent FM link,

$$b=\frac{\left\langle\left|[h_1(t)-h_2(t)]*\dot{n}_R(t)\right|^2\right\rangle}{\left\langle \dot{n}_R^2(t)\right\rangle} \tag{A.27}$$

b ranges from 0 for two perfectly matched photodetectors to 1 for a single photodetector.

A.3 Noise in Optically Amplified Angle Modulated Links

The single-sided noise power of the ASE component in each polarization is [3]

$$\left\langle n_{OA\hat{s}\,bp}^2\right\rangle=\left\langle n_{OA\hat{o}\,bp}^2\right\rangle=(G-1)hfn_{sp}B \tag{A.28}$$

where hf represents the average energy of the spontaneously emitted photons, n_{sp} is the amplifier spontaneous emission factor, and B is the signal bandwidth. The power spectral density of the spontaneous-spontaneous (sp-sp) noise is given in [4] as

$$\left\langle n_{sp-sp\,bp}^2\right\rangle=\left((G-1)hfn_{sp}\right)^2 2B_{opt}B \tag{A.29}$$

where B_{opt} is the bandwidth of the optical filter. No optical filter is needed in the DD link or in the interferometric links for high powers since the sp-sp noise is dominated by the signal-spontaneous (and reference-spontaneous in the interferometric links) noises.

The noise power in a bandwidth $B = f_{max}-f_{min}$ of a general $\dot{n}(t)$ is the integral from f_{min} to f_{max} of the power spectral density $(2\pi f)^2 \eta$, where η is the power spectral density of $\dot{n}(t)$. Therefore,

$$\left\langle \dot{n}_{bp}^2 \right\rangle = \frac{(2\pi)^2}{3} \eta \left(f_{\max}^3 - f_{\min}^3 \right) \tag{A.30}$$

As a result, the noise powers in the FM SNR expression are simply

$$\left\langle \dot{n}_{OA\hat{s}\,bp}^2 \right\rangle = \left\langle \dot{n}_{OA\hat{o}\,bp}^2 \right\rangle = (G-1)hfn_{sp} \frac{(2\pi)^2}{3} \left(f_{\max}^3 - f_{\min}^3 \right) \tag{A.31}$$

$$\left\langle \dot{n}_{sp-sp\,bp}^2 \right\rangle = \left((G-1)hfn_{sp} \right)^2 2B_{opt} \frac{(2\pi)^2}{3} \left(f_{\max}^3 - f_{\min}^3 \right) \tag{A.32}$$

A.4 References

[1] L. G. Kazovsky, "Performance analysis and laser linewidth requirements for optical PSK heterodyne systems," *J. Lightwave Technol.*, vol. LT-4, pp. 415-425, 1986.

[2] S. L. Woodward, T. L. Koch, and U. Koren, "RIN in multisection MQW-DBR lasers," *IEEE Photon. Technol. Lett.*, vol. 2, no. 2, pp. 104-108, 1990.

[3] P. S. Henry, "Error-rate performance of optical amplifiers," in *Tech. Dig. OFC '89*, Feb. 1989 (Houston, TX), paper THK3.

[4] T. Okoshi and K. Kikuchi, *Coherent Optical Fiber Communications*, KTK Scientific Publishers, Tokyo, 1988.

Appendix B

Derivation of Amplitude Modulated Link Equations

B.1 2-port 90° Optical Hybrid Homodyne WIRNA System

Let the signal to be transmitted be $x(t)$. The electric field of the optical signal obtained by the external amplitude modulator can be written, using phasor notation, as:

$$E_S = \sqrt{\frac{P_S}{2}}\left(e^{jx(t)} + e^{j\frac{\pi}{2}}\right) \tag{B.1}$$

where P_S represents the total optical power. In homodyne systems, the optical center frequency of the local oscillator is same as that of the signal light. The electric field of the local oscillator can be written as:

$$E_{LO} = \sqrt{P_{LO}}e^{-j\phi(t)} \tag{B.2}$$

where $f(t)$ is the phase difference between the optical signal and local oscillator, and it represents the total phase noise. Using the optical 90° hybrid, the two optical signals are combined. As outputs of the optical hybrid, two signals are obtained with different phase relations:

$$E_1 = \sqrt{L}(E_S + E_{LO}) \tag{B.3}$$

$$E_2 = \sqrt{L}\left(E_S + E_{LO}e^{j\frac{\pi}{2}}\right) \tag{B.4}$$

The output currents from the photodetectors are proportional to the optical power, $|E|^2$. They can be written as:

$$i_1 = |E_1|^2 R = A\left[P_S + P_{LO} + P_S \sin x + \sqrt{2P_S P_{LO}}\left\{\cos(x+\phi) - \sin\phi\right\}\right] + n_1 \tag{B.5}$$

$$i_2 = |E_2|^2 R = A\left[P_S + P_{LO} + P_S \sin x + \sqrt{2P_S P_{LO}}\left\{\sin(x+\varphi) + \cos\varphi\right\}\right] + n_2 \qquad \text{(B.6)}$$

where $A \equiv RL$ and n_1 and n_2 are the additive noises with power spectral densities of $\eta_1 = \eta_2 = \eta = \eta_{th} + 2qRL(P_s + P_{LO})$. After the DC block, wideband filter, and square-law detector, two processed signals are obtained as below:

$$w_1 = \left[(i_1 - DC) * h_1\right]^2 = A^2 \left[\begin{array}{l} 2P_S P_{LO}\left\{\cos^2(x+\phi) + \sin^2\phi - 2\cos(x+\phi)\sin\phi\right\} \\ +\left(P_S \sin x\right)^2 + 2P_S \sin x\sqrt{2P_S P_{LO}}\left\{\cos(x+\phi) - \sin\phi\right\} \end{array}\right] \\ +\left(n_1 * h_1\right)^2 + 2\left(n_1 * h_1\right)A\left[P_S \sin x + \sqrt{2P_S P_{LO}}\left\{\cos(x+\phi) - \sin\phi\right\}\right] \qquad \text{(B.7)}$$

$$w_2 = \left[(i_2 - DC) * h_1\right]^2 = A^2 \left[\begin{array}{l} 2P_S P_{LO}\left\{\sin^2(x+\phi) + \cos^2\phi + 2\sin(x+\phi)\cos\phi\right\} \\ +\left(P_S \sin x\right)^2 + 2P_S \sin x\sqrt{2P_S P_{LO}}\left\{\sin(x+\phi) + \cos\phi\right\} \end{array}\right] \\ +\left(n_2 * h_1\right)^2 + 2\left(n_2 * h_1\right)A\left[P_S \sin x + \sqrt{2P_S P_{LO}}\left\{\sin(x+\phi) + \cos\phi\right\}\right] \qquad \text{(B.8)}$$

From the multiplication of $\cos(x+\phi)$ and $\sin\phi$ terms, the original signal can be recovered. Many other noise terms, however, are produced by the same operation. By adding two branches, the strongest noise terms with the same dependency on *Ps* as the signal are either canceled or converted into DC current. The remaining terms can be separated into 5 terms:

$$y = (w_1 + w_2 - DC) * h_2 = Signal + 2ndHD + Direct{:}phase + White{:}phase + White{:}white \qquad \text{(B.9)}$$

where

$$Signal = 4P_S P_{LO} A^2 \sin x \qquad \text{(B.10)}$$

$$2ndHD = A^2 P_S^2 \cos 2x \qquad \text{(B.11)}$$

$$Direct{:}phase = \left(4A^2 P_S \sqrt{2P_S P_{LO}} \sin x \cos\phi\right) * h_2 \qquad \text{(B.12)}$$

$$\begin{aligned} Signal{:}white = {} & 2(n_1 * h_1)A\left[P_S \sin x + \sqrt{2P_S P_{LO}}\left\{\cos(x+\phi) - \sin\phi\right\}\right] * h_2 \\ & +2(n_2 * h_1)A\left[P_S \sin x + \sqrt{2P_S P_{LO}}\left\{\sin(x+\phi) + \cos\phi\right\}\right] * h_2 \end{aligned} \tag{B.13}$$

$$White{:}white = (n_1 * h_1)^2 * h_2 + (n_2 * h_1)^2 * h_2 \tag{B.14}$$

The white:phase cross term can be simplified considering that signal $P_S \sin x$ is relatively small compared to the phase noise term $\sqrt{2P_S P_{LO}}\left\{\cos(x+\phi) - \sin\phi\right\}$.

$$White{:}phase \cong 4(n_1 * h_1)A\sqrt{P_S P_{LO}} \sin\varphi * h_2 + (similar,\ independent\ term) \tag{B.15}$$

Assume $x = m\sin\omega_m t$ and $\sin x \equiv m\sin\omega_m t$. Evaluating the power of each term, we obtain the expressions below.

$$P_{signal} = 8A^4 P_S^2 P_{LO}^2 m^2 \tag{B.16}$$

$$P_{2ndHD} = \frac{1}{2}A^4 P_S^4 m^4 \tag{B.17}$$

To evaluate $P_{direct:phase}$, first evaluate the auto-correlation function.

$$R_1(\tau) = 8A^4 P_S^3 P_{LO} m^2 \cos(\omega_m t) e^{-\pi\Delta\nu|\tau|} \tag{B.18}$$

Using this function, we get

$$\begin{aligned} P_{direct:phase} &= \int_{-B_2}^{B_2} S_1(f)df = \int_{-B_2}^{B_2} FT\left[R_1(\tau)\right]df \\ &= \frac{8}{\pi}A^4 P_S^3 P_{LO} m^2 \int_{-\infty}^{\infty} \sin(2\pi B_2\tau)\cos(\omega_m\tau)e^{-\pi\Delta\nu|\tau|}\frac{1}{\tau}d\tau \\ &= \frac{8}{\pi}A^4 P_S^3 P_{LO} m^2 \left\{\tan^{-1}\left[\frac{4\Delta\nu B_2}{\Delta\nu^2 - B_2^2 + f_m^2}\right] + \pi\right\} \\ &= 8A^4 P_S^3 P_{LO} m^2 (1 - \Gamma_1) \end{aligned} \tag{B.19}$$

where

$$\Gamma_1 \equiv \begin{cases} \frac{1}{\pi}\tan^{-1}\frac{4\Delta\nu B_2}{4B_2^2-\Delta\nu^2} & , \quad if\ \Delta\nu < 2B_2 \\ 1-\frac{1}{\pi}\tan^{-1}\frac{4\Delta\nu B_2}{\Delta\nu^2-4B_2^2} & , \quad if\ \Delta\nu > 2B_2 \end{cases} \tag{B.20}$$

Similarly, for $P_{white:phase}$,

$$R_2(\tau) = 8A^2P_SP_{LO}\eta B_1 \sin c(2B_1\tau)e^{-\pi\Delta\nu|\tau|} \tag{B.21}$$

$$\begin{aligned} P_{white:phase} &= 2\int_{-B_2}^{B_2} FT[R_2(\tau)]df \\ &= \frac{8}{\pi^2}A^2P_SP_{LO}\eta\int_{-\infty}^{\infty}\sin(2\pi B_1\tau)\sin(2\pi B_2\tau)e^{-\pi\Delta\nu|\tau|}\frac{1}{\tau^2}d\tau \\ &= \frac{8}{\pi^2}A^2P_SP_{LO}\eta\left[\begin{array}{l} 2\pi B_1\tan^{-1}\left[\frac{4\Delta\nu B_2}{\Delta\nu^2+4B_1^2-4B_2^2}\right]+2\pi B_2\left\{\tan^{-1}\left[\frac{4\Delta\nu B_1}{\Delta\nu^2+4B_2^2-4B_1^2}\right]+\pi\right\} \\ +\frac{\pi\Delta\nu}{2}\ln\left\{\frac{\Delta\nu^2+4(B_1-B_2)^2}{\Delta\nu^2+4(B_1+B_2)^2}\right\} \end{array}\right] \\ &\equiv 16A^2P_SP_{LO}\eta B_2(1-\Gamma_2) \end{aligned} \tag{B.22}$$

where

$$\Gamma_2 \equiv \frac{\Delta\nu}{2\pi B_2}\ln\frac{B_1+B_2}{B_1-B_2} \tag{B.23}$$

$$P_{white:white} = 2\eta^2B_2(4B_1-B_2) \tag{B.24}$$

Finally, we obtain the signal to noise ratio as

$$\begin{aligned} SNR &= \frac{P_{signal}}{P_{2ndHD}+P_{direct-phase}+P_{white-phase}+P_{white-white}} \\ &= \frac{8A^4P_S^2P_{LO}^2m^2}{\frac{1}{2}A^4P_S^4m^4+8A^4P_S^3P_{LO}m^2(1-\Gamma_1)+16A^2P_SP_{LO}B_2\eta(1-\Gamma_2)+2\eta^2B_2(4B_1-B_2)} \end{aligned} \tag{B.25}$$

The fundamental limit of the dynamic range becomes

$$FLDR = \frac{8A^4P_s^2P_{LO}^2}{\frac{1}{2}A^4P_s^4 + 8A^4P_s^3P_{LO}(1-\Gamma_1) + 16A^2P_sP_{LO}B_2\eta(1-\Gamma_2) + 2\eta^2B_2(4B_1 - B_2)} \tag{B.26}$$

B.2 K-port Optical Hybrid Homodyne WIRNA System

The optical signal and the local oscillator light are combined through K-port optical hybrid. The output electric field from the k-th port of the optical hybrid can be written as:

$$E_k = \sqrt{L}\left(E_S + E_{LO}e^{j\frac{2\pi}{N}k}\right) \tag{B.27}$$

The output current of the k-th photodetector is

$$i_k = |E_k|^2 R = RL\left[P_S + P_{LO} + P_S\sin x + \sqrt{2P_SP_{LO}}\left\{\cos\left(x - \phi - \frac{2\pi}{K}k\right) + \sin\left(\phi + \frac{2\pi}{K}k\right)\right\}\right] + n_k \tag{B.28}$$

After squaring, each signal becomes

$$w_k = \left[(i_1 - DC) * h_1\right]^2 = A^2\left[\begin{array}{l} 2P_SP_{LO}\left\{\begin{array}{l}\cos^2\left(x - \phi - \frac{2\pi}{K}k\right) + \sin^2\left(\phi + \frac{2\pi}{K}k\right) \\ +2\cos\left(x - \phi - \frac{2\pi}{K}k\right)\sin\left(\phi + \frac{2\pi}{K}k\right)\end{array}\right\} + (P_S\sin x)^2 \\ +2P_S\sin x\sqrt{2P_SP_{LO}}\left\{\cos\left(x - \phi - \frac{2\pi}{K}k\right) + \sin\left(\phi + \frac{2\pi}{K}k\right)\right\}\end{array}\right]$$
$$+(n_k * h_1)^2 + 2(n_k * h_1)A\left[P_S\sin x + \sqrt{2P_SP_{LO}}\left\{\cos\left(x - \phi - \frac{2\pi}{K}k\right) + \sin\left(\phi + \frac{2\pi}{K}k\right)\right\}\right] \tag{B.29}$$

Taking the sum of all signals leads to an expression similar to Eq. (B.9):

$$y = \sum_{k=1}^{N} (w_k - DC) * h_2 = Signal + 2ndHD + Direct:phase + White:phase + White:white \tag{B.30}$$

where

$$Signal = 2NP_S P_{LO} A^2 \sin x \tag{B.31}$$

$$2ndHD = \frac{K}{2} A^2 P_S^2 \cos 2x \tag{B.32}$$

Because of the symmetry introduced by the K-port optical hybrid, *Direct:phase* cross terms are canceled.

$$Direct:phase = A^2 2P_S \sin x \sqrt{2P_S P_{LO}} \sum \left\{ \cos\left(x - \phi - \frac{2\pi}{K} k \right) + \sin\left(\phi + \frac{2\pi}{K} k \right) \right\} = 0 \tag{B.33}$$

$$Signal:white = \sum 2(n_k * h_1) A \left[P_S \sin x + \sqrt{2P_S P_{LO}} \left\{ \cos\left(x - \phi - \frac{2\pi}{N} k \right) + \sin\left(\phi + \frac{2\pi}{N} k \right) \right\} \right] * h_2 \tag{B.34}$$

$$White:white = \sum (n_k * h_1)^2 * h_2 \tag{B.35}$$

Similarly, the *White:phase* term is simplified to

$$White:phase \equiv \sum 4(n_k * h_1) A \sqrt{P_S P_{LO}} \sin \varphi * h_2 \tag{B.36}$$

The power of each term is evaluated as:

$$P_{signal} = 2K^2 A^4 P_S^2 P_{LO}^2 m^2 \tag{B.37}$$

$$P_{2ndHD} = \frac{K^2}{8} A^4 P_S^4 m^4 \tag{B.38}$$

$$P_{white:white} = K\eta^2 B_2 (4B_1 - B_2) \tag{B.39}$$

$$P_{white:phase} = N\int_{-B_2}^{B_2} FT[R_2(\tau)]df$$

$$= \frac{4N}{\pi^2}A^2P_SP_{LO}\eta\left[\begin{array}{l} 2\pi B_1\tan^{-1}\left[\frac{4\Delta\nu B_2}{\Delta\nu^2+4B_1^2-4B_2^2}\right]+2\pi B_2\left\{\tan^{-1}\left[\frac{4\Delta\nu B_1}{\Delta\nu^2+4B_2^2-4B_1^2}\right]+\pi\right\} \\ +\frac{\pi\Delta\nu}{2}\ln\left\{\frac{\Delta\nu^2+4(B_1-B_2)^2}{\Delta\nu^2+4(B_1+B_2)^2}\right\}\end{array}\right]$$

$$\equiv 8NA^2P_SP_{LO}\eta B_2(1-\Gamma_2) \tag{B.40}$$

The FLDR becomes

$$FLDR = \frac{P_{signal}}{P_{2ndHD}+P_{white-phase}+P_{white-white}}$$

$$= \frac{2N^2A^4P_s^2P_{LO}^2}{\frac{N^2}{8}A^4P_s^4+8NA^2P_sP_{LO}B_2\eta(1-\Gamma_2)+N\eta^2B_2(4B_1-B_2)} \tag{B.41}$$

B.3 2K-port Optical Hybrid Homodyne WIRNA System

We treat k-th output and (k+K)th output as a pair and make balanced receiver to cancel direct detection term before the squaring operation. The electric fields are

$$E_k = \sqrt{L}\left(E_S + E_{LO}e^{j\frac{2\pi}{2K}k}\right) \tag{B.42}$$

$$E_{k+K} = \sqrt{L}\left(E_S + E_{LO}e^{j\frac{2\pi}{2N}(k+K)}\right) \tag{B.43}$$

The photodetector output currents are

$$i_k = |E_k|^2R = RL\left[P_S+P_{LO}+P_S\sin x+\sqrt{2P_SP_{LO}}\left\{\cos\left(x-\phi-\frac{\pi}{K}k\right)+\sin\left(\phi+\frac{\pi}{K}k\right)\right\}\right]+n_k \tag{B.44}$$

$$i_{k+K} = |E_{k+K}|^2 R = RL\left[P_S + P_{LO} + P_S \sin x - \sqrt{2P_S P_{LO}}\left\{\cos\left(x - \phi - \frac{\pi}{K}k\right) + \sin\left(\phi + \frac{\pi}{K}k\right)\right\}\right] + n_{k+K} \tag{B.45}$$

The actual output from the balanced receiver is

$$I_k \equiv i_k - i_{k+K} = 2A\sqrt{2P_S P_{LO}}\left\{\cos\left(x - \phi - \frac{\pi}{K}k\right) + \sin\left(\phi + \frac{\pi}{K}k\right)\right\} + n'_k \tag{B.46}$$

where $n'_k \equiv n_k - n_{k+K}$ with power spectral density of $\eta_3 = \eta_{sh} + 4qRL(P_s + P_{LO})$. This expression shows that inessential terms are canceled and there is no 2nd harmonic noise nor *direct:phase* noise term. The output of the square-law detector becomes

$$\begin{aligned} w_k &= [I_k * h_1]^2 \\ &= 8A^2 P_S P_{LO}\left\{\cos^2\left(x - \phi - \frac{\pi}{K}k\right) + \sin^2\left(\phi + \frac{\pi}{K}k\right) + 2\cos\left(x - \phi - \frac{\pi}{K}k\right)\sin\left(\phi + \frac{\pi}{K}k\right)\right\} \\ &\quad + (n'_k * h_1)^2 + 4(n'_k * h_1)A\sqrt{2P_S P_{LO}}\left\{\cos\left(x - \phi - \frac{\pi}{K}k\right) + \sin\left(\phi + \frac{\pi}{K}k\right)\right\} \end{aligned} \tag{B.47}$$

By adding all signals, we obtain

$$y = \sum_{k=1}^{K}(w_k - DC) * h_2 = Signal + White{:}phase + White{:}white \tag{B.48}$$

where

$$Signal = 8KA^2 P_S P_{LO} A^2 \sin x \tag{B.49}$$

$$\begin{aligned} Signal{:}white &= \sum 4(n'_k * h_1)A\sqrt{2P_S P_{LO}}\left\{\cos\left(x - \phi - \frac{\pi}{K}k\right) + \sin\left(\phi + \frac{\pi}{K}k\right)\right\} * h_2 \\ &\equiv \sum 8(n'_k * h_1)A\sqrt{P_S P_{LO}} \sin\phi * h_2 \end{aligned} \tag{B.50}$$

$$White{:}white = \sum (n'_k * h_1)^2 * h_2 \tag{B.51}$$

Evaluating the power of each term, we get

$$P_{signal} = 8(2K)^2 A^4 P_S^2 P_{LO}^2 m^2 \tag{B.52}$$

$$P_{white:white} = \frac{2K}{2}\eta_3^2 B_2(4B_1 - B_2) \tag{B.53}$$

$$P_{white:phase} \cong 16(2K)A^2 P_S P_{LO}\eta_3 B_2(1-\Gamma_2) \tag{B.54}$$

There is no noise term dependent on the modulation index. As the result we achieve an FLDR of

$$\begin{aligned} FLDR &= \frac{P_{signal}}{P_{white-phase} + P_{white-white}} \\ &= \frac{8(2K)^2 A^4 P_s^2 P_{LO}^2}{16(2K)A^2 P_s P_{LO} B_2 \eta_3(1-\Gamma_2) + \frac{2K}{2}\eta_3^2 B_2(4B_1 - B_2)} \end{aligned} \tag{B.55}$$

Table B-1. Definition of the Variables

E_S , E_{LO}	Phasor of the optical signal and local oscillator
E_1, E_2	Output phasor of the optical hybrid port 1 and port 2
w_S, w_{LO}	Optical signal and local oscillator frequency
j_S, j_{LO}	Phase noise of the optical signal and local oscillator
$f(t)$	Combined linewidth of the signal and the local oscillator lasers
m	Modulation index to the external modulator
$x(t)$	Normalized RF input signal to the modulator
P_S	Received optical power
P_{LO}	Local oscillator optical power
L	Total loss of the optical hybrid from an input port to an output port
A	=RL; coefficient of the signal amplitude
B_1	Bandwidth of the lowpass filter (first stage: wide bandwidth)
B_2	Bandwidth of the lowpass filter (last stage: narrow bandwidth)

Appendix C

Derivation of Angle Modulated Link Equations

In this appendix, the link equations relating to the angle-modulated links discussed in Chapters 8 and 9 are derived. These include, among others, derivations of SNR and SFDR. Section C.1 contains derivations for Chapter 8, which covers both directly and externally modulated coherent PM and FM links. Section C.2 contains derivations for Section 9.5, which covers the heterodyne interferometric links (HIPM and HIFM). Section C.3 contains derivations for Section 9.6, which covers the homodyne interferometric phase modulated (HPM) link. Section C.4 contains references.

C.1 Coherent PM and FM Links

In this section, the derivations for the coherent PM and FM links are provided. Section C.1.1 contains the parallel derivations of SFDR. Section C.1.2 contains the parallel derivations of RF power transfer ratio and noise figure. Section C.1.3 contains derivations relating to the maximum available modulation depth for externally modulated FM links.

C.1.1 SFDR of Coherent PM and FM Links

The incident optical signal field at each photodetector for the PM and FM links is given by

$$e_{PM}(t) = \sqrt{\frac{P_s}{2}\left[1 + n_{RS}(t)\right]}\exp i\left[\omega_S t + \varphi_\Delta x(t) + \varphi_{nS}(t)\right] \tag{C.1}$$

$$e_{FM}(t) = \sqrt{\frac{P_s}{2}\left[1 + n_{RS}(t)\right]}\exp i\left[\omega_S t + \omega_\Delta \int x(t)dt + \varphi_{nS}(t)\right] \tag{C.2}$$

where P_S is the total received signal optical power at each receiver, $n_{RS}(t)$ is the relative intensity noise (RIN) of the signal laser, ω_S and $\varphi_{nS}(t)$ are the optical frequency and

phase noise of the signal laser, respectively, $x(t)$ is the normalized applied signal, φ_Δ is the phase deviation, and ω_Δ is the frequency deviation. We assume that the laser is perfectly linear and that its FM response is uniform in the case of direct FM, and that the integrator is perfectly linear in the externally modulated cases.

The local oscillator field at each photodetector for the coherent links is given by

$$e_{LO}(t) = \sqrt{\frac{P_{LO}}{2}\left[1 + n_{RLO}(t)\right]}\exp i\left[\omega_{LO}t + \varphi_{nLO}(t)\right] \tag{C.3}$$

where P_{LO} is the total received local oscillator power at the photodetector, $n_{RLO}(t)$ is the relative intensity noise (RIN) of the LO laser, and ω_{LO} and $\varphi_{nLO}(t)$ are the optical frequency and phase noise of the LO laser, respectively.

Neglecting DC terms, the detected currents (indicated by the subscript '1') in the PM and FM links are given by

$$\begin{aligned} i_{PM1}(t) = \left[h_1(t) + h_2(t)\right] * \Big\{ & R\sqrt{P_S P_{LO}\left[1 + n_{RS}(t)\right]\left[1 + n_{RLO}(t)\right]} \\ & \times \cos\left[\omega_{IF}t + \varphi_\Delta x(t) + \varphi_{nS}(t) - \varphi_{nLO}(t)\right] + n_{sh}(t)\Big\} + n_{th}(t) \\ & + \left[h_1(t) - h_2(t)\right] * \frac{1}{2} R\left[P_S n_{RS}(t) + P_{LO} n_{RLO}(t)\right] \end{aligned} \tag{C.4}$$

$$\begin{aligned} i_{FM1}(t) = \left[h_1(t) + h_2(t)\right] * \Big\{ & R\sqrt{P_S P_{LO}\left[1 + n_{RS}(t)\right]\left[1 + n_{RLO}(t)\right]} \\ & \times \cos\left[\omega_{IF}t + \omega_\Delta \int x(t)dt + \varphi_{nS}(t) - \varphi_{nLO}(t)\right] + n_{sh}(t)\Big\} + n_{th}(t) \\ & + \left[h_1(t) - h_2(t)\right] * \frac{1}{2} R\left[P_S n_{Rs}(t) + P_{LO} n_{RLO}(t)\right] \end{aligned} \tag{C.5}$$

where R is the responsivity of the photodetectors, $h_1(t)$ and $h_2(t)$ are the impulse responses of the two photodetectors, and $n_{sh}(t)$ and $n_{sh}(t)$ are due to shot and thermal noise, respectively. The shot noise is defined per photodetector in each system (see Appendix A.2.2). Since the thermal noise is added after detection, it is not affected by the impulse responses of the detectors. Ideally, the impulse responses of the photodetectors in a balanced receiver are perfectly matched; in practice, they are somewhat different. We will assume that the transfer functions of the photodetectors are approximately flat over the received signal bandwidth, and that they differ by a small

factor. Under this assumption, we can write $[h_1(t)+h_2(t)]*A(t)\equiv 2A(t)$ and $\Delta h(t)\equiv h_1(t)-h_2(t)$.

Now we derive expressions for the output currents of the links. We neglect high-order noise terms and products between the noise and the modulated signal (which does not include the IF carrier component) since analog links have high SNRs and small modulation depths. The PM signal is recovered by a chain consisting of a limiter, phase discriminator, and envelope detector.

After the limiter, the RIN terms multiplying the cosine term are eliminated and the quadrature components of the amplitude noise terms become part of the cosine argument,

$$i_{PM2}(t)=2R\sqrt{P_S P_{LO}}\cos\left[\omega_{IF}t+\varphi_\Delta x(t)+\varphi_{n\,tot}(t)\right] \tag{C.6}$$

where the total noise in the phase of the signal is given by

$$\varphi_{n\,tot}(t)=\varphi_{nS}(t)-\varphi_{nLO}(t)+\frac{1}{2R\sqrt{P_S P_{LO}}}\left(RP_S n_{RSq}(t)+RP_{LO}n_{RLOq}(t)+n_{Dq}(t)\right) \tag{C.7}$$

The delay-line filter has a transfer function given by

$$H(f)=\cos\left(\frac{\pi}{2}\frac{f}{f_{IF}}\right) \tag{C.8}$$

where we have chosen the filter delay $t = 1/2f_{IF}$. For a signal centered at f_{IF}, we can expand the transfer function as

$$H(f)\equiv -\frac{\pi}{2f_{IF}}(f-f_{IF})+\frac{1}{6}\left[\frac{\pi}{2f_{IF}}(f-f_{IF})\right]^3 \tag{C.9}$$

Using the Fourier derivative theorem to relate the input current to the discriminator to the output current, we obtain [1]:

$$i_{PM\,3}(t) = KR\sqrt{P_S P_{LO}}\left\{-\frac{1}{4f_{IF}}\left[\varphi_\Delta \dot{x}(t) + \dot{\varphi}_{n\,tot}(t)\right] + \frac{1}{6}\left(\frac{1}{4f_{IF}}\right)^3\left[\varphi_\Delta \dddot{x}(t) - i3\varphi_\Delta^2 \dot{x}(t)\ddot{x}(t) - \varphi_\Delta^3 \dot{x}^3(t)\right]\right\}$$
$$\times\cos\left[2\pi f_{IF} t + \varphi_\Delta x(t) + \varphi_{n\,tot}(t) + \varphi_o\right] \tag{C.10}$$

In Eq. (C.10), we have neglected higher order noise and signal cross noise terms (which are small compared to the first-order signal and noise terms). After the envelope detector and the integrator, we have

$$i_{PM\,out}(t) = KR\sqrt{P_S P_{LO}}\left\{-\frac{1}{4f_{IF}}\left[\varphi_\Delta x(t) + \varphi_{n\,tot}(t)\right] + \frac{1}{6}\left(\frac{1}{4f_{IF}}\right)^3\left[\varphi_\Delta \ddot{x}(t) - i\frac{3}{2}\varphi_\Delta^2 \dot{x}^2(t) - \varphi_\Delta^3 \int \dot{x}^3(t)dt\right]\right\} \tag{C.11}$$

It can be shown that, for a sub-octave signal band, the only significant intermodulation terms falling within the signal band are those coming from the term proportional to $\varphi_\Delta{}^3$, and we thus arrive at Eq. (C.11).

The only difference between the FM and PM receivers is the absence of an integrator after the envelope detector in the FM case. This results in

$$i_{FM\,out}(t) = TR\sqrt{P_S P_{LO}}\left\{-\frac{1}{4f_{IF}}\left[\omega_\Delta x(t) + \dot{\varphi}_{n\,tot}(t)\right] + \frac{1}{6}\left(\frac{1}{4f_{IF}}\right)^3\left[\omega_\Delta \ddot{x}(t) - i3\omega_\Delta^2 x(t)\dot{x}(t) - \omega_\Delta^3 x^3(t)\right]\right\} \tag{C.12}$$

It can be shown that, for a sub-octave signal band, the only significant intermodulation terms falling within the signal band are those coming from the term proportional to $\omega_\Delta{}^3$, and we thus arrive at Eq. (C.12).

The corresponding signal-to-noise ratios (SNRs) for the PM and FM links are given by

$$SNR_{PM} = \varphi_\Delta^2 \frac{4R^2 P_S P_{LO}\left\langle x^2(t)\right\rangle}{4R^2 P_S P_{LO}\left\langle\left(\varphi_{nS} - \varphi_{nLO}\right)^2\right\rangle + \frac{1}{4}b\left(RP_S\right)^2\left\langle n_{RS\,bp}^2\right\rangle + \frac{1}{4}b\left(RP_{LO}\right)^2\left\langle n_{RLO\,bp}^2\right\rangle + \left\langle n_{D\,bp}^2\right\rangle}$$
$$= \varphi_\Delta^2 SNR_{PMo} \tag{C.13}$$

$$SNR_{FM} = \left(\frac{\omega_\Delta}{B}\right)^2 \frac{4B^2R^2P_SP_{LO}\langle x^2(t)\rangle}{4R^2P_SP_{LO}\left\langle(\dot{\varphi}_{ns}-\dot{\varphi}_{nLO})^2\right\rangle+\frac{1}{4}b(RP_S)^2\langle \dot{n}^2_{RS\,bp}\rangle+\frac{1}{4}b(RP_{LO})^2\langle \dot{n}^2_{RLO\,bp}\rangle+\langle \dot{n}^2_{D\,bp}\rangle}$$

$$= \left(\frac{\omega_\Delta}{B}\right)^2 SNR_{FMo} \tag{C.14}$$

where B is the bandwidth of the baseband signal $x(t)$ and b is the photodetector matching factor, which is defined in Appendix C. The normalized SNRs SNR_{PMo}, and SNR_{FMo} are the SNRs for each of the links for a unity modulation index; note that the modulation indices may exceed unity. The various noise expressions in Eqs. (C.13) and (C.14) are evaluated in Appendix A.2.

Eqs. (C.13) and (C.14) indicate that the SNR increases monotonically with the modulation index. The maximum useful modulation index is limited by intermodulation distortion associated with nonlinear effects. In the next section, we derive expressions for the maximum useful modulation index and the associated spurious-free dynamic range.

As presented in Section 8.2.3, the SFDR of the links can be expressed by

$$SFDR = \left[\frac{8SNR_o}{3|b_3|}\right]^{2/3} \tag{C.15}$$

where SNR_o is defined in Eqs. (C.13) and (C.14) and $|b_3|$, the third-order nonlinearity coefficient, is $\frac{1}{6}\left(\frac{\pi f_{max}}{2f_{IF}}\right)^2$ for the coherent PM link and $\frac{1}{6}\left(\frac{B}{4f_{IF}}\right)^2$ for the coherent FM links.

C.1.2 RF Power Transfer Ratio and Noise Figure

*C.1.2.1. Definition of RF Power Transfer Ratio and Noise Figure**

The **RF power transfer ratio,** or RF power gain G, of the link is defined as the ratio of the RF power at the link output to the power delivered to the link RF input by the source:

* Much of this section appeared in section 1.2.1. of the progress report for the period 12/1/92 - 3/1/93. There are, however, small but important changes in the text.

$$G = \frac{S_o}{S_i} \tag{C.16}$$

It is easily obtained by measuring the input and output signal power levels and finding their ratio according to the above equation.

In general, RF amplifiers can be added before and after the optical link as shown in Fig. C-1.

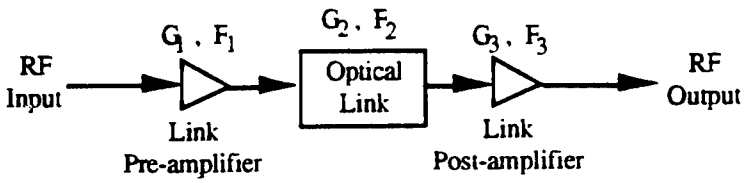

Fig. C-1. Optical link with a pre-amplifier and a post-amplifier.

The overall gain G of this amplifier- optical link - amplifier system is given by:

$$G = G_{in} G_{opt} G_{out} \tag{C.17}$$

where G_{opt} is the optical link gain, and G_{in} and G_{out} are the gains due to preamplification and postamplification, respectively. G_{opt} is determined by the electrical to optical and optical to electrical conversion efficiencies of optical components and the conversion losses of microwave components in the link.

G_{opt} for the externally modulated direct detection link is given by:

$$G_{opt.DD} = \left(\frac{\pi}{2V_\pi}\right)^2 (rP_S)^2 R_S^2 \tag{C.18}$$

where R_S is the source impedance, r is the photodetector responsivity, P_S is the received optical power, P_{LO} is the local oscillator power, and V_π is the voltage required to generate a modulator phase shift of π. The value of $G_{opt.DD}$ is dependent on the choice of modulator operating point; in this case the operating point is chosen at the half-power point of the sinusoidal modulator characteristic.

Noise figure measures the degradation in the signal-to-noise ratio (SNR) between the input and output of a link and is defined as:

$$F = \frac{\frac{S_i}{N_i}}{\frac{S_o}{N_o}} = \frac{N_o}{GN_i} \tag{C.19}$$

where S_i and N_i are the input signal and noise powers, and S_o and N_o are the output signal and noise powers. By definition, the input noise power is the noise power from a matched resistor, $N_i = kTB$, where k is Boltzmann's constant, T is the resistor temperature, and B is the signal bandwidth [2]. The output noise power can be expressed by:

$$N_O = GN_i + \eta B \tag{C.20}$$

where hB is the additive noise introduced in the device or link. Substituting $N_i = kTB$, we can express the noise figure as:

$$F = 1 + \frac{\eta}{GkT} \tag{C.21}$$

For the direct detection optical link, the noise figure is

$$F_{DD} = 1 + \frac{\eta_{DD}}{G_{DD}kT} \tag{C.22}$$

where

$$\eta_{DD} = R_S\left[\frac{r^2P_S^2}{4}10^{\frac{RIN}{10}} + 2qrP_S + \frac{4kT}{R_S}\right] \tag{C.23}$$

The total noise figure for the system shown in Fig. C-1 can be determined using the following expression:

$$F = F_{in} + \frac{F_{opt} - 1}{G_{in}} + \frac{F_{out} - 1}{G_{in}G_{opt}} \tag{C.24}$$

For the case of optical links $G_{in}G_{opt} << 1$ so that

$$F \approx \frac{F_{out} - 1}{G_{in} G_{opt}} \tag{C.25}$$

Expressing the terms in dB,

$$F \approx F'_{out} - G_{in} - G_{opt} = F'_{out} - G + G_{out}, \qquad \text{(dB)} \tag{C.26}$$

This means that the noise figure can be minimized (a) using a high gain pre-amplifier G_{in} and (b) increasing the optical power (corresponds to increasing G_{opt}). The sum of the noise figure and RF transfer ratio for the optical link is constant:

$$F + G \approx F'_{out} + G_{out} = \text{constant} \tag{C.27}$$

Therefore, it is possible to construct a system having both desirable features of high gain and low noise figure.

C.1.2.2. RF Power Transfer Ratios of Angle-Modulated Links

A detailed derivation of the RF power gain for an externally modulated coherent FM link is given in this section. The derivations for the directly modulated coherent FM link and the externally modulated coherent PM link are very similar and are not explicitly given, but points of interest are described. The RF power gains which we present in this section correspond to the gain G_{opt} of the optical link section in Fig. C-1 and do not include the impact of pre/post-amplification. G_{opt}, therefore, represents a measure of the losses from imperfect electrical to optical and optical to electrical conversion efficiencies of optical components and the conversion losses of microwave components in the link.

A block diagram of an externally modulated coherent FM link is shown in Fig. C-2. The input voltage is of the form $V(t) = Vx(t)$, where V is the signal amplitude and $x(t)$ is a dimensionless time-varying signal. The integrator, for simplicity, is assumed to be an RC lowpass filter with a voltage transfer characteristic

$$\frac{V_{out}(\omega)}{V_{in}(\omega)} = \frac{1}{1 + j\omega RC} \tag{C.28}$$

This filter, which can be built in microstrip or with lumped elements, serves as a good integrator for signals composed of frequencies far from baseband, such that $\omega RC >> 1$. It

is for frequencies in this range, therefore, that it is reasonable to expect that receiver nonlinearities will have the dominant effect on link SFDR. If $V_{in}(t) = V(t)$, then

$$V_{out}(t) = \frac{V}{RC}\int_{-\infty}^{t} x(t')dt' \tag{C.29}$$

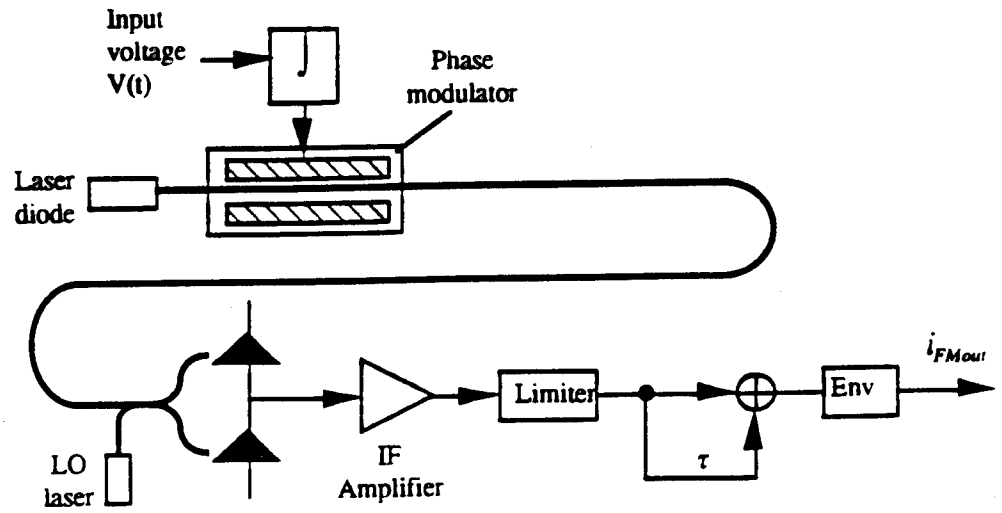

Fig. C-2. Externally modulated coherent FM link.

Assuming that a π phase shift is obtained from the modulator with a drive voltage V_π, the modulator output is

$$\sqrt{P_T}\exp\left[j\left(\omega_{opt}t + \frac{\pi V}{V_\pi RC}\int_{-\infty}^{t} x(t')dt' + \varphi_{nS}(t)\right)\right] \tag{C.30}$$

where P_T is the optical power at the modulator output. Assuming that the photodetectors are well-matched, the output current is*

$$i_{FM\,out}(t) \equiv \frac{1}{4f_{IF}}\left\{2r\sqrt{P_S P_{LO}}\left[\omega_\Delta x(t) - \frac{\omega_\Delta^3}{6}\left(\frac{1}{4f_{IF}}\right)^2 x^3(t)\right] + 2r\sqrt{P_S P_{LO}}\left[\dot{\varphi}_{nS}(t) - \dot{\varphi}_{nLO}(t)\right] + \dot{n}_{D\,bp}(t)\right\} \tag{C.31}$$

* This expression is from the derivation presented in Section 2.1.1 of the progress report for the period 3/193 - 6/1/93.

where P_S is the received optical power, $\varphi_{nS}(t)$ is the phase noise of the signal laser, f_{IF} is the receiver intermediate frequency, and w_D is the angular frequency deviation. In this case, $\omega_\Delta = \frac{\pi V}{V_\pi RC}$. P_{LO} is the total received local oscillator power at the photodetector and $j_{nLO}(t)$ is the phase noise of the LO laser. $n_{D\,bp}(t)$ is the receiver output noise process.

Assuming that the link input and output are impedance-matched with resistance R_S and that the input signal $x(t) = \cos\omega t$, the output RF power S_o is easily found to be

$$S_o = \left(\frac{1}{4f_{IF}}\right)^2 2r^2 P_S P_{LO} \left(\frac{\pi V}{V_\pi RC}\right)^2 R_S L_{nl} \tag{C.32}$$

L_{nl} is the loss of RF signal power due to the generation of nonlinearities in the limiter and the envelope detector. The input RF power $S_i = \frac{V^2}{2R_S}$. The RF power transfer ratio is

$$G_{opt\,(ext.\,FM)} = \frac{S_o}{S_i} = \left(\frac{1}{4f_{IF}}\right)^2 4r^2 P_S P_{LO} \left(\frac{\pi}{V_\pi RC}\right)^2 R_S^2 L_{nl} \tag{C.33}$$

The RF power transfer ratios for the other links were derived in a similar manner. For the externally modulated coherent PM link, the RF gain is

$$G_{opt\,(ext.\,PM)} = \left(\frac{1}{4f_{IF}}\right)^2 4r^2 P_S P_{LO} \left(\frac{\pi}{V_\pi RC}\right)^2 R_S^2 L_{nl} \tag{C.34}$$

which is identical to that of the externally modulated coherent FM link.

For the directly modulated coherent FM link, the RF gain is

$$G_{opt\,(dir.\,FM)} = \left(\frac{500\pi\gamma}{f_{IF}}\right)^2 4r^2 P_S P_{LO} L_{nl} \tag{C.35}$$

where γ is the FM response of the transmitter laser diode in GHz/mA and $\frac{V\gamma}{R_S}$ is the frequency deviation. Compared to the frequency deviation $\frac{V}{2V_\pi RC}$ of the externally modulated coherent FM link, it is clear that the required value of the applied voltage V for

a given frequency deviation will depend on the respective values of the transmitter laser FM response and the RC time constant of the integrator.

C.1.2.3. Noise Figures of Angle Modulated Links

In angle-modulated links, the noise at the link output is not always of the form ηB in Eq. (C.20) due to the nonlinear discrimination process. However, the derivation of noise figure is still fairly straightforward using the formula

$$F_{(link)} = 1 + \frac{noise\ power\ at\ link\ output}{G_{(link)} kTB} \tag{C.36}$$

We give below the output noise powers for the coherent PM and FM links. The noise figure is then obtained directly from Eq. (C.36).

The noise power at the output of the externally modulated coherent FM link is

$$\eta_{(ext.\,FM)} = R_S \left(\frac{1}{4f_{IF}}\right)^2 \left[4r^2 P_S P_{LO}[4\pi \Delta\upsilon B] + \frac{(2\pi)^2}{3}\left(4qr(P_S + P_{LO}) + \frac{4kT}{R_S}\right)\left(f_{max}^3 - f_{min}^3\right)\right] \tag{C.37}$$

where $\Delta\upsilon$ is the laser linewidth, B is the signal bandwidth, q is the electron charge, and f_{min} and f_{max} are the minimum and maximum frequencies in the signal band, respectively.

The noise power at the output of the directly modulated coherent FM link is

$$\eta_{(dir.\,FM)} = R_S \left(\frac{1}{4f_{IF}}\right)^2 \left[4r^2 P_S P_{LO}[4\pi \Delta\upsilon B] + \frac{(2\pi)^2}{3}\left(4qr(P_S + P_{LO}) + \frac{4kT}{R_S}\right)\left(f_{max}^3 - f_{min}^3\right)\right] \tag{C.38}$$

which is identical to the output noise power for the externally modulated coherent FM link.

The noise power at the output of the externally modulated coherent PM link is

$$\eta_{(ext.\,PM)} = R_S \left(\frac{1}{4f_{IF}RC}\right)^2 \left[4r^2 P_S P_{LO}\left[\frac{\Delta\upsilon}{\pi}\left(\frac{1}{f_{min}} - \frac{1}{f_{max}}\right)\right] + \left(4qr(P_S + P_{LO}) + \frac{4kT}{R_S}\right)B\right] \tag{C.39}$$

C.1.3 Modulation Depth Limitations for External PM and External FM

For the low received powers (< 100 μW) at which coherent links are frequently operated, thermal noise is the dominant noise at the receiver. Since the thermal noise power is independent of the transmitted optical power while the IMD power is clearly dependent on optical power, the optimum modulation depth (corresponding to the SFDR) increases with decreasing optical power. Under these conditions, it is important to know the modulation depth limitations of devices which will be used to generate externally modulated PM and FM signals.

From our experience in our laboratory, phase modulators can normally be comfortably operated for voltages up to 1.5 times V_π. This means that the maximum available modulation depth is about 4.71 (or 1.5 π) for an applied signal normalized to lie between 1 and -1. This modulation depth is not exceeded for any point in the plots of Chapter 8 or Chapter 9.

External frequency modulation requires an integrator followed by an external phase modulator. For an integrator which can be modeled by a single-pole lowpass filter, there will be a significant power loss since the rolloff of the lowpass filter will be inversely proportional to ω for $\omega R_{int} C_{int} >> 1$. It is clear that the FM modulation index $\frac{\omega_\Delta}{\omega_{max}} = \frac{\pi V}{V_\pi \omega_{max} R_{int} C_{int}}$ from the Section C.1.2.2, and hence that to attain the maximum available modulation depth of 4.71, RF amplification must be applied after integration to compensate for the power loss. A sufficiently linear region in the integrator characteristic must be chosen such that link operation is satisfactory, but this may reduce the available modulation depth depending on the available RF amplification. With careful construction, an integrator can be built which will have a highly linear region which is not also high loss.

C.2 Heterodyne Interferometric Links

In this section, the derivations for the HIPM and HIFM links are provided. Section C.2.1 contains the parallel derivations of SFDR for the two links. Section C.2.2 contains the parallel derivations of RF power transfer ratio and noise figure for the two links.

C.2.1 SFDR of HIPM and HIFM Links

To derive the SFDR of the HIPM and HIFM links, it is first necessary to derive expressions for the link SNRs and nonlinearity coefficients. Both of these are easily obtainable from the link output current. After that, the SFDR can be simply obtained from Eq. (C.15).

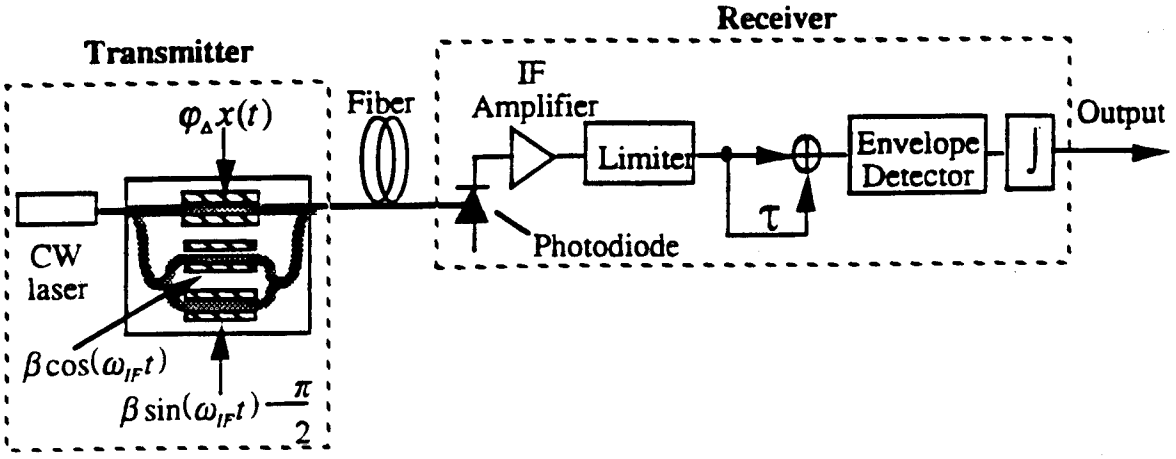

Fig. C-3. Phase-modulated implementation of HIPM link with novel electro-optic modulator.

A diagram of an HIPM link is provided in Fig. C-3 for reference. The optical fields contributed by the three arms of the modulator are given at the detector by

$$e_1(t) = \sqrt{\varepsilon_1 P[1+n_R(t)]}\exp i\left[\omega_o t + \varphi[x(t)] + \varphi_p(t)\right] \tag{C.40}$$

$$e_2(t) = \sqrt{\varepsilon_2 P[1+n_R(t)]}\exp i\left[\omega_o t + \beta_s \sin\omega_{IF} t - \frac{\pi}{2} + \varphi_p(t)\right] \tag{C.41}$$

$$e_3(t) = \sqrt{\varepsilon_3 P[1+n_R(t)]}\exp i\left[\omega_o t + \beta_c \cos\omega_{IF} t + \varphi_p(t)\right] \tag{C.42}$$

where $x(t)$ is the normalized input signal, $\varphi[\ ]$ refers to the type of modulation (either phase or frequency), w_{IF} is the angular intermediate frequency (IF), b_c and b_s are the phase deviations of the IF terms, ε_1, ε_2, and ε_3 are the splitting coefficients within the modulator, P is the laser optical power with link and modulator excess losses assumed compensated by amplification in the link, $n_R(t)$ is the laser RIN, and $j_p(t)$ is the laser phase noise. The delays through the arms of the modulator are assumed to be matched.

The current generated at the photodiode, $i_1(t)$, is given by

$$\begin{aligned} i_1(t) = RP[1+n_R(t)]\{&4\sqrt{\varepsilon_1\varepsilon_2}J_1(\beta_s)\sin[\omega_{IF}t+\varphi[x(t)]] \\ &+4\left(\sqrt{\varepsilon_1\varepsilon_3}J_1(\beta_c)-\sqrt{\varepsilon_1\varepsilon_2}J_1(\beta_s)\right)\sin[\varphi[x(t)]]\cos\omega_{IF}t \\ &+4\sqrt{\varepsilon_2\varepsilon_3}\left([-J_0(\beta_s)J_1(\beta_c)+J_2(\beta_s)J_3(\beta_c)-\ldots]\cos\omega_{IF}t\right. \\ &\left.+[J_0(\beta_c)J_1(\beta_s)+J_2(\beta_c)J_3(\beta_s)-\ldots]\sin\omega_{IF}t\right) \\ &+D.\,C.\ terms+2\omega_{IF}t\ terms+3\omega_{IF}t\ terms+\ldots\}+n_D(t)+An_R(t) \end{aligned} \tag{C.43}$$

where R is the photodetector responsivity, $n_D(t)$ is the contribution from the receiver thermal noise and the shot noise, and A the coefficient of the DC RIN. The phase noise is eliminated due to the equal optical path lengths through the three legs of the modulator. The first term is the desired phase-modulated term at the IF. The second term can be eliminated by choosing $\varepsilon_1 = \varepsilon_2 = \varepsilon_3 = 1/3$ and $\beta_s = \beta_c = \beta$. The third term can be eliminated by choosing $\beta \approx 1.8$. This creates only a 0.35 dB penalty from the maximum value of $J_1(\beta)$, which occurs at $\beta \approx 2.2$. If the maximum signal frequency is much smaller than the IF, the signal bands around w_{IF}, $2w_{IF}$, $3w_{IF}$, ... are well separated and we can filter out all terms not around w_{IF}. The current after the limiter is given by

$$i_2(t) = \frac{4}{9}RPJ_1(\beta)\sin[2\pi f_{IF}t+\varphi[x(t)]+\varphi_n(t)] \tag{C.44}$$

where K is the amplitude of $i_2(t)$. The limiter suppresses all variations in the envelope of the signal, resulting in suppression of the RIN term in the signal amplitude. To avoid threshold effects in the limiter, the carrier-to-noise ratio (CNR) before the limiter must be at least 12 dB [1]. The noise contribution to the phase is given by

$$\varphi_n(t) = \frac{9}{4RPJ_1(\beta)}\left[n_{Dq}(t)+\frac{RP}{3}\left(1+\frac{2}{3}J_0(\beta)\right)n_{Rq}(t)\right] \tag{C.45}$$

where $n_{Dq}(t)$ and $n_{Rq}(t)$ are the quadrature components within the IF band of $n_D(t)$ and $n_R(t)$, respectively. Applying the identical discriminator analysis as in Appendix C.1 gives output currents for PM and FM, respectively, of the form

$$i_{HIPM\ out}(t) = K\left\{-\frac{1}{4f_{IF}}\left[\varphi_\Delta x(t) + \varphi_n(t)\right] + \frac{1}{6}\left(\frac{1}{4f_{IF}}\right)^3\left[\varphi_\Delta \ddot{x}(t) - i\frac{3}{2}\varphi_\Delta^2 \dot{x}^2(t) - \varphi_\Delta^3 \int \dot{x}^3(t)dt\right]\right\} \tag{C.46}$$

$$i_{HIFM\ out}(t) = T\left\{-\frac{1}{4f_{IF}}\left[\omega_\Delta x(t) + \dot{\varphi}_{n\ tot}(t)\right] + \frac{1}{6}\left(\frac{1}{4f_{IF}}\right)^3\left[\omega_\Delta \ddot{x}(t) - i3\omega_\Delta^2 x(t)\dot{x}(t) - \omega_\Delta^3 x^3(t)\right]\right\} \tag{C.47}$$

The SNRs can then be written in the simple forms

$$SNR_{HIPM} = \varphi_\Delta^2\left[\left(\frac{4RPJ_1(\beta)}{9}\right)^2 \frac{\langle x^2(t)\rangle}{\langle n_{shot\ bp}^2\rangle + \langle n_{thermal\ bp}^2\rangle + \left(\frac{RP}{3}\right)^2\left(1+\frac{2}{3}J_0(\beta)\right)^2\langle n_{RIN\ bp}^2\rangle}\right] \tag{C.48}$$

$$SNR_{HIFM} = \left(\frac{\omega_\Delta}{B}\right)^2\left[\left(\frac{4RPJ_1(\beta)}{9}\right)^2 \frac{B^2\langle x^2(t)\rangle}{\langle \dot{n}_{shot\ bp}^2\rangle + \langle \dot{n}_{thermal\ bp}^2\rangle + \left(\frac{RP}{3}\right)^2\left(1+\frac{2}{3}J_0(\beta)\right)^2\langle \dot{n}_{RIN\ bp}^2\rangle}\right] \tag{C.49}$$

where the noise expressions are evaluated in Appendix A.2. Then the SFDR of both links can be expressed by

$$SFDR = \left[\frac{8SNR_o}{3|b_3|}\right]^{2/3} \tag{C.50}$$

where SNR_o is defined as the terms in square brackets in Eqs. (C.48) and (C.49) and $|b_3|$, the third-order nonlinearity coefficient, is $\frac{1}{6}\left(\frac{\pi f_{max}}{2f_{IF}}\right)^2$ for the HIPM link and $\frac{1}{6}\left(\frac{B}{4f_{IF}}\right)^2$ for the HIFM link. These terms are identical to those derived for the coherent PM and FM links in Appendix C.1.1, where the details of that derivation are contained.

C.2.2 RF Power Transfer Ratio and Noise Figure

The derivation of RF power transfer ratio and noise figure closely follows that given for the coherent FM link in Appendix C.1.2.2. The reader is advised to refer to that section for details.

The HIPM modulation index φ_Δ is equal to $\frac{\pi V}{V_\pi}$ (where V is the applied voltage and V_π is the voltage corresponding to a π phase shift in the modulator) and the HIFM modulation index $\frac{\omega_\Delta}{B}$ is equal to $\frac{\pi V}{V_\pi R_{int} C_{int} B}$, where R_{int} and C_{int} are parameters of the integrating lowpass filter. From the output currents given in Eqs. (C.46) and (C.47), the RF power transfer ratios of the two links are easily found to be

$$G_{opt\,(HIPM)} = G_{opt\,(HIFM)} = \left(\frac{1}{4f_{IF}}\right)^2 \frac{16}{81} R^2 P^2 J_1^2(\beta) \left(\frac{\pi}{V_\pi R_{int} C_{int}}\right)^2 R_S^2 L_{nl} \qquad \text{(C.51)}$$

This RF gain is in terms of the signal input power only; it does not include the two supplemental sinusoidal modulator inputs required for these two links.

The derivation of noise figure is straightforward using the formula (see Appendix C.1.2.1 for details)

$$F_{(link)} = 1 + \frac{noise\ power\ at\ link\ output}{G_{(link)} kTB} \qquad \text{(C.52)}$$

where the noise powers at the link outputs for the HIPM and HIFM links are

$$\eta_{(HIPM)} = R_S \left[\left\langle n^2_{shot\,bp} \right\rangle + \left\langle n^2_{thermal\,bp} \right\rangle + \left(\frac{RP}{3}\right)^2 \left(1 + \frac{2}{3} J_0(\beta)\right)^2 \left\langle n^2_{RIN\,bp} \right\rangle \right] \left(\frac{1}{4f_{IF} RC}\right)^2 \qquad \text{(C.53)}$$

$$\eta_{(HIFM)} = R_S \left[\left\langle \dot{n}^2_{shot\,bp} \right\rangle + \left\langle \dot{n}^2_{thermal\,bp} \right\rangle + \left(\frac{RP}{3}\right)^2 \left(1 + \frac{2}{3} J_0(\beta)\right)^2 \left\langle \dot{n}^2_{RIN\,bp} \right\rangle \right] \left(\frac{1}{4f_{IF}}\right)^2 \qquad \text{(C.54)}$$

The noise terms are given in Appendix A.2.

C.3 Homodyne Interferometric Links

In this section, the derivations for the HIPM and HIFM links are provided. Section C.3.1 contains the parallel derivations of SFDR for the two links. Section C.3.2 contains the parallel derivations of RF power transfer ratio and noise figure for the two links.

C.3.1 SFDR of HPM and HFM Links

To derive the SFDR of the HPM and HFM links, it is first necessary to derive expressions for the link SNRs and nonlinearity coefficients. Both of these are easily obtainable from the link output current. After that, the SFDR can be simply obtained from Eq. (C.15).

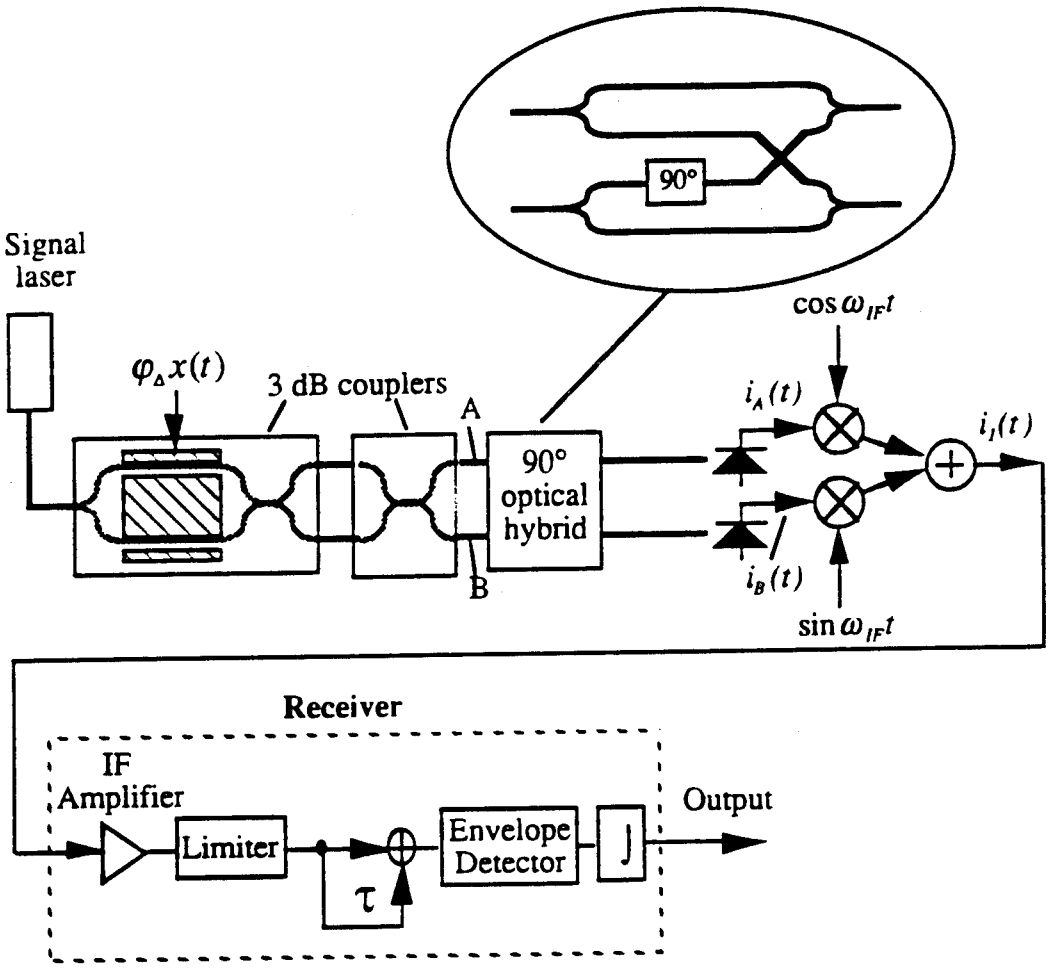

Fig. C-4. Homodyne interferometric phase modulated link.

A diagram of an HPM link is provided in Fig. C-4 for reference. Assuming a standard push-pull modulator structure and a 3-dB coupler transfer matrix of the form

$$\frac{1}{\sqrt{2}}\begin{bmatrix}1 & j\\ j & 1\end{bmatrix}, \tag{C.55}$$

the optical fields at points A and B in Fig. C-4 are given by

$$\begin{bmatrix} j\exp\left[j\left(\omega_o t+\frac{1}{2}\varphi[x(t)]+\frac{\varphi_b}{2}\right)\right]\\ j\exp\left[j\left(\omega_o t-\frac{1}{2}\varphi[x(t)]-\frac{\varphi_b}{2}\right)\right]\end{bmatrix}\sqrt{\frac{P}{2}(1+n_R(t))}\exp\left[j\varphi_p(t)\right] \tag{C.56}$$

where φ_b is an arbitrary bias phase associated with the modulator and all other symbols are as in the analysis in Appendix C.2.1.

A 90° optical hybrid has a transfer matrix relating the output fields, E_{out}, to the input fields, E_{in}, by

$$\begin{bmatrix}E_{A\,out}\\ E_{B\,out}\end{bmatrix}=\frac{1}{2}\begin{bmatrix}1 & 1\\ 1 & -j\end{bmatrix}\begin{bmatrix}E_{A\,in}\\ E_{B\,in}\end{bmatrix} \tag{C.57}$$

where the subscripts A and B refer to the two input and output ports. A 90° optical hybrid can be implemented as shown in Fig. C-4. Such a device has an excess loss of 3 dB and typically requires closed loop control of a bias voltage in a manner similar to biasing a Mach Zehnder modulator in its quasi-linear region of operation.

The currents $i_A(t)$ and $i_B(t)$ after the two photodetectors are given by

$$\begin{bmatrix}i_A(t)\\ i_B(t)\end{bmatrix}=\frac{RP}{4}(1+n_R(t))\begin{bmatrix}1+\cos(\varphi[x(t)])\\ 1-\sin(\varphi[x(t)])\end{bmatrix}+\begin{bmatrix}n_{recA}(t)\\ n_{recB}(t)\end{bmatrix} \tag{C.58}$$

where φ_b is set to zero for simplicity. The form of these currents allows for the creation of a phase-modulated IF signal through IF mixing after detection, in contrast to the frequency-shifting during optical modulation required in the heterodyne interferometric links. After mixing and combining, the current becomes

$$i_1(t) = \frac{RP}{4}(1+n_R(t))\left[\cos(\omega_{IF}t + \varphi[x(t)]) + \cos(\omega_{IF}t) + \sin(\omega_{IF}t)\right] + n_{recA}(t)\cos(\omega_{IF}t) + n_{recB}(t)\sin(\omega_{IF}t) \tag{C.59}$$

The first large term contains the desired phase-modulated signal. It also contains cross-terms between the baseband laser RIN and IF tones. This means that the impact of the laser RIN on the received IF signal will be the same as if that signal were at baseband. Therefore, the RIN suppression seen in the heterodyne interferometric links due to the high IF will not occur in the homodyne interferometric links. As in the heterodyne interferometric links, the RIN-cross-signal term will be essentially eliminated due to the use of a limiter. The noise terms $n_{recA}(t)$ and $n_{recB}(t)$ consist of shot and thermal noise and have worst-case power spectral densities

$$n_{recA}(t) = n_{recB}(t) = eRP + \frac{4kT}{R_r} \tag{C.60}$$

since the maximum received optical power at each photodetector is $P/2$.

Following the same procedure as in Appendices C.1.1 and C.2.1, the output currents for the HPM and HFM links are found to be

$$i_{HPM\,out}(t) = K\left\{-\frac{1}{4f_{IF}}\left[\varphi_\Delta x(t) + \varphi_n(t)\right] + \frac{1}{6}\left(\frac{1}{4f_{IF}}\right)^3\left[\varphi_\Delta \ddot{x}(t) - i\frac{3}{2}\varphi_\Delta^2 \dot{x}^2(t) - \varphi_\Delta^3 \int \dot{x}^3(t)dt\right]\right\} \tag{C.61}$$

$$i_{HFM\,out}(t) = T\left\{-\frac{1}{4f_{IF}}\left[\omega_\Delta x(t) + \dot{\varphi}_{n\,tot}(t)\right] + \frac{1}{6}\left(\frac{1}{4f_{IF}}\right)^3\left[\omega_\Delta \ddot{x}(t) - i3\omega_\Delta^2 x(t)\dot{x}(t) - \omega_\Delta^3 x^3(t)\right]\right\} \tag{C.62}$$

which are of identical forms to the output currents in Appendices C.1.1 and C.2.1. The difference is the noise contribution to the phase, which in this case is given by

$$\varphi_n(t) = \frac{4}{RP}\left(n_{recA\,q}(t) + n_{recB\,i}(t)\right) + n_R(t) \tag{C.63}$$

The quadrature and in-phase noise components have the same power spectral densities as the original noise components [3] and hence Eq. (C.60) can be substituted in directly to obtain the total noise power spectral density.

The SNRs can then be written in the simple forms

$$SNR_{HPM} = \varphi_{\Delta}^2 \left[\left(\frac{RP}{4} \right)^2 \frac{\langle x^2(t) \rangle}{\langle i_{recA\,bb}^2 \rangle + \langle i_{recB\,bb}^2 \rangle + \left(\frac{RP}{4} \right)^2 \langle i_{RIN\,bb}^2 \rangle} \right] \tag{C.64}$$

$$SNR_{HFM} = \left(\frac{\omega_{\Delta}}{B} \right)^2 \left[\left(\frac{RP}{4} \right)^2 \frac{B^2 \langle x^2(t) \rangle}{\langle i_{recA\,bb}^2 \rangle + \langle i_{recB\,bb}^2 \rangle + \left(\frac{RP}{4} \right)^2 \langle i_{RIN\,bb}^2 \rangle} \right] \tag{C.65}$$

where the noise expressions are evaluated in Appendix A.2. Since the received optical signal generates photocurrents at baseband, the noises in the homodyne interferometric links are all baseband noises. Then the SFDR of both links can be expressed by

$$SFDR = \left[\frac{8SNR_o}{3|b_3|} \right]^{2/3} \tag{C.66}$$

where SNR_o is defined as the terms in square brackets in Eqs. (C.64) and (C.65) and $|b_3|$, the third-order nonlinearity coefficient, is $\frac{1}{6}\left(\frac{\pi f_{\max}}{2 f_{IF}} \right)^2$ for the HPM link and $\frac{1}{6}\left(\frac{B}{4 f_{IF}} \right)^2$ for the HFM link. These terms are identical to those derived for the coherent PM and FM links in Appendix C.1.1 and to those derived for the heterodyne interferometric links in Appendix C.1.2.

C.3.2 RF Power Transfer Ratio and Noise Figure

The derivation of RF power transfer ratio and noise figure closely follows that given for the heterodyne interferometric links in Appendix C.2.2. The reader is advised to refer to that section for details.

From the output currents given in Eqs. (C.62) and (C.63), the RF power transfer ratios of the HPM and HFM links are easily found to be

$$G_{opt\,(HPM)} = G_{opt\,(HFM)} = \left(\frac{1}{4f_{IF}}\right)^2 \frac{1}{16} r^2 P_S^2 \left(\frac{\pi}{V_\pi RC}\right)^2 R_S^2 L_{nl} \alpha \tag{C.67}$$

where α is the conversion loss (on the order of 6 dB) of the microwave mixers required in the receivers of the HPM and HFM links.

The derivation of noise figure is straightforward using the formula (see Appendix C.1.2.1 for details)

$$F_{(link)} = 1 + \frac{noise\ power\ at\ link\ output}{G_{(link)} kTB} \tag{C.68}$$

where the noise powers at the link outputs for the HPM and HFM links are

$$\eta_{(HPM)} = R_S \left[\left\langle n^2_{recA\,bb} \right\rangle + \left\langle n^2_{recB\,bb} \right\rangle + \left(\frac{RP}{4}\right)^2 \left\langle n^2_{RIN\,bb} \right\rangle \right] \left(\frac{1}{4f_{IF}RC}\right)^2 \tag{C.69}$$

$$\eta_{(HFM)} = R_S \left[\left\langle i^2_{recA\,bb} \right\rangle + \left\langle i^2_{recB\,bb} \right\rangle + \left(\frac{RP}{4}\right)^2 \left\langle i^2_{RIN\,bb} \right\rangle \right] \left(\frac{1}{4f_{IF}}\right)^2 \tag{C.70}$$

The noise terms are given in Appendix A.2.

C.4 References

[1] P. F. Panter, *Modulation, Noise, and Spectral Analysis,* McGraw-Hill, Inc., New York, 1965.

[2] D. M. Pozar, *Microwave Engineering*, Addison-Wesley, New York, 1990.

[3] A. B. Carlson, *Communication Systems,* 3rd ed., McGraw-Hill, Inc., New York, 1986.

*U.S. GOVERNMENT PRINTING OFFICE: 1995-610-126-50123

MISSION

OF

ROME LABORATORY

Mission. The mission of Rome Laboratory is to advance the science and technologies of command, control, communications and intelligence and to transition them into systems to meet customer needs. To achieve this, Rome Lab:

a. Conducts vigorous research, development and test programs in all applicable technologies;

b. Transitions technology to current and future systems to improve operational capability, readiness, and supportability;

c. Provides a full range of technical support to Air Force Materiel Command product centers and other Air Force organizations;

d. Promotes transfer of technology to the private sector;

e. Maintains leading edge technological expertise in the areas of surveillance, communications, command and control, intelligence, reliability science, electro-magnetic technology, photonics, signal processing, and computational science.

The thrust areas of technical competence include: Surveillance, Communications, Command and Control, Intelligence, Signal Processing, Computer Science and Technology, Electromagnetic Technology, Photonics and Reliability Sciences.